

Love and Fear of Water

Water Dynamics around Charged and Apolar Solutes

ISBN 978-90-77209-79-0

© 2014, Sietse T. van der Post. All rights reserved.

Cover design: Photography by Ethan Oelman (www.ethan-oelman.com),
layout by Jorrit Thijn

Love and Fear of Water

Water Dynamics around Charged and Apolar Solutes

ACADEMISCH PROEFSCHRIFT

ter verkrijging van de graad van doctor
aan de Universiteit van Amsterdam
op gezag van de Rector Magnificus
prof. dr. D. C. van den Boom

ten overstaan van een door het college voor promoties ingestelde
commissie, in het openbaar te verdedigen in de Agnietenkapel
op vrijdag 7 februari 2014, te 10:00 uur

door

Sietse Thijmen van der Post

geboren te Zoetermeer

PROMOTIECOMMISSIE

Promotor: prof. dr. H. J. Bakker
Overige leden: prof. dr. W.-J. Buma
prof. dr. K. J. Hellingwerf
prof. dr. J. T. Hynes
prof. dr. F. Koenderink
prof. dr. L. D. Noordam
prof. dr. V. Subramaniam

Faculteit der Natuurwetenschappen, Wiskunde en Informatica

The work described in this thesis was performed at the FOM Institute AMOLF, Science Park 104, 1098 XG Amsterdam, The Netherlands. This work is part of the research programme of the *Stichting Fundamenteel Onderzoek der Materie* (FOM), which is financially supported by the *Nederlandse Organisatie voor Wetenschappelijk Onderzoek* (NWO).

Voor Bonnie

THIS THESIS IS BASED ON THE FOLLOWING PUBLICATIONS:

- S.T. van der Post and H.J. Bakker. The Combined Effect of Cations and Anions on the Dynamics of Water. *Phys. Chem. Chem. Phys.* *14*, 62806288 (2012). (*Chapters 8 and 9*)
- S.T. van der Post, S. Scheidelaar and H.J. Bakker. Femtosecond Study of the Effects of Ions on the Reorientation Dynamics of Water. *Journal of Mol. Liq.* *176*, 22-28 (2012). (*Chapter 9*)
- S.T. van der Post, K.J. Tielrooij, J. Hunger, E.H.G. Backus and H.J. Bakker. Femtosecond Study of the Effects of Ions and Hydrophobes on the Dynamics of Water. *Faraday Disc.* *160*, 171-189 (2013). (*Chapters 9, 10 and 11*)
- M. Pastorczyk, S.T. van der Post and H.J. Bakker. Cooperative Hydration of Carboxylate Groups with Alkali Cations. *Phys. Chem. Chem. Phys.* *15*, 17767-17770 (2013). (*Chapter 9*)
- S.T. van der Post, S. Scheidelaar and H.J. Bakker. Water Dynamics in Aqueous Solutions of Tetra-n-alkylammonium Salts: Hydrophobic and Coulomb Interactions Disentangled. *J. Phys. Chem. B* *117*, 1510115110 (2013). (*Chapter 10*)
- S.T. van der Post, J. Hunger, M. Bonn and H.J. Bakker. Observation of Water Separated Ion-Pairs between Cations and Phospholipid Headgroups. *Submitted*. (*Chapter 9*)
- C. Hsieh, S.T. van der Post, H.J. Bakker and M. Bonn. Inhomogeneous Vibrational Relaxation in Pure Water. *To be submitted*. (*Chapter 5*)
- S.T. van der Post and H.J. Bakker. Vibrational Relaxation of the OH-Stretch Overtone in Pure Liquid Water. *To be submitted*. (*Chapter 5*)
- S.T. van der Post and H.J. Bakker. Temperature Dependent Experimental Study of the Jump-Reorientation of Water. *To be submitted*. (*Chapter 6*)
- S.T. van der Post and H.J. Bakker. Water Reorientation in the Hydration Shell of TMU. *To be submitted*. (*Chapter 7*)

OTHER PUBLICATIONS BY THE SAME AUTHOR:

- K.J. Tielrooij, S.T. van der Post, J. Hunger, M. Bonn and H.J. Bakker. Anisotropic Water Reorientation around Ions. *J. Phys. Chem. B* *115*, 12638-12647 (2011).
- R. Ulbricht, S.T. van der Post, J.P. Goss, P.R. Briddon, R. Jones, R.U.A. Khan and M. Bonn. Single Substitutional Nitrogen Defects Revealed as Electron Acceptor States in Diamond using Ultrafast Spectroscopy. *Phys. Rev. B* *84*, 165202 (2011).

Contents

1	Introduction	11
2	Spectroscopy	17
2.1	Light-Matter Interaction	17
2.1.1	The Harmonic Oscillator	17
2.1.2	Non-Linear Systems	19
2.1.3	Quantum Mechanical Systems	22
2.2	Line Broadening and Spectral Diffusion	25
3	Experiment	29
3.1	Mid-Infrared Pump Probe	29
3.1.1	One Color Pump-Probe Setup	29
3.1.2	Two Color Pump-Probe Setup	31
3.2	Formalism of Polarization Resolved Experiments	33
3.3	Dielectric Relaxation Spectroscopy	40
3.3.1	THz spectroscopy	41
3.3.2	GHz spectroscopy	42
3.4	Samples	42
3.4.1	Wire Flow Cell	43
4	Data Analysis	45
4.1	Transient Absorption Spectra	45
4.2	Modeling Heat Dynamics	47
4.2.1	Simple Kinetic Model	48
4.2.2	Delayed Heat	49
4.3	Direct Probe of Heat Dynamics	50
4.3.1	Multiple Species	54
4.4	Anisotropy	56
4.4.1	Modeling of Anisotropy Dynamics	56
4.4.2	Self-Consistent Fit	58
4.4.3	Anisotropy and Exchange	59
4.5	Dielectric Relaxation	62

5	Vibrational Relaxation in Pure Water	65
5.1	Introduction	66
5.2	Experiment	66
5.2.1	Excitation of the Fundamental Transition	66
5.2.2	Excitation of Overtones	67
5.3	OH-stretch: Results and Interpretation	68
5.4	Overtones: Results and Interpretation	72
5.4.1	OH-stretch Overtone	72
5.4.2	Bend-Stretch Combination Tone	74
5.4.3	Calculation of the Overtone Spectrum of Hydrogen-bonded OH Groups	75
5.5	Discussion	78
5.5.1	Frequency Dependence of the OH-Stretch Vibrational Lifetime	78
5.5.2	The Stretch Overtone and Stretch-bend Combination Spectra	80
5.6	Conclusions	84
5.A	Appendix: Förster Transfer	85
6	Experimental Study of the Jump-Reorientation of Water	89
6.1	Introduction	90
6.2	Experimental	90
6.3	Results and Discussion	91
6.3.1	Thermalization Dynamics and Spectral Diffusion	91
6.3.2	Reorientation Dynamics at Room Temperature	94
6.3.3	Reorientation Dynamics at Elevated Temperature	99
6.4	Conclusions	100
6.A	Appendix: Narrow Pump and Anisotropy	102
7	Water Reorientation in the Hydration Shell of TMU	105
7.1	Introduction	106
7.2	Experimental	107
7.3	Results and Interpretation	107
7.3.1	Isotropic Results and Spectral Diffusion	107
7.3.2	Anisotropy Decay of Water Around TMU	108
7.4	Discussion	114
7.5	Conclusions	117
8	Exchange Dynamics in Salt Solutions	119
8.1	Introduction	120
8.2	Experimental	121
8.3	Results and Discussion	121
8.3.1	Linear spectra	121
8.3.2	Vibrational Relaxation and Exchange	121
8.3.3	Separation of the Anion-Bound Anisotropy	123
8.3.4	Contribution of Exchange to the Anisotropy	125

8.4	Conclusions	128
9	Cooperative Effects in Ion Hydration	129
9.1	Introduction	130
9.2	Samples and Linear Spectra	131
9.3	Results and Interpretation	132
9.3.1	Reorientation of Water in the Anion Hydration Shell . . .	132
9.3.2	Effect of Cations on the Anion Hydration Shell	135
9.3.3	Cooperative Effects of Cations combined with Formates or Phosphorylethanolamine	137
9.3.4	Lifetime of the PE-Na and PE-Ca Ion-pairs	141
9.4	Cooperative Ion Hydration: The Broad Picture	145
9.5	Summary	149
10	Hydrophobic and Coulomb Interactions Disentangled	151
10.1	Introduction	152
10.2	Experiment	153
10.3	Results and Analysis	153
10.3.1	Experimental Results	153
10.3.2	Modeling	155
10.3.3	Modeling Results	156
10.4	Discussion	159
10.4.1	Hydrophobic Effects on the Anion Hydration Shell	159
10.4.2	Formation of Aggregated Ion Clusters	162
10.5	Conclusions	164
11	Osmolytes and Denaturation	167
11.1	Introduction	168
11.2	Experimental	169
11.3	Results	170
11.3.1	THz Dielectric Relaxation	170
11.3.2	fs-IR Pump-Probe	171
11.4	Discussion	174
11.5	Conclusions	176
	Bibliography	179
	Summary	195
	Samenvatting	199
	Dankwoord	203

1

Introduction

THE REMARKABLE PROPERTIES OF WATER Without exaggeration water can be regarded as one of the most interesting compounds in nature. The water molecule is deceptively simple, consisting only of one oxygen and two hydrogen atoms. It is probably the one chemical that most people in the world actually know by its chemical formula: H_2O . The human body contains 65 % of water (men a bit more than women) and life as we know it would not be possible without it. That is: not possible without *liquid* water. The fact that water pours out of the tap as a liquid substance is actually quite remarkable. Any other substance of comparable molecular size and weight would be a gas under ambient conditions (eg. methane, ammonium, oxygen, carbondioxide).

Another fact present in the human consciousness is the floating of icecubes on water. Indeed, the density of ice is lower than that of liquid water and the density of liquid water increases upon heating. Interestingly, though, the minimum density of liquid water is not at zero degrees Celsius but actually at 4°C . As long as a body of water like a lake does not entirely cool down to 4°C ., warmer water will thus always well up to the surface. Dutch people know this very well, since this effect prevents ice skating on most small but deep lakes most winters, while sometimes the very large but shallow IJsselmeer is covered with ice.

The examples given above are just two out of a long list of 'anomalies' of water (some count 46, others more than 60) [1]. At the heart of many of these (apparent) anomalies is the special structure of water on a molecular level. The water molecule is unique in its property of both donating and accepting two hydrogen-bonds. A hydrogen-bond is an electromagnetic attraction between a slightly positively charged hydrogen-atom in a molecule and a lone electron pair on the oxygen (in the case of water) of another molecule (Fig. 1.1). This bond is not as strong as a typical covalent bond, but still has a quite high binding energy (5.0 kcal/mol). By forming on average almost four of such bonds, water molecules form a tetrahedral network that is strongly bound. This hydrogen-bond network is the reason for many of the anomalies of water: its liquid phase at ambient conditions, unusually high viscosity, high specific heat capacity, high density, low compressibility and high surface tension, to name a few.

In spite of this strong binding, reorganization of the hydrogen-bond network

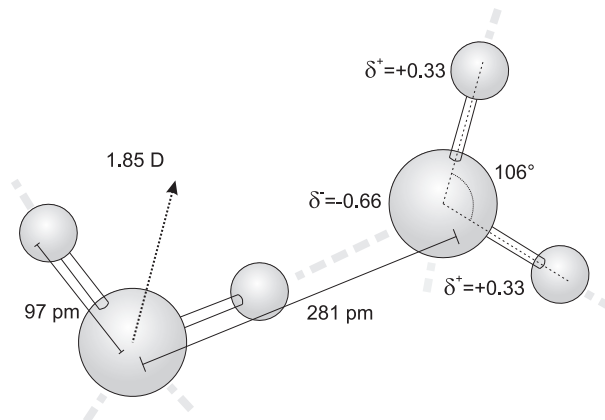


FIGURE 1.1. The positive net charge on the protons (+0.33) and the negative net charge on the oxygen atom (-0.66) results in the formation of a hydrogen-bond. Since the covalent bonds make an angle of 106° , the molecule has a net dipole of 1.85 D. The hydrogen-bond (oxygen-oxygen) distance of 281 pm is the average value in liquid water at ambient conditions.

takes place on a picosecond timescale. In a process involving concerted displacements of a number of surrounding water molecules, hydrogen-bonds are continuously broken and reformed [2, 3, 4]. This dynamical behavior leads to additional properties of importance: water can rapidly adapt to a change of chemical environment, enabling the solvation of ions and other solutes. Water is also a transport medium for chemical reactions. A special example is the transport of protons. The two protons of a water molecule are not at all tightly bound to the oxygen atom. In pure liquid water spontaneous (auto)ionization occurs and low concentrations of OH^- and H_3O^+ ions exist. As a result of the fast reorganization of hydrogen-bonds and the ease at which the protic covalent bonds are broken and formed, excess protons show an extremely fast diffusive behavior in water [5]. It is however not one proton that finds its way through the hydrogen-bond network, but rather a relay race of innumerable proton exchanges that lead to transfer of the proton charge. This mechanism is called the Grotthuss mechanism [6].

WATER AS A SOLVENT All the above properties make water a very complicated substance and a topical subject of research even in its pure form [7, 8, 9]. However, the property that makes water special in a much broader context is its role as a solvent. Crucial in this aspect is the conformation of the molecule: the two covalent bonds make an angle of 106° . Since the oxygen atom has a larger electron affinity than the two protons, this conformation result in a net electric dipole of 1.85 Debye (Fig. 1.1). This charge distribution in combination with the small molecule size makes water an extremely good solvent for ions. Water

is the most polar solvent known ^a, and its high dielectric constant (~ 80 at room temperature [10]) shields the charge of an ion such that for many anion/cation combinations ion recombination followed by precipitation does not occur up to very high concentrations.

A consequence of the strong polarity is that water is a very poor solvent for apolar compounds like alkanes: Oil and water do not mix. Such compounds go by the name of hydrophobes, they fear water. Although other polar solvents have a dislike for hydrophobes as well, the affinity mismatch between fatty molecules and water does not find an equal in nature [11]. Recent theoretical research on the microscopic origins of the phase segregation of water and hydrophobic compounds showed that the hydrogen-bond network acts as a driving force of hydrophobic assembly [11]. The size of the hydrophobic molecule does however play an important role. For apolar molecules larger than about one nanometer, hydrogen-bonds need to be broken to make a cavity in which the molecule can reside. The energy cost involved in the breaking of those hydrogen-bonds scales with the surface of the hydrophobic molecule, and aggregation naturally becomes favorable to limit this energy cost [11]. For anything smaller than one nanometer, the hydrogen-bond network is flexible enough to fold itself around it while keeping the hydrogen-bonds intact. The size dependence can be compared with a densely crowded mob of people: A child that wants to move through will find no problem in sneaking in between the legs, but a big fat person will have to excuse him/herself all the time.

In nature, hydrophobes are often combined with a charged or polar molecular group, thus forming an amphiphilic molecule. Examples are plentiful: any soap or detergent, the alcohol in a glass of wine or the lipids that make up the cell membranes in the body. For such solutes, water reveals its unique properties as a solvent best. The affinity of water for the polar moieties and its enmity for the hydrophobic parts of an amphiphile drives the formation of membranes and numerous other processes in organisms. Proteins in organisms rather shield their hydrophobic parts from interacting with water in a process called the hydrophobic collapse. The three-dimensional structure that such molecules thereby assume give them their function. It is for this reason that water is often referred to as the solvent of life.

THE LOOK OF WATER In this thesis we study the properties of water that are fundamental to the properties that were described above. We study the dynamics of the ever changing hydrogen-bond network and how this network is affected by the presence of charged, polar or hydrophobic solutes. But how does one look at something as small as a water molecule? Especially since its size is not the only challenge. Moreover, for water all relevant dynamical processes take place on ultrashort timescales between 50 femtoseconds and a couple of picoseconds. The atoms are not even tightly fixed to each other

^aSome solvents, like DMSO or acetonitrile, have a larger dipole than water. Their dielectric constant, which can be regarded as a measure of how well the solvent shields an electric charge, is however smaller. For this reason, water is nonetheless considered more polar than any other solvent.

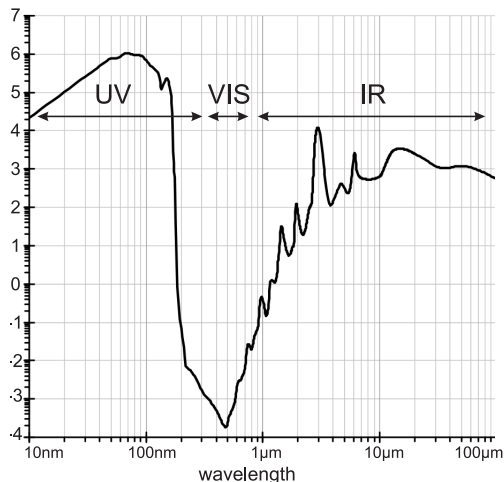


FIGURE 1.2. The linear absorption spectrum of pure liquid water (adapted from [12]). Absorption in the UV region is due to electronic transitions. The absorption bands at $3\mu\text{m}$ and $6\mu\text{m}$ are the OH-stretch and H_2O -bend vibrations, respectively. Absorption at wavelengths longer than $8\mu\text{m}$ are librational and translational motions, while all other bands between the visible region and than $3\mu\text{m}$ are vibrational overtones and combination bands.

(proton transfer and hydrogen-bond switching). The solution to this problem is water's interaction with light. The interaction with light of the right wavelength has the same result on a water molecule as a soundwave of the right pitch has on a guitar string: it will induce a vibration.

In daily life water appears to us as a clear, transparent liquid. The transparency of water to visible light is nonetheless an exception that was exploited by evolution when it came to the 'choice' to which part of the electromagnetic spectrum the eyes of organisms should be sensitive. Fig. 1.2 shows the absorption spectrum of water from the UV to the microwave spectral region. The absorption at shorter wavelengths of the visible gap are due to electronic transitions, while the rich structure of bands at longer wavelengths are due to vibrations and (for yet longer wavelengths) librational motions and hydrogen-bond vibrations. It is the vibrational region that is of most interest to us in this thesis.

A water molecule (and any molecule in general) is all but a rigid structure made out of sticks and balls. The covalent bonds are flexible enough to give freedom for the atoms to vibrate. A classical picture of a water molecule would thus be one of springs and balls. A close-up of the vibrational modes that are of importance to this thesis are shown in Fig. 1.3. Water molecules have three normal modes of vibration: the bending mode (absorbing light of $6\mu\text{m}$), the symmetric stretching mode and the asymmetric stretching mode (absorbing light of $3\mu\text{m}$). These modes have overtones with much lower absorption cross section, causing small additional absorption peaks at wavelengths shorter than

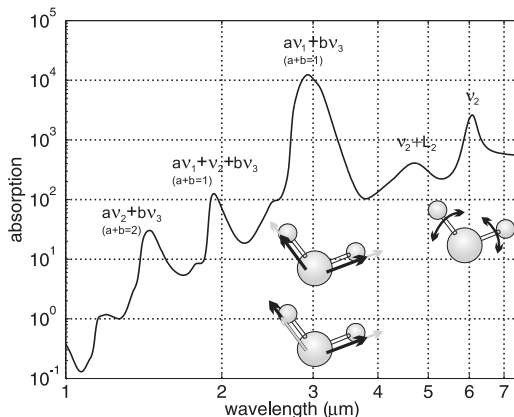


FIGURE 1.3. The main part of the vibrational absorption spectrum of pure liquid water. The three vibrational modes are depicted by ν_1 (symmetric OH-stretch), ν_2 (H_2O -bend) and ν_3 (asymmetric OH-stretch). At shorter wavelengths, all kinds of combination and overtone bands occur of increasingly lower amplitude.

$2.5 \mu\text{m}$. The extension of the overtones into the region of visible light causes water to appear blue.

The techniques that are used in this thesis to study water exploit the vibrations of water. The vibrational modes are excited with laser pulses tuned to the vibrational frequencies. These excitations change the absorption spectrum of water and the time evolution of these absorption changes can provide information on the water molecules and the structure and dynamics of the hydrogen-bond network. Although the water molecule itself has only three intramolecular vibrational modes, the coupling to the network of the hydrogen-bonds highly complicates the analysis of the absorption changes. All molecules are connected, and making one spring vibrate will quickly lead to a response of many other vibrations [9]. It is exactly this interconnectedness that makes water such an interesting liquid, but also one that is very challenging to study.

OUTLINE OF THIS THESIS The following three chapters are a general introduction to the measurement and analysis techniques we used. We first discuss the theory behind the spectroscopic experiments. The harmonic oscillator lies at the heart of many topics in physics and vibrational spectroscopy is certainly one of them. From there we proceed to the more realistic picture of a quantum anharmonic oscillator, which is closer to most oscillators in nature including the vibrations of a water molecule. Subsequently, the experimental details of the used experimental setups are discussed, with extra emphasis to the manipulations of the laser-light polarization in polarization resolved measurements. The three chapters are concluded with an extensive treatise of the techniques used to analyze and to interpret the experimental data.

After these introductory chapters, the thesis describes a number of studies of aqueous solutions. The chapters are organized such that we start with the

most fundamental aspects of water and as the chapters progress, systems with more direct biological implications are studied. Chapter 5 and 6 consider the vibrational dynamics and reorientation in pure water, followed in chapter 7 by a study of the fundamental aspects of hydrophobic hydration. Chapter 8 and 9 are concerned with the dynamics of water molecules in solutions of ions. In chapter 10 the results of chapters 7 and 9 are used to study a system in which both coulomb effects and hydrophobic hydration combined play a role. Finally, chapter 11 makes a comparison of the reorientation of water and the properties of denaturation agents in aqueous solutions of various osmolytes.

2

Spectroscopy

2.1 LIGHT-MATTER INTERACTION

Many phenomena in nature can be readily described by oscillations. An oscillation is the natural response of a system that is pushed out of a stable equilibrium by a stimulus. On the molecular scale, the displacement of atoms will lead to molecular vibrations. Although an idealized situation, the harmonic oscillator is the natural starting point for any treatise of oscillatory behavior. We will start with classical systems, since these provide a more intuitive picture that can still be related to molecular vibrations. Since transitions are not explained by classical theory, we eventually provide a (concise) quantum description as well. Along the way, the relation of the theory to physical systems is highlighted.

2.1.1 THE HARMONIC OSCILLATOR

The classical harmonic oscillator (CHO) is a system in which a mass m experiences a linear restoring force in case it is displaced from its equilibrium position x_0 in the vibrational coordinate x . The common example is a mass-spring system with spring force constant k . In the analog to a molecular vibration, the mass corresponds to the reduced mass of the total system of an atom that is covalently bonded (the spring) to the rest of the molecule. The equation of motion (EOM) of the CHO including damping and driving terms is given by,

$$m\ddot{x} + 2\gamma m\dot{x} + kx = V(t) \quad (2.1)$$

where k is the linear force constant, γ the damping coefficient and $V(t)$ the driving force. In the absence of any damping or a driving force, the fundamental frequency of the oscillator is given by $\omega_0 = \sqrt{k/m}$.

Coupling of the oscillator to its environment leads to damping. Without the driving force, the general solution to the EOM of the damped oscillator is given by,

$$x(t) = A \cos(\Omega t + \phi) e^{-\gamma t}, \quad \Omega = \sqrt{\frac{k}{m} - \gamma^2} \quad (2.2)$$

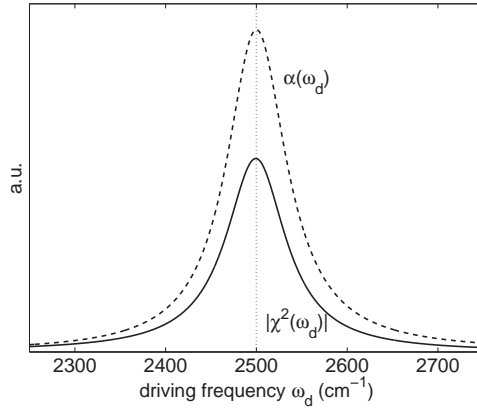


FIGURE 2.1. The power spectrum of the susceptibility and the associated absorption coefficient calculated for a resonance at 2500 cm^{-1} with the damping factor $\gamma = 40\text{ cm}^{-1}$.

where the integration constants A (amplitude) and ϕ (phase) follow from the boundary conditions. Damping thus has two consequences: The fundamental frequency of the mode is shifted and the vibration decays with a time constant γ . The stronger the coupling of the oscillator to its environment is, the larger the damping constant γ and the faster the decay will be.

In order to be able to study molecular vibrations by vibrational spectroscopy, they need to couple to light, that is, to electromagnetic field oscillations. We therefore consider the driving force to be an oscillating electric field with frequency ω_d and amplitude E_0 interacting with charges positioned on the oscillating masses (ie. the atoms in a molecule),

$$V(t) = qE(t) = qE_0 \cos(\omega_d t) \quad (2.3)$$

The solutions to the EOM Eq. (2.1) are then given by,

$$x(t) = \frac{qE_0 |\chi(\omega_d)|}{m} \cos(\omega_d t + \arg(\chi(\omega_d))) \quad (2.4)$$

where $\chi(\omega_d)$ denotes the linear susceptibility,

$$\chi(\omega_d) = \frac{1}{\omega_0^2 - \omega_d^2 + 2i\gamma\omega_d} \quad (2.5)$$

The susceptibility can be regarded as a measure of how easily the oscillator responds to the driving stimulus. The power spectrum $|\chi(\omega_d)|^2$ is shown in Fig. 2.1. The largest amplitude is naturally at the resonance frequency ω_0 . The spectrum has a Lorentzian lineshape with far extending shoulders, indicating that a small but nonzero cross section exists to drive the oscillator with a frequency ω_d far away from the resonance frequency ω_0 . If the driving

field is exactly resonant with the oscillator, the phase shift of the response is $\arg(\chi(\omega_0)) = 90^\circ$.

The susceptibility also constitutes the ability of the medium to polarize in response to the driving electric field. This relation can be written as,

$$\vec{P} = \varepsilon_0 \chi^{(1)}(\omega) \vec{E} \quad (2.6)$$

The superscript (1) in the susceptibility anticipates to the introduction of additional (non-linear) terms to the polarization later in this chapter. Other microscopic effects like the polarizability of electronic wave functions also contribute to the macroscopic polarization. An electromagnetic oscillation as driving force thus induces an oscillating polarization, which re-emits an electromagnetic field. We showed in Eq. (2.4) that at resonance the polarization field is 90° out of phase with the driving field. The re-emitted field is therefore 180° out of phase with the driving field and both will destructively interfere. This is a way of picturing absorption. The complex index of refraction is related to the susceptibility by,

$$\hat{n}(\omega) = n(\omega) + i\kappa(\omega) = \sqrt{1 + \chi(\omega)} \quad (2.7)$$

The imaginary part of the refractive index $\kappa(\omega)$ is the extinction coefficient, which is directly related to the absorption coefficient $\alpha(\omega)$ by,

$$\alpha(\omega) = \frac{2\kappa(\omega)\omega}{c} \quad (2.8)$$

Fig. 2.1 shows the frequency dependence of the absorption coefficient for a resonance at 2500 cm^{-1} . From Eq. (2.4) it is clear that $\chi(\omega)$ has a lorentzian shape of which the width is determined by the damping factor γ . This shape is quite well maintained in the absorption coefficient and explains why the lorentzian lineshape is frequently encountered in nature.

2.1.2 NON-LINEAR SYSTEMS

A purely harmonic oscillator is an approximation that is rarely encountered in nature. For most systems, a large displacement from the equilibrium position results in a restoring force that is not linear in the displacement anymore. A commonly used example is that of an atom covalently bound to another atom. In this situation, a large displacement will eventually lead to dissociation of the atoms. The potential of such a system can be modeled by the Morse-potential,

$$V_m(x) = V_0(e^{-2\beta x} - 2e^{\beta x}) \quad (2.9)$$

where V_0 is the binding energy and β a parameter that defines the width of the potential. The solutions to the equations of motion in the Morse-potential without damping or driving are written for small displacements as [13],

$$x(t) = \frac{1}{\beta} \ln(1 - C_1 \cos(\omega_0 t) - C_2 \sin(\omega_0 t)) \quad (2.10)$$

where C_1 and C_2 are constants following from the boundary conditions and ω_0 is the fundamental frequency in the harmonic limit. This solution to the EOM clearly shows very nontrivial oscillatory behavior. A power expansion of the natural logarithm yields,

$$x(t) = \frac{C_1}{\beta} (\cos(\omega_0 t) + \sin(\omega_0 t)) - \quad (2.11)$$

$$\frac{C_1^2 - C_2^2}{4\beta} (1 - \cos(2\omega_0 t)) + \quad (2.12)$$

$$\frac{C_1 C_2}{2\beta} \sin(2\omega_0 t) + O(3) \quad (2.13)$$

where the quadratic second order terms were rewritten. As can be seen, the oscillations in the Morse-potential contain frequencies of higher order than the fundamental frequency ω_0 .

In analogy to the Morse potential, in certain dielectric media the induced polarization does not depend linearly on the driving electromagnetic field. As a result, the electromagnetic field that is radiated by the induced polarization will contain higher order frequencies similar to what we saw above. Typically, the polarization is written as a function of the driving field $\vec{E}(t)$ in Eq. (2.6) can be expanded to encompass these higher orders as,

$$\vec{P}(\omega) = \varepsilon_0 \left(\chi^{(1)} \vec{E}(\omega) + \chi^{(2)} \vec{E}^2(\omega) + \chi^{(3)} \vec{E}^3(\omega) + \dots \right) \quad (2.14)$$

where $\chi^{(i)}$ is the i -th order susceptibility. Since the susceptibility may be different for the various polarization directions, the $\chi^{(i)}$ are tensors. The values of the susceptibilities depend on the properties of the dielectric medium and the higher order susceptibilities are in general very small. Therefore very large electric fields are needed to induce a non-linear polarization. Lasers can provide such large electric fields.

The non-linear terms in Eq. (2.14) give rise to a large variety of responses. Consider the driving field to be a superposition of two electromagnetic waves with different frequencies ω_i ($i = 1, 2$),

$$\vec{E}(\vec{x}, t) = \vec{E}_1 e^{i(\vec{k}_1 \cdot \vec{x} - \omega_1 t)} + \vec{E}_2 e^{i(\vec{k}_2 \cdot \vec{x} - \omega_2 t)} + c.c. \quad (2.15)$$

where $\vec{k}_i = \vec{n}(\omega_i) \omega_i / c$ is the wave vector in a medium with refractive index \vec{n} for frequency ω_i and the $c.c.$ denote the complex conjugate terms. It is quite straightforward to calculate the second order ($\chi^{(2)}$) non-linear response of the

polarization for a dispersion-free medium,

$$\begin{aligned}
\vec{E}^2(\vec{x}, t) &= |\vec{E}_1|^2 e^{i(2\vec{k}_1 \cdot \vec{x} - 2\omega_1 t)} + c.c. & (SHG) & \quad (2.16) \\
&|\vec{E}_2|^2 e^{i(2\vec{k}_2 \cdot \vec{x} - 2\omega_2 t)} + c.c. & (SHG) & \\
&2\vec{E}_1 \cdot \vec{E}_2 e^{i((\vec{k}_1 + \vec{k}_2) \cdot \vec{x} - (\omega_1 + \omega_2)t)} + c.c. & (SFG) & \\
&2\vec{E}_1 \cdot \vec{E}_2 e^{i((\vec{k}_1 - \vec{k}_2) \cdot \vec{x} - (\omega_1 - \omega_2)t)} + c.c. & (DFG) & \\
&2(|\vec{E}_1|^2 + |\vec{E}_2|^2) & (OR) &
\end{aligned}$$

A medium driven by the electromagnetic field described above thus emits light at frequencies that are completely different from the fundamental frequencies of the driving fields. The process leading to the production of light at the doubled frequencies $2\omega_1$ and $2\omega_2$ is called second harmonic generation (SHG), at $\omega_1 + \omega_2$ sum frequency generation (SFG), to light at $\omega_1 - \omega_2$ difference frequency generation (DFG) and to a static field called the optical rectification (OR). The non-linear susceptibility of a material can thus be used to convert light to different frequencies.

The non-linear response generates an oscillating polarization that emits light at the new frequency at every point in the medium along the propagation direction of the incident light. However, in general the phase-velocity of the re-emitted light will be unequal to that of the incident light. Light that was emitted at one point will then have a different phase than the light emitted further along the propagation direction. Over distances larger than the coherence length the light destructively interferes. Only under a detailed balancing of the refractive indices at different frequencies, the phase velocities of the light components are matched such that constructive interference is achieved. For instance for the process of SFG ($\omega_3 = \omega_1 + \omega_2$) optimal conversion is achieved if:

$$\vec{k}_1 + \vec{k}_2 = \vec{k}_3 \rightarrow \vec{n}(\omega_1)\omega_1 + \vec{n}(\omega_2)\omega_2 = \vec{n}(\omega_3)\omega_3 \quad (2.17)$$

This requirement is called the phase matching condition. Similar conditions can be written for the SHG and DFG responses. A birefringent medium has different refractive indices in different directions of the crystal structure that can be used for phase-matching. In the simplest case of an uniaxial crystal, the refractive index is identical in two spatial directions and different in a third. This third axis is called the optic axis. β -Barium borate (BBO), frequently used in the experiments describe in this thesis, is uniaxial. Light incident on such a crystal will experience different refractive indices for different polarization directions only if the propagation direction is not coinciding with the optic axis. The effective refractive indices can be tuned by rotating the crystal around an axis different from the optic axis. This method of angle-tuning is used to chose a geometry in which the phase matching condition is met for the desired frequencies and light conversion process.

2.1.3 QUANTUM MECHANICAL SYSTEMS

Up to now we considered classical systems as these already provide an intuitive picture of the dependence of absorption on driving fields etc. However, oscillations on a molecular level should be treated quantum mechanically. A bound quantum oscillator possesses eigenstates $|\phi_n\rangle$ ($n=1,2,\dots$) of which the energies E_n are the eigenvalues that follow from the Schrödinger equation,

$$\hat{H}_0 |\phi_n\rangle = E_n |\phi_n\rangle, \quad \hat{H}_0 = \frac{\hat{p}^2}{2m} + \frac{1}{2}k\hat{x}^2 \quad (2.18)$$

where \hat{H}_0 is the unperturbed hamiltonian of the harmonic oscillator. The first and second term in \hat{H}_0 describe the kinetic and potential energy, respectively. \hat{p} and \hat{x} are the momentum and position operators. The eigenvalues that follow from this equation are,

$$E_n = \hbar\omega_0(n + \frac{1}{2}) \quad (2.19)$$

with $\omega_0 = \sqrt{k/m}$ the fundamental frequency of the classical oscillator we derived above.

A perturbation of the system, for example by interaction with an external electromagnetic field, may induce a transition from one energy state to another. Such a process is described by the time-dependent Schrödinger equation,

$$i\hbar \frac{d}{dt} |\phi\rangle = \hat{H} |\phi\rangle \quad (2.20)$$

where $\hat{H} = \hat{H}_0 + \hat{V}_{int}(t)$ is the perturbed hamiltonian. The interaction can be described as,

$$\hat{V}_{int}(t) = \frac{1}{2}\vec{\mu} \cdot \vec{E}_0(e^{i\omega_a t} + e^{-i\omega_a t}) \quad (2.21)$$

where $\vec{\mu}$ is the dipole moment operator. $\vec{\mu}$ reflects the distribution of charges q_i in a molecule and is a function of the position operators \vec{x}_i :

$$\vec{\mu} = \sum_i q_i \vec{x}_i \quad (2.22)$$

$V_{int}(t)$ is defined here in perfect analogy to the driving force that we defined in Eq. (2.3) for the classical oscillator, with the cosine written in its complex notation. From Eq. (2.20) the rate $W_{i \rightarrow j}$ at which a transition occurs from state $|\phi_i\rangle$ to another state $|\phi_j\rangle$ can be derived. This is known as Fermi's Golden Rule, which is written to first order in the perturbation as,

$$\begin{aligned} W_{i \rightarrow j} &= \frac{2\pi}{\hbar^2} |\langle \phi_j | \hat{V}_{int}(t) | \phi_i \rangle|^2 \delta(\omega_{ij} \pm \omega_a) \\ &= \frac{\pi E_0^2}{2\hbar^2} \cos^2(\theta) |\langle \phi_j | \hat{\mu} | \phi_i \rangle|^2 \delta(\omega_{ij} \pm \omega_a) \end{aligned} \quad (2.23)$$

given that state $|\phi_i\rangle$ is sufficiently populated. The delta functions assure that only transitions occur at the transition frequency $\omega_{ij} = (E_i - E_j)/\hbar$. The \pm sign

in the delta function indicates that not only transitions from a low energy state to a high energy state can happen. The transition from a high energy state to a low energy state is allowed as well and is referred to as stimulated emission. Both transitions have the same probability. The excitation probability is proportional to $\cos^2(\theta)$, where θ is the angle between the polarization of the driving field and the dipole moment operator. This property is used in polarization resolved pump-probe experiments, where a linearly polarized light pulse excites a subset of oscillators that have their transition dipole moment preferentially aligned parallel to the polarization direction.

The transition rate in Eq. (2.23) is quadratically proportional to the transition dipole moment $\mu_{i,j}$,

$$\mu_{i,j} = \langle \phi_j | \hat{\mu} | \phi_i \rangle \quad (2.24)$$

In Eq. (2.22) the dipole moment operator $\hat{\mu}$ was defined in terms of an ordinary Cartesian coordinate system. In considering vibrational transitions, it makes more sense to define $\hat{\mu}$ in terms of the normal coordinates of vibrations Q_i . All molecules with N atoms have $3N - 6$ of such normal coordinates ($3N - 5$ in case the molecule is linear). Expanding $\hat{\mu}$ in all Q_i for small displacements from the equilibrium positions $Q_i = 0$ yields,

$$\hat{\mu} = \mu_0 + \sum_i \left(\frac{\partial \hat{\mu}}{\partial Q_i} \right)_0 Q_i + \frac{1}{2} \sum_i \sum_j \left(\frac{\partial^2 \hat{\mu}}{\partial Q_i \partial Q_j} \right)_0 Q_i Q_j + O(3) \quad (2.25)$$

where μ_0 is the dipole moment of the molecule in equilibrium position. For the water molecule, the normal modes correspond to the bending mode, symmetric OH stretch mode and asymmetric OH stretch mode. The transition dipole moment $\mu_{\nu_{OH}\nu'_{OH}}$ for transitions in the (symmetric) OH stretch coordinate is thus given by,

$$\begin{aligned} \mu_{\nu_{OH}\nu'_{OH}} = & \left(\frac{d\hat{\mu}}{dQ_{OH}} \right)_0 \langle \nu'_{OH} | Q_{OH} | \nu_{OH} \rangle + \\ & \frac{1}{2} \left(\frac{d^2\hat{\mu}}{dQ_{OH}^2} \right)_0 \langle \nu'_{OH} | Q_{OH}^2 | \nu_{OH} \rangle + O(3) \end{aligned} \quad (2.26)$$

where the expansion is around the equilibrium position $Q_{OH} = 0$ and ν_{OH} denotes the energy level of the mode. A vibrational transition thus requires a change of the dipole moment in the corresponding vibrational coordinate.

Two approximations are often made. First, the second and higher derivatives in Eq. (2.26) are assumed to be zero (no electrical anharmonicity), and secondly the wave functions $|\nu_{OH}\rangle$ are those of the harmonic oscillator (no mechanical anharmonicity, ie. no anharmonic potential). Under this double harmonic approximation, only transitions between adjacent states can occur, since all other matrix elements are zero,

$$\langle \nu'_{OH} | Q_{OH} | \nu_{OH} \rangle = \begin{cases} 1 & \text{if } \nu'_{OH} = \nu_{OH} \pm 1 \\ 0 & \text{if } \nu'_{OH} \neq \nu_{OH} \pm 1 \end{cases} \quad (2.27)$$

This means that transitions directly from the ground state $|\nu_{OH} = 0\rangle$ to an overtone state $|\nu_{OH} \geq 2\rangle$ are forbidden. The formation of a hydrogen-bond makes the OH stretch vibration in liquid water quite anharmonic. Lippincott and Schroeder developed a potential based on empirical data that describes the energy levels of the OH stretch vibration and is given by [14],

$$V_{LS}(r, R_{OO}) = D_{Ia} \left(1 - e^{-n_{Ia}(r-r_0)^2/2r}\right) + D_{Ib} \left(1 - e^{-n_{Ib}(R_{OO}-r-r_0)^2/2(R_{OO}-r)}\right) \quad (2.28)$$

where r is the oxygen-proton distance and R_{OO} is the oxygen-oxygen distance between the hydrogen-bonding water molecules. $D_{Ia} = 38750 \text{ cm}^{-1}$ is the binding energy of the OH covalent bond, $N_{Ia} = 9.8 \text{ \AA}^{-1}$ is the parameter defining the OH stretch vibrational frequency and $r_0 = 0.97 \text{ \AA}$ is the gas phase OH bond length. D_{Ib} and n_{Ib} are obtained from comparison of the model to empirical values [14]. The potential is shown in Fig. 2.2 for an oxygen-oxygen distance $R_{OO} = 2.81 \text{ \AA}$, which is the average distance in liquid water at room temperature. The wave functions were calculated using a Numerov integration scheme. From these wave functions, it can be shown that transitions with $\Delta\nu_{OH} > 1$ have a non-zero transition dipole moment and hence are allowed.

In addition, the mechanical anharmonicity leads to a difference in the transition frequencies ω_{01} and ω_{12} . This difference is fundamental to vibrational pump-probe spectroscopy, in which a vibrational mode is excited and the resulting absorption changes (transient absorption) are subsequently probed. The excitation leads to an induced absorption at ω_{12} , reduced absorption due to stimulated emission at ω_{01} and an equal reduced absorption at ω_{01} due to the depleted ground state. For the harmonic oscillator, the transition $\nu = 1 \rightarrow 2$ has twice the cross section as the $\nu = 0 \rightarrow 1$ transition. Since in addition all ω_{ij} are identical for $j = i \pm 1$ in the harmonic potential, the total absorption change is zero. The anharmonic potential leads to different ω_{01} and ω_{12} frequencies and therefore a non-zero transient absorption spectrum.

If the electrical harmonic approximation is also abandoned, higher orders in Eq. (2.26) can also contribute to the overtone transition dipole moment $\nu_{OH} = 0 \rightarrow 2$. In case the partial charges on the atoms of the molecule are independent on the distance, $\mu_{\nu_{OH}\nu'_{OH}}$ varies linearly with the extension of the covalent bond for small displacements in the Q_{OH} coordinate. If this is not the case, $d^2\hat{\mu}/dQ_{OH}^2$ is non-zero and the second term in Eq. (2.26) will have a contribution to $\mu_{0,2}$ given that the matrix element $\langle 2|Q_{OH}^2|0\rangle$ is not vanishing. This last condition is true for both the harmonic and the Lippincott-Schroeder potential.

Finally, in analogy to overtones, combination modes like the H₂O-bend/OH-stretch mode in water are only allowed if both oscillations are anharmonically coupled. In such a case, the second order cross term between the vibrational coordinates of both modes in Eq. (2.25) is not vanishing,

$$\frac{1}{2} \left(\frac{d^2\hat{\mu}}{dQ_{OH}dQ_{bend}} \right)_0 \langle \nu'_{OH}, \nu'_{bend} | Q_{OH} Q_{bend} | \nu_{OH}, \nu_{bend} \rangle \quad (2.29)$$

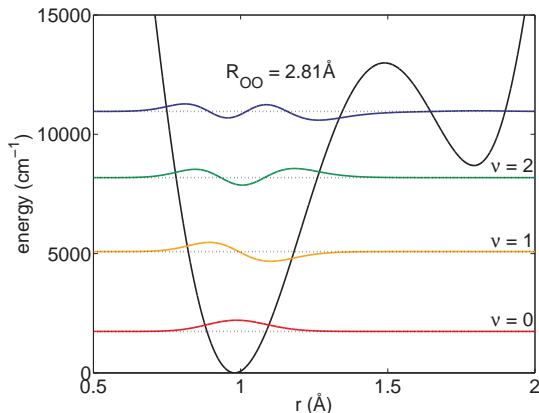


FIGURE 2.2. The Lippincott-Schroeder potential for an oxygen-oxygen distance of $R_{OO} = 2.81 \text{ \AA}$. The wave functions of the first four states were calculated using a Numerov integration scheme. Due to the anharmonicity of the potential, non-zero transition dipole moments exist between the ground state and the $|\nu_{OH} = 2\rangle$ overtone state.

2.2 LINE BROADENING AND SPECTRAL DIFFUSION

In section 2.1.1 we found that the absorption coefficient of a single, damped oscillator has a lorentzian dependence on frequency, the width of the lineshape being determined by the damping parameter γ . γ was found to be related to the vibrational lifetime of the oscillator. The vibrational lifetime of the OD stretch vibration of HDO molecules in water is 1.8 ps, implying a homogeneous linewidth of $\gamma \approx 6 \text{ cm}^{-1}$. Clearly, the linear absorption spectrum of the OD stretch vibration is much broader than that. A number of processes in water lead to additional line-broadening that results in the observed broad absorption spectrum. The line-broadening of a single oscillator is called homogeneous line-broadening. Inhomogeneous line-broadening occurs if the absorption spectrum of a collection of oscillators shows an broadening additional to the homogeneous linewidth.

The parameters of homogeneous broadening are difficult to obtain due to inhomogeneous broadening and spectral diffusion. Coupling of the vibrational modes of a single water molecule to the environment by hydrogen-bonds causes the resonance frequencies to be shifted. A stronger hydrogen-bond for example induces a larger red-shift on the OH stretch transition frequency ω_{01} . Water exists of an inhomogeneous mixture of oscillators that donate hydrogen-bonds of different strengths, resulting in a distribution of lorentzian lineshapes. This is referred to as inhomogeneous line broadening. Finally, the total cross section $\sigma_c(\omega_{01})$ of a single oscillator depends on its hydrogen-bond strength and thus on its resonance frequency ω_{01} . Such a dependence is called a Non-Condon effect [15].

In the following we set up a simple model to demonstrate the static effects

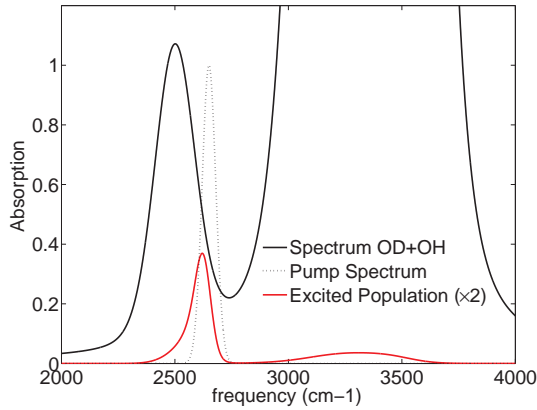


FIGURE 2.3. The results of the calculation of the number density of excited OH/OD oscillators (lower solid line) by a narrow-band excitation pulse (dotted line). The homogeneous linewidth was assumed to be 40 cm^{-1} . Although the excitation pulse is far off-resonant from the OH stretch absorption band, still a third of the excited oscillators are OH oscillators.

of an excitation of the inhomogeneously broadened OD stretch absorption band by a narrow-band pump pulse. To this end, we assume that the lineshape of a single oscillator with resonance frequency ω_{01} is lorentzian with a FWHM of 40 cm^{-1} and denote this by $L(\omega; \omega_{01})$. Let $G_{OD}(\omega)$ be the distribution function of OD oscillators, normalized such that,

$$\int d\omega G_{OD}(\omega) = 1 \quad (2.30)$$

The absorption spectrum $S_{OD}(\omega)$ is then given by the convolution of the homogeneous lineshape and the inhomogeneous broadening,

$$S_{OD}(\omega) = \int d\omega_{01} G_{OD}(\omega_{01}) \sigma_c(\omega_{01}) L(\omega; \omega_{01}) \quad (2.31)$$

The number density $n_{OD}(\omega)$ of excited OD oscillators with resonance frequency ω_{01} after excitation by a pump with spectral shape $P(\omega)$ is proportional to,

$$n_{OD}(\omega_{01}) = G_{OD}(\omega_{01}) \sigma_c(\omega_{01}) \int \omega P(\omega) L(\omega; \omega_{01}) \quad (2.32)$$

The spectrum of the excited oscillators finally reads,

$$S_e = \int d\omega_{01} n_{OD}(\omega_{01}) \sigma_c(\omega_{01}) L(\omega; \omega_{01}) \quad (2.33)$$

For simplicity we assume that the hydrogen-bond distributions of the OD stretch and OH stretch oscillators multiplied by the cross sections follow the

linear spectra of isotopically diluted OD in H₂O. Fig. 2.3 shows the evaluation of $n_{OD}(\omega)$ and $n_{OH}(\omega)$ under these conditions. Although the excitation spectrum was positioned far off resonance of the OH-stretch band, still one third of the excited oscillators are OH oscillators. This effect can be assigned to the far extending lorentzian shoulders of the homogeneous lineshapes. For similar reasons, the frequency maximum of the OD stretch oscillators is red-shifted compared to the excitation band. These results depend on the choice of the homogeneous linewidth: broader lines enhances these effects. If the linewidth is broader for red-absorbing (strongly hydrogen-bonded) oscillators, the relative number of excited OH oscillators will be still larger.

As a result of dynamic processes, the number density $n_{OD}(\omega)$ of excited oscillators will eventually be redistributed according to the static distribution function $G_{OD}(\omega)$. The time-evolution to this randomized state is called spectral diffusion and three molecular processes can be identified that contribute to this. First, librational motions can result in a very fast change of hydrogen-bond strength and thus ω_{01} on a timescale of 100 fs. Secondly, translational motions lead to a structural reorganization that has the same effect on a timescale of 1 ps. Finally, excitation energy may transfer in a resonant way from an excited oscillators to an accepting mode nearby in a process called Förster transfer. Since the accepting mode can have a slightly different resonance frequency, this process also leads to spectral diffusion. The timescale of this process in pure liquid water is 50 fs but becomes slower for isotopically diluted systems, since this process is strongly dependent on the distance between the donating and (resonant) accepting mode.

3

Experiment

3.1 MID-INFRARED PUMP PROBE

In this section we describe the femtosecond infrared pump-probe (fs-IR) setups that were used to obtain many results described in this thesis. As elaborated on in chapter 4 the concept of the technique is to excite a vibrational mode with an intense laser pulse, the pump, after which the induced absorption changes are monitored by a weaker probe pulse as a function of the delay time between the two pulses. From the analysis of the absorption changes information is obtained on the vibrational lifetime of the excitation, energy transfer and molecular re-orientation.

3.1.1 ONE COLOR PUMP-PROBE SETUP

In a one color pump-probe experiment the pulses have the same spectral shapes. The laser system used in these experiments is a regenerative Ti:Sapphire laser (Hurricane, Spectra-Physics) that generates 800 nm pulses with a duration of 110 fs and energy of 0.9 mJ at a repetition rate of 1 kHz. Using a beamsplitter, the output is split into two portions of 70% and 30% of the total energy. The first part is used to pump a white-light seeded commercial Optical Parametric Amplifier (OPA, Spectra-Physics) based on a β -bariumborate (BBO) crystal. The angle of the BBO crystal is tuned to generate light at $\sim 1.3 \mu\text{m}$ (signal) and $\sim 2 \mu\text{m}$ (idler). The idler is frequency doubled in a second BBO crystal to a wavelength of $\sim 1 \mu\text{m}$. This 1 μm pulse is used as a seed in a parametric amplification process (difference frequency mixing, DFG) in a potassium niobate crystal (KNB) crystal that is pumped with the remaining 30% portion of the 800 nm beam. In the DFG process, mid-IR pulses are generated with a full-width-half-maximum (FWHM) of 100 cm^{-1} that are *s*-polarized. The central wavelength can be tuned between 2300 cm^{-1} and 2700 cm^{-1} by varying the angles of the crystals. The pulses have a duration of 150 femtoseconds an energy of 5-9 μJ depending on the frequency.

The $\sim 2500 \text{ cm}^{-1}$ pulses are sent onto a wedged CaF_2 plate. The transmitted part ($\sim 90 \%$) serves as the pump pulse. The reflection from the front side is sent into a variable delay stage with a time-resolution of 6.6 fs. This fraction

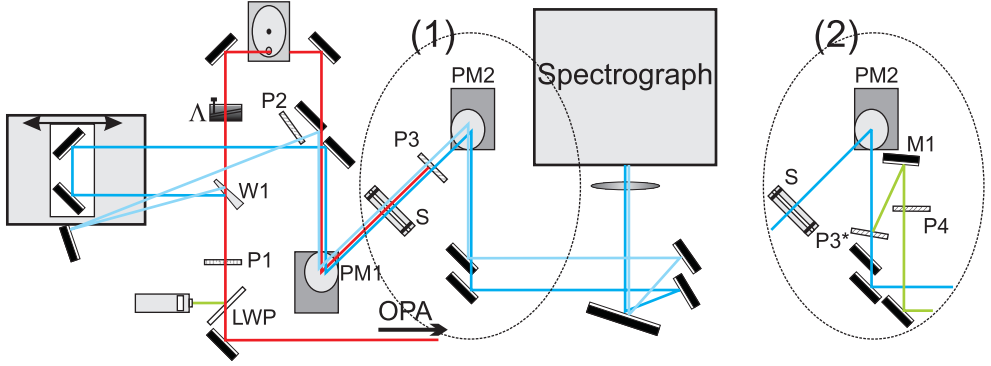


FIGURE 3.1. Detection scheme of the one-color pump-probe setup. After the long wave pass filter to remove any residual signal and idler (LWP), the polarization of the mid-IR light from the Spectra-Physics OPA is first cleaned-up by a polarizer (P1). The CaF_2 wedge (W1) splits the beam in a pump (transmitted), probe (front reflection) and reference pulse (back reflection). The polarization of the pump light is rotated by 45° using a tilting half-wave plate (Λ), after which every second pump pulse is blocked by a chopper. The polarization of the reference pulse is cleaned-up by polarizer P2. All pulses are focussed on the sample S by the 45° parabolic mirror PM1. After this point two detection schemes were used. (1) The polarization components of the probe light parallel and perpendicular to the pump polarization are selected by rotating polarizer P3, after which the probe and reference beams are recollimated on PM2 and guided into the detector. (2) An alternative detection method collects the reflection of a polarizer P3, which is now placed after the recollimating parabolic mirror PM2. The polarization of the reflected beam is cleaned-up by polarizer P4, after which all beams are guided into the detector. The reference beam has in this case been omitted for clarity.

forms the probe. With the delay stage we vary the time delay t between pump and probe. The reflection from the back side of the wedged CaF_2 plate serves as a reference pulse. The pump is transmitted through a $\lambda/2$ plate to rotate its polarization at 45 degrees with respect to that of the probe. The pump, probe and reference are all focussed in the sample using a gold-coated parabolic mirror, but only the pump and the probe are in spatial overlap. After the sample, a mechanically rotated polarizer selects either the polarization component of the probe pulse parallel or perpendicular to the pump polarization. After recollimation of the beams with a second parabolic mirror, the probe and the reference are dispersed with an Oriel monochromator and detected on two separate lines of an Infrared Associates 3×32 mercury-cadmium-telluride (MCT) detector array. The measurement of the reference thus allows for a frequency-resolved correction for shot-to-shot fluctuations of the probe-pulse energy.

The MCT detector has a third array that allows for a different detection scheme that is used in some of the experiments. This detection scheme is identical to that described above till after the sample. Instead of first selecting the parallel or perpendicular component with the rotating polarizer, the probe

and reference are first recollimated with the parabolic mirror. Subsequently, the probe and reference are transmitted through a static polarizer that is positioned such that the vector normal to its surface is under a small angle with the direction of incident probe beam. The polarizer is aligned such that the transmitted probe light is the polarization component that, at the sample position, is perpendicular to the pump polarization. The reflected light thus yields the parallel component. A small fraction of the perpendicular component is reflected as well and an additional polarizer is placed to clean up the polarization of the reflected beam. Both polarization components are detected simultaneously on different array lines of the MCT detector, thereby reducing the measurement time by half. In addition, synchronous measurement of both polarization components improves the signal-to-noise ratio.

3.1.2 TWO COLOR PUMP-PROBE SETUP

In a two color pump-probe experiment the pulses are generated in two separate infrared generation stages, thereby enabling for different pulse spectra of both pulses. The infrared pulses used for this experiment were generated using the output of a regenerative Ti:Sapphire laser (Coherent), providing pulses at 800 nm with a duration of 35 fs and a pulse energy of 3.5 mJ at a repetition rate of 1 kHz. The output of the laser is split in three portions of interest: (1) 850 μJ to pump a homebuilt optical parametric amplifier (OPA) to generate the probe light, (2) 850 μJ to pump a TOPAS (LightConversion) and (3) 1.3 mJ to pump a difference frequency mixing stage after the TOPAS to generate mid-IR pulses that are used as pump (Fig. 3.2).

The pump pulses are generated by pumping a TOPAS (LightConversion) based on super-fluorescence. The TOPAS down-converts the pulses in a BBO crystal to signal (*p*-polarized) and idler (*s*-polarized) pulses in the range of ~ 1600 nm till ~ 2400 nm with a total energy of 280 μJ . In most experiments the idler pulses are doubled in a 1 mm BBO crystal to create $\sim 1 \mu\text{m}$ pulses, which are finally difference frequency mixed with the 1.3 mJ portion of 800 nm light out of the Ti-Sapphire laser. This last conversion step yields light pulses with a central frequency tunable between 2900 cm^{-1} and 3600 cm^{-1} (using KTP as DFG crystal) or between 2300 cm^{-1} and 2800 cm^{-1} (using LiNbO_3 as DFG crystal). The spectral bandwidth is 150 cm^{-1} and pulse energy 50 μJ . The cross-correlate between the pump and probe pulses as obtained in a thin germanium window is 150 fs, mainly determined by the pump pulse duration.

To generate the narrow band pump light the idler out of the TOPAS was upconverted to 1000 nm using a relatively long BBO crystal of 4mm. The acceptance bandwidth of the crystal is thereby used to make the pulse spectrally more narrow. In a third step the doubled idler was difference frequency mixed in a Lithium Niobate (LN) crystal with 1 mJ pulses of 800 nm to generate mid infrared pulses. The LN crystal we used had a thickness of 10 mm to narrow the spectral bandwidth even further. The light pulses that we eventually obtained had a pulse energy of 16 μJ and a spectral bandwidth of 50 cm^{-1} full width half maximum (FWHM).

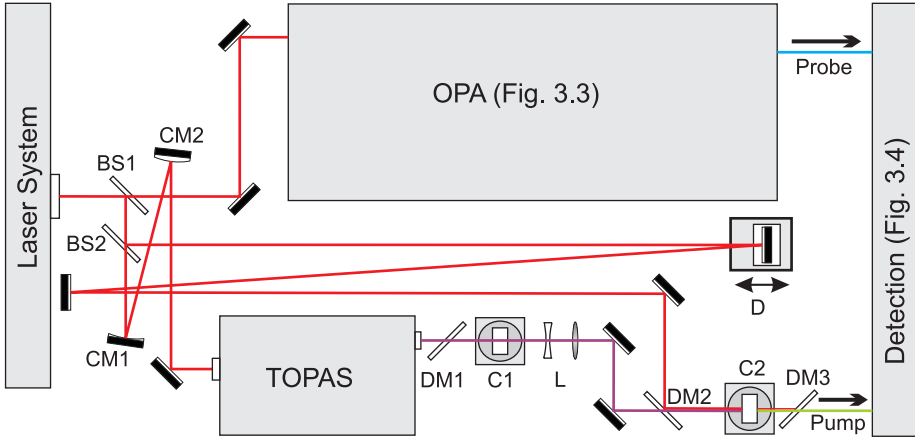


FIGURE 3.2. Overview of the two-color setup. With beamsplitters BS1 and BS2, the output of the Ti:Sapphire laser is split into three portions. The beam size of one portion is decreased by the mirror telescope CM1-CM2 and used as a pump in a LightConversion TOPAS to generate signal and idler pulses. The signal pulses are removed by a dichroic mirror (DM1), after which the idler is frequency-doubled in a BBO crystal (C1). The beam size of the doubled idler is blown up by a factor of two in telescope L. The doubled idler and another portion of the 800 nm light are spatially overlapped in a second crystal (C2), the nature of which depends on the desired frequency (see text). Temporal overlap is tuned with delay stage D. Dichroic mirror DM3 removes any residual 800 nm and doubled idler.

The homebuilt OPA (Fig. 3.3) is built according to the geometry developed by the group of Peter Hamm. The OPA is white-light seeded and generates a signal and idler pulse in a parametric amplification process in a BBO crystal (2 mm), very much like the commercial OPA discussed in the previous subsection. The signal and idler are difference frequency mixed in a silver-gallium-disulfide crystal (1.2 mm), yielding mid-IR pulses of which the wavelength can be tuned between $8\ \mu\text{m}$ and $2.5\ \mu\text{m}$. At $4\ \mu\text{m}$ wavelength, the pulse energy is $5\ \mu\text{J}$, the FWHM of the pulse spectra is $300\ \text{cm}^{-1}$. The generated pulses are *s*-polarized.

The detection scheme is shown in Fig. 3.4 and is very similar to what was described for the one color setup. Instead of CaF_2 we used a ZnSe wedge to split off larger portions of the output of the homebuilt OPA as the probe and reference light. The light transmitted through the wedge is dumped on a beamblock. Close to the sample the polarizations of both the probe and the reference are cleaned using two polarizers. In this setup the third array of the MCT detector is used to detect (a small fraction of) the pump light. During actual measurements this beam path is blocked by a mechanical switch to avoid pump scatter on the probe and reference arrays.

In some experiments we directly used either the signal or the idler pulses directly out of the TOPAS or homebuilt OPA as the pump or probe (chapter 5). A neutral density filter was used to attenuate the pulse energy in case this was

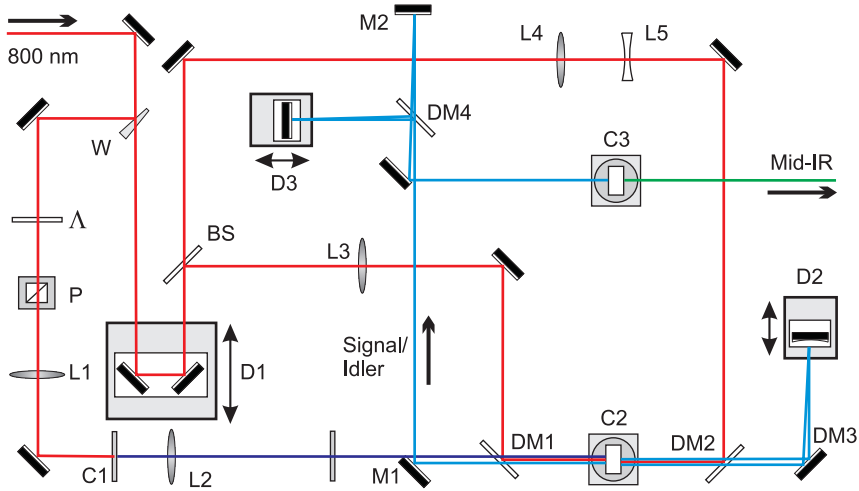


FIGURE 3.3. The homebuilt OPA, used in the two-color pump-probe setup, is pumped with 800 nm pulses of $850 \mu\text{J}$. First, a few percent of the 800 nm light is reflected from the front side of a CaF_2 wedge (W). A combination of a half-lambda plate (Λ) and a polarizer-cube (P) is used to obtain p -polarized light of tunable intensity, which is focussed by lens L1 on a sapphire plate (C1) to generate white light. The white light is refocussed (L2) on a BBO crystal (C2). A second fraction ($\sim 10\%$) of the 800 nm light is split of by a beamsplitter (BS) and focussed by lens L3 on the BBO crystal to spatially overlap with the white light. Temporal overlap is tuned by delay D1. The generated signal pulses are isolated by dichroic mirror DM3 and recollimated by a concave mirror on delay D2. D2 is tuned such that the pulses are in temporal overlap with the remaining part of the 800 nm light in the BBO crystal C2 for a second amplification step. The residual 800 nm light after amplification is removed by dichroic mirror DM1 after which the signal and idler enter the DFG stage. A combination of a dichroic mirror (DM4) and a delay stage (D3) to adjust the path length of the idler pulses is used to have the signal and idler overlapped both in space and time on a silver gallium disulfide crystal (C3) to generate the mid-IR pulses.

needed. Since the energy of photons of the signal is larger than the bandgap in germanium, we used silicium to determine the cross correlate between the pulses. We found in this case the cross correlate between the two signal pulses to be 100 fs.

3.2 FORMALISM OF POLARIZATION RESOLVED EXPERIMENTS

All infrared experiments in this thesis are polarization resolved. The characterization of the polarization of a light pulse in the experiment is less trivial than measuring the power, but extremely important. A small irregularity may lead to artefacts that are difficult to correct for. In this section we set up a machin-

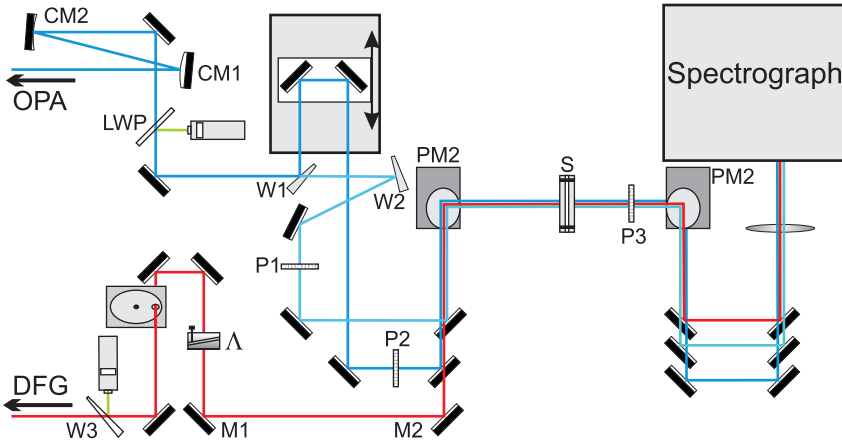


FIGURE 3.4. Detection scheme of the two-color pump-probe setup. The light from the (homebuilt) OPA is used for the probe and the reference pulses. The beamsize is first increased by a factor of 2.5 by the telescope CM1 and CM2. The long wave pass filter LWP filters out the signal and idler light and transmits the mid-IR. The LWP is also used to overlap a green laser pointer with the mid-IR for alignment. W1 is a ZnSe wedge that reflects 10% of the light into the delay stage to use as the probe. From the transmitted light a second portion of 10% is reflected by a similar wedge (W2) to use as the reference. The polarization of both beams is cleaned up by polarizers P1 and P2. The pump light is generated in the DFG stage (see text). A dielectric-coated wedge (W3) removes the remaining signal and idler from the beam and reflects a laser pointer with the mid-IR for alignment. Every second pump pulse is blocked by a chopper, and the polarization is tuned by a tilting half-wave plate (Λ , see text). Pump, probe and reference are focussed on the sample S by a parabolic mirror PM1. After the sample, different polarization components of the probe are selected by a mechanically rotated polarizer P3. The beams are recollimated by parabolic mirror PM2, after which the light is steered into the spectrograph. Finally, the light is detected with a liquid nitrogen cooled three line MCT array detector.

ery to carefully determine the effects of different optics on the light polarization and eventually our observables. To do this we use the Jones formalism of polarization [16]. In this formalism the polarization of light is represented as a vector that spans both the phase and field amplitude in a plane orthogonal with respect to the direction of light propagation. Convenient for most purposes is the frame in which the first element represents the component in the horizontal plane in the lab frame and the second element represents the component in the vertical plane. A light wave with frequency ω and wavenumber k traveling in the z -direction can thus be written as,

$$\vec{E}(\vec{x}, t) = \begin{pmatrix} E_{0,x} e^{i\phi_x} \\ E_{0,y} e^{i\phi_y} \end{pmatrix} e^{i(kz - \omega t)} \quad (3.1)$$

where the x -axis is the horizontal axis and the y -axis is the vertical axis perpendicular to the light beam. $E_{0,i}$ and ϕ_i denote the i -component of the field

amplitude and relative phase, respectively. The vector of Eq. (3.1) is called the Jones vector and can be regarded as the polarization state of the light. In Dirac notation such a state is written as,

$$\begin{pmatrix} E_{0,x}e^{i\phi_x} \\ E_{0,y}e^{i\phi_y} \end{pmatrix} = |\Phi\rangle \quad (3.2)$$

The vector space that the polarization state belongs to has two normalized eigenvectors. A logical choice is the p -polarization direction and the s -polarization direction,

$$|P\rangle = \begin{pmatrix} 1 \\ 0 \end{pmatrix}, \quad |S\rangle = \begin{pmatrix} 0 \\ 1 \end{pmatrix} \quad (3.3)$$

Since in our experiment nearly all reflections and refractions are in the horizontal plane, however, this choice coincides with the horizontal and vertical states. The polarization state of a p -polarized light wave can thus be written as,

$$|\Phi\rangle = E_{0,x} |H\rangle \quad (3.4)$$

Here the convention is used that the arbitrary phase ϕ_x of an initial state is set to zero. The intensity follows from taking the inner product between the bra and the ket, which for a general polarization state $|\Phi\rangle$ yields,

$$I(\omega) = \frac{1}{2}c\varepsilon_0 \langle \Phi | \Phi \rangle = \frac{1}{2}c\varepsilon_0 (E_{0,x}^2 + E_{0,y}^2) \quad (3.5)$$

Every optical element that interacts with this light can now be represented by a matrix operator, which will be denoted by a boldface capital. Optical elements may introduce mixing of polarization components, phase shifts and absorptions. In the remainder of this section it is assumed that all optical elements are perfect, in the sense that they do not lead to additional losses. An example of an optical element is the polarizer \mathbf{P} , which may be positioned to transmit light in the p -polarization or s -polarization direction and is represented by,

$$\mathbf{P}_p = \begin{pmatrix} 1 & 0 \\ 0 & 0 \end{pmatrix} \quad \mathbf{P}_s = \begin{pmatrix} 0 & 0 \\ 0 & 1 \end{pmatrix} \quad (3.6)$$

Polarizers are found in the detection scheme of the two-color setup in positions P1, P2 and P3 (Fig. 3.4). It is trivial to show that \mathbf{P}_s acting on the state denoted in Eq. (3.4) yields zero, while \mathbf{P}_p fully preserves the state. For the less trivial case of a polarizer under an angle ϕ with the horizontal plane of the experiment, it is most convenient to rotate the coordinate frame of the polarization state such that the trivial operators \mathbf{P} from Eq. (3.6) can be used. Let $|\Phi_f\rangle$ be the final state, then this operation can be written as,

$$|\Phi_f\rangle = \mathbf{R}(-\phi)\mathbf{P}_p\mathbf{R}(\phi)|\Phi\rangle \quad (3.7)$$

where $\mathbf{R}(\phi)$ is the matrix of rotation under an angle ϕ in a cartesian coordinate system,

$$\mathbf{R}(\phi) = \begin{pmatrix} \cos(\phi) & \sin(\phi) \\ -\sin(\phi) & \cos(\phi) \end{pmatrix} \quad (3.8)$$

The last operator $\mathbf{R}(-\phi)$ in Eq. (3.7) is needed to rotate the state back to the labframe. Thanks to the off-diagonal elements in the operator sequence in Eq. (3.7), a mixing will occur between the components of the initial polarization state. This is of course well known: a light wave transmitted through a polarizer that is under $\phi = 45^\circ$ with the initial polarization of the light will obtain a polarization component in the perpendicular direction of initial polarization. Polarizer P3 in Fig. 3.4 rotates mechanically under an angle of $\phi = \pm 45^\circ$ to select different polarization components of the transmitted probe light.

Another optical element of interest is the phase retarder (Λ in Fig. 3.4). This element consists of a birefringent material that introduces different phase delays in different polarization directions. The Jones-operator $\mathbf{\Lambda}$ belonging to this element is given by,

$$\mathbf{\Lambda} = \begin{pmatrix} e^{i\phi_x} & 0 \\ 0 & e^{i\phi_y} \end{pmatrix} \quad (3.9)$$

If $\mathbf{\Lambda}$ acts on a real Jones vector, polarization dependent phase-shifts are introduced. For $\phi_x \neq \phi_y + n\pi$ ($n=1,2,3\dots$), this corresponds to an elliptical polarization of the light. In our setup we use a special case of the phase retarder, the half-wave plate. This element introduces a phase difference $\phi_x - \phi_y = \pm\pi$. Since the initial phase ϕ_x is arbitrary, we can choose it such that $\mathbf{\Lambda}$ becomes a real valued matrix that only flips the sign of $E_{0,y}$. This does not change a polarization state that was initially p -polarized. However, the half-wave plate can be rotated around the axis along the light beam. This action is achieved in the Jones formalism by a rotation of the polarization state equivalent to Eq. (3.7). The half-wave plate thus rotates the polarization of the light while preserving its complex phases: A linearly polarized light wave remains linearly polarized after transmission.

The half-wave plate used in our experiments has an extra degree of freedom: Tilting the optical axis of the birefringent material. This has the advantage that the phase velocities (and hence the phase delays) can be tuned according to the wavelength of the light. Without this degree of freedom the half-wave plate would be specified only for one fixed wavelength. There is another advantage, though. By tilting the half-wave plate, the phase delays can be tuned such that $\phi_x - \phi_y$ is no longer equal to $\pm\pi$ with as a result an ellipticity of the polarization after transmission. As we will demonstrate below this is important for polarization resolved experiments.

At this point it should be noted that the light pulses used in our experiment have a finite bandwidth and thus consists of a distribution of frequencies. The birefringent material of half-wave plate introduces different phase delays for different frequencies in the pulse spectrum. A rigorous treatment would

therefore utilize a vector of polarization states that allows every frequency component to have its own phase and amplitude components. Let us to this end consider a light pulse in the frequency domain with a certain spectral shape, for which $E_{0,x}(\omega)$ and $E_{0,y}(\omega)$ are the spectral envelopes of the pulse in the x and y polarization directions, respectively,

$$\vec{E}(\vec{x}, t) = \begin{pmatrix} E_{0,x}(\omega)e^{i\phi_x(\omega)} \\ E_{0,y}(\omega)e^{i\phi_y(\omega)} \end{pmatrix} e^{i(k(\omega)z - \omega t)} \quad (3.10)$$

The initial polarization state of such a pulse can thus be written in the previously defined basis as,

$$|\Phi(\omega)\rangle = E_{0,x}(\omega) |P\rangle + E_{0,y}(\omega)e^{i(\phi_y(\omega) - \phi_x(\omega))} |S\rangle \quad (3.11)$$

The third optical element we discuss here is the mirror. As we will show below, the reflection by a mirror has a non-trivial effect on the polarization of light in case its initial polarization state is not purely $|P\rangle$ or $|S\rangle$. In our experiment we mainly use gold mirrors. Reflection by a metallic surface is expressed in the Fresnel factors r_p and r_s , which are given in terms of the angle of incidence θ_i by [16],

$$r_p(\nu, \theta_i) = \frac{\sqrt{n^2(\nu) - \sin^2(\theta_i)} - n^2(\nu) \cos(\theta_i)}{\sqrt{n^2(\nu) - \sin^2(\theta_i)} + n^2(\nu) \cos(\theta_i)} \quad (3.12)$$

$$r_s(\nu, \theta_i) = \frac{\cos(\theta_i) - \sqrt{n^2(\nu) - \sin^2(\theta_i)}}{\cos(\theta_i) + \sqrt{n^2(\nu) - \sin^2(\theta_i)}} \quad (3.13)$$

where $n(\nu)$ is the complex index of refraction. With these Fresnel factors, the Jones operator for reflection \mathbf{M} is then given by the matrix,

$$\mathbf{M}(\nu, \theta_i) = \begin{pmatrix} -r_p(\nu, \theta_i) & 0 \\ 0 & r_s(\nu, \theta_i) \end{pmatrix} \quad (3.14)$$

Using the index of refraction of gold, the reflection under $\theta_i = 45^\circ$ on a gold mirror of light with a frequency of $\nu = 2500 \text{ cm}^{-1}$ yields,

$$\mathbf{M} = \begin{pmatrix} 0.95 + 0.22i & 0 \\ 0 & 0.98 + 0.11i \end{pmatrix} \quad (3.15)$$

An initial Jones vector with equal phase and amplitude for both polarization directions will acquire a phase difference between the two polarization components after reflection. This is analogue to saying that a light pulse, initially linearly polarized under an angle of 45° with the horizontal lab frame) acquires an ellipticity in its polarization. In our setup this occurs on mirrors M1, M2 and PM1 after the pump polarization was rotated using the half-wave plate

\mathbf{A} (Fig. 3.4). For the half-wave plate we found that for certain angles of the optical element we introduce an ellipticity in the transmitted light. In practice this ellipticity is tuned such that it compensates for phase delays acquired by the subsequent reflections. Using Eq. (3.15) it can easily be shown that for $4\ \mu\text{m}$ light the required polarization state immediately after the half-wave plate must be,

$$|\Phi\rangle = E_0 \begin{pmatrix} 0.51 \\ 0.49 \cdot e^{0.35i} \end{pmatrix} \quad (3.16)$$

in order to pre-compensate for the subsequent reflections on the gold mirrors. At the sample position \mathbf{S} , the pump light will then be linearly polarized again, under 45° with the horizontal plane. Since the refractive index is dependent on the wavelength of the incident light, so is \mathbf{M} . Different frequency components of a light pulse with a finite bandwidth thus obtain (very small) different polarization ellipticities after reflection.

We will now translate a polarization resolved pump-probe experiment to the formalism described above. To this end we assume a certain response in the sample and investigate how the *measured* response depends on the (mis)alignment of certain optical components. In absence of a preceding pump pulse, the probe light will be partially absorbed by the sample,

$$\mathbf{S}_0(\omega) = e^{-\frac{1}{2}\alpha(\omega)} \begin{pmatrix} 1 & 0 \\ 0 & 1 \end{pmatrix} \quad (3.17)$$

where $\alpha(\omega)$ is the absorption in the sample. The factor $\frac{1}{2}$ in the exponent arises from the fact that \mathbf{S}_0 is an operator acting on the polarization state, which will be squared to obtain the intensity.

An intense pump pulse excites modes in the sample that lead to absorption changes $\Delta\alpha(\omega, t)$ that depend on the polarization direction and the waiting time after the excitation. Following the notation of chapter 4, we can write the absorption of the probe light after excitation by a pump pulse that is s -polarized as follows,

$$\mathbf{S}(\omega, t) = e^{-\frac{1}{2}\alpha(\omega)} \begin{pmatrix} e^{-\frac{1}{2}\Delta\alpha_\perp(\omega, t)} & 0 \\ 0 & e^{-\frac{1}{2}\Delta\alpha_\parallel(\omega, t)} \end{pmatrix} \quad (3.18)$$

where the anisotropy $R(\omega, t)$ leads to different absorption changes in the directions orthogonal and parallel to the pump polarization according to,

$$\Delta\alpha_\parallel(\omega, t) = (1 + 2R(\omega, t))\Delta\alpha(\omega, t) \quad (3.19)$$

$$\Delta\alpha_\perp(\omega, t) = (1 - R(\omega, t))\Delta\alpha(\omega, t) \quad (3.20)$$

A nonzero anisotropy thus rotates the polarization state of the transmitted probe.

The equation for $\mathbf{S}(\omega, t)$ above assumes that the angle between the propagation vector of the pump pulse and the z -axis equals zero degrees. In reality, this is experimentally not possible and the angle is rather on the order of $\delta = 10^\circ$ (see Fig. 3.5). To take this angle into account, we have to perform an additional

rotation of the probe frame in the y - z plane. So far, we did not consider the z -coordinate, as this is the propagation direction of the probe light. However, the inclination of the pump beam results in a mixing of the response in the z and y direction according to,

$$\mathbf{S}(\omega, t) = e^{-\frac{1}{2}\alpha(\omega)} \begin{pmatrix} e^{-\frac{1}{2}\Delta\alpha_{\perp}(\omega, t)} & 0 \\ 0 & e^{-\frac{1}{2}(\cos^2(\delta)\Delta\alpha_{\parallel}(\omega, t) + \sin^2(\delta)\Delta\alpha_{\perp}(\omega, t))} \end{pmatrix} \quad (3.21)$$

This expression follows from the fact that the absorption changes in the two directions orthogonal to the pump polarization are identical. In our experiment, the pump is typically not s -polarized but rather has its polarization at an angle of 45° with the vertical plane. In analogy to the treatment of the polarizer operator (Eq. (3.7)), this is achieved by sandwiching $\mathbf{S}(\omega, t)$ between rotation operators.

The pump-probe experiment now yields an incoming p -polarized probe pulse $|\Phi_p(\omega)\rangle$ that either is, or is not, preceded by a pump pulse with a polarization under $\theta_p = 45^\circ$ with the vertical plane. After the sample, a mechanically rotating polarizer \mathbf{P} rotates over an angle $\phi = \pm 45^\circ$ with respect to the probe polarization to select either the polarization component of the probe light parallel or perpendicular to the initial polarization of the pump (see Fig. 3.5). The final polarization states with preceding pump can thus be written as,

$$|\Phi_{f\pm}(\omega, t)\rangle = \mathbf{R}(\mp\phi)\mathbf{P}_p\mathbf{R}(\pm\phi)\mathbf{R}(-\theta_p)\mathbf{S}(\omega, t)\mathbf{R}(\theta_p)|\Phi_p(\omega)\rangle \quad (3.22)$$

where the upper signs refer to the parallel polarization component and the lower signs to the perpendicular polarization component of the probe. The final polarization states without preceding pump $|\Phi_{f\pm}^0(\omega)\rangle$ are obtained by replacing $\mathbf{S}(\omega, t)$ by $\mathbf{S}_0(\omega)$. After the rotating polarizer only the intensity of the light is of interest and further optics can thus be ignored. The detected pump-probe signal of Eq. (4.1) is a function of the intensities measured on the detector and can be expressed in terms of the polarization states as,

$$\Delta\alpha_{\parallel/\perp}(\omega, t) = -\ln \frac{\langle \Phi_{f\pm}(\omega, t) | \Phi_{f\pm}(\omega, t) \rangle}{\langle \Phi_{f\pm}^0(\omega) | \Phi_{f\pm}^0(\omega) \rangle} \quad (3.23)$$

We now assume a frequency independent anisotropy of the form $R(\omega, t) = 0.4e^{-0.4t}$. The probe spectrum is assumed to have properties similar to the specifications of the one color setup described in section 3.1.1 of this chapter. If Eq. (3.23) is evaluated with these input parameters we can obtain the detected anisotropy using Eq. (4.3). Clearly, in case $\theta_p = 45^\circ$, $\phi = \pm 45^\circ$ and $\delta = 0^\circ$ we reobtain the same dynamics $R(\omega, t)$ as the actual response that was put in. If θ_p , ϕ and δ assume different values, the detected anisotropy will be different. Firstly, we show a number of anisotropy curves for different values of ϕ in Fig. 3.6A. Such a situation occurs when the rotating polarizer is not well aligned. For increasing deviations of ϕ from $\pm 45^\circ$ (for every lower curve δ is 2° smaller), the anisotropy starts at a lower value. A simple rescaling does not

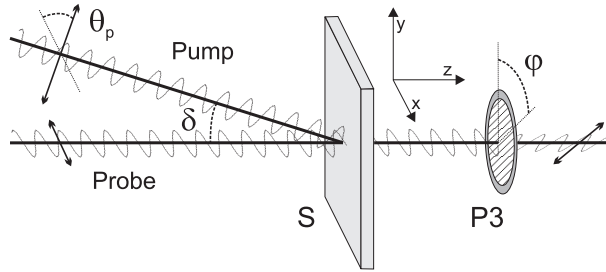


FIGURE 3.5. Pump and probe polarization and beam angles at the sample position. The p -polarized probe has its electric field oscillations in the horizontal (x - z) plane in the lab frame and propagates in the z -direction. The propagation direction of the pump makes an angle δ with the propagation direction of the probe in the vertical (y - z) plane. The polarization direction of the pump makes an angle of $\theta_p = 45^\circ$ with the polarization direction of the probe. After the sample S, a mechanically rotating polarizer (P3) selects different polarization components of the probe light by rotating over an angle $\phi = \pm 45^\circ$ with the probe polarization direction.

yield the same result, since the dynamics are also different. A second example is given in Fig. 3.6B. Here we varied the inclination angle δ between the pump and the probe in steps of 10° . It should be noted that an inclination of 10° does not yet alter the detected anisotropy strongly: the initial anisotropy at $t = 0$ is $< 2\%$ smaller than 0.4. Finally, the detected anisotropy decays calculated for different angles between the pump and probe polarization are shown in Fig. 3.6C (variation of θ_p in steps of 2°). These results are quite similar to the first example, although the deviation between the curves resulting from different angles is not persistent for longer delay times.

We also evaluated the detected anisotropy in case the rotating polarizer P3 is not positioned between the sample S and the second parabolic mirror PM2 but rather after PM2 (see Fig. 3.4). Before the polarization components are selected by the polarizer, one more reflection by a parabolic mirror occurs and Eq. (3.22) is thus to be extended with an additional reflection operator $\mathbf{M}(\omega, \theta)$. As we have seen, reflections by gold mirrors induce different phase shifts for different polarization directions and we thus may wonder how strongly the repositioning of the rotating polarizer affects the detected anisotropy. We found that indeed a very small decrease of $R(\omega, t)$ is present for increasing frequencies in case the probe pulse contains a spatial chirp. This frequency dependence is less than a percent of the initial amplitude of the anisotropy per 100 cm^{-1} and flips sign in case the polarization of the probe is changed from p to s .

3.3 DIELECTRIC RELAXATION SPECTROSCOPY

The purpose of dielectric relaxation spectroscopy (DRS) is to measure (a part of) the complex permittivity spectrum of a sample, mostly in the sub-THz frequency regime. The permittivity of a dielectric medium is a measure of how

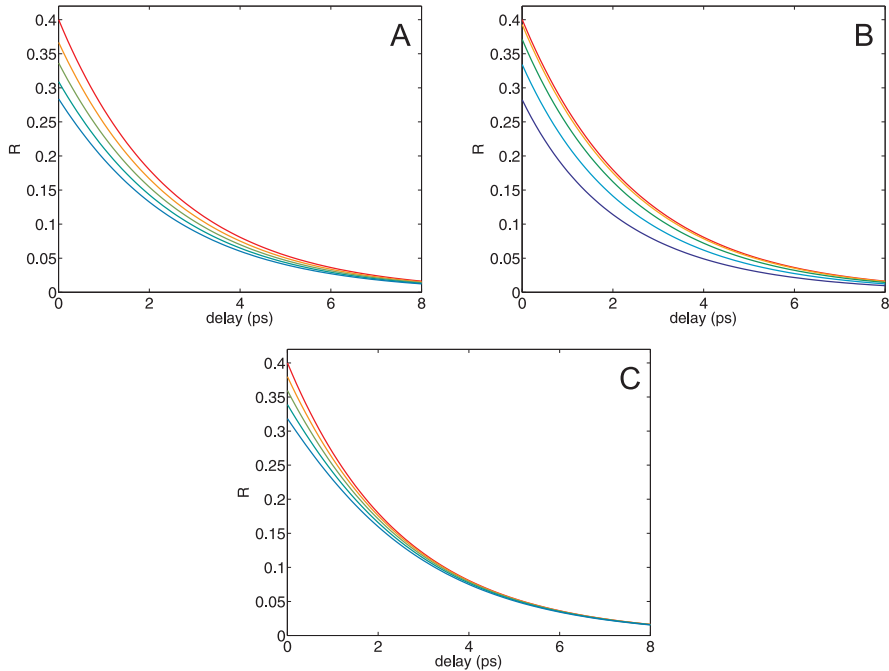


FIGURE 3.6. Calculated anisotropy decays as would be measured for identical sample responses (red lines) but suboptimal setup parameters due to misalignment. **(A)** The angle of rotation ϕ of the rotating polarizer (P3 in Fig. 3.4) is smaller than $\pm 45^\circ$ by steps of 2° . **(B)** The inclination angle δ between the pump and the probe is nonzero, by steps of 10° . **(C)** The angle θ_p between the pump and probe polarization is smaller than 45° by steps of 2° .

strongly the medium polarizes upon the application of an external field. The permittivity spectrum of a dipolar solution therefore provides information on the reorientation of dipoles in the solution. At lower frequencies, electromagnetic waves are not easily confined anymore in a collimated beam propagation. We use two types of setups: (1) a far field setup that makes use of freely propagating laser pulses in the THz regime and (2) a near-field setup that measures the reflection of electromagnetic waves in the GHz regime in a waveguide.

3.3.1 THZ SPECTROSCOPY

In THz dielectric relaxation spectroscopy the permittivity spectrum is probed by characterizing a THz pulse after transmission through the sample. The far-infrared THz pulse is generated by optical rectification in a ZnTe crystal pumped by (a part of) the output of a Ti:Sapphire pulsed laser (800 nm, ~ 110 fs, $\sim 75 \mu\text{J}$). The resulting pulse typically comprises a single cycle of the electric field and has a duration of ~ 1 ps. Fourier transformation of the pulse yields a frequency spectrum between 0.4 and 1.2 THz. The pulse shape cannot be

detected directly. Instead, we make use of the optical Kerr effect in a second ZnTe crystal. The strong electric field of the THz pulse causes a change in refractive index in the crystal, of which the magnitude and sign depends on the field intensity and direction, respectively. An 800 nm laser pulse is spatially overlapped with the THz pulse in the crystal with varying delay time between the pulses. Depending on which part of the single cycle THz pulse is in temporal overlap with the 800 nm pulse, a different change in polarization is induced on the 800 nm pulse by the change in refractive index. After the crystal the polarization components are split using a quarter wave plate and a polarizing beamsplitter. The polarization changes are monitored as a function of pulse delay by a differential detector. Measurements of an empty cuvette and without any cuvette are done to subtract their contribution to the signal. The complex index of refraction $\hat{n}(\nu)$ is obtained from the change in amplitude (due to absorption $\kappa(\nu)$) and delay (due to refraction $n(\nu)$) of the THz pulse upon propagation through the sample [17],

$$\hat{n}(\nu) = n(\nu) - i\kappa(\nu) \quad (3.24)$$

From the complex index of refraction the permittivity spectrum is obtained by,

$$\hat{\epsilon}(\nu) = \hat{n}^2(\nu) \quad (3.25)$$

3.3.2 GHz SPECTROSCOPY

The permittivity spectrum in the GHz spectral regime is measured using a Vector Network Analyzer (VNA, Rhode & Schwarz GmbH & Co KG, Germany, model ZVA67). The VNA is connected by a phase stable coaxial cable (Rhode-Schwartz, ZV-Z96) to various homebuilt probes to cover different parts of the GHz spectral domain. In the low frequency domain (10 MHz - 2 GHz) we used a probe cell in which the outer coaxial electrode extends several centimeters from the base plane to contain the sample fluid and the coaxial pin sticks 1.8 mm into the sample [18, 19]. For the high frequency domain (0.5 - 67 GHz) we used a probe that exists of a sample container with a coaxial end of which the outer conductor is attached to a circular flange and the inner conductor is capped with a glass bead to prevent sample fluid to enter the coaxial cable [20]. $\hat{\epsilon}(\nu)$ is obtained by measuring phase-resolved the reflections of the oscillatory electromagnetic fields provided by the VNA. In order to calibrate the spectra, known dielectrics were measured like pure water, *N,N*-dimethylacetamide, methanol, ethanol or 2-propanol.

3.4 SAMPLES

In most of the work we used isotopically diluted water as the solvent. Millipore H₂O was purified further in a deionizer. D₂O (99.99% purity) was purchased from Sigma-Aldrich. Throughout this thesis, the isotope dilution mostly used is 4% D₂O in H₂O (mol percent). All other solutes used were purchased from Sigma-Aldrich, the details of which are treated in every chapter separately.

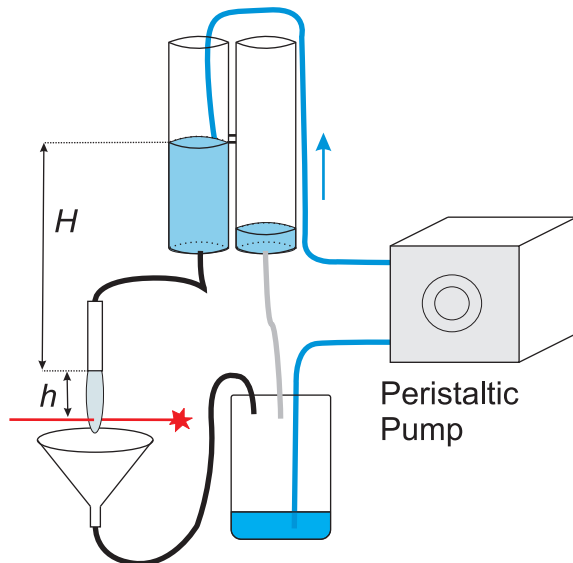


FIGURE 3.7. Schematic picture of the wire flow cell. Water (or another solvent) is pumped by a peristaltic pump into a reservoir in which the content level is kept constant (by means of an overflow) to maintain a constant pressure at the nozzle position. Under the film, the liquid is collected for reuse. Increasing H will put a larger pressure on the nozzle and increase the flow rate, making the film thicker. The film will become thinner further away from the nozzle (increasing h).

3.4.1 WIRE FLOW CELL

A frequently used conventional sample holder consists of two CaF_2 or BaF_2 windows, separated by a thin spacer to create a waterfilm of 10-1000 μm thickness. Unfortunately, in some experiments the energy of the pump pulses is high enough to create a third order polarization in such windows, emitting radiation known as white-light. This broad band light appears in the measurement results as a very unstable background artefact, obscuring the signal of interest. To solve this problem we made use of a wire flow cell that was constructed similar to the description in reference [21]. Water from a reservoir is gently released from a flat nozzle bearing an elongated tungsten wire loop of 125 μm thickness (Fig. 3.7). The width of the loop is approximately 5 mm. At the bottom of the tungsten wire loop the water is collected in a glass funnel and pumped back into the reservoir using a peristaltic pump. Thanks to the surface tension, the water forms a stable thin film floating in mid air in between the wires. This enables measurements on the sample without any windows. The thickness of the water film depends on the flow rate and distance from the nozzle h . The flow rate is increased by increasing the elevation difference H between the nozzle and the water level in the reservoir. The film becomes thinner for lower flow rates and at positions further away from the nozzle due to the gravitational pull on the

water. Stable configurations are obtained with film thicknesses of 25-125 μm . A linear spectrum taken from the film close to the nozzle using a fast flow rate resembled closely a linear spectrum from a water-filled conventional sample cell with a 115 μm spacer. For this optical pathlength the absorbance of a pure H_2O sample is ~ 2 O.D. at the OH-stretch/ H_2O -bend combination band and ~ 0.5 O.D. at the first OH-stretch overtone. The wire flow cell was also tested and found to work with solvents that have a lower viscosity/surface tension than water (e.g. methanol, ethanol and acetone).

4

Data Analysis

4.1 TRANSIENT ABSORPTION SPECTRA

In our mid-infrared pump-probe experiment we use a probe pulse to measure the absorption change in a sample due to the excitation of a vibrational mode by an intense pump pulse. The difference between the transmission spectra with ($I(\nu, t)$) and without ($I_0(\nu)$) a preceding pump-excitation is called a transient spectrum $\Delta\alpha(\nu, t)$ and can be written in terms of the measured intensities as,

$$\Delta\alpha(\nu, t) = -\ln\left(\frac{I(\nu, t)}{I_0(\nu)}\right) \quad (4.1)$$

where ν denotes the frequency and t the delay time between the pump and the probe pulses. Typically the transmission spectra I are normalized to the spectrum of a reference pulse that is not overlapping with the pump pulse in order to divide out intensity fluctuations of the laser. Most pump-probe experiments in this thesis are performed on the OD stretch vibrational mode of the HDO molecule in isotopically diluted water (a few percent HDO in H_2O). The transient spectra measured on this and similar vibrational modes contain three main contributions. First, the pump excites the OD stretch mode of a small percentage of HDO molecules to their first excited state $|\nu_s=1\rangle$. Due to the decreased population in the ground state, the excitation results in a reduced absorption at the $\nu_s = 0 \rightarrow 1$ transition frequency of this mode. The reduced absorption ($\Delta\alpha(\nu, t)$ is negative) is called the ground state bleach. Second, stimulated emission out of the $|\nu_s=1\rangle$ state occurs and contributes to the absorption decrease at the $\nu_s = 0 \rightarrow 1$ transition frequency. Finally, the absorption of the probe pulse due to the $\nu_s = 1 \rightarrow 2$ excitation of pump-excited modes leads to an induced absorption ($\Delta\alpha(\nu, t)$ is positive). Since the OD stretch vibrational mode is anharmonic, the spectrum associated with the $\nu_s = 1 \rightarrow 2$ transition is red-shifted by $\sim 180 \text{ cm}^{-1}$ from the $\nu_s = 0 \rightarrow 1$. With increasing pump-probe delay, an increasing number of excited HDO molecules have relaxed to their ground state, causing all three contributions to the transient spectra to decrease in amplitude. Time resolved transient spectra $\Delta\alpha(\nu, t)$ thus contain information on the decay of the probed vibrational mode.

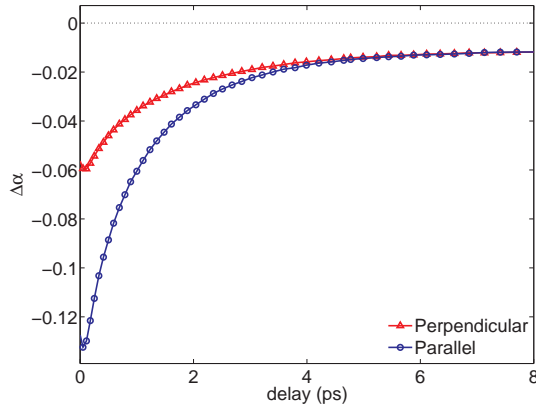


FIGURE 4.1. The transient absorption difference probed at 2500 cm^{-1} with a probe pulse with its polarization parallel (circles) and perpendicular (triangles) to the pump polarization. The parallel signal is initially larger due to the anisotropic excitation. After a couple of picoseconds both signals become identical due to molecular reorientation.

In case the excitation pulse was linearly polarized, the measured response depends on the polarization of the probe pulse. The reason is that the excitation probability scales with $\cos^2(\alpha)$, where α is the angle between the excitation polarization and the transition dipole moment of the vibrational mode. Immediately after excitation, the absorption changes probed parallel to the pump polarization will therefore be larger than those probed perpendicular to the pump polarization. After a certain delay time the OD stretch modes will be less ordered due to molecular reorientation. As a consequence, the absorption changes will depend increasingly less on the direction of the probe polarization, i.e. become more isotropic. An example of the parallel and perpendicular absorption changes probed in 8% HDO in H_2O at 2500 cm^{-1} for different delay times is shown in Fig. 4.1. The dynamical behavior of such a polarization resolved experiment thus not only depends on the vibrational decay of the excited mode, but on the reorientation dynamics as well. To obtain the transient spectra that are completely independent on molecular reorientation and thus reflect the vibrational decay only we have to take the weighted difference between the parallel and perpendicular signals according to,

$$\Delta\alpha_{\text{iso}}(\nu, t) = \frac{\Delta\alpha_{\parallel}(\nu, t) + 2\Delta\alpha_{\perp}(\nu, t)}{3} \quad (4.2)$$

where the perpendicular absorption changes appear twice to take into account the fact that we probe the three-dimensional sample in a two-dimensional plane orthogonal to the beam propagation. All probed dipoles are projected on this plane .

A parameter that exclusively depends on the reorientation of the excited

transition dipole moments is the anisotropy $R(\nu, t)$ given by,

$$R(\nu, t) = \frac{\Delta\alpha_{\parallel}(\nu, t) - \Delta\alpha_{\perp}(\nu, t)}{\Delta\alpha_{\parallel}(\nu, t) + 2\Delta\alpha_{\perp}(\nu, t)} \quad (4.3)$$

Using Eq. (4.2) and Eq. (4.3), the parallel and perpendicular absorption changes can be written as a combination of the vibrational decay and reorientation dynamics according to,

$$\Delta\alpha_{\parallel}(\nu, t) = (1 + 2R(\nu, t))\Delta\alpha_{\text{iso}}(\nu, t) \quad (4.4)$$

$$\Delta\alpha_{\perp}(\nu, t) = (1 - R(\nu, t))\Delta\alpha_{\text{iso}}(\nu, t) \quad (4.5)$$

From the converging behavior of the parallel and perpendicular signals it is clear that the anisotropy of the OD stretch vibration in isotopically diluted water decays on a timescale of several picoseconds (Fig. 4.1). Both signals do not decay completely but rather reach an endlevel after ~ 10 ps. This response at long delay times is not due to excited OD oscillators, and needs to be subtracted from the data to obtain the anisotropy dynamics of the OD stretch transition dipole moment only. An important part of the data analysis of anisotropy measurements involves the subtraction of this endlevel and in the following sections we elaborate on a number of methods to achieve this.

4.2 MODELING HEAT DYNAMICS

As we have seen in the previous section, the transient pump-probe response in isotopically diluted water is virtually always superimposed on another response. This response is found to grow in on a similar timescale as the decay of the excitation and remains constant for longer delay times, at least on the timescale of the experiment (100 ps). The origin of this contribution is the rise in temperature of the sample due to dissipation of the vibrational energy into thermal bath modes. The typical pump energy used to excite OD-stretch oscillators in the experiment described in section 3.1.1 is $5 \mu\text{J}$, focused in the sample on a spot with a radius of $100 \mu\text{m}$. If we assume that about 90% of the energy is absorbed by the sample, the sample thickness is $25 \mu\text{m}$ and that energy diffusion in the direction orthogonal to the laser propagation direction is negligible on the timescale of the experiment, the probed volume of water experiences a temperature increase of about 10 Kelvin after vibrational relaxation is complete. As a response to the new energy content, the hydrogen-bonds in the solution will weaken. OD-oscillators with a weaker hydrogen-bond have a lower cross section and their resonance frequency is shifted towards blue frequencies. This explains the spectral shape of the thermal endlevel found in our experiments: a bleach at red frequencies and a much smaller induced absorption a blue frequencies. This spectral shape can be reproduced by subtracting the linear spectrum of the sample at room temperature from that at an elevated temperature: the thermal difference spectrum. The thermal endlevel thus forms an observable from our non-linear experiment that can be compared to an observable obtained with linear spectroscopy.

4.2.1 SIMPLE KINETIC MODEL

In most of our work we are interested in retrieving the vibrational lifetimes and the reorientation dynamics of the excited OD oscillators. To isolate the OD-stretch response, we therefore need to subtract the contribution of the heat signal from the measured pump-probe data. Subtracting the thermal endlevel as a constant offset ignores the fact that in the first few picoseconds most energy is still present as localized vibrations rather than thermal modes. To account for this effect we use a kinetic model for vibrational decay in which the dynamics of the population in the thermalized ground state is related to the vibrational decay of the excitation through rate equations. In the simplest possible model the population in the excited state directly decays to the thermalized ground state. The population $N_1(t)$ in the excited state and the population $N_H(t)$ in the thermalized ground state are then obtained for all pump-probe delay-times t by solving the differential equations,

$$\frac{d}{dt}N_1(t) = -k_1N_1(t) \quad (4.6)$$

$$\frac{d}{dt}N_H(t) = +k_1N_1(t) \quad (4.7)$$

where k_1 is the vibrational decay rate of the excited state. This can conveniently be written into a vector notation in which we introduce a rate matrix $\mathbf{M}(\mathbf{k})$,

$$\frac{d}{dt}\mathbf{N}(t) = \mathbf{M}(\mathbf{k}) \cdot \mathbf{N}(t) \quad (4.8)$$

$$= \begin{pmatrix} -k_1 & 0 \\ +k_1 & 0 \end{pmatrix} \begin{pmatrix} N_1(t) \\ N_H(t) \end{pmatrix}. \quad (4.9)$$

where \mathbf{k} denotes the set of parameters of the model. The trivial solutions to these coupled equations are,

$$N_1(t) = N_1(0)e^{-k_1t} \quad (4.10)$$

$$N_H(t) = N_1(0)(1 - e^{-k_1t}) \quad (4.11)$$

Typically the total population in the model is normalized and hence the initial condition is set to $N_1(0) = 1$. Both states thus have a time dependent contribution to the measured transient spectra $\Delta\alpha_{\text{iso}}(\nu, t)$ according to,

$$\Delta\alpha_{\text{iso}}(\nu, t) = \sum_{i=1}^2 N_i(t)\sigma_i(\nu) \quad (4.12)$$

$$= N_1(t)\sigma_1(\nu) + N_H(t)\sigma_H(\nu) \quad (4.13)$$

where $\sigma_1(\nu)$ and $\sigma_H(\nu)$ represent the transient spectra associated with both states. The model is fit to the data by minimizing the following χ^2 function by varying the rate of decay k_1 ,

$$\chi_{\text{iso}}^2(\mathbf{k}) = \int \int dt d\nu \left(\frac{\Delta\alpha(\nu, t) - \sum_i N_i(t; \mathbf{k})\sigma_i(\nu)}{\epsilon_{\Delta\alpha}(\nu, t)} \right)^2 \quad (4.14)$$

where $\epsilon_{\Delta\alpha}(\nu, t)$ represent the variances of the data points $\Delta\alpha(\nu, t)$ and $N_i(t; \mathbf{k})$ represent the population dynamics according to the model parameters \mathbf{k} . The state spectra for a given set of population dynamics are obtained by calculating the minimum of $\chi_{iso}^2(\mathbf{k})$ with respect to the spectral amplitudes $\sigma_i(\nu_j)$ of every measured frequency ν_j ,

$$\frac{d}{d\sigma_i(\nu_j)} \int dt \left(\frac{\Delta\alpha(\nu_j, t) - \sum_i N_i(t; \mathbf{k})\sigma_i(\nu_j)}{\epsilon_{\Delta\alpha}(\nu_j, t)} \right)^2 = 0 \quad (4.15)$$

The spectral contribution of heating the sample is isotropic and hence equal in both the parallel and perpendicular probed signal. To obtain the contribution to both signals that is solely from the OD-stretch excitation we subtract the contribution of the thermalization,

$$\widetilde{\Delta\alpha}_{\parallel}(\nu, t) = \Delta\alpha_{\parallel}(\nu, t) - N_H(t)\sigma_H(\nu) \quad (4.16)$$

$$\widetilde{\Delta\alpha}_{\perp}(\nu, t) = \Delta\alpha_{\perp}(\nu, t) - N_H(t)\sigma_H(\nu) \quad (4.17)$$

These pure signals can be used to calculate the anisotropy parameter $R(\nu, t)$ following Eq. (4.3),

$$R(\nu, t) = \frac{\widetilde{\Delta\alpha}_{\parallel}(\nu, t) - \widetilde{\Delta\alpha}_{\perp}(\nu, t)}{\widetilde{\Delta\alpha}_{\parallel}(\nu, t) + 2\widetilde{\Delta\alpha}_{\perp}(\nu, t)} \quad (4.18)$$

4.2.2 DELAYED HEAT

It has been demonstrated that the simple model of the previous section does not describe very well the isotropic transient spectra measured on the OD stretch in a few percent HDO in H₂O [22]. A much better description is obtained when the vibrationally excited state is allowed to decay to an intermediate state first [22]. The population in the intermediate state subsequently decays into the thermalized ground state. Effectively this leads to a delayed ingrowth of the heat. Such a delay is supported by measurements on the vibrational decay of the OH-stretch vibration and subsequent thermalization in pure liquid water [23]. While the vibrational lifetime of the OH-stretch in pure water is only ~ 200 fs, the thermal endlevel was found to grow in with a timeconstant of at least ~ 600 fs. In the formalism described in the previous section the rate equations for such a model look like,

$$\frac{d}{dt}\mathbf{N}(t) = \begin{pmatrix} -k_1 & 0 & 0 \\ +k_1 & -k_{int} & 0 \\ 0 & +k_{int} & 0 \end{pmatrix} \begin{pmatrix} N_1(t) \\ N_{int}(t) \\ N_H(t) \end{pmatrix} \quad (4.19)$$

where $N_{int}(t)$ is the population dynamics and k_{int} the decay rate of the intermediate state. This delayed thermal response can be due to the transient population of a particular non-thermal state in the vibrational relaxation of the OD stretch vibration. Such a non-thermal state may involve the HOD bending mode and/or the librational modes. However, the intermediate state was

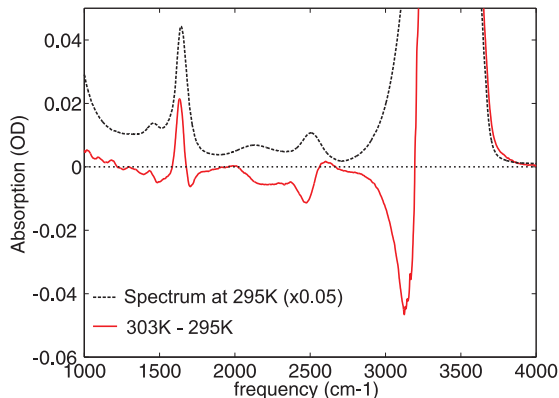


FIGURE 4.2. Linear spectrum of a sample of 8% HDO in H_2O at 295K (multiplied by 0.05, dashed line), and the difference spectrum between a linear spectrum at 295K and a linear spectrum of the same sample at 303K. The difference spectrum shows a rich structure of features, caused by the shifting of bands and change in cross sections upon a rise of temperature.

observed to have no spectral signature [22], which means that its absorption spectrum is identical to that of the OD stretch vibration before the excitation by the pump. Therefore, the delayed rise of the thermal response is likely not due to the transient excitation of a specific mode like the HOD bending vibration, because such an excitation would lead to an anharmonic frequency shift of the absorption spectrum of the OD stretch vibration. Instead, the delayed rise is probably rather due to the relatively slow adaptation of the coordinates of low-energy degrees of freedom (hydrogen-bond bend and stretch) to the higher energy content that results from the relaxation of the OD stretch vibration. The relaxation of the OD stretch vibration leads to a rapid increase of the energy content of the lower-energy degrees of freedom, and these coordinates need some time to evolve to the new equilibrium positions corresponding to this higher energy content.

4.3 DIRECT PROBE OF HEAT DYNAMICS

For increasingly complicated systems, as also described in this thesis, it may become more difficult to accurately describe the data with a kinetic model. Until now we considered systems that were homogeneous in the sense that the excited oscillators were evenly distributed over the absorption band at time-zero and could be treated as behaving identical. Although this is most of the time an approximation, it often provides a good description of the data. Some systems, however, are strongly inhomogeneous and the approximation breaks down. The vibrational lifetime may be strongly frequency dependent or the

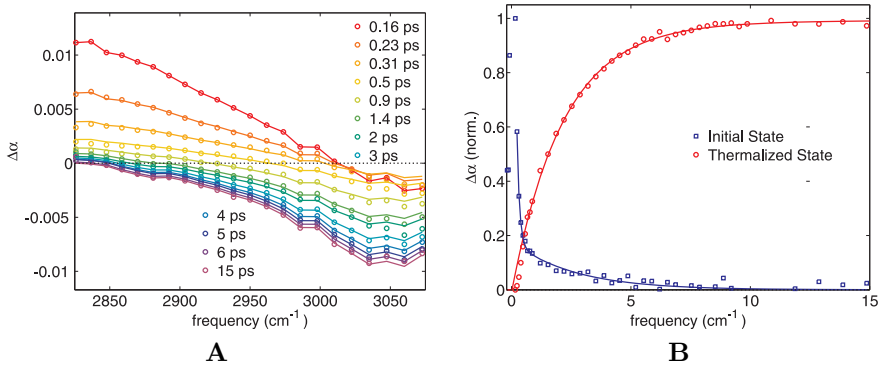


FIGURE 4.3. (A) Transient spectra for different delay times probed around 2900 cm^{-1} after exciting the OD stretch vibration in a sample of 8% HDO:H₂O with a pump centered around 2650 cm^{-1} . The bleach that grows in with increasing delay time is the thermal difference spectrum of the red shoulder of the OH stretch vibration. (B) The dynamics that resulted from a decomposition of the spectra shown in panel A.

excitation is inhomogeneous. The latter case may happen by using a pump-pulse with a narrow spectral width. As described in section 2.2, this leads to spectral diffusion and as a result the transient state spectrum $\sigma_1(\nu)$ in Eq. (4.12) may not be constant in time anymore.

A kinetic model to describe the isotropic transient absorption data becomes in such a case quickly too complicated to obtain reliable values for the fit parameters. The main problem in obtaining the dynamics of the heat contribution from our data is that the contributions of both the thermalized ground state and the excitation are overlapping. A solution is to obtain the dynamics of the thermal difference spectrum by an independent method. Fig. 4.2 shows that upon heating a sample containing 8% HDO:H₂O by a few degrees, virtually all modes in the linear spectrum of water from 400 cm^{-1} to 4000 cm^{-1} either shift or change in amplitude. We are thus able to measure the dynamics of the thermal difference spectrum by probing an entirely different part of the spectrum.

An ideal window of probing has a strong thermal response, a not too strong linear absorption, and is free from any response due to the direct vibrational excitation. The spectral area around the H₂O bending mode at 1600 cm^{-1} is meeting these criteria very well. Probing in this region is experimentally relatively involved since the absorption of water vapor in the air requires the setup to be tightly flushed with dry air. A good alternative is the large thermal response at the red shoulder of the OH-stretch vibration around 3000 cm^{-1} . The only potential complication is a possible contribution of OH-oscillators that are anharmonically coupled to excited OD-oscillators in HDO molecules. This is not a major problem, as will be shown later.

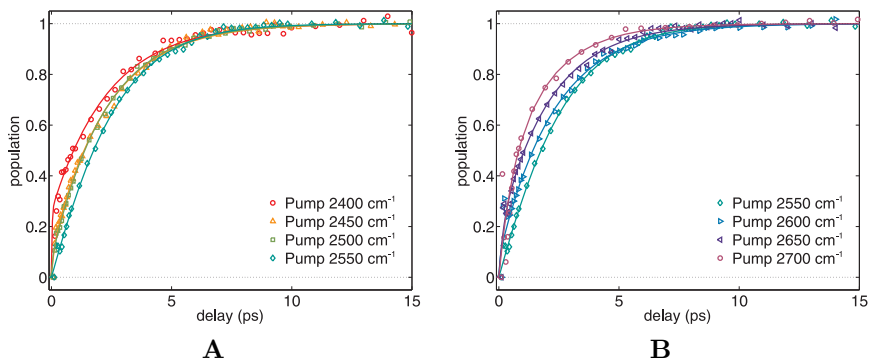


FIGURE 4.4. Different thermalization dynamics obtained for center frequencies of the pump red-shifted (**A**) and blue-shifted (**B**) from the center of the OD stretch band. For increasing red-shifts or blue-shifts the dynamics becomes faster.

Fig. 4.3A shows the results of a measurement for which the OD stretch vibration is excited by using pump pulses of which the spectrum was centered around 2650 cm^{-1} and the probe around 2900 cm^{-1} . For very short delay times there is an induced absorption at low frequencies. This feature quickly decays, after which a bleach at higher frequencies grows in at a much slower rate. We recognize the shape of the bleach as the thermal difference spectrum in this spectral region in Fig. 4.2. The spectral response at short delay times probably arises from the $\nu = 1 \rightarrow 2$ transition of OH oscillators that are excited in the very far red wing of the OH stretch absorption band. As was shown in section 2.2, an excitation pulse of which the spectrum is very red-shifted from the center of the OH stretch band can still excite OH oscillators.

The OH stretch excited state spectrum $\sigma_{OH}(\nu)$ and thermal difference spectrum $\sigma_H(\nu)$ have quite a different shape. For this reason it is possible to disentangle the population dynamics of both states by doing a spectral decomposition of the transient spectra obtained at all delay times. To do this decomposition, we use for $\sigma_H(\nu)$ the transient spectrum at long delay times (100 ps) and for $\sigma_{OH}(\nu)$ the transient spectrum at 200 fs. At this delay time the pump and probe pulse are not overlapping anymore and the contribution of the coherent artefact becomes negligible. The results of such a spectral decomposition is shown in Fig. 4.3B. It should be noted that for the thermalization dynamics nearly identical results are obtained in case a delay trace of the raw data is taken at $\nu \approx 3000\text{ cm}^{-1}$ for which the OH stretch contribution is very small.

Fig. 4.4 shows the thermalization dynamics that were obtained for a solution of 8% HDO:D₂O. For the different curves the center frequency of the pump spectrum (FWHM of 60 cm^{-1}) was shifted from 2400 cm^{-1} to 2700 cm^{-1} . The dynamics clearly depend on the excitation spectrum, with a faster initial rise in case the OD stretch band is not pumped in the center of its absorption

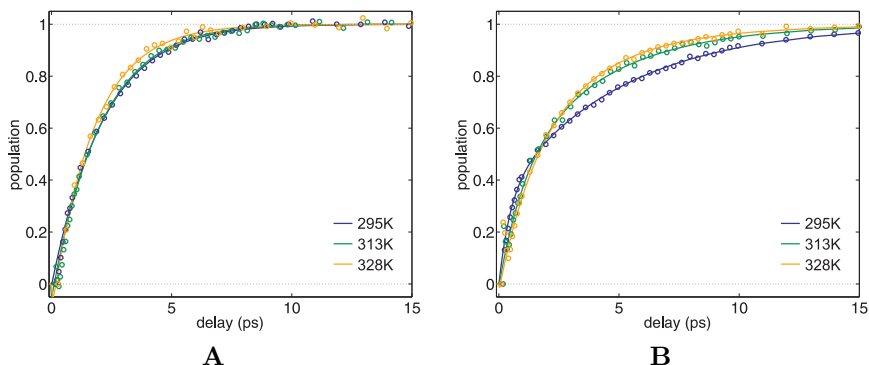


FIGURE 4.5. Temperature dependence of the thermalization dynamics after excitation at 2650 cm^{-1} in (A) neat 8% HDO:H₂O and (B) a solution of 6 mol/kg TMU.

spectrum at 2500 cm^{-1} . If the pump spectrum is shifted to frequencies higher than 2550 cm^{-1} (Fig. 4.4A), this can be explained by the collateral excitation of OH oscillators that decay much more rapidly than OD oscillators and as a result lead to a faster thermalization. For excitation frequencies at the red shoulder of the OH stretch band (Fig. 4.4A), the collateral excitation of the blue shoulder of the H₂O-bend plus libration band at 2200 cm^{-1} plays a similar role.

Fig. 4.5A shows the thermalization dynamics in 8% HDO:D₂O for several sample temperatures. The OD stretch band is in this case excited homogeneously by a spectrally broad pump (FWHM of 150 cm^{-1}). For increasing temperatures the dynamics become faster, which is a result of the faster decay time T_1 of the OD stretch vibration. It should be noted here that the rate of thermalization is not exactly proportional T_1 , due to the delay in thermalization that was discussed in section 4.2.2 of this chapter.

Finally, by the use of kinetic models it has been shown that the thermalization dynamics in water becomes slower upon the addition of the small amphiphilic molecule tetramethylurea TMU [24]. We therefore compare the thermalization dynamics of a concentrated solution of TMU in water (6 mol/kg) for different temperatures in Fig. 4.5B. It is evident that the dynamics is slower compared to neat 8% HDO:H₂O. However, the dynamics at short delay times does not seem to show the characteristics of a long delay of the thermalization after vibrational decay. Fig. 4.6 shows a comparison of the thermalization dynamics for both neat isotopically diluted water and a solution of 6 mol/kg TMU obtained by the two methods described in this chapter: Direct measurement by probing the red shoulder of the OH stretch band and by fitting a kinetic model to the data that includes an intermediate state accounting for the delayed thermalization. Both methods yield thermalization dynamics that are similar at longer delay times, but have a quite different character at short delays. The kinetic model thus seems to underestimate the contribution of the thermal difference

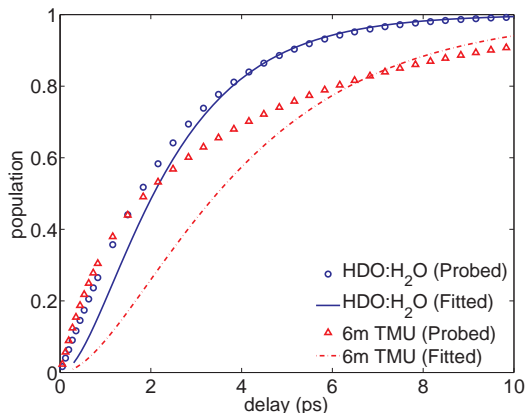


FIGURE 4.6. Comparison of the thermalization dynamics in neat 8% HDO:H₂O and 6 mol/kg TMU as obtained from a fit of a kinetic model to the isotropic transient spectra (lines) and from a spectral decomposition as described in this section (symbols). For short delay times there is a considerable deviation.

spectrum in the first few picoseconds. How much influence the underestimation of the thermal contribution has on the calculation of the anisotropy parameter depends on the relative size of the excited state with respect to the thermal difference spectrum. At short delay times, the excited state contribution is still relatively large and an incorrect subtraction of the thermal contribution does not affect the anisotropy as calculated by Eq. (4.18) much.

The thermalization dynamics obtained by the methods described above can be used to subtract the heat component from a measurement on the excitation (eg. the OD stretch vibration) for which an identical pump is used. To this end, a multi-exponential function is fitted to the thermalization curve to capture the dynamics $N_H(t)$. No assumptions are made on the fit based on physical interpretation, since it merely serves the purpose of describing the measured dynamics. Typically, a function of three exponentials were found to accurately describe the curves. For the thermal difference spectrum $\sigma_H(\nu)$, the transient spectrum at long delay time is used of the dataset of which the thermal contributions is to be subtracted. For improved signal-to-noise, typically the average transient spectrum of at least three delay times between 70 and 100 ps were used. Having obtained a description of $N_H(t)$ and $\sigma_H(\nu)$, finally Eq. (4.16) is used to obtain the heat subtracted transient spectra.

4.3.1 MULTIPLE SPECIES

In section 4.2.1 we implicitly assumed in the kinetic model that all OD-oscillators decay with equal decay rate k_1 . For neat isotopically diluted water this is shown to provide an accurate description of the data [22], as long

the spectrum of the pump pulse is broad enough to overlap with the whole OD-stretch absorption band. This condition is required since spectral diffusion (see section 2.2) is for most systems studied happening at a similar timescales as the vibrational relaxation. In some more complicated solutions there may be different species of oscillators i that have different excited state transient spectra $\sigma_i(\nu)$, population dynamics $N_i(t)$ and reorientation dynamics $R_i(\nu, t)$. Information on $N_i(t)$ and $\sigma_i(\nu)$ can be obtained from a fit of a kinetic model to the isotropic transient spectra, which are free from any contribution of the reorientation dynamics. In order to do so, we need to extend the model described in Eq. (4.19) with an additional excited state to incorporate the excited state response of the second species. The rate equations that follow are written as,

$$\frac{d}{dt}\mathbf{N}(t) = \begin{pmatrix} -k_1 & 0 & 0 & 0 \\ 0 & -k_2 & 0 & 0 \\ +k_1 & +k_2 & -k_{int} & 0 \\ 0 & 0 & +k_{int} & 0 \end{pmatrix} \begin{pmatrix} N_1(t) \\ N_2(t) \\ N_{int}(t) \\ N_H(t) \end{pmatrix}. \quad (4.20)$$

where k_1 and k_2 are the vibrational decay rates of species 1 and 2, respectively. The initial conditions are $(N_1(0), N_2(0), N_{int}(0), N_H(0)) = (1-p, p, 0, 0)$, where p is a free fit parameter and denotes the relative initial population in the second state. p must assume values between 0 and 1 to assure the total population in the model is normalized to one. In this model it is assumed that both excited states decay to the same intermediate state, which subsequently decays to the thermalized ground state.

The parallel and perpendicular signals can then in analogy to Eq. (4.4) and Eq. (4.12) be written as the sum of both contributions,

$$\Delta\alpha_{\parallel}(\nu, t) = [1 + 2R_1(t)]N_1(t)\sigma_1(\nu) + [1 + 2R_2(t)]N_2(t)\sigma_2(\nu) + N_H(t)\sigma_H(\nu) \quad (4.21)$$

$$\Delta\alpha_{\perp}(\nu, t) = [1 - R_1(t)]N_1(t)\sigma_1(\nu) + [1 - R_2(t)]N_2(t)\sigma_2(\nu) + N_H(t)\sigma_H(\nu) \quad (4.22)$$

Assuming that we have subtracted the heat contribution, the anisotropy that would be obtained using Eq. (4.3) yields,

$$R(\nu, t) = \frac{\sum_{i=1}^2 R_i(t)N_i(t)\sigma_i(\nu)}{\sum_{i=1}^2 N_i(t)\sigma_i(\nu)} \quad (4.23)$$

This expression poses a problem. If one of the species has slower population dynamics, $R(\nu, t)$ will represent a weighted sum of the reorientation dynamics of both species with weighting factors $N_i(t)$ that differ for every pump-probe delay time. It is much more instructive if both $R_1(t)$ and $R_2(t)$ could be resolved separately, which is in fact possible in case also the spectral response of both

species (ie. $\sigma_1(\nu)$ and $\sigma_2(\nu)$) is different. In such a case it is more convenient to consider the not-normalized difference between the parallel and perpendicular signals $D(\nu, t)$ given by,

$$D(\nu, t) = \frac{\Delta\alpha_{\parallel}(\nu, t) - \Delta\alpha_{\perp}(\nu, t)}{3} = \sum_{i=1}^n R_i(t)N_i(t)\sigma_i(\nu) \quad (4.24)$$

With the knowledge of the population dynamics and spectral responses of both species from the isotropic fit, we can resolve the reorientation dynamics by performing a spectral decomposition analogous to Eq. (4.15),

$$\frac{d}{dR_i(t_j)} \int d\nu \left(\frac{D(\nu, t_j) - \sum_i R_i(t_j)N_i(t)\sigma_i(\nu)}{\epsilon_D(\nu, t_j)} \right)^2 = 0 \quad (4.25)$$

Alternatively, the heat subtracted parallel and perpendicular transient spectra can be decomposed directly to obtain the dynamical components from both species,

$$\frac{d}{dA_i(t_j)} \int d\nu \left(\frac{\Delta\alpha_{\parallel}(\nu, t_j) - \sum_i A_i(t_j)\sigma_i(\nu)}{\epsilon_{\Delta\alpha_{\parallel}}(\nu, t_j)} \right)^2 = 0 \quad (4.26)$$

and similar for the perpendicular transient spectra. $A_{i,\parallel}(t)$ and $A_{i,\perp}(t)$ contain all the dynamical behavior of species i ,

$$A_{i,\parallel}(t) = [1 + 2R_i(t)]N_i(t) \quad (4.27)$$

$$A_{i,\perp}(t) = [1 - R_i(t)]N_i(t) \quad (4.28)$$

The anisotropy of both species is thus evaluated by,

$$R_i(t) = \frac{A_{i,\parallel}(t) - A_{i,\perp}(t)}{A_{i,\parallel}(t) + 2A_{i,\perp}(t)} \quad (4.29)$$

The multiple-species model can in principle be extended to incorporate any number of species. Whether such an extension does not lead to an over-determination of the data depends on how well separated the species are spectrally, how different the vibrational lifetimes are and the quality of the data.

4.4 ANISOTROPY

4.4.1 MODELING OF ANISOTROPY DYNAMICS

In the previous section we described how we obtain the anisotropy dynamics $R(\nu, t)$ from a polarization resolved measurement. In the following discussion we assume that $R(\nu, t)$ is the anisotropy of the transition dipole moment of the OD or OH stretch vibration of water, since this is most relevant for this thesis. It can be shown that the anisotropy is proportional to the second order orientational correlation function of the transition dipole of vibration $\boldsymbol{\mu}_s$ [25],

$$R(t) = \frac{2}{5} \langle P_2(\boldsymbol{\mu}_s(0) \cdot \boldsymbol{\mu}_s(t)) \rangle \quad (4.30)$$

where P_2 is the second order Legendre polynome. Immediately after excitation, the anisotropy thus has a maximum value of 0.4. Its subsequent decay depends on the chemical environment and is primarily governed by four different processes. First, librational motions make the transition dipole wobble over a cone. The librational decay process takes place on a very fast timescale (~ 100 fs). Since the angle of the cone is often limited by the chemical environment (eg. the hydrogen-bond of the OD/OH oscillator), this reorientation process does not lead to a complete decay of the anisotropy. Secondly, an OD/OH oscillator may jump to a new hydrogen-bonding partner. Although the actual jump takes only a few hundred femtoseconds, the rate of jumps is on the order of $\sim 0.5 \text{ ps}^{-1}$. Such a jump is found to involve a rotation of the transition dipole moment over a large angle ($\sim 60^\circ$) [2], and thus results in a complete loss of orientation. The third process of anisotropy decay is frame rotation. A transition dipole moment that remains hydrogen-bonded to the same partner will on average point along the oxygen-oxygen coordinate. As a result of the dynamic hydrogen-bond network surrounding it, this coordinate also experiences a slow reorientation. Finally, $R(\nu, t)$ can decay due to the resonant transfer of the vibrational excitation from the initially excited mode to a neighboring oscillator. This is not a reorientation process, but the transition dipole moment of the accepting mode can be different from that of the donating mode. As a result, the orientational correlation decreases. The rate of transfer strongly depends on the distance between the donating and accepting modes and is extremely fast in pure liquid water (< 100 fs), but can be neglected in solutions of sufficient isotopic dilution [26].

After a short equilibration time, all OD oscillators in a solution of 8% HDO in H_2O can be approximated as belonging to a single species due to fast spectral diffusion (see section 2.2). The anisotropy in such a solution therefore decays mono-exponentially after a few hundred picoseconds. In previous sections we also considered systems in which two different species can be identified. In particular, it was assumed that the species have different population dynamics, spectral response and reorientation dynamics. In a solution containing multiple species, there are in fact a number of relevant situations that may occur, for some of which a spectral decomposition as described above is not possible. First, it can happen that although the population dynamics are different for both species, their spectral response may overlap. If the species with slower vibrational relaxation also has slower reorientation dynamics, the total anisotropy can show a recurrence behavior. This was observed for water in reverse micelles, for which the anisotropy was found to increase again after an initial decay [27]. Secondly, both the spectral response and the population dynamics can be very similar for both species. The bimodal behavior will then only become apparent in the anisotropy dynamics and $R(t)$ will in such case not be a mono-exponential function anymore. This has been observed for solutions of amphiphiles in water [28] (see also chapter 7 and chapter 10). It was typically found that the anisotropy could be modeled with a separate exponent for both species, yielding separate reorientation times and amplitudes. Finally, the spectral responses

of the species can be different, but their vibrational lifetimes are the same. In this case a spectral decomposition is still possible if the excited state spectra are known, but it is not possible to obtain those spectra from the isotropic data using a kinetic model as described in section 4.3.1. An indication of this situation is when the anisotropy has a frequency dependence even if the isotropic relaxation has not.

4.4.2 SELF-CONSISTENT FIT

It may happen that in a system with two species the spectral separation between the associated transient state spectra $\sigma_i(\nu)$ is small. A decomposition of the anisotropy according to the procedure described in the section 4.3.1 may in such a case be prone to cross-talk (assignment of spectral amplitude to the incorrect state). One solution to this problem is found in fitting simultaneously a kinetic model for vibrational decay to the isotropic data and functional forms of the reorientation dynamics to the heat corrected anisotropy data. Instead of minimizing only Eq. (4.14) for a two-species model, we thus need to minimize at the same time an error function that incorporates a model for the reorientation dynamics. To that end we consider again the difference $D(\nu, t)$ between the measured parallel and perpendicular transient spectra, which is expressed in terms of our state model as,

$$D(\nu, t) = \sum_{i=1}^2 R_i(t; \mathbf{p}) N_i(t; \mathbf{k}) \sigma_i(\nu) \quad (4.31)$$

where both the third and fourth term from the original equation (Eq. (4.24)) vanish as a result of the assumptions that $\sigma_{int}(\nu) = 0$ and that the thermal ground state is isotropic. $R_1(t; \mathbf{p})$ and $R_2(t; \mathbf{p})$ are the functional forms of the reorientation dynamics of OD-oscillators of the first or second species, respectively, for a set of free fit parameters \mathbf{p} . The population dynamics $N_i(t)$ and state spectra $\sigma_i(\nu)$ are obtained from the results of Eq. (4.14) and Eq. (4.15). We can thus extend the χ^2 function of Eq. (4.14) by,

$$\chi_{ani}^2(\mathbf{p}) = \int \int dt d\nu \left(\frac{D(\nu, t) - \sum_i R_i(t; \mathbf{p}) N_i(t; \mathbf{k}) \sigma_i(\nu)}{\epsilon_D(\nu, t)} \right)^2 \quad (4.32)$$

where $\epsilon_D(\nu, t)$ are the variances of $D(\nu, t)$.

The additional restriction on the fit by Eq. (4.32) comes from the choice of the functional forms of the anisotropy functions $R_i(t; \mathbf{p})$. Datapoints obtained by the conventional calculation of the anisotropy dynamics, as described earlier in this chapter, are frequently fitted with exponential functions [22, 28, 29, 30]. A logical choice is thus to have $R_i(t; \mathbf{p})$ decay exponentially. Depending on the system studied and previous observations, more than one exponential component can be included. A self-consistent fit with such a choice of $R_i(t; \mathbf{p})$ gives a large penalty to χ^2 for parameters \mathbf{p} that lead to anisotropy dynamics that increase with time or that do not decay to zero. The advantage over a

conventional fit after which a similar functional form is fitted to $R_i(t)$ is thus that unphysical description are excluded from the solutions.

This approach does not resolve the data points of the anisotropy of both species. To obtain the data points $R_i^D(t)$ of the anisotropy decay of a single species i , the fitted contribution of the other species is subtracted from the raw data according to,

$$R_{i=1}^D(t) = \frac{D(\nu, t) - [R(t)N(t)\sigma(\nu)]_{i=2}}{[N(t)\sigma(\nu)]_{i=1}} \quad (4.33)$$

This method strictly yields an overestimation of systematic errors in the data, since the same error ends up in both collection of anisotropy points $R_1^D(t)$ and $R_2^D(t)$.

4.4.3 ANISOTROPY AND EXCHANGE

In section 4.3.1 we considered the possibility of having multiple species of OD oscillators with different spectral response and dynamics. An example of such systems are aqueous salt solutions, in which OD oscillators hydrogen-bonded to anions and those hydrogen-bonded to other water molecules can be treated as two different species. However, the two species are both OD stretch modes and are thus intrinsically not different. They reflect different chemical environments and it is expected that the two species exchange population as a result of dynamics in the liquid. This chemical exchange occurs by a large rotational motion in or out the anion hydration shell and is accompanied with a large loss in orientation. This mechanism is discussed in chapter 8 and in this section we elaborate on the effects of such jumps on the observed anisotropy decay of both species.

The kinetic model from Eq. (4.20) is extended to incorporate this exchange. The exchange model is described by the rate equations,

$$\frac{d}{dt}\mathbf{N}(t) = \begin{pmatrix} -k_1 - k_{1\curvearrowright 2} & +k_{2\curvearrowright 1} & 0 & 0 \\ +k_{1\curvearrowright 2} & -k_2 - k_{2\curvearrowright 1} & 0 & 0 \\ +k_1 & +k_2 & -k_{int} & 0 \\ 0 & 0 & +k_{int} & 0 \end{pmatrix} \begin{pmatrix} N_1(t) \\ N_2(t) \\ N_{int}(t) \\ N_H(t) \end{pmatrix}. \quad (4.34)$$

where k_1 and k_2 are again the vibrational decay rates of species 1 and 2, respectively, and $k_{1\curvearrowright 2}$ and $k_{2\curvearrowright 1}$ are the rates of exchange between the species. The initial conditions are defined identically to the model described in Eq. (4.20). A graphical representation of this model is shown in Fig. 4.7.

In the coming discussion we denote an OD oscillator that at the time of excitation resides in chemical environment 1 or 2 as **1** and **2**, respectively. At any given time after excitation the OD oscillator may either still be in the same chemical environment, denoted by $1\curvearrowright 1$ and $2\curvearrowright 2$, or may have exchanged to the other chemical environment, denoted by $1\curvearrowright 2$ and $2\curvearrowright 1$. We can of course consider even higher order processes, like $1\curvearrowright 2\curvearrowright 1$, but we will not do this for a number of reasons. First, in case the vibrational lifetime is shorter than the exchange

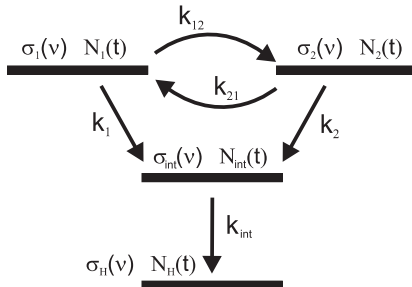


FIGURE 4.7. Graphical representation of the two-state model that includes exchange between the two species. The symbols are explained in the text.

time, the probability of higher order exchange processes decreases quickly. In the studied system this is indeed the case. Secondly, a quick back-exchange is likely accompanied with a recovery of the orientation of the OD oscillator. Further decay of the orientation will in such a case thus be independent on the temporary excursion. For simplicity we assume that an OD oscillator that exchanges from one chemical environment to the other loses its orientation completely. It can be shown that this is the case for a jump over an angle of 54.7° , which is in fact very close to the physical situation when considering exchange in and out of the anion hydration shell (see chapter 8).

The effect of exchange events on the reorientation dynamics as obtained from the analysis elaborated on in section 4.3.1 can now be described as follows. Immediately after excitation, the transient state spectrum $\sigma_1(\nu)$ of OD oscillators in chemical environment 1 represents the response of the collection of all $\mathbf{1}$. Therefore, the resolved anisotropy $R_1(\nu, 0)$ reflects the orientation of all $\mathbf{1}$. As time evolves, an increasing number of oscillators become $\mathbf{1} \rightarrow \mathbf{2}$. Since those oscillators now contribute to the spectral response of $\sigma_2(\nu)$ (they increase $N_2(t)$), their orientation is not contributing to $R_1(\nu, t)$ anymore. However, at the time of excitation there will be $\mathbf{2}$ that at later times become $\mathbf{2} \rightarrow \mathbf{1}$. Since those oscillators now have their spectral response at $\sigma_1(\nu)$ (increase of $N_1(t)$), they will contribute to $R_1(\nu, t)$. In the process of exchange they lost all their orientation and therefore they effectively lower $R_1(\nu, t)$. This process can be formalized by treating the $\mathbf{1} \rightarrow \mathbf{1}$, $\mathbf{1} \rightarrow \mathbf{2}$, $\mathbf{2} \rightarrow \mathbf{2}$ and $\mathbf{2} \rightarrow \mathbf{1}$ as four separate species. Let us assume that the thermal contribution is already subtracted from the data obtained for such a system. The rate equations describing the population dynamics of the species of Eq. (4.20) can then be rewritten as,

$$\frac{d}{dt} \mathbf{N}(t) = \begin{pmatrix} -k_1 - k_{\mathbf{1} \rightarrow \mathbf{2}} & 0 & 0 & 0 \\ +k_{\mathbf{1} \rightarrow \mathbf{2}} & -k_1 & 0 & 0 \\ 0 & 0 & -k_2 - k_{\mathbf{2} \rightarrow \mathbf{1}} & 0 \\ 0 & 0 & +k_{\mathbf{2} \rightarrow \mathbf{1}} & -k_2 \end{pmatrix} \begin{pmatrix} N_{\mathbf{1} \rightarrow \mathbf{1}}(t) \\ N_{\mathbf{1} \rightarrow \mathbf{2}}(t) \\ N_{\mathbf{2} \rightarrow \mathbf{2}}(t) \\ N_{\mathbf{2} \rightarrow \mathbf{1}}(t) \end{pmatrix}. \quad (4.35)$$

where the dynamics of $N_{int}(t)$ and $N_H(t)$ are omitted. The total isotropic

transient spectra are then written as,

$$\Delta\alpha(\nu, t) = \sum_{i,j=1}^2 N_{i\rightsquigarrow j}(t)\sigma_j(\nu) \quad (4.36)$$

and in a similar fashion the difference signal $D(\nu, t)$ as,

$$D(\nu, t) = \sum_{i,j=1}^2 R_{i\rightsquigarrow j}(t)N_{i\rightsquigarrow j}(t)\sigma_j(\nu) \quad (4.37)$$

We assumed that orientation is completely lost in a jump and using the previous two expressions and the definition of the anisotropy we can write,

$$R_{1\rightsquigarrow 1}(t) = \sum_{i=1}^2 \frac{N_{i\rightsquigarrow 1}(t)R_1(t)}{N_{1\rightsquigarrow 1}(t)} \quad (4.38)$$

where $R_1(t)$ is the anisotropy that resulted from the spectral decomposition. All the rates needed to calculate the dynamics from Eq. (4.35) were already determined from the isotropic fit, and the intrinsic anisotropy dynamics $R_{1\rightsquigarrow 1}(t)$ and $R_{2\rightsquigarrow 2}(t)$ can thus readily be evaluated.

In case the state spectra $\sigma_1(\nu)$ en $\sigma_2(\nu)$ are of very similar shape and strongly overlapping, the exchange rates k_{12} and k_{21} are hard to obtain from a free fit of the kinetic model to the isotropic data. However, the anisotropy data provides additional information that can aid in determining these rates. To this end, we use the fact that in case the pump spectrum is tuned over the absorption spectrum, different ratio's of the initial $N_{1\rightsquigarrow 1}(0)$ and $N_{2\rightsquigarrow 2}(0)$ populations are excited. In case the pump has a stronger overlap with $\sigma_1(\nu)$ than with $\sigma_2(\nu)$, the response measured for the second species will represent more $1\rightsquigarrow 2$ relative to $2\rightsquigarrow 2$ and vice versa. As a result, the anisotropy dynamics as obtained from a spectral decomposition $R_i(t)$ are different for various spectral positions of the pump. The intrinsic anisotropy dynamics $R_{1\rightsquigarrow 1}(t)$ and $R_{2\rightsquigarrow 2}(t)$ are by definition invariant under the change of the pump spectrum and the relation between them was given in Eq. (4.38). The exchange parameters k_{12} and k_{21} can therefore be constraint in a fit that includes data obtained with different pump frequencies. The additional weight χ_{ex}^2 to the χ^2 function of the isotropic fit is provided by the requirement of the invariance of the intrinsic anisotropy dynamics. For n datasets with different center frequencies of the pump spectrum χ_{ex}^2 can be written as,

$$\chi_{ex}^2 = \frac{1}{2} \int dt \sum_{i \neq j}^n \frac{(R_{1\rightsquigarrow 1}^i(t; \mathbf{k}) - R_{1\rightsquigarrow 1}^j(t; \mathbf{k}))^2}{\epsilon_{R^i}^2(t) + \epsilon_{R^j}^2(t)} \quad (4.39)$$

and similar for the intrinsic $R_{2\rightsquigarrow 2}(t)$ anisotropy. Here is $\epsilon_{R^i}(t)$ the variance of the intrinsic anisotropy of dataset i and \mathbf{k} the parameters of the kinetic model including the exchange parameters.

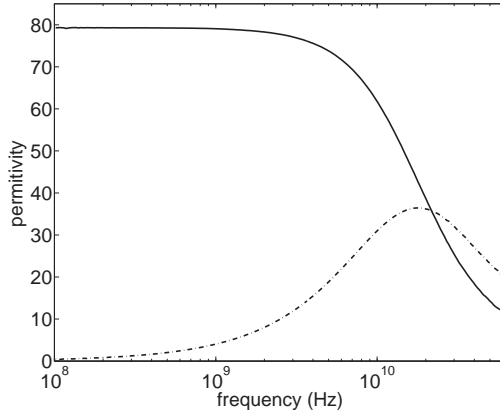


FIGURE 4.8. Real (solid line) and imaginary (dashed-dotted line) part of the permittivity spectrum of pure liquid water. The out-of-phase response peaks at ≈ 20 GHz, which frequency corresponds to a dipole reorientation time of 8.4 ps.

4.5 DIELECTRIC RELAXATION

In this section we describe how the complex permittivity spectra obtained by either THz or GHz dielectric relaxation spectroscopy (DRS) are analyzed. To this end, we first elaborate a bit on the molecular origin of the permittivity spectrum of pure liquid water.

DRS measures the correlation function of the macroscopic polarization of the sample as a response to an externally applied electric field. Generally, an applied electric field partially aligns the permanent dipoles of the water molecules against the thermal fluctuations. The resulting induced macroscopic polarization is proportional to the applied field,

$$\mathbf{P} = \varepsilon_0(\hat{\varepsilon}(\nu) - 1)\mathbf{E} \quad (4.40)$$

where ε_0 is the permittivity in vacuum and $\hat{\varepsilon}(\nu) = \varepsilon'(\nu) - i\varepsilon''(\nu)$ is the frequency-dependent complex permittivity. At frequencies lower than the characteristic timescale at which reorientation processes of water molecules take place, the dipoles can follow the electric field oscillations and the built-up polarization is only limited by the thermal fluctuations of the dipole orientations. At high frequencies, the dipoles fail to follow the oscillations of the applied electric field. The transition from the low-frequency to the high-frequency domain is marked by a strong response in the imaginary dielectric function due to a phase lag in the reorienting dipoles relative to the externally applied oscillating electric field (the out-of-phase response).

Fig. 4.8 shows the real and imaginary part of the complex permittivity for pure water. For single-component molecular liquids, for which the polarization decays with a single-exponential functional shape, the measured permittivity

can often be described by a Debye relaxation model,

$$\hat{\epsilon}(\nu) - \epsilon_\infty = \frac{S}{1 + 2\pi i\nu\tau}, \quad (4.41)$$

where ϵ_∞ is the permittivity at infinite frequency, τ is the characteristic relaxation time and S the amplitude of the Debye mode. The maximum of the out-of-phase response in pure water is found at 20 GHz, corresponding to a timescale τ_{bulk} of ≈ 8.4 ps [31]. This time constant is often referred to as the Debye relaxation time and has been assigned to the timescale of the spontaneous restructuring of the hydrogen-bond network. At higher frequencies (~ 0.9 THz, $\tau_{\text{fast}} \approx 350$ fs), a contribution with a much lower amplitude has been found. This additional mode has been assigned either to quick jumps of undercoordinated water [2, 32], interaction-induced components in the water relaxation mechanism [33, 34] or a small angular rotation preceding a large angle jump [8]. The dielectric function $\hat{\epsilon}(\nu)$ of water is thus modeled as a sum of two Debye modes with time constants τ_{bulk} and τ_{fast} ,

$$\hat{\epsilon}_{\text{H}_2\text{O}}(\nu) = \frac{S_{\text{bulk}}}{1 + 2\pi i\nu\tau_{\text{bulk}}} + \frac{S_{\text{fast}}}{1 + 2\pi i\nu\tau_{\text{fast}}} + \epsilon_\infty, \quad (4.42)$$

The fraction of water molecules that reorient with time constant τ_n is proportional to the amplitude S_n . For pure water $S_{\text{bulk}} \approx 70$ and $S_{\text{fast}} \approx 2$.

To compare the reorientation time obtained with dielectric relaxation spectroscopy with the reorientation time obtained with fs-IR pump-probe spectroscopy, it should be realized that they differ by a linear conversion factor. The reason for this difference is that both experiments measure a different observable. GHz-DRS measures the first order correlation function $C_1(t)$. The decay time τ_{bulk} of $C_1(t)$ thus represents the collective reorientation of all water molecules. The fs-IR experiment measures the second order correlation function $C_2(t)$ of the transition dipole moments of the OD stretch vibration. The decay time t_{bulk} of $C_2(t)$ is a measure of the reorientation of single water molecules. Assuming a jump-reorientation model or diffusive reorientation model (small amplitude angular reorientations) yields an ratio $\tau_{\text{bulk}}/t_{\text{bulk}}$ of the two time constants of 2.5 and 3, respectively. Dipole-dipole coupling between water molecules however leads to a further increase of τ_{bulk} . The ratio between the rotational correlation times of the two different experiments including dipole-dipole coupling was found to be 3.4, independent on the temperature [35].

For a mixture of different dipolar species that show distinct time constants, it can be assumed that each species is described with a separate Debye mode. The amplitude S of each relaxation mode is proportional to the corresponding concentration c of dipoles and their effective dipole strength μ_{eff} through the Cavell equation [36],

$$S = \frac{\epsilon_s}{3(\epsilon_s + \frac{1}{3}(1 - \epsilon_s))} \frac{N_A}{k_B T \epsilon_0} \mu_{\text{eff}}^2 c \quad (4.43)$$

where ϵ_s is the static permittivity.

For electrolyte solutions the translation of the ions, as determined by the macroscopic conductivity σ_c , gives rise to an additional contribution $\kappa(\nu)$ to the imaginary part ε'' of the permittivity, given by,

$$\kappa(\nu) = \frac{-i\sigma_c}{2\pi\nu\epsilon_0} \quad (4.44)$$

Due to its ν^{-1} dependence, this conductivity term becomes dominating for low frequencies. Typically, this contribution is subtracted from the data by assuming $\varepsilon'' = \kappa(\nu)$ for the low frequency domain [37, 19].

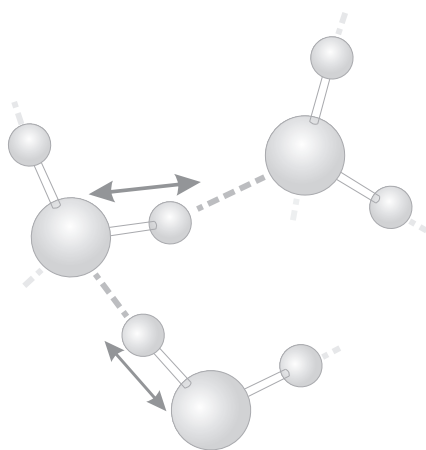
The addition of a solute often leads to a (concentration dependent) decrease of $\hat{\varepsilon}(\nu)$ (depolarization), as a result of three contributions. First, in a constant volume there is a decreased number of water molecules that contribute to the signal because of dilution when a solute is added. This effect is corrected for by calculating the water density in the solution from the solution density and water concentration. Secondly, the water molecules in the hydration shell of the solute molecules may have different reorientation dynamics. As a result they no longer contribute to the bulk water Debye mode but to a separate mode at different frequencies. In case of strongly hydrating cations, water molecules are bound so strongly that their contribution to $\hat{\varepsilon}(\nu)$ is shifted out of the measurement window [38]. Finally there is the effect of kinetic depolarization that results from the movement of charges in an electric field. This depolarization component $\Delta S_{kd}(c)$ is proportional to the macroscopic conductivity and given by [39, 38, 37],

$$\Delta S_{kd}(c) = -\frac{2}{3}\tau_D\sigma_c(c) \cdot \frac{\varepsilon_s(0) - \varepsilon_\infty(c)}{\varepsilon_s(0)\varepsilon_0} \quad (4.45)$$

where $\varepsilon_s(0)$ is the static permittivity of pure water and $\varepsilon_\infty(c)$ the permittivity at infinite frequency for a solution of solute concentration c .

It should finally be noted that the THz-DRS experiment described in chapter 3 probes at frequencies between 0.4 and 1.2 THz and is not very sensitive to the frequency dependence of the dielectric relaxation modes that peak at much lower frequencies. The frequency window of the generated THz pulses does not reach down to the maximum of the main Debye response of water at 20 GHz, but the high frequency wing of this response extends to THz frequencies. The depolarization of the main Debye mode of water can therefore be measured by THz-DR. Conversely, the GHz-DRS experiment measures in the range of 10 MHz to 70 GHz. The low amplitude high frequency mode at 0.9 THz in pure water can therefore be neglected in the analysis of the permittivity spectra measured in this range.

Vibrational Relaxation in Pure Water



A crucial parameter in any type of time-resolved vibrational spectroscopy is the excited state lifetime of the vibrational modes in the sample. In this thesis we almost exclusively make use of the OH- or OD-stretching vibration in pure or isotopically diluted water. The vibrational lifetime (T_1) thereby provides the limiting timescale over which observables like the reorientation dynamics or vibrational couplings can be measured. The T_1 of the OH-stretch vibration in pure liquid water has been measured to be very short (200 ± 50 fs) in comparison to for example the T_1 of the OD-stretch vibration of HDO in H_2O (1.8 ± 0.1 ps). This difference is probably due to the strong resonant coupling of the OH-stretch vibration to the overtone of the H_2O -bend. **In this chapter we show that not for all OH-stretching modes in pure liquid water $T_1 = 200$ fs.** Very weakly hydrogen-bonded OH-oscillators have a vibrational lifetime that is almost a factor of three slower compared to that of strongly hydrogen-bonded OH-oscillators. In addition, we demonstrate that weakly hydrogen-bonded oscillators dominate the overtone spectrum of the OH-stretch vibration. These results show that pure water is quite an inhomogeneous liquid.

5.1 INTRODUCTION

In previous work it was shown that in spite of the structure of the OH-stretch absorption band of water, spectral diffusion due to Förster transfer equilibrates any excited subset within hundred femtoseconds [40, 41, 42, 43]. It was also found that the vibrational lifetime of the OH-stretch is 200–240 fs, independent on the excitation frequency [44, 41].

The structure of the linear absorption spectrum of the OH-stretch vibration is still a topic of debate [45, 15, 46, 47]. Most interpretations involve contributions from the symmetric and asymmetric stretch, and the H₂O-bend overtone vibrations [48, 46, 40, 49]. It was also proposed that the H₂O-bend overtone leads to a Fermi-resonance with the symmetric OH-stretch vibration [46, 47, 50, 51]. Mixing of the wave functions of both modes forms a decreased cross section in the broad symmetric stretch band, known as an Evans window [47]. Surprisingly, the overtone spectrum of the OH-stretch vibration is extremely smooth [52, 53]. The underlying molecular origin of this smoothness is likely far from simple. The complexity becomes clear when considering the linear spectrum of a small percentage of HDO molecules in heavy water. In such a solution no H₂O-bend or (a)symmetric OH-stretch vibrations exist and the OH-stretch fundamental absorption spectrum is in this case almost a single gaussian. The OH-stretch overtone spectrum of HDO, however, shows a rich structure of several peaks [54]. The underlying structure of the smooth overtone spectrum in pure H₂O is thus expected to be rather complex [55].

Explanations of these phenomena have been sought in the structure of water [56, 55, 54, 45]. The OH-stretching vibration of the water molecule is a good probe of this structure. Its coupling to the hydrogen-bond causes the OH-stretch resonance frequency to be dependent on the hydrogen-bond strength: a stronger hydrogen bond lowers the resonance frequency. In this chapter we measure the vibrational lifetime and spectral response of OH oscillators in different spectral regions of the OH-stretch fundamental and overtone spectrum. We investigate whether the relaxation of the fundamental OH-stretch vibrational excitation is indeed as frequency independent as has been suggested previously. Subsequently we study the vibrational relaxation of the OH-stretch/H₂O-bend combination mode and of the OH-stretch overtone.

5.2 EXPERIMENT

5.2.1 EXCITATION OF THE FUNDAMENTAL TRANSITION

The experiments were performed with the two-color setup described in section 3.1.2. The absorption band of the OH-stretch fundamental vibrations of H₂O has a maximum at 3400 cm⁻¹ and a full width at half maximum (FWHM) of ~300 cm⁻¹ (see linear spectrum in Fig. 5.1, band 1). We excited the band using an intense pump pulse (10 μJ) with a center frequency tunable between 2900 cm⁻¹ and 3700 cm⁻¹. The spectral bandwidth of the pump pulses was 150 cm⁻¹ FWHM. The sample was probed at three different spectral positions:

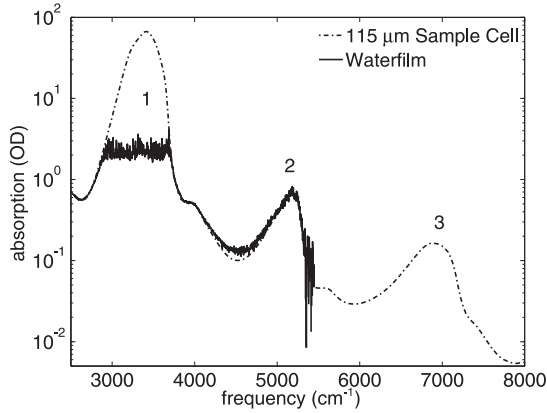


FIGURE 5.1. Logarithmic plot of the linear spectrum of the waterfilm (solid line) and that of pure water with $115\ \mu\text{m}$ path length (dashed line, scaled from the spectrum of a $1\ \mu\text{m}$ sample cell). In this chapter we focus on three bands: 1) the OH-stretch band centered at $3400\ \text{cm}^{-1}$, 2) the OH-stretch/ H_2O -bend combination band centered at $5150\ \text{cm}^{-1}$ and 3) the OH-stretch overtone band centered at $6900\ \text{cm}^{-1}$.

the $\nu = 0 \rightarrow 1$ transition around $3400\ \text{cm}^{-1}$, the $\nu_{\text{OH}} = 1 \rightarrow 2$ transition around $3000\ \text{cm}^{-1}$ and the $\nu_{\text{OH}} = 1 \rightarrow 2$ transition of the H_2O -bend vibration at $1550\ \text{cm}^{-1}$. The FWHM of the probe pulses was $300\ \text{cm}^{-1}$, and the FWHM of the cross-correlate with the pump pulses (measured in a thin germanium window) was $150\ \text{fs}$. Most of the data was taken by probing the $\nu_{\text{OH}} = 1 \rightarrow 2$ transition around $3000\ \text{cm}^{-1}$, since a strong thermal difference spectrum obscures the response of the excited OH oscillators at the $\nu_{\text{OH}} = 0 \rightarrow 1$ transition frequency.

For the measurements on the OH-stretch fundamental we used a sample cell consisting of two calcium fluoride windows of $0.5\ \text{mm}$ thickness, pressed against each other with small drop of water in between. This procedure resulted in a water film of approximately a few micrometers thickness, at which path length the maximum absorbance of the OH-stretch vibration is $\sim 2\ \text{OD}$. Since water vapor in the air causes a strong absorption around $3600\ \text{cm}^{-1}$ (rotation-vibrational lines of the free OH-stretch), the setup was purged with dry nitrogen to a humidity $< 5\%$.

5.2.2 EXCITATION OF OVERTONES

The OH-stretch/ H_2O -bend combination band is centered at $5150\ \text{cm}^{-1}$, and the OH-stretch overtone band is centered at $6900\ \text{cm}^{-1}$ with a FWHM of $\approx 600\ \text{cm}^{-1}$ (bands 2 and 3 in Fig. 5.1, respectively). Depending on the experiment either the signal (OH-stretch overtone) or the idler (OH-stretch/ H_2O -bend combination) output of the TOPAS was used as a pump. The spectral bandwidth of the pump was $250\ \text{cm}^{-1}$ FWHM. The pulse energy was typically $50\ \mu\text{J}$ for pumping

the combination band and 90 μJ for pumping the overtone.

The response of the system was probed at two different positions in the spectrum. First, we used the signal or idler output of the homebuilt OPA to directly probe the response of the overtone or combination band. Secondly, the OH-stretch vibration at the $\nu_{OH} = 1 \rightarrow 2$ transition at 3000 cm^{-1} was probed. In order to have sufficient absorption in the overtone region, the sample was made several tens to a hundred μm thick, resulting in an absorbance of > 30 OD at the OH-stretch fundamental vibration. For this reason the fundamental transition $\nu_{OH} = 0 \rightarrow 1$ could not be probed.

Unfortunately, the high (photon) energy of the pump pulses used in this experiment creates a third order polarization in CaF_2 windows resulting in white light generation. This broad-band light appears in our measurements as a very unstable background artefact, obscuring the signal of interest. To mitigate this problem, we used the wire flow cell described in section 3.4.1. Stable configurations of the waterfilm were obtained with film thicknesses of 25–125 μm . A linear spectrum taken from the film close to the nozzle using a fast flow rate resembled closely a linear spectrum from a water-filled conventional sample cell with a 115 μm spacer (Fig. 5.1). For this optical pathlength the absorbance of the sample is ~ 2 OD at the OH-stretch/ H_2O -bend combination band and ~ 0.5 OD at the OH-stretch overtone band.

It should be noted that the pump energies used in this experiment are close to being able to excite electrons in the sample in a multi-photon absorption process. Such excited electrons would give rise to an induced absorption signal that is highly non-linear with the pump intensity. By comparing the amplitudes of the measured signals for different pump intensities, we found that such a contribution is not present in our data.

5.3 OH-STRETCH: RESULTS AND INTERPRETATION

Fig. 5.2 shows the transient response around 3000 cm^{-1} of a sample of pure water that was excited at the blue shoulder of the OH-stretch band (3600 cm^{-1}). The positive transient spectrum at early pump-probe delay times is due to the $\nu_{OH} = 1 \rightarrow 2$ absorption of OH oscillators that were excited by the pump. The negative transient response at longer delay times is the thermal difference spectrum: the excitation energy has been transferred from the OH stretch mode into low frequency modes, giving rise to an increased sample temperature.

As explained in section 4.2.2 it was found in previous work that the thermalization does not follow immediately the vibrational relaxation but is delayed [23]. To obtain an accurate estimation of the vibrational relaxation time T_1 we therefore globally fit a kinetic model to the data in which we take the delayed thermalization into account (for a detailed description of the model see section 4.2.2). The solid lines in Fig. 5.2A represent the results of this fit.

Delay traces recorded at 3050 cm^{-1} are shown in Fig. 5.3A for different central frequencies of the pump spectrum (thermalization subtracted data). There is a clear correlation between the pump frequency and the vibrational relaxation

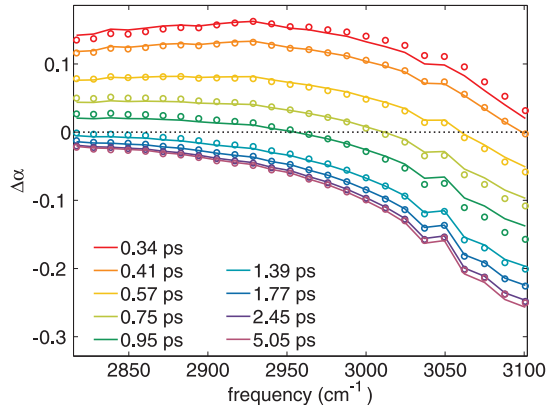


FIGURE 5.2. Transient spectra at different pump-probe delay times probed at the $\nu_{OH} = 1 \rightarrow 2$ transition. For this measurement the pump spectrum was centered at 3600 cm^{-1} .

dynamics. The maximum of the linear absorption spectrum of the OH-stretch band is at 3400 cm^{-1} . The dynamics become slower with an increasingly blue-shifted pump spectrum. Pumping the sample at frequencies red-shifted from this maximum, however, does not yield dynamics that are very different from when the sample is pumped at 3400 cm^{-1} .

The vibrational relaxation times obtained from the fits are summarized in Fig. 5.3B. For pump frequencies lower than 3400 cm^{-1} $T_1 \approx 230 \text{ fs}$. However, T_1 increases with frequency, and this increase becomes steeper. After excitation at 3700 cm^{-1} , we find that $T_1 = 540 \pm 70 \text{ fs}$. From the fits we also obtain the transient spectra $\sigma(\nu)$ of the excited OH oscillators (shown for different pump frequencies in Fig. 5.4A). If the pump spectrum is tuned to higher frequencies the transient spectra also blue-shift. This observation indicates that on the timescale of the experiment no full spectral equilibration takes place. The vibrational relaxation in pure liquid water is thus frequency dependent.

So far we focussed on the transient response at the $\nu_{OH} = 1 \rightarrow 2$ transition, since this response is not so much obscured by the contribution of the thermal difference spectrum. To study the vibrational dynamics for different pump frequencies further, we measured the transient response at different probe frequencies. Firstly, the thermal difference spectrum of the OH-stretch has a zero crossing around 3500 cm^{-1} . At this frequency, the thermal contribution is therefore small compared to the excited state spectrum. Another mode of interest is the H_2O -bending mode at 1640 cm^{-1} . It has been shown that this mode gives an almost instantaneous response upon excitation of the OH-stretch vibration [46]. We probed the H_2O -bending mode at its $\nu_b = 1 \rightarrow 2$ transition at 1550 cm^{-1} . The raw transient delay plots for these probing frequencies are shown in Fig. 5.4B for a pump centered at 3400 cm^{-1} and 3600 cm^{-1} . For all data the dynamics is significantly slower when the OH-stretch band is pumped at the blue shoulder.

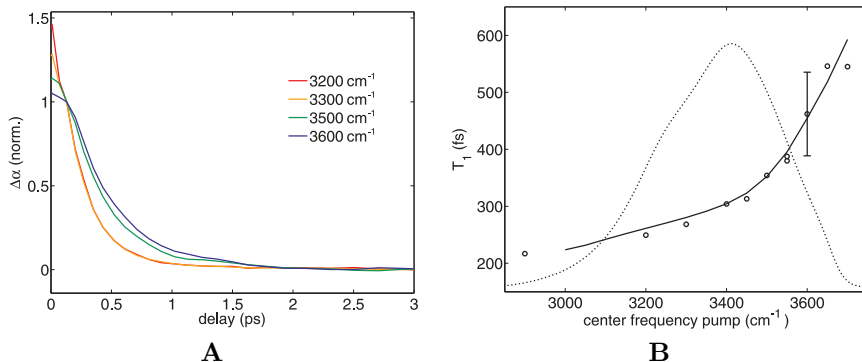


FIGURE 5.3. **(A)** Delay traces taken at 3050 cm^{-1} for measurements with the pump spectrum centered around various frequencies. The heat contribution is subtracted from this data according to the procedure described in the text. The vibrational relaxation is significantly slower when the OH-stretch band is pumped at its blue shoulder. **(B)** Relaxation time T_1 of the OH-stretch vibration obtained from the measured transient spectra as a function of the pump frequency. For low pump frequencies the relaxation time is similar to values that were found in other work. When the blue shoulder of the OH-stretch band is pumped, T_1 becomes up to a factor of 2.5 slower. The dotted line is the shape of the linear spectrum of the OH-stretch band. The solid line represents the result of a simulation, the details of which are elaborated on in the appendix, section 5.A.

By pumping the blue shoulder of the OH-stretch band we create an excited subset of OH oscillators that, at the time of excitation, are mainly in a weakly hydrogen-bonded state. This subset is clearly out of equilibrium. We can distinguish two processes that lead to relaxation to the equilibrium distribution. Firstly, the excitation energy may be transferred to another OH oscillator by Vibrational Resonant Energy Transfer (VRET), also called Förster transfer, a process that is caused mainly by dipole-dipole coupling [57, 58, 59]. This may be to a neighboring molecule or to an OH oscillator on the same molecule (intramolecular coupling). The donating and accepting oscillators should be in close vicinity of each other, since the rate of transfer is inversely proportional to the sixth power of their mutual distance. In addition, the rate of transfer is proportional to the overlap integral of the cross sections of both oscillators. A second contribution to the equilibration of the hydrogen-bond distribution is formed by translational motions of the water molecules that increase or decrease the oxygen-oxygen distance and thus the hydrogen-bond strength [60, 61, 62]. This last process is relatively slow ($\sim 1 \text{ ps}$ [63, 64, 65, 66, 60, 67, 68]).

VRET is known to cause extremely fast spectral diffusion in water [41]. It has even been claimed that within hundred femtoseconds *all* memory of the initial out-of-equilibrium excitation is lost and the excited subset smeared out over the full absorption band [69, 42]. Such a complete loss of memory is however

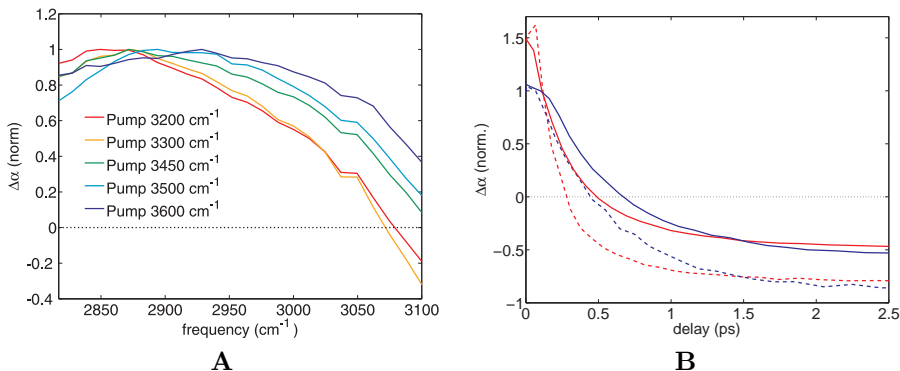


FIGURE 5.4. (A) The excited state spectra obtained from fitting the kinetic model described in the text to the transient spectra. For increasingly blue-shifted pump spectra the excited state spectra blue-shift as well. This progression indicates that spectral diffusion is incomplete on the timescale of the measurements (~ 1 ps). The spectra are normalized to their maximum value. (B) Delay traces at the H₂O-bend $\nu_{\text{bend}} = 1 \rightarrow 2$ (dashed lines) and OH-stretch $\nu_{\text{OH}} = 1 \rightarrow 2$ (solid lines) response upon pumping the OH-stretch band at 3400 cm^{-1} (red lines) and at 3600 cm^{-1} (blue lines). For all measurements the dynamics are slower when the OH-stretch band is pumped in its blue shoulder compared to when it is pumped in the center of the band. No thermalization contribution was subtracted and the curves are normalized at 200 fs.

incompatible with our current findings. We find that the vibrational lifetime is dependent on the excitation frequency. The vibrational lifetime for a sample pumped at the peak position of the OH-stretch band is less than $T_1 = 300$ fs. If equilibration was to happen on a 100 fs timescale, any oscillator excited at much higher frequencies would have equilibrated fast enough to effectively decay with $T_1 < 300$ fs. Our results thus imply that at the blue side of the spectrum VRET must become less efficient.

The qualitative molecular picture of the reduced rate of VRET is probably as follows. The concentration of oscillators that absorb on the blue extreme of the spectrum is low. Therefore the probability of finding other oscillators that are spectrally overlapping is also low. All adjacent oscillators likely have a considerably lower resonance frequency, and energy transfer to those oscillators is unfavorable. The transfer of vibrational energy from weakly bound oscillators to more strongly bound oscillators by VRET is thus suppressed. A quantitative description of this suppression is found in the appendix (section 5.A), in which we set up a model to simulate this effect. The solid line in Fig. 5.3 are the values of T_1 that result from this simulation and reproduce our experimental data very accurately.

The above arguments are based on the assumption that initially weak hydrogen-bonds remain weakly bound at least on the timescale of the vibrational relaxation (~ 500 fs). This is perfectly consistent with the timescale

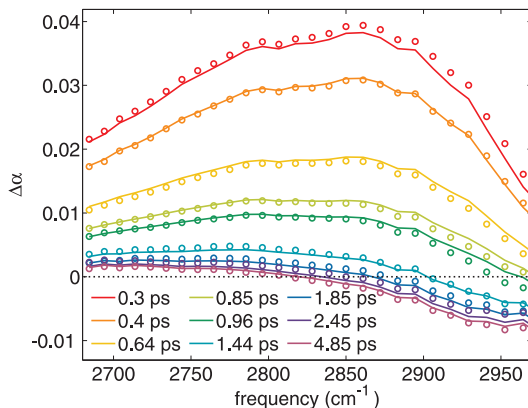


FIGURE 5.5. Transient spectra obtained for a measurement in which the OH-stretch overtone was pumped at 7000 cm^{-1} and the $\nu_{OH} = 1 \rightarrow 2$ transition was probed. The transient spectra show an induced absorption. This can be explained by an extremely fast relaxation of the overtone from the $\nu_{OH} = 2$ state to the $\nu_{OH} = 1$ state. The $\nu_{OH} = 1$ state decays significantly slower.

of translational motions. The translation of water molecules to increase or decrease the oxygen-oxygen distance occurs with a time constant of ~ 1 ps [66, 63, 65, 68, 67, 64, 60]. The suppression of the rate of spectral diffusion due to VRET is further evidenced by the shifted transient state spectra presented in Fig. 5.4A. For a pump spectrum that is tuned to 3600 cm^{-1} , the transient response is blue-shifted by more than 100 cm^{-1} compared to the transient response of a sample pumped at the maximum of the OH-stretch spectrum. An OH oscillator initially excited at the blue side of the spectrum thus remains blue on timescales on the order of 0.5 ps.

5.4 OVERTONES: RESULTS AND INTERPRETATION

5.4.1 OH-STRETCH OVERTONE

The most straightforward way to investigate the relaxation of the OH-stretch overtone vibration is to pump and probe the overtone band directly. The cross section of the overtone, however, is a factor ~ 500 times smaller than that of the OH-stretch fundamental (see Fig. 5.1). In a one-color experiment, the pump=probe signal is proportional to the square of the absorption cross section, and the signals would be too small to measure with our signal-to-noise ratio. We therefore pump the overtone and probe the $\nu_{OH} = 1 \rightarrow 2$ transition. The results from a measurement in which the pump was tuned to the maximum of the overtone band at 7000 cm^{-1} are shown in Fig. 5.5. The transient spectra have a strong resemblance to those obtained with the pump spectrum tuned to

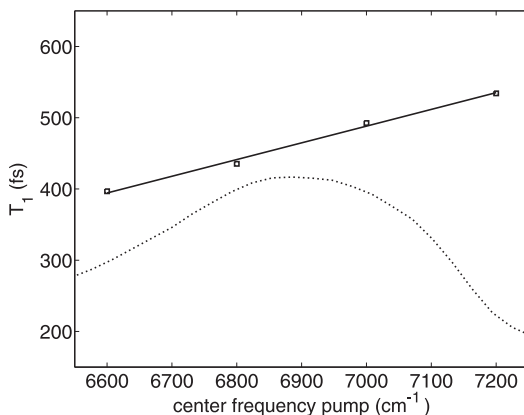


FIGURE 5.6. The vibrational relaxation times T_1 of $\nu_{OH} = 1 \rightarrow 0$ after excitation of the OH-stretch overtone at different frequencies (horizontal axis). Excitation of the blue shoulder of the overtone leads to a longer T_1 compared to an excitation at the red shoulder. The dotted line is the shape of the linear spectrum of the overtone band.

the blue side of the OH-stretch fundamental, shown in Fig. 5.2A. For early delay times we observe an induced absorption, which decays to a bleaching signal caused by the thermalized ground state. We use the same approach as before and globally fit a kinetic model for vibrational decay to the data to obtain the time constants T_1 . The results are summarized for various center frequencies of the pump spectrum in Fig. 5.6. The first thing to notice is that the T_1 values are again much larger than 200 fs. Secondly, there exist a dependence on the pump frequency: in case the overtone band is pumped at higher frequencies, the relaxation of the induced absorption measured at 2850 cm^{-1} decays slower.

When populating the $|\nu_{OH} = 2\rangle$ state, one naively may expect a bleach at the $\nu_{OH} = 1 \rightarrow 2$ transition (due to stimulated emission) and an induced absorption at the $\nu_{OH} = 2 \rightarrow 3$ transition. It may therefore seem somewhat surprising that the excitation of the OH-stretch overtone gives rise to an induced absorption at the frequencies of the $\nu_{OH} = 1 \rightarrow 2$ transition. The spectra of Fig. 5.5 thus imply that the overtone excitation is nearly instantaneously transferred to the $|\nu_{OH} = 1\rangle$ excitation, either by vibrational relaxation or by splitting of the overtone excitation into two $|\nu_{OH} = 1\rangle$ excitations.

The subsequent $\nu_{OH} = 1 \rightarrow 0$ relaxation occurs significantly slower than 200 fs. In addition, the transient state spectrum (transient spectrum at early delays in Fig. 5.5) is shifted to higher frequencies compared to the transient state spectrum after excitation of the OH stretch fundamental at 3300 cm^{-1} (Fig. 5.4A). There is thus a strong resemblance with the results obtained when the OH-stretch fundamental is pumped at 3600 cm^{-1} . Additionally, the vibrational lifetime T_1 increases when tuning the pump spectrum from 6600 cm^{-1} to 7100 cm^{-1} , similar to the increase in T_1 when tuning the pump spectrum

over the fundamental transition from 3400 cm^{-1} to 3600 cm^{-1} . Our interpretation of these results is that the OH-stretch overtone spectrum is dominated by weakly hydrogen-bonded OH oscillators. By pumping the maximum of the overtone band at 6900 cm^{-1} we apparently excite mainly those OH oscillators that have a weak hydrogen-bond, for which Förster transfer and vibrational decay is slower as was pointed out in section 5.3. This interpretation is supported by the spectral position of the OH stretch overtone spectrum. The OH oscillator is anharmonic and the $\nu_{OH} = 0 \rightarrow 2$ transition maximum is expected to be at a frequency of $\sim 6500\text{ cm}^{-1}$ ($3400+3100$), considerably lower than twice the fundamental transition energy (6800 cm^{-1}). From Fig. 5.1 it is clear that the maximum of the $\nu_{OH} = 0 \rightarrow 2$ band is actually higher than 6800 cm^{-1} . This maximum shift indicates that the $\nu_{OH} = 0 \rightarrow 2$ transition is much stronger for weakly hydrogen-bonded OH oscillators than for strongly hydrogen-bonded OH oscillators.

5.4.2 BEND-STRETCH COMBINATION TONE

Since the H_2O -bend/OH-stretch combination tone is stronger than the OH-stretch overtone, a direct pump-probe measurement (in which we probe the excited mode) could be performed. The transient spectra for different delay times obtained with both the pump and probe spectra centered at 5100 cm^{-1} are shown in Fig. 5.7. At short delay times an induced absorption is present at 5200 cm^{-1} . This signal is small, however, and rapidly decays into the much larger thermal difference spectrum. Close examination of the delay dependence at the frequencies for which the thermal difference spectrum is negligible ($\sim 5190\text{ cm}^{-1}$), reveals that the induced absorption decays on a $\sim 0.5\text{ ps}$ timescale. A detailed analysis is unfortunately challenging due to the overwhelming heat contribution.

For this reason we again probe the response of the $\nu_{OH} = 1 \rightarrow 2$ transition of the fundamental OH stretch vibration. The results of such a measurement for which the pump spectrum was centered at 5000 cm^{-1} are shown in Fig. 5.8A. The transient spectra show an induced absorption that is very similar to that observed when exciting the overtone (see Fig. 5.5). Since we excite the H_2O -bend/OH-stretch combination tone, this response can be naturally identified as the excited state absorption of the OH stretch vibration. The decay of the induced absorption is considerably slower than 200 fs . We analyzed the spectra in a similar fashion as was done in the previous sections. For three pump spectra, overlapping with different regions of the H_2O -bend/OH-stretch combination band, the normalized decay traces of the excited state are shown in Fig. 5.8B. We find that an excitation of the band at 5170 cm^{-1} results in a slightly slower relaxation time ($590 \pm 70\text{ fs}$) than an excitation at the red shoulder of the band ($500 \pm 70\text{ fs}$).

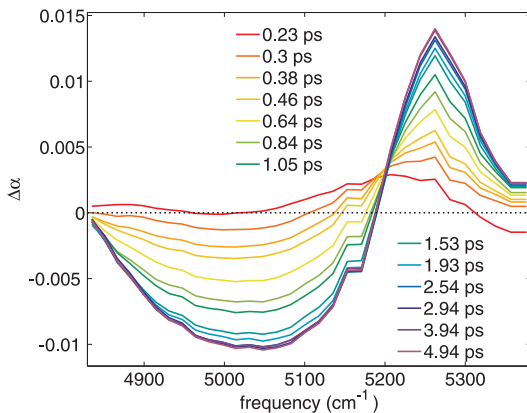


FIGURE 5.7. Transient spectra obtained for a measurement in which the OH-stretch/H₂O-bend combination tone is pumped and probed around at 5100 cm⁻¹. Already at quite short delay times the thermal difference spectrum is the dominant contribution. Around 5150 cm⁻¹ the transient spectra are positive for short delay times, decay through zero at about 550 fs and eventually equilibrate at negative values. This behavior is indicative for an induced excited state absorption at early delays.

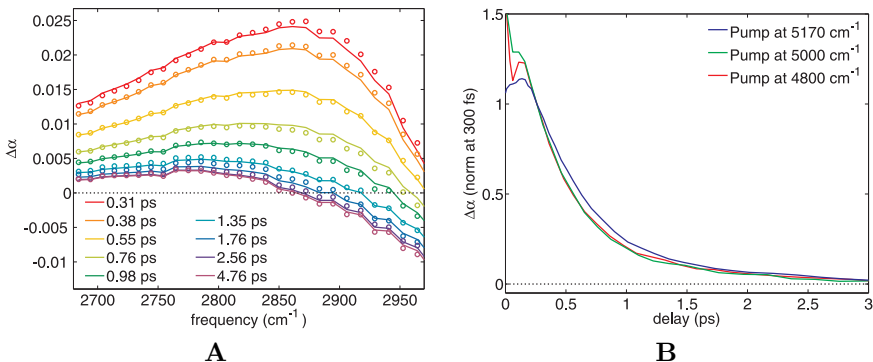


FIGURE 5.8. (A) Transient spectra obtained with the pump spectrum centered at 5000 cm⁻¹ and the probe at the $\nu_{OH} = 1 \rightarrow 2$ transition of the OH-stretch. (B) Delay trace of the measurement in panel A compared to a measurement in which the OH-stretch was pumped directly at 3400 cm⁻¹. The dynamics of the combination mode is considerably slower.

5.4.3 CALCULATION OF THE OVERTONE SPECTRUM OF HYDROGEN-BONDED OH GROUPS

In this section we will demonstrate that for strongly hydrogen-bonded oscillators, a cancellation occurs in the transition dipole moment to the overtone. This

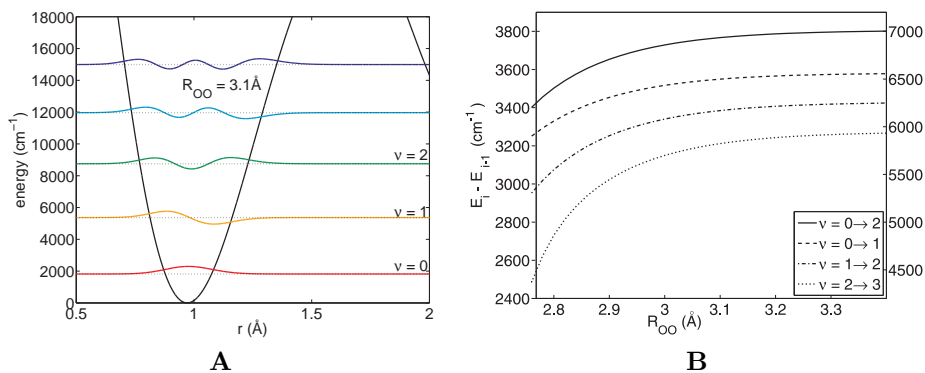


FIGURE 5.9. (A) The Lippincott-Schroeder potential as a function of the OH bond length r for an hydrogen-bonded OH-group of a water molecules. For the potential shown we used a hydrogen-bond length (oxygen-oxygen distance) of $R_{OO} = 3.1$ Å, corresponding to an oscillator donating a weak hydrogen-bond. The energy levels were calculated using a Numerov integration scheme. (B) The transition frequencies of $\nu_{OH} = 0 \rightarrow 1$ (dashed), $\nu_{OH} = 1 \rightarrow 2$ (dashed-dotted) and $\nu_{OH} = 0 \rightarrow 2$ (solid line, right axis) calculated for different hydrogen-bond lengths R_{OO} . Only weakly hydrogen-bonded OH groups have a $\nu_{OH} = 0 \rightarrow 2$ transition frequency higher than 6600 cm^{-1} .

cancelation explains why the OH-stretch overtone spectrum is dominated by weakly hydrogen-bonded OH oscillators. We analyze the linear overtone spectrum in the context of the Lippincott-Schroeder (LS) model, which has been shown to provide a good description of the coupling between the OH stretch vibration and the hydrogen-bond (see also section 2.1.3).

We calculate the wave functions of the LS-potential using a Numerov integration scheme for different hydrogen-bond lengths R_{OO} . Fig. 5.9A shows the LS-potential for an oxygen-oxygen distance of $R_{OO} = 3.1$ Å, with the calculated wave functions of the first four energy levels. The transition energies that correspond to the $\nu_{OH} = 0 \rightarrow 1$, $\nu_{OH} = 1 \rightarrow 2$, $\nu_{OH} = 2 \rightarrow 3$ and $\nu_{OH} = 0 \rightarrow 2$ transitions are shown as a function of hydrogen-bond length in Fig. 5.9B.

The transition probability of an excitation from the $|\nu_{OH}\rangle$ state to the $|\nu'_{OH}\rangle$ state is proportional to transition dipole moment $\mu_{\nu_{OH}\nu'_{OH}}$, which is the matrix element of the dipole moment operator $\hat{\mu}$ given by

$$\mu_{\nu_{OH}\nu'_{OH}} = \langle \nu'_{OH} | \hat{\mu} | \nu_{OH} \rangle, \quad (5.1)$$

where $\hat{\mu}$ is the dipole moment operator, defined in section 2.1.3. As discussed there, the transition dipole moment can be expanded for small displacements

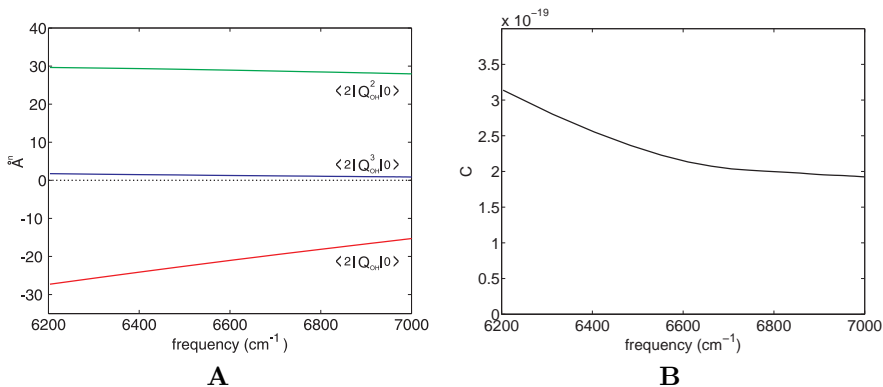


FIGURE 5.10. (A) The matrix elements of the linear, quadratic and cubic displacements of the $\nu_{OH} = 0 \rightarrow 2$ transition (the vertical axis is in units of \AA , \AA^2 or \AA^3 , respectively). The matrix elements were calculated for different hydrogen-bond lengths, which were mapped to the $\nu_{OH} = 0 \rightarrow 2$ transition frequency according to the relation in Fig. 5.9B. (B) The second derivative of the transition dipole moment as a function of the $\nu_{OH} = 0 \rightarrow 2$ transition frequency.

of the vibrational coordinate Q_{OH} around its equilibrium position,

$$\begin{aligned} \mu_{\nu_{OH}\nu'_{OH}} &= \left(\frac{d\hat{\mu}}{dQ_{OH}} \right)_0 \langle \nu'_{OH} | Q_{OH} | \nu_{OH} \rangle + \\ &\frac{1}{2} \left(\frac{d^2\hat{\mu}}{dQ_{OH}^2} \right)_0 \langle \nu'_{OH} | Q_{OH}^2 | \nu_{OH} \rangle + \dots \end{aligned} \quad (5.2)$$

Using the wave equations of the LS-potentials, we calculate the matrix elements for the $\nu_{OH} = 0 \rightarrow 2$ transition of the linear, quadratic and cubic displacements,

$$\langle 2 | Q_{OH} | 0 \rangle \quad (\text{linear}) \quad (5.3)$$

$$\langle 2 | Q_{OH}^2 | 0 \rangle \quad (\text{quadratic}) \quad (5.4)$$

$$\langle 2 | Q_{OH}^3 | 0 \rangle \quad (\text{cubic}) \quad (5.5)$$

for various hydrogen-bond lengths. The results are shown in Fig. 5.10A. The linear and quadratic displacements are of leading order, while the cubic (and higher, not shown) order contributions are much smaller. Note that the vertical axis shows the values in units of \AA , \AA^2 or \AA^3 , depending on the order of the displacement. Due to the opposite signs of the linear and quadratic displacements, a cancellation between the first and second term in Eq. (5.2) can occur. The first derivative of the dipole moment $\hat{\mu}$ increases with increasing hydrogen-bond strength (i.e. decreasing R_{OO}) and was empirically found to depend on

the fundamental transition frequency according to [54],

$$\frac{d\hat{\mu}}{dQ_{OH}}(\omega) \approx \left(1.21 + \sqrt{3.34 - \frac{2.15\omega}{\omega_f}} \right) \cdot 10^{-18} C; \quad (5.6)$$

where $\omega_f = 3719.65 \text{ cm}^{-1}$ is the absorption frequency of the free OH-stretch mode in the gas phase. The overtone absorption cross section $\sigma_{0,2}(\omega)$ is written as a function of the transition dipole moment as,

$$\sigma_{0,2}(\omega) = \frac{\pi\omega}{3\hbar c \varepsilon_0} |\mu_{0,2}(\omega)|^2 \quad (5.7)$$

The transition dipole moment $\mu_{0,2}(\omega)$ is given by Eq. (5.2). We used the calculated linear and quadratic displacements (Fig. 5.10A) and $d\hat{\mu}/dQ_{OH}$ from Eq. (5.6) to directly obtain $d^2\hat{\mu}/dQ_{OH}^2$ from Eq. (5.2) by ignoring the terms of higher order than Q_{OH}^2 . The overtone spectrum was described by the values of $d^2\hat{\mu}/dQ_{OH}^2$ shown in Fig. 5.10B. Fig. 5.11 demonstrates that for the values of the second derivative shown indeed a cancelation occurs between the first and second order terms in Eq. (5.2) for strongly hydrogen-bonded OH oscillators. The value of $d^2\hat{\mu}/dQ_{OH}^2$ increases for increasing hydrogen-bond strength (lower transition frequencies). This dependence has an intuitive rationalization: the stronger coulomb interaction of the OH group with the lone pair of the hydrogen-bond acceptor makes the transition dipole more non-linear in the Q_{sOH} displacement. However, due to the opposite signs of the $\langle 2|Q_{OH}|0\rangle$ and $\langle 2|Q_{OH}^2|0\rangle$ matrix elements, this leads to a cancelation of the first two terms in the transition probability (Eq. (5.2)) for strongly hydrogen-bonded OH oscillators and a domination of weakly hydrogen-bonded OH oscillators in the OH-stretch overtone band.

5.5 DISCUSSION

5.5.1 FREQUENCY DEPENDENCE OF THE OH-STRETCH VIBRATIONAL LIFETIME

Relaxation of the OH-stretch vibration leads to a very strong thermal response that almost completely obscures the transient response at the $\nu_{OH} = 0 \rightarrow 1$ transition frequencies [23]. This effect is similar in nature and even stronger than for example the thermalization response shown for the H₂O-bend/OH-stretch combination band in Fig. 5.7. To improve the determination of the vibrational lifetime of the OH-stretch vibration we therefore probed the induced absorption at the $\nu_{OH} = 1 \rightarrow 2$ transition in most experiments presented in this chapter. In pure liquid water this induced absorption is believed to arise from a combination of six transitions between the symmetric and asymmetric stretching vibrations [40], causing it to be significantly broader than the fundamental transition. Due to the anharmonicity of the OH-stretch mode the $\nu_{OH} = 1 \rightarrow 2$ band is red-shifted from the fundamental transition. It seems natural to assume

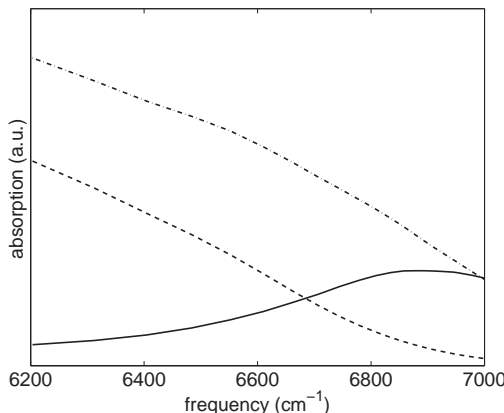


FIGURE 5.11. Calculated OH stretch overtone spectrum for the first-order contribution to the transition dipole moment μ_{02} (dashed line), the second order contribution to μ_{02} (dashed-dotted line) and both contributions (solid line). When both contributions are taken into account, an interference occurs for strongly hydrogen-bonded OH oscillators. The linear absorption spectrum of the overtone is with both terms well described.

that the lifetime of the $\nu_{OH} = 1 \rightarrow 2$ transition is identical to that of the $\nu_{OH} = 0 \rightarrow 1$ transition. However, in ice it was found that the $\nu_{OH} = 1 \rightarrow 2$ decay is about 10% faster than the $\nu_{OH} = 0 \rightarrow 1$ decay due to an intermediate state that is present in the decay channel [70, 71, 72]. The time constant of the $\nu_{OH} = 1 \rightarrow 0$ decay may therefore be 10% slower than the vibrational lifetime that we obtained from probing the $\nu_{OH} = 1 \rightarrow 2$ transition.

Various studies found a value of the OH-stretch vibrational lifetime $T_1 = 200$ fs [23, 73, 46, 44]. Ample evidence exists that the main pathway of vibrational decay is the H₂O-bend overtone centered at 3250 cm^{-1} [48, 74, 67, 46, 44, 75]. At elevated temperatures, the average hydrogen-bond strength decreases, leading to a blue-shift of the OH-stretch band and a red-shift of the H₂O-bend overtone. As a result the spectral overlap decreases, leading to an increase of T_1 [74, 67]. Even though the H₂O-bend overtone band overlaps with the red shoulder of the OH-stretch band, T_1 was always considered to be independent of frequency [46, 44]. This was explained by the paradigm that any inhomogeneity in the OH-stretch band is averaged out within 50 fs by spectral diffusion. The underlying mechanism of this rapid spectral diffusion is the ultrafast hopping of vibrational energy quanta between oscillators (Förster transfer) [57, 58, 59]. Blue-excited oscillators thus spectrally migrate within 50 fs to the red side of the spectrum by Förster transfer, where the overlap with the H₂O-bend overtone band acts as a sink for vibration decay.

In this chapter we have shown clear evidence that the vibrational lifetime in fact does depend on the excitation frequency. Such a dependence requires the excitation to keep its frequency for at least as long as the vibrational lifetime, in apparent contradiction to the presence of rapid Förster transfer within 50 fs.

However, we also observe a blue-shift of the transient spectrum with increasing excitation frequency (Fig. 5.4A), which implies that for high excitation frequencies ($> 3600 \text{ cm}^{-1}$), the excited oscillators do not spectrally equilibrate within 0.5 ps.

In the appendix we show that this observation is in fact consistent with the presence of Förster transfer. An oscillator that is excited in the very blue shoulder of the OH-stretch band, first needs to spectrally diffuse to overlap with the H_2O -bend overtone band in order to decay. However, the spectral overlap with this spectral region required for Förster hopping is very small. In addition, the probability of finding an oscillator with a more favorable spectral overlap nearby is small since the number density of such oscillators in the blue wing is small. As a result, the rate of Förster transfer from a donating OH oscillator resonant at 3700 cm^{-1} to an accepting OH oscillator overlapping with the H_2O -bend overtone band is about 20 times smaller than the rate from a donating oscillator at 3250 cm^{-1} to the same acceptor (Fig. 5.13). This result is in line with previous work that suggested that weakly hydrogen-bonded OH oscillators undergo slower spectral diffusion than strongly hydrogen-bonded OH oscillators [41]. Förster transfer thus strongly decelerates with increasing OH frequency. However, a significant deviation from the 200 fs decay time constant occurs only in the very blue shoulder of the absorption band, and this may explain why the frequency dependence was not noticed before [46, 44].

The lower Förster rate also has consequences for the reorientation dynamics probed by polarization resolved fs-IR pump-probe spectroscopy. This technique measures the reorientation dynamics of water by probing the decay of an anisotropically excited subset of OH-stretch oscillators [22]. In pure liquid water the anisotropy was found to decay nearly instantaneously [69, 40, 42]. This fast decay is not due to the reorientation of independent OH groups, but to the ultrafast hopping of the vibrational excitation to accepting OH modes with different orientation than the donating modes. Due to the slower Förster rates for OH oscillators with high OH-stretch frequencies, the anisotropy is expected to decay much slower upon excitation of the high-frequency wing of the absorption band. This is indeed what we observe (Fig. 5.12).

5.5.2 THE STRETCH OVERTONE AND STRETCH-BEND COMBINATION SPECTRA

It is surprising that excitation of the OH-stretch overtone ($\nu_{\text{OH}} = 0 \rightarrow 2$) leads to an induced absorption at $\nu_{\text{OH}} = 1 \rightarrow 2$ frequencies, where a bleach due to $\nu_{\text{OH}} = 2 \rightarrow 1$ stimulated emission would be expected. There are two possible explanations for this observation. First, the induced absorption may arise from a $\nu_{\text{OH}} = 2 \rightarrow 3$ or even $\nu_{\text{OH}} = 2 \rightarrow 4$ transition. We performed an analysis in the framework of the Lippincott-Schroeder model and find that especially the $\nu_{\text{OH}} = 2 \rightarrow 4$ transition can have a considerable cross section in the probed spectral region. Both cross section and transition frequency however strongly depend on the hydrogen-bond strength (defined by the oxygen-oxygen distance). Since we do not see such a strong difference of the transient response

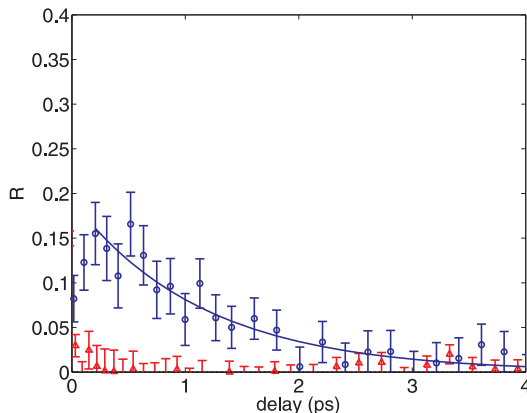


FIGURE 5.12. The anisotropy dynamics of the OH stretch vibration in pure water after excitation at 3650 cm^{-1} (circles) or 3400 cm^{-1} (triangles). The probed frequency is 3500 cm^{-1} , at which the thermal response is zero. Excitation at 3400 cm^{-1} is followed by an instantaneous drop of the anisotropy to zero. Consistent with the lower rate of Förster transfer, the reorientation dynamics after excitation at 3650 cm^{-1} have a component that is much slower than those after excitation at 3400 cm^{-1} .

for different pump frequencies, this explanation can be ruled out. The induced absorption can more likely be identified as the $\nu_{OH} = 1 \rightarrow 2$ transition. The presence of this feature in the transient spectrum for pump-probe delay times of 200 fs therefore implies an ultrafast relaxation of $\nu_{OH} = 2 \rightarrow 1$. Possibly, a single OH oscillator excited in the $|\nu_{OH} = 2\rangle$ state rapidly transfers one quantum of vibrational energy to a neighboring oscillator, resulting in two $|\nu_{OH} = 1\rangle$ excitations.

The subsequent $\nu_{OH} = 1 \rightarrow 0$ decay is $T_1 = 450 \pm 50$ fs, much slower than the main relaxation time after excitation of $\nu_{OH} = 0 \rightarrow 1$ fundamental transition directly ($T_1 \approx 200$ fs). In addition, we observe that the $\nu_{OH} = 1 \rightarrow 2$ induced absorption spectrum is more blue-shifted after excitation of the overtone compared to the induced absorption after excitation of the fundamental transition at 3400 cm^{-1} (Fig. 5.4A). It rather resembles the $\nu_{OH} = 1 \rightarrow 2$ spectrum after excitation of the very blue wing of the fundamental transition. It may be argued that these effects are due to a temperature increase of the environment in close vicinity of the excited oscillator due to the thermalization of one of the two OH stretch quanta. The thermalization of the vibrational energy was however found to be on a picosecond timescale, much slower than the vibrational lifetime of the OH stretch [23, 46, 75]. In addition, the temperature dependence of T_1 that has been reported is too small to account for the large effect that we observe [74, 67]. Instead, we assign the blue-shifted induced absorption and slower T_1 to the predominant excitation of weakly hydrogen-bonded OH groups. This is because that the OH stretch overtone spectrum is dominated by such species. This interpretation is in line with previous work that suggested that

the overtone spectrum of the OH stretch vibration of HDO molecules in D₂O can be explained by a strong dependence of the transition dipole moment on the hydrogen-bond strength [54], see also section 5.4.3.

The rich structure of bands in the OH-stretch overtone band of HDO has in several studies been interpreted as arising from different hydrogen-bonding species in water [76, 56, 45]. Similar suggestions have been made for pure liquid water: By dissolving a small amount of pure water in acetone, the otherwise smooth overtone spectrum breaks up in several peaks of which the relative amplitudes change with temperature [55]. These studies made a very discrete separation of 1, 2 or 3 hydrogen-bonded species [76, 56, 55, 45], a picture that is not supported by modern molecular dynamics simulations [77, 78]. Based on a theoretical interpretation of the linear absorption spectrum of HDO:D₂O, the overtone spectrum could be well explained from a destructive interference effect in the cross section of the overtone transition of strongly hydrogen-bonded water molecules [54]. Hence, instead of a discrete division in species, the calculations show that the electrical and mechanical anharmonicities have different dependencies on the hydrogen-bond strength. Their contributions to the transition dipole moment destructively interfere for some hydrogen-bond strengths and yield a net transition dipole moment for others.

We find strong evidence that in pure liquid H₂O a similar cancelations occurs. The absorption spectrum of the OH stretch overtone in pure H₂O has its maximum at 6900 cm⁻¹, more than twice the average frequency of the fundamental transition. The strongly anharmonic potential of the OH stretch vibration rather predicts a frequency maximum around 6500 cm⁻¹ (Fig. 5.9B). This would indeed be the case if non-Condon effects could be neglected. Non-Condon effects, the dependence of the transition dipole moment on the low-frequency (hydrogen-bond) coordinates, are however strong in water [15]. The transition dipole moment of the fundamental OH stretch transition μ_{01} strongly depends on the hydrogen-bond strength of the oscillator. In fact, the number density of weakly hydrogen-bonding OH groups that have their resonance frequency at 3600 cm⁻¹ has been found to be quite large. However, since their μ_{01} is much smaller than that of strongly hydrogen-bonded OH groups, their contribution to the linear spectrum of the fundamental transition is small [15, 68, 79, 7]. For the overtone transition dipole moment μ_{02} , the dependence on the hydrogen-bond strength is reversed due to the interference of the electrical and mechanical anharmonicities (section 5.4.3). We found that μ_{02} strongly depends on the hydrogen-bond strength and almost completely disappears for strongly hydrogen-bonded OH oscillators. The overtone spectrum is thus dominated by weakly hydrogen-bonded OH oscillators.

These considerations based on the linear spectra and the Lippincott-Schroeder model are perfectly in line with our experimental results. OH oscillators with a $\nu_{OH} = 0 \rightarrow 2$ transition frequency at the overtone maximum of 6900 cm⁻¹, have a fundamental transition of ~ 3600 cm⁻¹. The relatively large number density that was found for oscillators resonant at 3600 cm⁻¹ therefore also contributes to the large overtone cross section at 6900 cm⁻¹. The vibrational lifetimes that we find after an excitation at 3600 cm⁻¹ or 6900 cm⁻¹ match perfectly.

The results on the H₂O-bend/OH-stretch combination band suggest a similar frequency dependence of the transition dipole moment. After excitation of this band, we find an induced absorption at the $\nu_{OH} = 1 \rightarrow 2$ frequencies with similar characteristics as we found after excitation of the OH stretch overtone band: a blue-shifted excited state response and a relatively long vibrational lifetime ($T_1 = 500 \pm 70$ fs). In analogy to the overtone band, the combination band shows a very asymmetric tail towards lower frequencies and has a maximum at a higher frequency (5150 cm^{-1}) than the sum of the H₂O-bend and OH-stretch band maxima ($\omega_{01,bend} + \omega_{01,OH} = (1640 + 3400) \text{ cm}^{-1}$). The anharmonic coupling between the two vibrations [80], would rather suggest a lower transition frequency for the combination band.

For the transition dipole moment $\mu_{(0,0),(1,1)}$ of an excitation of the H₂O-bend/OH-stretch combination tone $\nu_{bend}, \nu_{OH} = (0, 0) \rightarrow (1, 1)$ a similar analysis as for the overtone (Eq. (5.2)) can be made. The first and second-order contributions to $\mu_{(0,0),(1,1)}$ can be written as,

$$\begin{aligned} \mu_{(0,0),(1,1)} = & \left(\frac{d\hat{\mu}}{dQ_{OH}} \right)_0 \langle \nu_{bend/OH} = 1 | Q_{OH} | (0, 0) \rangle + \\ & \frac{1}{2} \left(\frac{d^2\hat{\mu}}{dQ_{OH}^2} \right)_0 \langle \nu_{bend/OH} = 1 | Q_{OH}^2 | (0, 0) \rangle + \\ & \frac{1}{2} \left(\frac{d^2\hat{\mu}}{dQ_{OH}dQ_{bend}} \right)_0 \langle \nu_{bend/OH} = 1 | Q_{OH}Q_{bend} | (0, 0) \rangle \end{aligned} \quad (5.8)$$

where the bend/stretch combination wave function can be written as a mixed state,

$$|\nu_{bend/OH} = 1\rangle = \alpha |1, 1\rangle + \beta |0, 2\rangle + \gamma |0, 1\rangle, \quad (\alpha^2 + \beta^2 + \gamma^2 = 1) \quad (5.9)$$

in which the wave function of the H₂O-bend/OH-stretch combination tone is a superposition of the product wave function $|1, 1\rangle$ of the $\nu = 1$ states of the uncoupled stretch and bend vibrations, the wave function of the OH stretch first excited state $|0, 1\rangle$ and that of the OH stretch overtone state $|0, 2\rangle$. The amplitude of $\mu_{(0,0),(1,1)}$ does not only depend on the amplitudes of the dipole moment derivatives, but also on the anharmonic coupling between the H₂O-bend and OH-stretch modes. Evidence exists that the wave functions of the vibrational modes in water all show a very mixed behavior [9]. The $|0, 1\rangle$ term will add a large contribution to the transition dipole moment, which could explain the surprisingly large cross section of the combination band. These latter wave functions are admixed by anharmonic couplings like $Q_{OH}^2 Q_{bend}$ or even by a linear coupling $Q_{OH} Q_{bend}$. The shape and position of the combination band suggest that for this band a similar destructive interference effect in the cross section occurs as for the overtone band. The mixing of the overtone wave function for example yields a similar interference behavior as was described above in the first and second term in Eq. (5.8) in case the $|1, 1\rangle$ state is replaced by the superposition state Eq. (5.9).

5.6 CONCLUSIONS

We studied the inhomogeneity of some of the most important vibrational absorption bands of pure water: the OH stretch fundamental band, the OH stretch overtone band and the H₂O-bend/OH-stretch combination band. We measured the vibrational relaxation of the $|\nu_{OH} = 1\rangle$ state by probing the induced absorption at the $\nu_{OH} = 1 \rightarrow 2$ transition after excitation of these bands at different frequencies. We find that the spectral position of the induced absorption blue-shifts for excitation frequencies that are higher than the average OH stretch absorption frequency ($> 3400 \text{ cm}^{-1}$). The excited vibrations thus keep the same resonant frequencies on the timescale of the experiment ($\sim 0.5 \text{ ps}$). Normally, ultrafast spectral diffusion by vibrational resonant excitation (Förster) transfer would equilibrate any inhomogeneity within a few hundred femtoseconds. However, the number density of oscillators in the high frequency wing of the absorption band is relatively small and have an unfavorable spectral overlap with nearby chromophores. The Förster transfer rates are therefore low for these oscillators and spectral diffusion is mostly determined by structural diffusion (1 ps). Excitation of the OH stretch fundamental band at frequencies $\geq 3600 \text{ cm}^{-1}$ yields a much longer T_1 than excitation at the center or on the low frequency wing of the band. The longer T_1 for high excitation frequencies follows from an unfavorable overlap of the resonance frequency of high-frequency OH oscillators with the H₂O-bend overtone band at 3250 cm^{-1} , which is the main decay channel of the OH stretch vibration.

After excitation of the OH-stretch overtone at 6900 cm^{-1} , the oscillators decay within $< 100 \text{ fs}$ to the $|\nu_{OH} = 1\rangle$ state. For this reason we observe an induced absorption at the $\nu_{OH} = 1 \rightarrow 2$ transition that is very similar to the response after excitation of the OH stretch fundamental. The induced absorption after excitation of the OH-stretch overtone is equally blue-shifted and its vibrational decay is equally slow as after direct excitation of the OH stretch fundamental at 3600 cm^{-1} . This shows that the overtone band is dominated by weakly hydrogen-bonded OH oscillators. An analysis in the context of the Lippincott-Schroeder model of the OH stretch vibration reveals that a cancellation occurs in the transition dipole moment of strongly hydrogen-bonded OH oscillators. The OH oscillators that are probed after excitation of the OH stretch overtone band at 6900 cm^{-1} have the same hydrogen-bond strength as the oscillators excited in the OH stretch fundamental band at 3600 cm^{-1} . This explains why their spectral response and vibrational lifetime are identical. For the stretch-bend combination tone we observe similar results, i.e. a blue-shifted spectrum and a relatively slow vibrational relaxation. This result indicates that for the stretch-bend transition a similar destructive interference effect occurs as for the overtone.

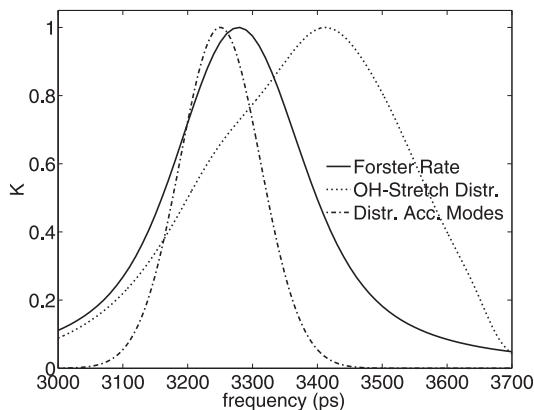


FIGURE 5.13. Relative Förster rates (solid line) from donating oscillators (horizontal axis) to a distribution of oscillators overlapping with the H₂O-bend overtone (dashed-dotted line). At 3600 cm⁻¹ the rate of transfer is more than 10 times lower than for oscillators resonant around 3250 cm⁻¹.

5.A APPENDIX: FÖRSTER TRANSFER

The rate for Förster transfer k_{DA} from a donating oscillator D to an accepting oscillator A is proportional to the overlap integral of their spectra $\sigma_D(\nu)$ and $\sigma_A(\nu)$, respectively, and inversely proportional to their distance \vec{R} to the sixth power according to [58],

$$k_{DA} \propto \frac{C}{|\vec{R}|^6} \int d\nu \sigma_D(\nu) \sigma_A(\nu) \quad (5.10)$$

where C is a prefactor containing the transition dipole moments of both oscillators and a geometrical factor that accounts for the relative orientations of the oscillators. Here, we will consider relative values of k_{DA} and assume an isotropic distribution of oscillators such that C can be treated as a constant. All oscillators are assumed to have a Lorentzian line profile at a certain center frequency ν_c ,

$$\sigma(\nu) = L(\nu - \nu_c) = L_{\nu_c}(\nu), \quad (5.11)$$

with the homogeneous linewidth gradually increasing from 40 cm⁻¹ at the low frequency wing of the spectrum to 80 cm⁻¹ at the high frequency wing of the spectrum.

We calculate $k_{DA}(\nu_{c,D}, \nu_{c,A})$ for a single donating oscillator with center frequency $\nu_{c,D}$ and an accepting oscillator with center frequency $\nu_{c,D}$. The density of oscillators in the bath as a function of their center frequencies is assumed to follow a distribution function $G(\nu)$ that is normalized such that,

$$\int d\nu G(\nu) = 1 \quad (5.12)$$

Eventually, we will take the normalized linear spectrum of the OH-stretch band as the distribution function. This is an approximation, as the cross section of blue OH oscillators is in fact smaller than that of red oscillators. If ρ is the density of oscillators, then $R_0 = (3/4\pi\rho)^{1/3}$ denotes the radius around an oscillator that contains one other oscillator. With the distribution function $G(\nu)$ the number of oscillators $\eta(r, \nu_{c,A})$ that have their center frequency at $\nu_{c,A}$ in a sphere of radius r is then given by,

$$\eta(r, \nu_{c,A}) = \left(\frac{r}{R_0}\right)^3 G(\nu_{c,A}) \quad (5.13)$$

The exact value of R_0 will be divided out when normalizing the rates and is thus of no importance. The number density $N(R, \nu_{c,A})$ of accepting oscillators at $\nu_{c,A}$ at a spherical shell of radius R and thickness dR around the donating oscillator is thus given by,

$$N(R, \nu_{c,A}) = \frac{3R^2}{R_0^3} G(\nu_{c,A}) dR \quad (5.14)$$

The rate k_{DA} for Förster transfer from an excited oscillator with center frequency $\nu_{c,D}$ to an accepting oscillator with center frequency $\nu_{c,A}$ is thus,

$$k_{DA}(\nu_{c,D}, \nu_{c,A}) = \int_{R_0}^{\infty} dR \int d\nu \frac{C}{|R|^6} N(R, \nu_{c,A}) L_{\nu_{c,D}}(\nu) L_{\nu_{c,A}}(\nu) \quad (5.15)$$

where the integration over R has a lower boundary cut-off at the radius R_0 .

As a first comparison we assume a distribution of accepting modes $B(\nu)G(\nu)$, where $B(\nu)$ is the lineshape of the overtone of the bending vibration. The exact shape of this band is not known for pure liquid water, but for our purpose we assume a linewidth which is 1.5 times that of the fundamental bend (88 cm^{-1}) and a center frequency of 3250 cm^{-1} . The total rate $K(\nu_{c,D})$ for transfer from a subset of donating oscillators $L_{\nu_{c,D}}(\nu)$ to the distribution overlapping with the bend overtone is found when we integrate over the accepting modes distribution,

$$K(\nu_{c,D}) = \int d\nu_{c,A} k_{DA}(\nu_{c,D}, \nu_{c,A}) B(\nu_{c,A}) G(\nu_{c,A}) \quad (5.16)$$

This integral is evaluated for different center frequencies $\nu_{c,D}$ of the donating oscillator. The results are normalized to the maximum rate and shown in Fig. 5.13. There is a strong frequency dependence of K . At 3600 cm^{-1} the transfer rate is more than a factor of 11 slower compared to 3250 cm^{-1} .

To get a description of the population dynamics, we performed a simulation that also includes dynamics effects other than Förster transfer. To this end, we divide the OH stretch linear absorption spectrum between 3000 cm^{-1} and 3800 cm^{-1} in bins with a lorentzian absorption profile with central frequencies ν_i , 2 cm^{-1} apart. Förster transfer from bin i to bin j is calculated according to

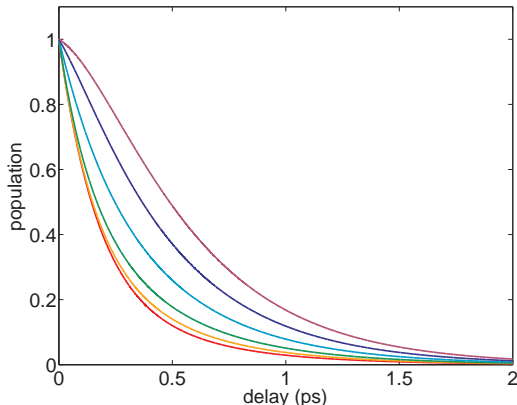


FIGURE 5.14. Population dynamics simulated for an initial population in frequency bins between 3000 cm^{-1} and 3700 cm^{-1} , with steps of 100 cm^{-1} (red to blue curves) according to the model described in the text. The population dynamics becomes much slower at blue excitation frequencies in spite of ultrafast Förster transfer. The time constants of exponential fits to the curves between 0.2 and 1 ps are shown in Fig. 5.3B.

Eq. (5.15). The rates are normalized such that the rate from an oscillator in the center of the band to any other oscillator is,

$$\int d\nu k_{DA}(3400, \nu) = 20\text{ps}^{-1}. \quad (5.17)$$

In addition to Förster transfer, reorientational jumps and structural diffusion also lead to spectral diffusion. The jump rate is assumed to be $k_j = 0.5\text{ ps}^{-1}$ for bins higher than 3500 cm^{-1} and zero for others. Oscillators that undergo a reorientational jump are distributed over all other bins according to the distribution function $G(\nu)$. Structural diffusion is described by letting bins exchange population with their neighbors with rate constants that depend on the slope of $G(\nu)$,

$$k_{s,i \rightarrow i+1} = k_g G(\nu_{i+1}) / G(\nu_i) \quad (5.18)$$

where k_g is related to the time constant of the frequency correlation function $\tau_c = 700\text{ fs}$ according to $k_g^{-1} = \tau_c(1 - \sqrt{1 - 4/w^2})$ [81]. Here is w the half width at $1/e$ of the maximum of the equilibrium distribution. For our simulation and bin size, this yields $k_g^{-1} = 1.0\text{ fs}$.

The decay rate of the OH stretch vibration is assumed to be proportional to the spectral overlap of the lorentzian lineshape of a certain bin and the H_2O -bend overtone,

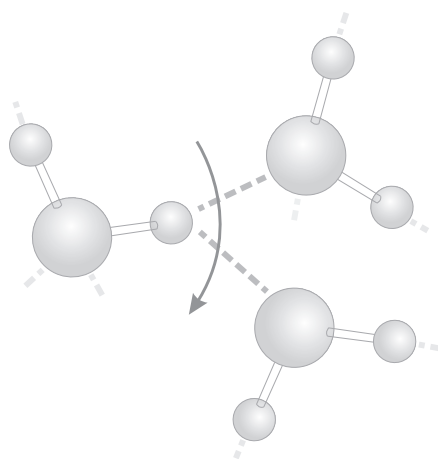
$$k_b(\nu_i) \propto \int d\nu L_{\nu_i}(\nu) B(\nu) \quad (5.19)$$

The rates are normalized such that the rate for oscillators with the maximum spectral overlap $k_b(\nu = 3250) = 1/170\text{ fs}^{-1}$. Bins at lower frequencies than 3250 cm^{-1} are all assumed to have a decay rate of $1/170\text{ fs}^{-1}$ (due to strong

coupling). As initial condition, one bin at a particular frequency contains a population (is assumed to be excited). The subsequent population dynamics are obtained by iteration over time with a step size of 0.2 fs. For a number of excitation frequencies (bins), the results are shown in Fig. 5.14. Exponential fits to the dynamics between 0.2 and 1 ps yield the vibrational relaxation times that are shown as a solid line in Fig. 5.3B. The experimental results are very well reproduced.

6

Experimental Study of the Jump-Reorientation of Water



Molecular dynamics simulations showed that the largest contribution to the reorientation of water molecules is formed by hydrogen-bond switching events, in which a water molecule breaks a hydrogen-bond and forms a new one with another water molecule. This change of hydrogen-bonding partners was found to happen over large sudden jumps rather than in a continuous fashion. We use pump-probe spectroscopy on the OD-stretch vibration of HDO molecules in water to measure the reorientation of the vector along the transition dipole of this vibrational mode. **We find experimental evidence that supports the jump mechanism of water reorientation.** We also find that for increasing temperatures both the rate of spectral diffusion and the reorientation dynamics become faster. The activation energy that we obtain from the spectral diffusion data is 2.6 ± 0.5 kcal/mol.

6.1 INTRODUCTION

The hydrogen-bond network of water is both robust and dynamic at the same time. The binding energy of a hydrogen bond is 5.0 kcal/mol, about one twentieth of the OH covalent bond energy and still well above the energy of thermal fluctuations at room temperature. This does not mean that hydrogen-bonds do not easily break. Water molecules switch hydrogen-bonding partners at a rate of 0.3 ps^{-1} [61, 2, 68, 82, 3]. In this concerted process, the hydrogen-bond is never completely broken, but the hydroxyl group rather forms an intermediate bifurcated hydrogen-bond to the oxygen atoms of two nearby water molecules [2]. It was found that this transition state lowers the activation energy of a hydrogen-bond switch to about 3.1–3.5 kcal/mol [83, 84, 85, 86, 87, 88].

The transition through the bifurcated state happens on a timescale of 100 fs and involves a large angular jump of the hydroxyl group [2]. Classical molecular dynamics (MD) simulations found this process to be the main contributor to the molecular reorientation of water [2, 86]. For increasing temperatures the reorientation of water has been found to become faster and it is therefore likely that the jump mechanism speeds up. This chapter aims at obtaining more knowledge on the jumping process and its temperature dependence.

The stretching vibration of the hydroxyl groups is particularly sensitive to its chemical environment and offers an ideal probe of the hydrogen-bond network. A strong hydrogen-bond leads to a red-shift of the resonance frequency of the OH stretch vibration, whereas a weak hydrogen-bond leads to a blue-shift. The transition state of a molecular jump can be regarded as a very weak hydrogen-bond [89]. The evolution from a linear hydrogen bond to the bifurcated transition state is therefore accompanied by a large change in vibrational frequency. Therefore there exists an intimate relation between the reorientation of water and spectral diffusion of the OH stretch vibrational frequency.

We use the strong coupling of the hydrogen-bond to the OH stretch vibration to study the jump reorientation of water molecules at different temperatures. To this end, we performed two-color infrared pump-probe spectroscopy on neat (isotopically diluted, 8% D_2O in H_2O) liquid water. By using a narrow-band excitation pulse positioned the blue wing of the OD stretch vibrational band, we excite the stretch vibration of a subset of OD groups that donate very weak hydrogen-bonds. These OD groups have a much higher chance of being within a few hundred femtoseconds from a reorientational jump compared to OD groups that donate hydrogen-bonds of average strength [89]. We first analyze the isotropic response, including spectral diffusion. Subsequently we consider the reorientation dynamics of OD groups with different hydrogen-bond strengths, first at room temperature and finally for elevated temperatures.

6.2 EXPERIMENTAL

The measurements in this chapter were performed using the two-color setup described in section 3.1.2 with the central frequency of the probe spectrum

tuned to 2200 cm^{-1} , 2550 cm^{-1} or 3000 cm^{-1} . For some of the measurements we used a spectrally broad pump pulse (full width half maximum (FWHM) 200 cm^{-1}), tuned to the center of the OD stretch band at 2500 cm^{-1} . Such a spectral shape of the pump assures a homogeneous excitation of OD oscillators over the whole absorption band. For most measurements we used a spectrally narrow pump pulse (FWHM 60 cm^{-1}) to selectively excite a part of the OD-stretch oscillators in their first excited state. With the center frequency tuned to the blue shoulder of the absorption band (eg. 2650 cm^{-1}), preferably OD groups that have a very weak hydrogen-bond will be excited. To make pulses with such a narrow spectrum, the idler coming from the TOPAS was frequency doubled to $\sim 1000\text{ nm}$ using a BBO crystal of 4 mm thickness. We thereby used the narrow acceptance bandwidth of the crystal to generate pulses that are spectrally more narrow. To generate mid-infrared pulses we performed difference frequency mixing of this pulse with 1 mJ pulses of 800 nm in a lithiumniobate crystal with a length of 10 mm. The use of this relatively long crystal was to narrow the spectral bandwidth even further. The generated light pulses that we eventually obtained had a pulse energy of $16\text{ }\mu\text{J}$.

We used D_2O (99.9 % pure, Sigma Aldrich) and millipore water to make isotopically diluted water samples (8 mol% D_2O in H_2O). We used this isotope ratio to obtain an optimal contrast between the signal from the OD-stretch vibration and the undesired thermalization of excited OH-stretch vibrations. Resonant Förster energy transfer is at this HDO concentration still quite limited [26]. The sample cell consisted of a stainless steel ring with two calcium fluoride windows (0.5 mm), pressed against each other with a $25\text{ }\mu\text{m}$ spacer in between. For the temperature dependent measurements we used a peltier element with dedicated controller to heat up the aluminium base plate of the sample cell. A thermocouple attached to the sample cell was used to maintain a constant temperature ($\Delta T \approx \pm 1\text{ K}$) in the temperature range between 295K and 343K.

6.3 RESULTS AND DISCUSSION

6.3.1 THERMALIZATION DYNAMICS AND SPECTRAL DIFFUSION

The isotropic transient spectra are constructed from the parallel and perpendicular data using Eq. (4.2) and are shown in Fig. 6.1. The transient spectra for short delay times show a bleach at blue frequencies. With increasing delay times this bleach shifts to lower frequencies and decays. The frequency shift within the first picosecond is attributed to fast spectral diffusion of the excited oscillators. After 30 ps the spectrum is not changing anymore with further increasing delay time within the experimentally accessible range (1 ns). This quasi-static spectrum is the thermal difference spectrum elaborated on in section 4.3.

Immediately after excitation, the thermal difference spectrum is already relatively large with respect to the excited state response. Previous measurements on the same system with a spectrally broad pump centered around the center of the OD stretch band (2500 cm^{-1}) yielded a thermal difference spectrum

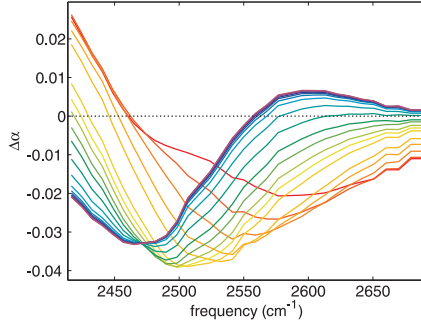


FIGURE 6.1. Raw isotropic transient spectra for pump-probe delay times between 0.09 ps (red line) and 50 ps (purple line). At short delay times the transient spectra mainly show a bleach at frequencies $>2450 \text{ cm}^{-1}$. The bleach subsequently shifts to the red and decays. At long delay times the transient spectrum takes the form of a thermal difference spectrum.

with a relatively smaller amplitude (data not shown, [24]). In principle this could be due to very fast relaxation of OD oscillators within the first hundred femtoseconds or so. This would require a strong coupling between those OD oscillators and their environment. However, since the pump spectrum is tuned to the blue side of the OD-stretch spectrum, the excited subset of OD oscillators rather contains weakly coupled oscillators. More likely is that the pump also excites OH oscillators which are relaxing with a time constant of $\approx 200 \text{ fs}$ [74]. Although 2650 cm^{-1} is far off from the OH-stretch maximum at 3400 cm^{-1} , the cross section of the OH vibrations is non-zero due to the large amplitude of the band and inhomogeneous broadening. Since the OD-stretch band is pumped off-center, the relative contribution of the OH-stretch excitation is non-negligible and leads to a fast thermal response. More details on this collateral excitation can be found in section 2.2.

To obtain the reorientation dynamics using Eq. (4.18) we need to subtract the heating contribution from the parallel and perpendicular data. In previous work this was achieved by fitting a kinetic relaxation model to the isotropic data. As we have pointed out above, though, the transient spectra in Fig. 6.1 contain highly non-trivial thermalization dynamics. In addition, the excited state contribution is complicated due to the spectral diffusion. This renders the use of a simple kinetic model close to impossible. Therefore, we obtained the thermalization dynamics by probing the large thermal difference spectrum at the shoulder of the OH-stretch band at 3000 cm^{-1} (details are described in section 4.3). At this frequency there is no contribution of the excited OD oscillators and the thermalization dynamics can be measured directly. These dynamics are used to subtract the thermal difference spectrum from the data of Fig. 6.1. An additional advantage of this method is that no assumptions need to be made on the rate and mechanism of the relaxation of the OD vibrations.

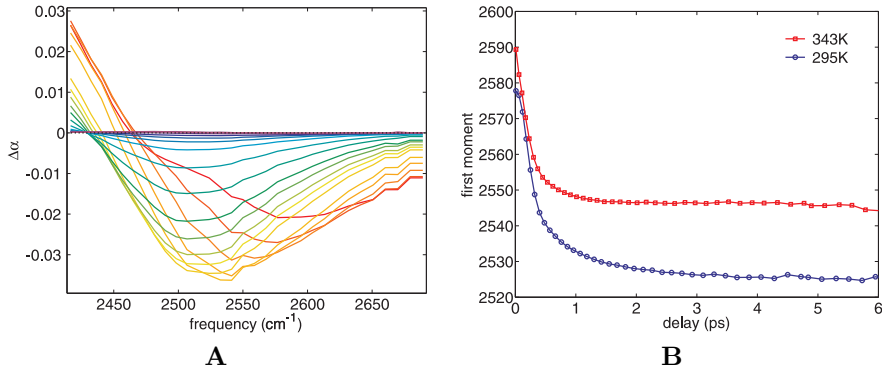


FIGURE 6.2. **(A)** Isotropic transient spectra from which the thermalization component is subtracted. The first moment of the spectra is plotted in panel **(B)** for sample temperatures of 295K and 343K. The time evolution of the first moment reflects the spectral diffusion in the samples. At delay times >1 ps an equilibrium is reached. At 343K the spectral diffusion is faster and the center of the band is blue-shifted by 20 cm^{-1} .

The isotropic data obtained after subtraction of the thermal difference spectrum are shown in Fig. 6.2A. The spectral diffusion is apparent as a red-shift of the spectral maximum and the zero-crossing with increasing delay times. To quantify the spectral diffusion we evaluate the first moment M_1 of the negative (bleaching) part of the heat-corrected transient spectra. The first moments are plotted as a function of the pump probe delay time in Fig. 6.2B. In anticipation to the temperature dependent measurements presented later in this chapter, M_1 is shown for sample temperatures 295K and 343K. The first thing to notice is that within a few hundred femtoseconds M_1 has already relaxed to $\sim 2560 \text{ cm}^{-1}$. The decay progresses still further in the subsequent 1.5 ps and equilibrates at 2530 cm^{-1} . At 343K the endlevel of M_1 is higher and the decay is somewhat faster than at 295K.

Before we interpret the dynamics of the M_1 decays we explain why it does not start at 2650 cm^{-1} , the maximum of the excitation spectrum. The OD stretch band is an inhomogeneously broadened collection of homogeneous lorentzian lineshapes, the number density of which falls off in the wings. The overlap of the spectrum of the excitation pulse at 2650 cm^{-1} with the lineshapes of OD oscillators red-shifted from 2650 cm^{-1} is larger than that with OD oscillators that are resonant at 2650 cm^{-1} . As a result, the maximum of the number density of excited OD oscillators is at 2610 cm^{-1} (see also section 2.2).

The excited OD oscillators have high frequencies, meaning that they donate a very weak hydrogen-bond. There are two main molecular configurations corresponding to a weak hydrogen-bond: Either 1) the hydrogen-bonding (OD-O) angle between the vector pointing along the OD covalent bond and the oxygen-

oxygen vector is large, or 2) the oxygen-oxygen distance (R_{OO}) of the two water molecules involved in the hydrogen-bond is large [60].

From classical MD simulations it is known that for the excited subensemble in this experiment more than 20% of the OD oscillators is within 125 fs from a molecular jump [86]. In comparison, for an excitation around the OD stretch absorption maximum this is less than 5%. Therefore, the excited subset exists of two groups with different near future events: shortly after excitation either 1) evolves to the bifurcated state, resulting in a rapid successful jump over a large angle to a new hydrogen-bonding partner or switches back to its original hydrogen-bonding partner in an unsuccessful jump, or 2) ordinary structural diffusion leads to a gradual evolution to stronger hydrogen-bonds.

Let us now consider how these hydrogen-bond configurations and structural dynamics influence our observables. In case the OD group was at the time of excitation close to a transition state, it will either rapidly switch back to its current hydrogen-bonding partner or jump. In either case, in the final state the hydrogen-bond is much more linear (and hence stronger) and the resonance frequency of the OD oscillator thus quickly decreases. As a result, these processes lead to fast spectral diffusion to lower frequencies. The typical time associated with a reorientation jump are on the order of a few hundred femtoseconds [2, 4] and we associate this process with the very fast decay of M_1 that we find in Fig. 6.2B.

In other cases, the OD oscillator was donating a weak hydrogen-bond due to its large oxygen-oxygen distance R_{OO} and will remain wobbling in the librational cone of its current hydrogen-bonding partner. It will not be much restricted by its coulomb interaction with the nearest water molecule [60] and has a lot of freedom to wobble: its librational cone is large [89]. While wobbling, its hydrogen-bond strength will on average remain weak and the wobbling thus has a limited contribution to spectral diffusion. For the oscillator to spectrally diffuse to lower frequencies, the R_{OO} distance should become smaller. This can happen by translational motions that occur in pure liquid water on a ~ 1 ps timescale [66, 63, 65, 68, 67, 64, 60]. Such an initially blue-excited OD oscillator thus likely remains to give a response at blue frequencies within the first picosecond. This process is associated with the slower decay of M_1 in Fig. 6.2B.

6.3.2 REORIENTATION DYNAMICS AT ROOM TEMPERATURE

After subtraction of the thermal component of the parallel and perpendicular transient spectra we calculated the anisotropy dynamics at various probe frequencies using Eq. (4.18). The results are shown in Fig. 6.3A. The anisotropy in the first picosecond shows a strong dependence on the probe frequency, while for longer delay times the dynamics are completely frequency independent.

The low values of the initial anisotropy and subsequent rise in the first picosecond that we find for low probe frequencies (eg. 2500 cm^{-1}) is a feature that requires cautious consideration. This feature finds its origin in a frequency dependence of the anisotropy. To understand the observed frequency dependence in detail, we need to consider all contributions to the transient spectra carefully.

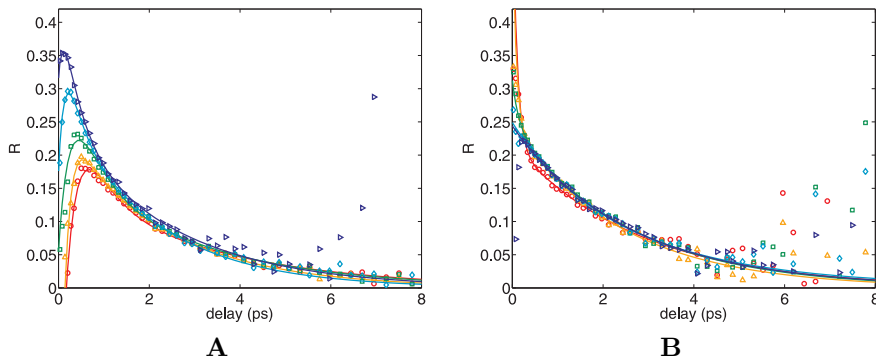


FIGURE 6.3. Anisotropy dynamics of OD groups in neat HDO:H₂O. For these measurements the sample was excited with a narrow band pump at 2650 cm⁻¹. **(A)** Probe frequencies in the $\nu = 0 \rightarrow 1$ region (2490, 2500, 2520, 2560 and 2600 cm⁻¹, red to blue curves). For short delay times the anisotropy has a strong dependence on the probe-frequency, which disappears entirely after 1 ps. The anisotropy at 2600 cm⁻¹ initially decays significantly faster than 2.5 ps, the timescale of reorientation found using a spectrally broad pump centered around 2500 cm⁻¹ [22]. **(B)** Probe frequencies in the $\nu = 1 \rightarrow 2$ region (2100, 2150, 2200, 2250 and 2300 cm⁻¹, red to blue curves). The anisotropy dynamics show no dependence on the probe frequency and decay with a time constant of 2.3 ± 0.2 ps.

The total transient spectrum is a combination of a (negative) bleaching signal at the $\nu = 0 \rightarrow 1$ transition frequencies and a (positive) induced absorption signal at the $\nu = 1 \rightarrow 2$ transition frequencies. Due to the anharmonicity of the OH-stretch vibration the induced absorption is red-shifted about 200 cm⁻¹ with respect to the bleach. Therefore a considerable spectral region exists in which both features overlap. As a result, the total measured transient absorption at 2500 cm⁻¹ is in fact the sum of the bleach at 2500 cm⁻¹ and the blue wing of the induced absorption. The blue wing of the induced absorption is the $\nu = 1 \rightarrow 2$ response of weakly hydrogen-bonded oscillators that have a ground-state absorption at 2700 cm⁻¹, while the bleach at 2500 cm⁻¹ rather represents the $\nu = 0 \rightarrow 1$ response of OD oscillators with an average hydrogen-bond strength. If the reorientation dynamics is the same for any hydrogen-bond strength of the OD oscillators, the anisotropy at any probe frequency of either the bleach or induced absorption would be the same for a given delay time. Addition of the two signals would not make any difference. If however the reorientation dynamics *does* change with oscillator strength and thus probe frequency, the anisotropy at 2500 cm⁻¹ is a non-trivial combination of both the reorientation dynamics of OD oscillators that absorb at the blue wing of the linear spectrum ($\nu = 0 \rightarrow 1$) and those that absorb at the center of the linear spectrum ($\nu = 1 \rightarrow 2$). More specific, the anisotropy at 2500 cm⁻¹ is the sum of the reorientation dynamics of the $\nu = 0 \rightarrow 1$ and $\nu = 1 \rightarrow 2$ response, weighted to their isotropic spectral

amplitude. At probe frequencies where the total isotropic response is zero, this weighted sum leads to an asymptotic behavior of the anisotropy. The small (and even negative) values for the anisotropy at 2500 cm^{-1} in Fig. 6.3A are thus artificial, but do represent an anisotropy that decreases with decreasing frequency. A formal description of this interference effect is found in the appendix 6.A.

The complicated competition within the bleaching of the OD stretch band can be avoided by probing the red wing of the induced absorption only. This approach comes at a cost: For a subset of oscillators with $\nu = 0 \rightarrow 1$ resonances at one single frequency there is a distribution of $\nu = 1 \rightarrow 2$ frequencies. The absence of a unique mapping results in a smearing effect that partly averages out spectral differences in reorientation dynamics. The anisotropy dynamics measured between 2100 cm^{-1} and 2300 cm^{-1} using the same spectrally narrow excitation pulse centered around 2650 cm^{-1} are shown in Fig. 6.3B. To obtain these results we used the same method of subtraction of the thermalization contribution. These probe frequencies cover the red wing of the induced absorption part of the transient spectrum: Since the anharmonic shift is about 200 cm^{-1} , the oscillators probed at 2300 cm^{-1} approximately correspond to the oscillators probed at 2500 cm^{-1} . Between 2100 cm^{-1} and 2300 cm^{-1} we observe no significant frequency dependence in the reorientation dynamics. It should be noted, though, that the initial value of the anisotropy R_0 at 2300 cm^{-1} is lower than R_0 at 2600 cm^{-1} .

The frequency dependence of the anisotropy following a narrow-band blue excitation is consistent with earlier work [90]. Previous fs-IR studies found that the reorientation time of OD groups in a similar solution is $2.5 \pm 0.1\text{ ps}$ and is independent on the probe frequency [22]. Those experiments were performed with a spectrally broad pump, centered around the maximum of the OD-stretch band at 2500 cm^{-1} . For the subset excitation used in the present experiment, we observe that the dynamics of the anisotropy at different frequencies is governed by an interplay of the reorientational jumps and the structural diffusion. Librational motions also lead to a decay of the anisotropy, but is completed within hundred femtoseconds [89, 91], and therefore only shows in our results as a lower starting value of the anisotropy (Fig. 6.3). This loss of orientation originates from the wobbling motion of an OD group while keeping its hydrogen-bond intact. Librational motions do not contribute to spectral diffusion, since the hydrogen-bond strength remains similar.

For the interpretation of the subsequent anisotropy dynamics we will again consider the different configurations and structural dynamics of weakly hydrogen-bonded oscillators described in the previous section. We find that at very short delay times the anisotropy is lower on the red side than on the blue side of the spectrum (Fig. 6.3). This difference can be fully understood by the jump reorientation of blue-excited OD oscillators. Classical molecular dynamics (MD) studies have shown that more than 20% of such weakly hydrogen-bonded OD groups are within 125 fs of an orientational jump to a new hydrogen-bonding partner [86]. Such a jump event requires a large angular change of the OD group that leads to an almost complete decay of

the anisotropy [2]. As we have argued in the previous section, a jump event is accompanied with fast spectral diffusion of the OD oscillator to lower frequencies. These OD oscillators therefore have little contribution to the reorientation dynamics probed at 2600 cm^{-1} immediately after their jump. They rather dominate the signal at lower frequencies, eg. 2500 cm^{-1} , where initially no OD oscillators were excited at all. The anisotropy measured in the first few hundred femtoseconds at 2500 cm^{-1} thus mostly represents OD oscillators that lost part of their orientation in a jump. As a consequence, the anisotropy at red probe frequencies is initially lower than the anisotropy at 2600 cm^{-1} . For the anisotropy measured at 2500 cm^{-1} this effect is magnified by the competition between the bleach and the induced absorption at these frequencies, which was described above. A better comparison is obtained if we compare the anisotropy dynamics at 2600 cm^{-1} with those probed at 2300 cm^{-1} (Fig. 6.3). The response measured at 2300 cm^{-1} corresponds to the $\nu = 1 \rightarrow 2$ transition of oscillators that absorb at 2500 cm^{-1} . The anisotropy indeed shows a lower value in the first picosecond.

The second contribution to the anisotropy dynamics comes from structural diffusion by the variation of oxygen-oxygen distances R_{OO} [43]. As a result, R_{OO} decreases for those OD groups that initially had a large value of the oxygen-oxygen distance, thereby spectrally shifting the resonance frequency of those oscillators to lower frequencies. This shift we found as the ~ 1 ps decay component in the spectral diffusion represented by the first moment in Fig. 6.2B. The process of the structural diffusions process will thus 'feed' the red side of the spectrum with oscillators that still possess relatively a lot of orientation. Conversely, there are oscillators that made a rapid orientational and spectral jump from the blue wing of the spectrum to 2500 cm^{-1} . By the slower spectral diffusion process of translational motions, these oscillators diffuse back to the blue wing. Since they lost all their orientation already in the first few hundred femtoseconds, their contribution to the anisotropy measured at the blue side of the spectrum leads to a decay. Translational motions thus wash away any remaining memory of the out-of-equilibrium excitation, causing the anisotropy curves for all probe frequencies to become identical after ~ 1.5 ps. After spectral diffusion is completed, the anisotropy is therefore independent on the spectral position of the excited OD oscillators.

The subsequent reorientation dynamics after spectral equilibration is not different from the anisotropy dynamics after a homogeneous excitation by a spectrally broad pump. These dynamics are dominated by the large angular jump hydrogen-bond switching and frame reorientation [2]. From an exponential fit to the data for delay times larger than 2 ps we indeed find a time constant of the anisotropy decay of 2.4 ± 0.3 ps. This time constant is in excellent agreement with previous findings on the reorientation of OD groups in isotopically diluted water (2.5 ps) [22].

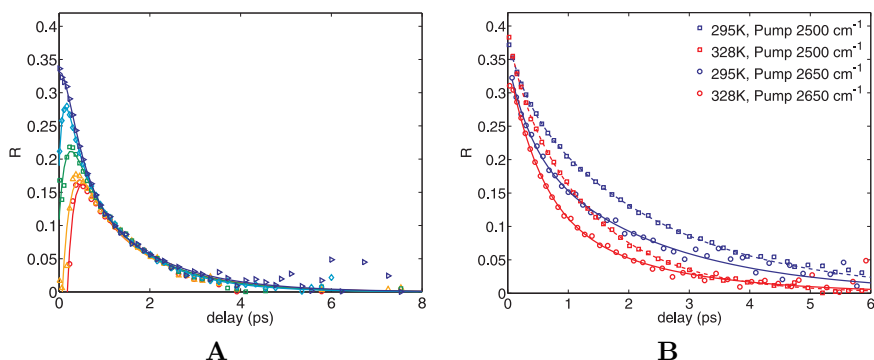


FIGURE 6.4. (A) Similar figure as Fig. 6.3A (identical probe frequencies) for a sample temperature of 328K. The reorientation dynamics in neat 16% HDO:H₂O is faster than that at 295K. (B) Anisotropy decay probed at 2600 cm^{-1} after excitation with a spectrally narrow pump centered around 2650 cm^{-1} (solid lines) and anisotropy decay after excitation with a spectrally broad pump centered around 2500 cm^{-1} (dotted lines) at 295K and 343K. The anisotropy decays faster in case the sample is pumped at 2650 cm^{-1} compared to when the sample is excited with a spectrally broad pump. This also holds for elevated temperatures: although increasing the sample temperature speeds up the reorientation dynamics, pumping the blue wing of the OD-stretch band makes the anisotropy decay still faster.

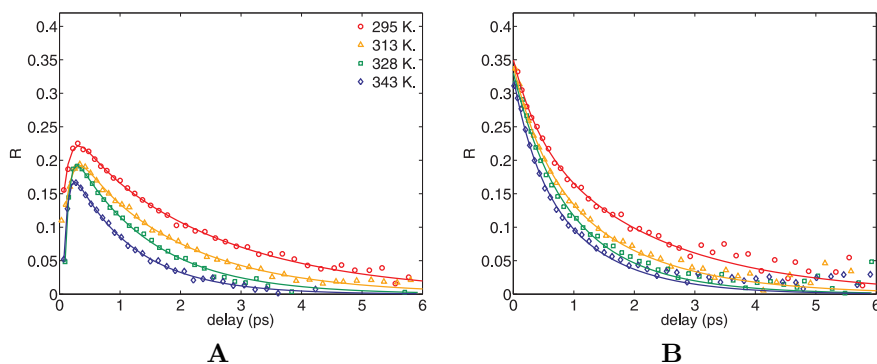


FIGURE 6.5. Anisotropy decay probed at 2500 cm^{-1} (A) and at 2600 cm^{-1} (B) after excitation by a spectrally narrow pump centered around 2650 cm^{-1} , at a sample temperature of 295K (circles), 313K (triangles), 328K (squares) and 343K (diamonds). For increasing temperatures the dynamics become faster.

6.3.3 REORIENTATION DYNAMICS AT ELEVATED TEMPERATURE

All anisotropy results that we considered until this point were obtained at room temperature. We will now compare the frequency dependent measurements for neat 16% HDO:H₂O at different temperatures. It should be noted that the vibrational lifetime T_1 of the OD-stretch vibration becomes longer for increasing temperature [88, 35]. A longer T_1 makes the determination of the anisotropy at longer delay times even more accurate.

Fig. 6.4A shows the frequency dependent reorientation dynamics obtained at $T = 328\text{K}$. The pump spectrum is again centered around 2650cm^{-1} with a FWHM of 60cm^{-1} . We compare these data to the results obtained at room temperature (295K) presented in Fig. 6.3. The most clear difference is that the relaxation at all frequencies is significantly faster at 328K than at 295K. In Fig. 6.4B we compare the anisotropy dynamics obtained for a spectrally broad excitation and a narrow blue excitation at different temperatures. The probe frequency used is 2600cm^{-1} , but it should be noted that for a broad excitation pulse the anisotropy decay does not significantly depend on the probe frequency [22]. At both 295K and 328K, the orientational relaxation after excitation with a spectrally narrow pump at 2650cm^{-1} is faster than after excitation with a spectrally broad pump. Independent on the type of excitation pulse used, the reorientation dynamics becomes faster at elevated temperatures. The anisotropy decays at 2500cm^{-1} and 2600cm^{-1} are shown in Fig. 6.5 for all sample temperatures measured.

The equilibration of the frequency dependence of the anisotropy in the first picosecond is faster at 328K compared to the data measured at 295K. This is quantified by fitting a straight line to the frequency dependent anisotropy at every delay time. The slope as function of delay time is shown in Fig. 6.7A for a number of temperatures. We compare these plots with the dynamics of the first moment in Fig. 6.7B. The first moments are obtained by the method described in section 6.3.1. We fitted mono-exponential functions to the data (solid lines), of which the decay constants are presented in Fig. 6.7 for all measured temperatures. The results show a strong correlation between the spectral diffusion and anisotropy equilibration, both becoming faster for increasing temperature.

In the previous section we found that the anisotropy decay following excitation with a spectrally narrow pump at 2650cm^{-1} are governed by an interplay of the reorientational jumps and spectral equilibration. For increasing temperatures, both components will become faster. Water reorientation by jumps is an activated process and thus this process becomes more frequent at elevated temperatures [88]. The rate limiting step of a jump event to occur is the approach of a new potential hydrogen-bonding partner. This process is sped up by faster structural diffusion and thus the frequency of jumps increases. R_{OO} distances become on average slightly larger at higher temperatures, as is also illustrated by the higher endlevel of the first moment at 343K in Fig. 6.2B. Fig. 6.7 demonstrates that structural diffusion becomes faster (see also [87]),

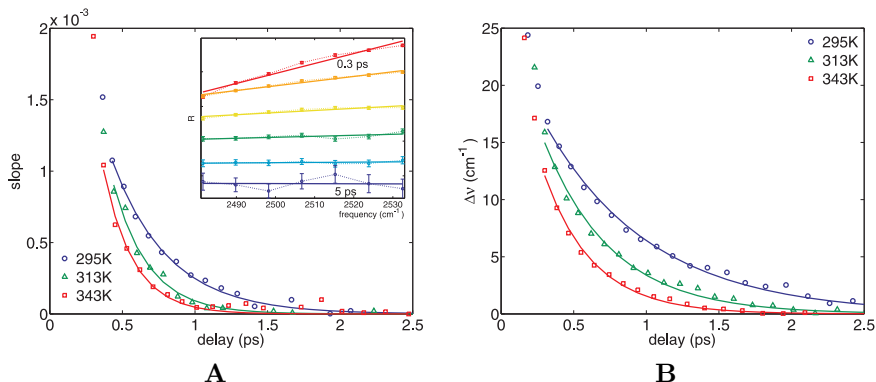


FIGURE 6.6. (A) The time-dependent slope of a straight line fitted to the frequency dependent anisotropy between 2485 cm^{-1} and 2530 cm^{-1} (see inset for the fits to the data taken at 295K). The vanishing of the slope at long delay times implies that full spectral equilibration has taken place. The solid lines are mono-exponential fits to the data. (B) Dynamics of the first moment M_1 obtained at different temperatures. The plots are vertically displaced such that they decay to a vanishing difference $\Delta\nu$ between M_1 at a given delay time and M_1 of the equilibrium spectrum that is reached after several picoseconds (see Fig. 6.2). The solid lines are mono-exponential fits to the data.

resulting in a faster equilibration of the anisotropy as a function of probe frequency. Due to the increased rate of the jumps and the accelerated spectral diffusion, the average reorientation speeds up. From the decay constants of spectral diffusion and the anisotropy equilibration we can determine the activation energy of these processes (fitted lines in Fig. 6.7). Both methods yield a value of $11 \pm 2\text{ kJ/mol}$, or $2.6 \pm 0.5\text{ kcal/mol}$. This value is in reasonable agreement with previous findings of $3.1\text{--}3.5\text{ kcal/mol}$ [83, 84, 85, 86, 87, 88].

6.4 CONCLUSIONS

We studied the reorientation dynamics of OD groups in isotopically diluted water at different temperatures after excitation by a narrow-band pump pulse, spectrally centered around 2650 cm^{-1} . This pump excites a subset of those OD oscillators that donate a weak hydrogen-bond. This subset offers a good probe of the hydrogen-bond switching process for two reasons: these OD oscillators have an increased probability of being close to an orientational jump event that results in a hydrogen-bond switch, and for short delay times the signal response at the red side of the spectrum will reveal the oscillators that have just experienced such a hydrogen-bond switch. We find that a few hundred femtoseconds after excitation the hydrogen-bond switching leads to a lower anisotropy at low frequencies compared to high frequencies. This spectral dependence of the

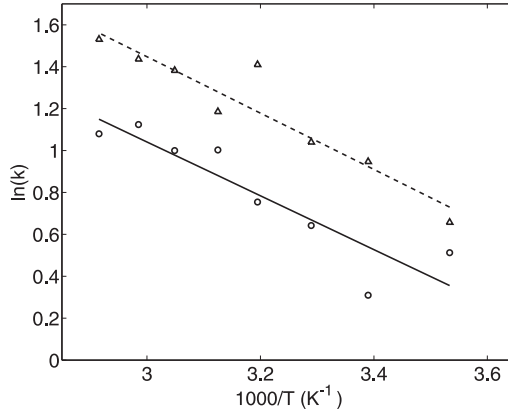


FIGURE 6.7. Natural logarithm of the decay rates that were obtained from an exponential fit to the dynamics of the first moment (circles) and slope of the frequency dependent anisotropy (triangles) from Fig. 6.7, as a function of inverse temperature. The activation energy that was found by taking the slope of a linear fit through the points is 11 ± 2 kJ/mol.

anisotropy vanishes on a 1 ps time scale due to structural diffusion. After equilibration, the reorientation dynamics is governed by the interplay of structural diffusion and hydrogen-bond switching events and are the same as found after homogeneous excitation of the absorption band. For elevated temperatures we find that both the spectral diffusion and the reorientation become faster. We find an activation energy of hydrogen-bond switching of 2.6 ± 0.5 kcal/mol.

6.A APPENDIX: NARROW PUMP AND ANISOTROPY

In this appendix we will describe in detail the amplification effect of a frequency dependence in the anisotropy dynamics that may occur following a narrow-band blue excitation. We assume a similar excitation spectrum as used in the experiment, with a FWHM of 60 cm^{-1} and centered around 2650 cm^{-1} . We recall from chapter 4 that the isotropic transient spectra may be written as the product of the population dynamics $N(t)$, reflecting the vibrational decay of the excitation, and the excited state transient absorption spectrum $\sigma(\nu)$ (Eq. (4.12)). Furthermore, we restate that $\sigma(\nu)$ consist of a negative contribution $\sigma_{01}(\nu)$ due to stimulated emission and ground state depletion (the bleach) at the $\nu_s = 0 \rightarrow 1$ transition frequency and a positive contribution $\sigma_{12}(\nu)$ due to excited state absorption at the $\nu_s = 1 \rightarrow 2$ transition frequency. The heat corrected isotropic transient spectra for a single species solution can thus be written as,

$$\widetilde{\Delta\alpha}_{\text{iso}}(\nu, t) = N(t)\sigma(\nu) = N(t) (\sigma_{01}(\nu) + \sigma_{12}(\nu)) \quad (6.1)$$

However, the absorption spectrum of OD-oscillators in isotopically diluted water is inhomogeneously broadened: oscillators with stronger or weaker hydrogen-bonds have their resonance frequency at different positions in the absorption band. In case of a narrow band excitation pulse with its center frequency at the blue side of the OD-stretch band, mainly those OD-oscillators are excited that have a weak hydrogen-bond. This results in a blue-shifted transient response of both $\sigma_{01}(\nu)$ and $\sigma_{12}(\nu)$ at time zero. Due to spectral diffusion, σ_{01} and σ_{12} have a time dependence and will eventually assume their equilibrium shape.

For simplicity we consider a gaussian shape for the bleach with central frequency ν_c^0 at time zero, exponentially relaxing to ν_c^∞ due to spectral diffusion with rate k_s . The spectral contribution of the bleach $\sigma_{01}(\nu, t)$ to the total transient absorption can then be written as,

$$\sigma_{01}(\nu, t) = A e^{-\frac{(\nu - \nu_c(t))^2}{2\Sigma^2}} \quad (6.2)$$

where A is the amplitude of the response and Σ the width of the gauss. We ignored here the fact that a narrow excitation also leads to a time dependent broadening of Σ . The time-dependent center frequency $\nu_c(t)$ can be written as,

$$\nu_c(t) = (\nu_c^0 - \nu_c^\infty) e^{-k_s t} + \nu_c^\infty \quad (6.3)$$

A similar relation can be derived for the spectral contribution of the induced absorption $\sigma_{12}(\nu, t)$, for which the sign of the amplitude will be different and the center frequency is shifted to the red side of the spectrum by the anharmonicity (180 cm^{-1}). Using Eq. (4.4) and using the expression for the anisotropy of Eq. (4.3) yields,

$$R_m(\nu, t) = \frac{\sigma_{01}(\nu, t)R_{01}(\nu, t) + \sigma_{12}(\nu, t)R_{12}(\nu, t)}{\sigma_{01}(\nu, t) + \sigma_{12}(\nu, t)} \quad (6.4)$$

The subscript m of the anisotropy R_m is added as a reminder that this parameter represents the measured anisotropy as opposed to the actual anisotropy

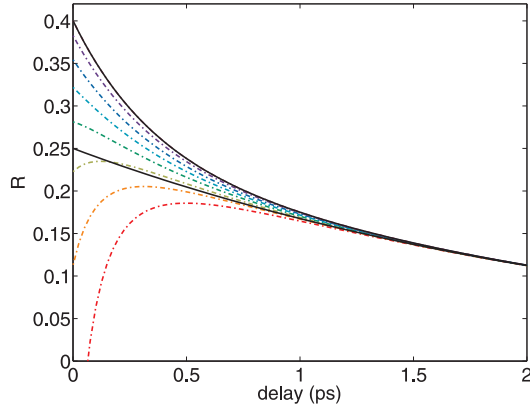


FIGURE 6.8. A simulation of the artefact that arises in the measured anisotropy dynamics in case the OD stretch vibration in isotopically diluted water is inhomogeneously excited by a narrow band pump centered at the blue shoulder of the absorption band. The solid black lines are the actual anisotropy dynamics at 2500 cm^{-1} (lower line) and 2600 cm^{-1} (upper line). The dashed-dotted lines are the anisotropy dynamics that were calculated as they would be measured for equidistant frequencies (step size 12.5 cm^{-1}) between 2500 cm^{-1} (lowest curve) and 2600 cm^{-1} (uppermost curve).

R_{01} and R_{12} . We explicitly took the anisotropy different for the bleach and the induced absorption. This is necessary because at a given frequency ν the spectral response of the bleach arises from different oscillators than the spectral response of the induced absorption, due to the anharmonicity of the OD stretch vibration. An oscillator that contributes to the bleach at 2500 cm^{-1} , therefore also contributes to the induced absorption at 2320 cm^{-1} . In terms of the associated reorientation dynamics we write this as,

$$R_{12}(\nu, t) = R_{01}(\nu + 180, t) \quad (6.5)$$

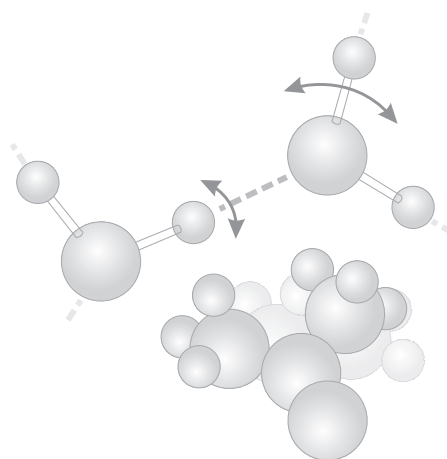
In case there is no frequency dependence in the anisotropy, the equality in Eq. (6.5) is trivial and $R_m(\nu, t)$ reduces to $R_{01}(t)$. For the experiment in this chapter, the anisotropy in fact does depend on the probe frequency. In line to what we found we define the frequency dependence as,

$$R_{01}(\nu, t) = \frac{2}{5} (0.25e^{-0.4t} + 0.15\rho e^{-3t}) \begin{cases} \rho = 0 (\nu < 2500) \\ \rho = \frac{\nu - 2500}{100} (2500 < \nu < 2600) \\ \rho = 1 (\nu > 2600) \end{cases} \quad (6.6)$$

We calculated $R_m(\nu, t)$ according to Eq. (6.4) for values of the spectral diffusion parameters that are describing a physical example of actually measured data presented in chapter 7. The results are plotted in Fig. 6.8 for a number of probe-frequencies. The black lines represent the actual anisotropy of the bleach at 2500 cm^{-1} and 2650 cm^{-1} . As can be seen, the amplitude of R_m

is heavily suppressed for short delay times, especially at frequencies close to 2500 cm^{-1} where an asymptotic behavior seems to be present. This behavior follows from the nominator of Eq. (6.4) than can become very small for frequencies at which $\sigma_{01}(\nu, t) \sim \sigma_{12}(\nu, t)$. Due to the difference between $R_{01}(\nu, t)$ and $R_{12}(\nu, t)$, the nominator is not necessarily small at these frequencies. This effect disappears for longer delay times for two reasons. 1) The definition of the anisotropy implicitly assumed a convergence of $R_{01}(\nu, t)$ and $R_{12}(\nu, t)$ and 2) the zero-crossing of $\sigma(\nu, t)$ shifts to frequencies lower than 2500 cm^{-1} , thereby diminishing the artefact. Both of these points are related to spectral diffusion. In case spectral diffusion would not be complete within the timescale of the experiment, $R_{01}(\nu, t)$ and $R_{12}(\nu, t)$ would not converge with a residual frequency dependence as a result.

Water Reorientation in the Hydration Shell of TMU



In aqueous solutions of amphiphiles the reorientation dynamics of a part of the water molecules is much slower than in bulk water. In chapter 10 we will show that the number of slower water molecules scales with the number of hydrophobic groups in the solution. Such a dependence strongly suggests that the slower water molecules are those that solvate the hydrophobic moieties of the amphiphile. **In this chapter we investigate in the underlying mechanism of the retardation of water molecules in the hydrophobic solvation shell.** We find that OD-groups around the methyl groups of tetramethylurea (TMU) have a lower rate of jumps. This effect is highly correlated with a component of extremely slow spectral diffusion in these solutions. These results are consistent with recent Raman MCR experiments in which it was found that the structure of the hydrogen-bond network around hydrophobic groups is more ordered. From these observations we conclude that reduced translational motions hinder the approach of a new hydrogen-bonding partner close to hydrophobic groups, a process that is essential for a successful jump to happen. We show that for increasing temperatures this effect rapidly disappears.

7.1 INTRODUCTION

The concepts of 'hydrophobic interaction' and 'hydrophobic hydration' have gained a lot of use in the past decades, but what *is* the hydrophobic effect? The use of the terms may be considered questionable, as hydrophobic groups are rather lacking direct interaction with solvating water molecules. Instead, the driving mechanism behind processes that are associated with the hydrophobic effect, like aggregation, is rather found in the hydrogen-bonding structure and dynamics around the hydrophobe.

Water consists of an extended network by forming on average almost four hydrogen-bonds per water molecule. To accommodate a small hydrophobic particle, this network is able to elastically bend to form a cavity. For larger particle sizes, bending the network is not sufficient anymore and hydrogen-bonds are broken, thereby forming an interface [92, 11]. The first process is entropic in nature and depends on the volume of the particle, while the second process is enthalpic and depends on the surface of the cavity. It is found that the transition between the two mechanisms takes place for particle sizes of about 1 nm [11]. The detailed balance between the free energy of a number of hydrated small hydrophobic molecules or one hydrated large aggregate determines whether aggregation is favored or not. Since this balance is partly enthalpic in nature, the aggregation effects are expected to depend on the temperature. Such a temperature dependence has indeed been found empirically for systems in which hydrophobic aggregation plays a role, like protein folding [93, 94, 95].

The remarkable change in heat capacity for aqueous solutions of amphiphiles previously lead Frank and Evans to propose the existence of highly structured water around hydrophobic groups, for which they coined the term 'icebergs' [96]. Although the iceberg model was proposed already in the fifties, evidence for such a strongly increased structure of water around hydrophobic groups was not found [97]. Only a recent Raman spectroscopy study found some structure enhancement in solutions of alcohols in water [98]. Contrasting to the lacking evidence for induced structure of water, compelling evidence exists by NMR [99, 100, 101, 102], femtosecond infrared spectroscopy [28, 17], dielectric relaxation spectroscopy [103, 17, 104], classical molecular dynamics (MD) simulations [105, 106, 107] and ab initio MD simulations [108] that the reorientation of water in solutions of amphiphiles is slower than in bulk water. The magnitude of the retardation and the extent of the effect is however not agreed upon.

In recent two-dimensional infrared (2D-IR) spectroscopy studies it was found that water molecules show very slow spectral dynamics around the hydrophobic groups of tert-butyl alcohol (TBA), trimethylamine-N-oxide (TMAO) and tetramethylurea (TMU) [109, 110]. The partial slowing down of the spectral diffusion was found to be highly correlated to the slower reorientation dynamics in these solutions [110]. This correlation suggests a common origin, and points to a strong hindrance of water in its evolution to a bifurcated hydrogen bond structure near hydrophobic groups. The hindrance can be explained by a distortion of the hydrogen-bond network by the presence of the hydrophobic molecular groups, allowing for less translational motions and jump reorientation events.

To investigate this proposition, we performed infrared pump-probe experiments on a concentrated solution of TMU in isotopically diluted water. By exciting the OD stretch vibration of a subset of HDO molecules that form very weak hydrogen-bonds, we are able to obtain information on the spectral diffusion and orientational dynamics of this subset. First we compare the spectral diffusion for both neat water and aqueous solutions of TMU, after which we consider the reorientation of water molecules in both solutions. Finally we explore the temperature dependence of water reorientation in the TMU solution. All results combined are consistently interpreted with a detailed molecular picture of reorientation dynamics in the hydrophobic solvation shell.

7.2 EXPERIMENTAL

The details of the experiments performed in this chapter are identical to those described in section 6.2 of the previous chapter. Instead of neat isotopically diluted water, we used a solution of TMU in isotopically diluted water. TMU was purchased from Sigma Aldrich (99.9 % pure) and added to 8 % D₂O in H₂O to obtain a solution of 6 molal (mol/kg solvent) TMU.

7.3 RESULTS AND INTERPRETATION

7.3.1 ISOTROPIC RESULTS AND SPECTRAL DIFFUSION

Fig. 7.1A shows the transient spectra obtained after excitation of the 6 molal TMU solution by the narrow band pump, centered at 2650cm⁻¹, at room temperature (295K). At short delay times t , the bleach is blue-shifted from the central absorption of the OD stretch band. For increasing t , the bleach undergoes complicated dynamics. First it shifts to lower frequencies while increasing in amplitude, later it decays again to a thermalized ground state. From close examination of the transient spectra obtained for the delay times 7 ps and 50 ps it can be seen that the amplitude at 2480 cm⁻¹ is becoming more negative again after 7 ps. This can only be explained if the excitation is not decaying immediately to the thermalized ground state but is somewhat delayed. This is fully in agreement with previous findings on the thermalization dynamics in similar systems [23, 22, 28] (see also section 4.2.2).

The thermalization contribution is subtracted in a procedure identical to what was described in the previous chapter and section 4.3. From the resulting thermalization-free transient spectra we determined the first moment M_1 as a measure of the spectral diffusion in the sample. The results are shown in Fig. 7.1B for the TMU solution (triangles) and for neat 16% HDO:H₂O (squares). A similar determination of M_1 was done for measurements with a spectrally broad excitation pulse centered around the OD-stretch band maximum of 2500 cm⁻¹ (Fig. 7.1B).

The M_1 curves for the broad-excitation pulse are nearly flat, positioned at \sim 2530 cm⁻¹ for neat 16% HDO:H₂O and blue-shifted by only a few wavenum-

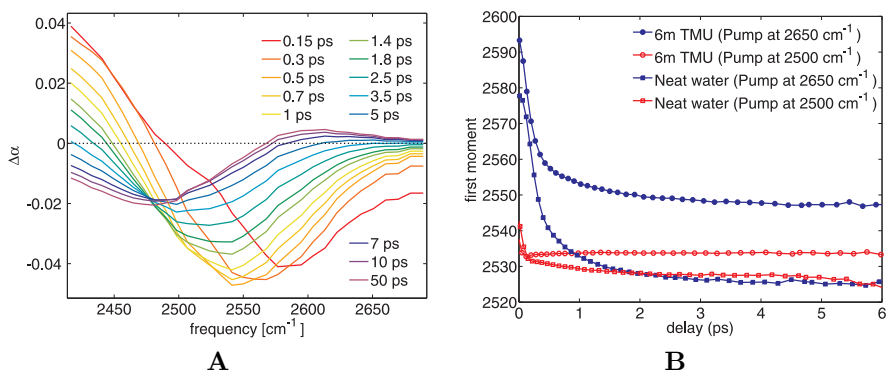


FIGURE 7.1. **(A)** The isotropic transient spectra for a number of pump-probe delay times. For short delay times the transient spectra mainly show a bleach at blue frequencies. The bleach subsequently shifts to the red and decays. For long delay times the transient spectrum is the thermal difference spectrum. Please note that the increase of amplitude of the transient spectra between 7 and 100 ps at 2480 cm⁻¹ is indicative for a delayed heat ingrowth as discussed in the text. **(B)** The first moment determined from the heat corrected transient spectra of the TMU solution and neat 16% HDO:H₂O (see chapter 6) at 295K. The open markers are the first moments obtained from measurements for which the pump spectrum was spectrally broad and centered around the maximum of the OD stretch absorption band (2500 cm⁻¹). For both solutions there is fast spectral diffusion for short delay times, but for TMU the diffusion is not complete. Subsequent decay occurs by a much slower process.

bers for the TMU solution. Since the broad pump pulse leads to a homogeneous excitation of the absorption spectrum, spectral diffusion has no effect on the excited lineshape and thus also not on M_1 . The value of $M_1 = 2530$ cm⁻¹ can thus be regarded as the equilibrium position of the bleach. In the case of excitation in the blue wing, the M_1 curves show a fast initial decay, followed by a slower decay to an endlevel. After 500 fs the values for M_1 deviate significantly for the different samples: Spectral diffusion in the TMU solution appears to level off at 2570 cm⁻¹, while for neat 16% HDO:H₂O the initial decay is deeper and the endlevel is at 2530 cm⁻¹. From these results we conclude that for neat 16% HDO:H₂O, spectral diffusion is completed after ~ 1.5 ps. In contrast, spectral equilibration in the TMU solution has not at all been completed within 6 ps. Apparently, a very slow component of spectral diffusion appears upon the addition of TMU to water.

7.3.2 ANISOTROPY DECAY OF WATER AROUND TMU

Fig. 7.2 shows delay curves of the transient absorption at two different probe frequencies probed parallel and perpendicular to the pump polarization. In the first picosecond the relative amplitude decay of the parallel signal probed at

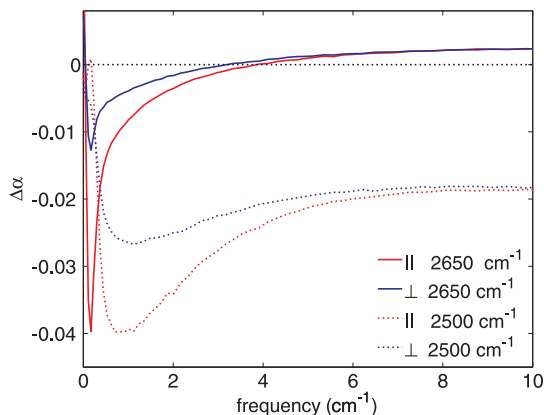


FIGURE 7.2. Delay traces at two probe-frequencies probed parallel and perpendicular to the pump polarization, obtained with a narrow band pump (center frequency 2650 cm^{-1}) for a 6 molal solution of TMU in 16% HDO:H₂O at room temperature. In the first picosecond the signals at 2650 cm^{-1} show a fast decay, while at 2500 cm^{-1} there is a fast rise. For long delay times both parallel and perpendicular signals assume a value that remains constant till at least 100 ps. This static transient signal is the thermal difference response due to sample heating after the vibrational relaxation. The difference between the parallel and perpendicular signals are a measure for the reorientation dynamics.

2650 cm^{-1} is much larger than that of the perpendicular signal at 2650 cm^{-1} . This shows that a large part of the initial anisotropy decays within the first picosecond. The parallel and perpendicular signals probed at 2500 cm^{-1} are crossing a few hundred femtoseconds after excitation. From this delay time onwards the anisotropy measured at this frequency is thus increasing, reaching a maximum somewhere between 0.5 ps and 1.5 ps after which it decays again.

We calculate the anisotropy dynamics (using equation Eq. (4.18)) after subtraction of the thermal contribution of the raw parallel and perpendicular transient spectra. The results for the TMU solution and for neat 16% HDO:H₂O, probed at the $\nu = 0 \rightarrow 1$ transition and at the $\nu = 1 \rightarrow 2$ transition, are shown in Fig. 7.3 for a sample temperature of 295K. There are two main differences between the results of the two samples. Firstly, for the TMU solution there is a frequency dependence of the anisotropy that is persistent for longer delays. This is the case for probe frequencies in both the $\nu = 0 \rightarrow 1$ and $\nu = 1 \rightarrow 2$ region. Secondly, after a fast decay in the first picosecond, the dynamics in the TMU solution show a much slower decay for the remaining anisotropy. At 8 ps the anisotropy is still quite large, implying that a large amount of orientation remains. The amplitude of this long-delay part is different for various probe frequencies.

We first consider the persistent frequency dependence. We recall from the previous chapter that for neat 16% HDO:H₂O the anisotropy dynamics after

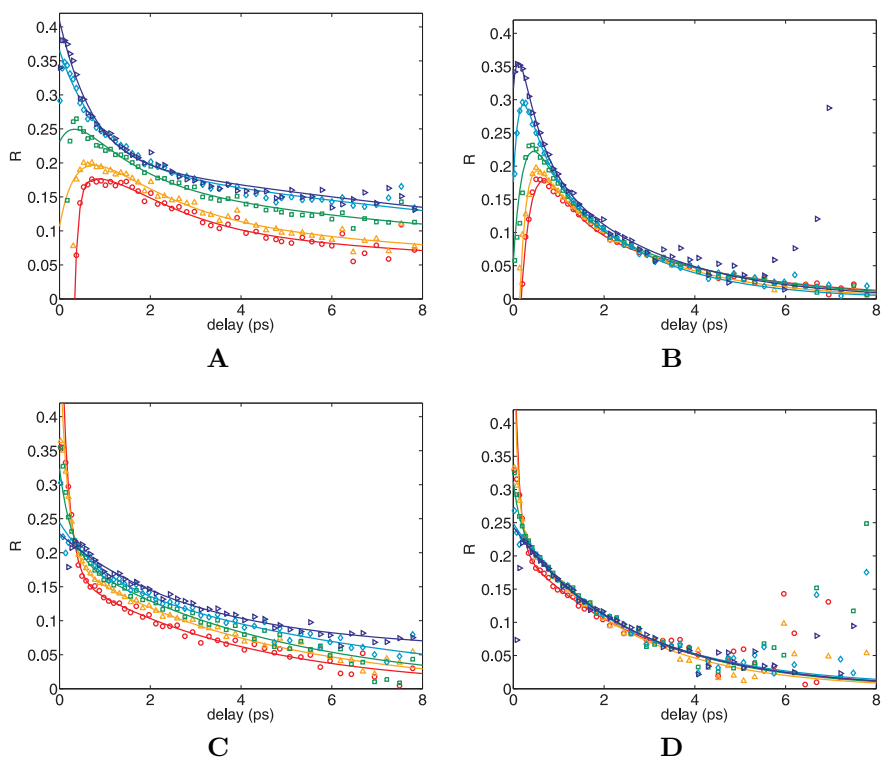


FIGURE 7.3. Anisotropy dynamics following narrow-band excitation at 2650 cm^{-1} , probed at $2490, 2500, 2520, 2560$ and 2600 cm^{-1} (red to blue curves) in the $\nu = 0 \rightarrow 1$ region (upper figures) and at $2100, 2150, 2200, 2250$ and 2300 cm^{-1} in the $\nu = 1 \rightarrow 2$ region (lower figures). The samples used were 6 molal TMU (panel **A** and **C**) and neat 16% HDO:H₂O (panel **B** and **D**). The frequency dependence of the anisotropy is persistent for the TMU solution, while for neat water spectral equilibration removes the frequency dependence after 1 ps. The solid lines are guides to the eye.

~ 1.5 ps is completely independent on the probe frequency due to spectral diffusion by translational motions in the liquid. The persistence of the frequency dependence in the TMU solution shown in Fig. 7.3 thus indicates that the spectral diffusion is not completed at 8 ps. As a result, the anisotropy at different frequencies (high in the blue wing, low in the red wing, following a 2650 cm^{-1} excitation) does not completely average out for delays < 8 ps.

The observation of such a persistent frequency dependence of the anisotropy agrees with the spectral diffusion curves we obtained from the analysis of the first moments M_1 of the transient spectra (Fig. 7.1). From that analysis we found that in neat 16% HDO:H₂O spectral diffusion is completed after ~ 2 ps, while in the TMU solution a very slow component exists that has not yet de-

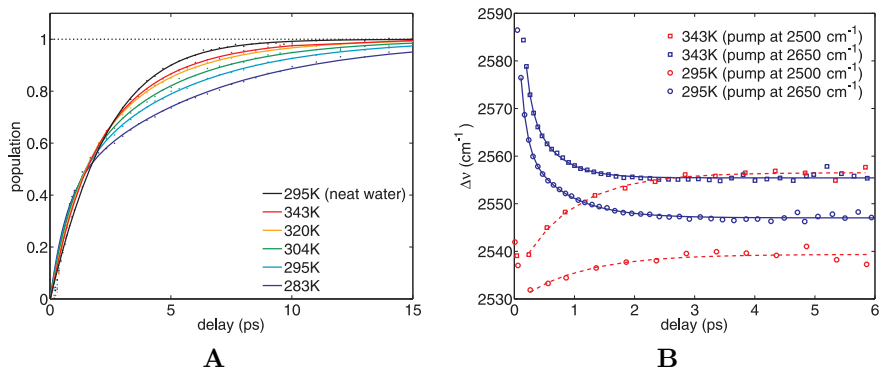


FIGURE 7.4. **(A)** Thermalization dynamics in a solution of 6m TMU at different lab temperatures. The slow component that is present at room temperature disappears almost entirely at 343K. For comparison the thermalization dynamics in neat water at 295K is shown (black curve). In neat water, the thermalization dynamics does not depend much on temperature (see section 4.3). **(B)** Dynamics of the first moment in a solution of 6m TMU at 295K and 343K after excitation at 2500 cm^{-1} and 2650 cm^{-1} . The difference in endlevel at 295 is indicative for a very slow spectral diffusion component. At 343K, this component has disappeared and spectral diffusion is complete after a few picoseconds.

cayed at 8 ps. We discussed two main mechanisms for spectral diffusion: Angular jumps to a stronger hydrogen-bond configuration and translational motion to smaller values of R_{OO} . Both mechanisms eventually lead to a complete equilibration of the hydrogen-bond strength distribution and thus decay of M_1 . The observation of incomplete spectral diffusion at delay times between 2 and 8 ps therefore implies that both mechanisms are altered.

A subset of the OD oscillators in the TMU solution thus have both a low rate of jumping and slow translational motions. As a result, the anisotropy of this subset decays much slower, as we indeed observe for delay times $t > 2$ ps. At early delays ($t < 2$ ps) the dynamics is in fact significantly faster than those following a broad excitation. A likely explanation is that both the fast reorientation component and the fast relaxation of M_1 of the TMU solution in the first ~ 2 ps is mainly associated with OD oscillators outside the hydrophobic hydration shell. This is analogous to the dynamics observed for neat 16% HDO:H₂O.

We performed the same experiment at elevated temperatures. At every temperature we performed an additional determination of the thermalization dynamics using the method from section 4.3. The results are shown in Fig. 7.4A. At low temperatures the thermalization happens on two very distinct timescales, but for increasing temperatures the slow component disappears. After removing the thermalization contribution from the data we determine the dynamics of the first moment M_1 . Fig. 7.1B shows the results for $T=295\text{K}$ and $T=343\text{K}$ for a

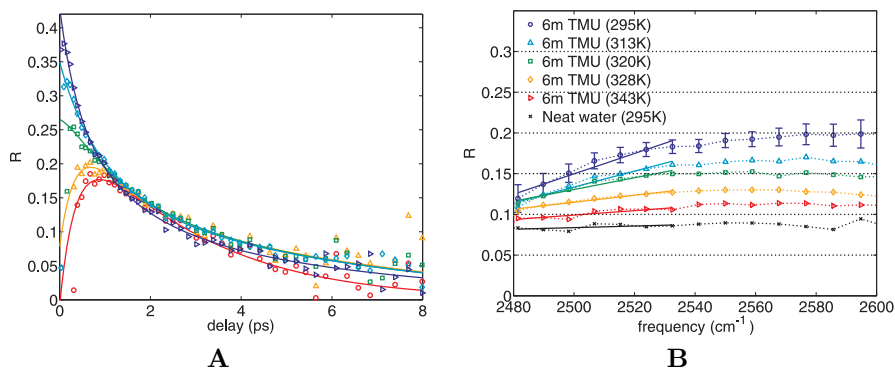


FIGURE 7.5. (A) Similar figure as Fig. 7.3A for 6 molal TMU at a sample temperature of 328K. The slow decaying part of the anisotropy has a smaller amplitude. In contrast to the results obtained at 295K, no frequency dependence for long delay times is observed. (B) The anisotropy values at 2.5 ps delay time are shown as a function of probe frequency for different temperatures. The frequency dependence that is observed for a sample temperature of 295K completely disappears at higher sample temperatures. For comparison the same plot is shown for neat 16% HDO:H₂O at 295K. The solid lines are fits of a straight line to the frequency region 2485–2530 cm^{-1} to quantify the spectral dependence of the anisotropy as a function of time.

pump spectrum centered at 2500 cm^{-1} and 2650 cm^{-1} . At room temperature the spectral diffusion seems to have come almost to a halt at 6 ps, while at 343K spectral diffusion is completed after a few picoseconds.

The reorientation dynamics obtained for the TMU solution at 328K are shown in Fig. 7.5A. In analogy to what we found for neat water in chapter 6, the anisotropy probed at 328K decays faster than that probed at 295K. However, we find that upon increasing the temperature the dynamics in the TMU hydration shell accelerates much more dramatically than in neat water. This finding is in agreement with previous work [17]. Additionally, the slow component of the spectral diffusion becomes faster and the frequency dependence of the anisotropy disappears. After ~ 2 ps the anisotropy values are completely independent on the probe frequency. The temperature dependence of this anisotropy dispersion is further illustrated in Fig. 7.5B. In this figure the value of the anisotropy at different probe frequencies is shown for four sample temperatures and a pump-probe delay time of 2.5 ps. We further quantify the anisotropy dispersion by fitting a straight line to the anisotropy in the frequency domain 2485–2530 cm^{-1} at every delay time (solid lines in Fig. 7.5B). The slope of the fits are shown as a function of delay time in Fig. 7.6A for a number of temperatures. The non-vanishing endlevels at low temperature are indicative for the persistent frequency dependence of the anisotropy we found in Fig. 7.3. The values of the endlevels are shown in Fig. 7.6B for different temperatures. For comparison we also plotted the difference in endlevel of the dynamics of the first moment (see

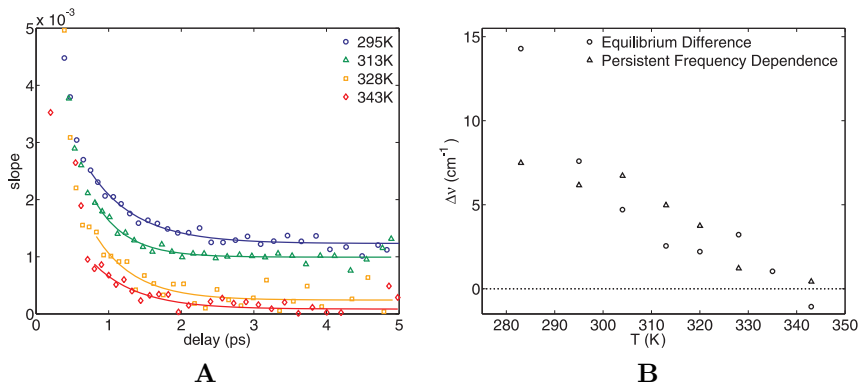


FIGURE 7.6. **(A)** Slope of a straight line fitted to the frequency dependent anisotropy (see Fig. 7.5B) as a function of delay time for different temperatures. For low temperatures the anisotropy is not equilibrated at 5 ps, resulting in the persistent slope. The solid lines are guides to the eye. The endlevels are a measure of inhomogeneity at long delay times and are plotted as a function of temperature in panel **(B)**. For comparison the difference in endlevel of the first moment is plotted, which is a measure for incomplete spectral diffusion (see Fig. 7.4B). Both parameters are correlated and vanish for increasing temperatures.

for example Fig. 7.4B). Both parameters show the same trend: for increasing temperatures both the persistent frequency dependence of the anisotropy and the slow component of the spectral diffusion gradually disappear.

In Fig. 7.7 we compare the anisotropy decay after excitation with a spectrally broad pump with the anisotropy decay after excitation with a spectrally narrow pump at 2650 cm^{-1} at a probe frequency of 2600 cm^{-1} . The anisotropy decay following the narrow-band blue excitation is faster in the first picosecond than the anisotropy decay following the spectrally broad excitation: The anisotropy after 6 ps is independent of the excitation pulse used for this probe frequency. This loss of memory of excitation is present for all measured temperatures. The slow component represents the dynamics in the TMU solvation shell, in which spectral diffusion is very slow. Hence, as long as these oscillators are excited, irrespective by a spectrally broad pump or a narrow blue pump, these dynamics will be seen. This is a different situation from neat water, where spectral diffusion does play a role and a narrow blue excitation effectively speeds up the dynamics probed at 2600 cm^{-1} . For the TMU solution, only the dynamics in the first few picoseconds becomes faster after a narrow blue excitation. These dynamics thus likely mainly represent OD oscillators outside the TMU solvation shell for which spectral diffusion is still fast and plays a dominant role in the dynamics.

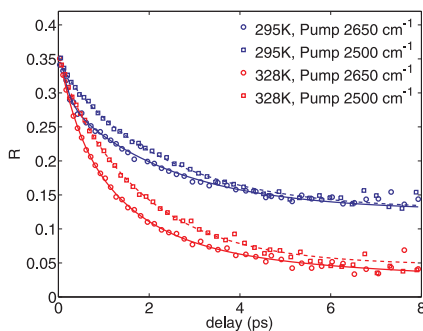


FIGURE 7.7. Comparison of the anisotropy dynamics obtained with a spectrally narrow pump centered around 2650 cm^{-1} (solid lines) and a spectrally broad pump centered around 2500 cm^{-1} (dotted lines) at 295K and 343K. The probe frequency is 2600 cm^{-1} . Similar to what was found for neat 16% HDO:H₂O in chapter 6, at short delay times a faster anisotropy decay is observed after a spectrally narrow blue excitation. The amplitude of the slow reorientation process, however, is conserved: for a probe frequency of 2600 cm^{-1} the anisotropy does not depend on the type of excitation anymore at 8 ps.

7.4 DISCUSSION

We find that spectral diffusion of the OD stretch vibration in a 6 molal solution of TMU in 16% HDO:H₂O has a very slow component that is not present in neat 16% HDO:H₂O (Fig. 7.1). This finding is in agreement with previous 2D-IR measurements on a similar system [109, 110]. Here we find that spectral diffusion also comes to an almost complete halt on the picosecond timescale of the experiment. Spectral diffusion can be due to excitation transfer and structural diffusion [43]. For the isotope dilution we used, the contribution of (Förster) excitation transfer is small [26]. Others have proposed that slow spectral diffusion in aqueous solutions of amphiphiles determined by 2D-IR may be due to the different interaction strength of OD/OH groups with the hydrophilic group of the amphiphile and other water molecules [105, 106]. However, the number of OD/OH groups hydrogen-bonded to the carbonyl group of TMU is likely limited to only two or three, while previous studies found that as many as 12 OD groups per TMU molecule are affected [24, 17]. In addition, in solutions of urea water was found to be hardly affected at all [111], while this molecule has an identical carbonyl group.

The slower spectral diffusion therefore likely arises from slower structural diffusion and a decreased rate of jump reorientation events near the hydrophobic part of the molecule. Recent work using Raman spectroscopy revealed that water around the hydrophobic groups of tert-butyl alcohol is more structured [98]. The methyl groups of TMU are small enough to reside in cavities in the hydrogen-bond network without the need of breaking hydrogen-bonds [11]. The folding of the network around TMU likely leads to a stiffening of the hydrogen-bond network that causes structural diffusion to be severely hindered.

The slower reorientation dynamics is closely related to the slow component of the spectral diffusion, as is also demonstrated in Fig. 7.6. Water dynamics is dominated by the process of hydrogen-bond switching according to the jump-mechanism of reorientation [2]. The rate limiting step for jump reorientation events is the structural reorganization of the hydrogen-bond network to allow the approach of the new hydrogen-bonding partner [89]. Slower structural diffusion thus inevitably also leads to a decreased rate of jump reorientation events and hence slower dynamics.

The reorientation dynamics probed in the blue wing contains contributions of both OD oscillators outside the hydrophobic hydration shell and OD oscillators that are strongly affected by TMU. In comparison to anisotropy measurements with a broad excitation spectrum, the anisotropy at the blue shoulder is initially decaying much faster (Fig. 7.7). This is fully consistent with the interpretation above of the OD groups outside the hydrophobic hydration shell that jump to the red side of the spectrum and diffuse back to the blue side, similar to what we observed for neat water (Fig. 7.3). Structural diffusion is very slow for the OD oscillators that are affected by TMU and for these OD oscillators jumps occur at a much lower rate than in bulk water [108]. The anisotropy decay of these oscillators is therefore much slower, and is in the absence of spectral diffusion mainly probed in the blue wing.

In the case of excitation at 2650 cm^{-1} , the anisotropy measured at low frequencies represents almost exclusively the response from OD oscillators that, after blue excitation, underwent relatively rapid spectral diffusion. These oscillators are thus not so much influenced by TMU. These structurally diffused oscillators either experienced a jump event or migrated from the blue side of the spectrum to the red side by structural diffusion. The decay of the anisotropy in the red wing is very similar to that of OD groups in neat water (Fig. 7.3).

Spectral diffusion leads to a complete randomization of the initially excited subset, after which the reorientation dynamics is independent on the probe frequency. For neat 16% HDO:H₂O this is indeed what we find (Fig. 7.3) and chapter 6 elaborated more extensively on this frequency dependence for short delay times. In contrast to the results for neat 16% HDO:H₂O, we find that the anisotropy dynamics in a 6 molal solution of TMU after excitation by the narrow-band pump pulse strongly depends on the probe frequency. Previous anisotropy measurements on aqueous TMU solutions did not show any frequency dependence for this concentration of TMU [24], but in those experiments the OD absorption band was homogeneously excited by a broad band pump.

At the TMU concentration used in our experiments, it is valid to question whether or not all water molecules are in the vicinity of a TMU molecule and whether a bimodal model as described above is justified [112, 105, 107]. There are a number of points to be taken into consideration to answer this question. TMU is found to aggregate at concentrations below 6 molal and it is therefore likely that nanopools of water exist between clusters of TMU molecules [113, 17, 107]. Water reorientation and spectral diffusion in these nanopools are likely similar to bulk water. Secondly, even water molecules in close vicinity of a TMU

molecule may possess an OD group of which the dynamics is hardly affected by the presence of TMU. This will be the case if the OD group hydrogen-bonds to a water molecule outside the TMU hydration shell or to the hydrophilic group of the TMU. Finally, recent *ab initio* calculations on TMU solution do suggest that even at concentrations as high as 11 molal, the water hydrogen-bond network percolates through regions of accumulating TMU molecules [114]. The average number of hydrogen-bonds per water molecule in a solution of 5.5 molal TMU was found to be 3.6, only marginally smaller than the coordination number in pure water (3.7). The hydrogen-bond network is thus maintained to a large extent at such high concentrations and likely contains regions where the reorientation proceeds similar as in bulk water.

A large increase in reorientation time around TMU has also in previous fs-IR and dielectric relaxation experiments been found for relatively low concentrations of TMU [17, 24]. This large increase has been disputed by classical molecular dynamics (MD) simulations [105, 106]. These simulations find a very modest retardation factor at low concentrations of 1.5 that was assigned to a shielding effect: OD/OH groups in the hydration shell of a hydrophobic group have less potential new hydrogen-bond partners, resulting in a lower frequency of jumps [105]. In this picture there is no collective effect like an enhancement of the hydrogen-bond structure around the hydrophobe. Simulations based on *ab initio* calculations did show an enhanced structure and much slower dynamics of water molecules in the TMU hydration shell [108]. It was found that the spectral diffusion of water around a hydrophobe contains three timescales of spectral diffusion: 70 fs, 1 ps and >10 ps [108]. The slower dynamics was assigned to a (five-fold) decreased rate of hydrogen-bond jumps that was related to the overcoordination of water molecules [108].

The slowing down of the water dynamics around hydrophobic groups seems therefore not only due to the local excluded volume of the hydrophobic moiety. The hydrogen-bond network is probably more globally jammed by accommodating the hydrophobic molecule. The hydrogen-bond rearrangements leading to reorientation is a collective process that requires the reorganization of multiple molecules [115, 61, 68, 86, 82]. The filling of the network cavities by the hydrophobic moieties leads to a strong slowing down of the structural reorganization (spectral diffusion) and thus of the rate of formation of hydrogen-bond configurations that would enable a successful reorientational jump.

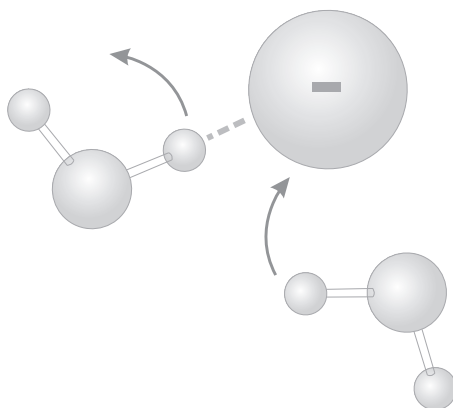
In agreement with previous work [116, 17] we find that the slow reorientation around TMU strongly accelerates upon increasing the temperature. This speed up probably finds its origin in the structural relaxation that becomes much faster at higher temperatures. All hydrogen-bonds become weaker and the formation of a cavity accommodating the hydrophobic groups has a much less restrictive effect on the hydrogen-bond network. The improved ability of the hydrogen-bond network to restructure, results in an increased rate of jumps for OD oscillators next to the hydrophobic groups and therefore a faster decay and spectral equilibration of the anisotropy (Fig. 7.7 and Fig. 7.6). This interpretation is corroborated by *ab initio* calculations, where it was found that the slowest timescale of both spectral diffusion and reorientation dynamics becomes

increasingly less important with increasing temperature [108].

7.5 CONCLUSIONS

We studied the reorientation of OD groups in a 6 molal solution of TMU in isotopically diluted water (16% HDO:H₂O). We used two-color infrared pump-probe spectroscopy to excite the blue wing of the OD stretch vibration and probe the $\nu = 0 \rightarrow 1$ and $\nu = 1 \rightarrow 2$ regions of this band. By exciting only OD oscillators with a blue resonance frequency, we selected those oscillators that have a very weak hydrogen-bond. We found that the spectral diffusion in the TMU solution has a slow component with a time constant > 10 ps. In addition, the reorientation dynamics show a persistent dependence on the probe frequency and hence hydrogen-bond strength of the OD oscillators. These results point at the presence of a less dynamic hydrogen-bond network that folds itself around the hydrophobic groups of the TMU molecule. The decreased ability of the network to restructure leads to much slower spectral diffusion. As a consequence, OD groups that form this cavity have a low rate of forming hydrogen-bond structures that would allow for a reorientational jump. At higher temperatures, the enhanced structuring of the hydrogen-bond network around the hydrophobic groups vanishes, leading to a strong acceleration of the spectral diffusion and the reorientation dynamics.

Exchange Dynamics in Salt Solutions



The solubility of salts in water relies on a subtle balance of the coulomb interaction between water molecules and the ions. If the attraction between the ions is strong compared to the ion-water interaction, the salt precipitates. In solution, a negatively charged anion forms hydrogen-bonds with the OD-groups of a number of water molecules in its direct vicinity. **This solvation shell is not static and in this chapter we describe the exchange of solvation water molecules with their bulk surroundings.** We make use of two properties of the stretching vibration of OD-groups that are hydrogen-bonded to halide anions: (1) its resonance frequency is blue-shifted and (2) its vibrational lifetime is significantly longer compared to that of bulk OD-stretch vibrations. These properties enable us to resolve the reorientation dynamics of both anion-bound and bulk OD-groups. We find that OD groups that are hydrogen-bonded to anions possess a wobbling motion. Small ions like Cl^- have a stronger interaction with the OD groups and therefore restrict the wobbling cone more than for example the larger anion I^- .

8.1 INTRODUCTION

Salts in aqueous solutions are often considered in the context of their ability to enhance or weaken the structural conformation of proteins and membranes. Depending on the surface charge density of the ions they may show an increased or decreased affinity for functional groups by coulomb interaction. These interactions also change the structure and dynamics of water itself and can take the form of a hydrogen-bond or can be purely electrostatic. The electric fields exerted by ionic charges can lead to a strong ordering of the surrounding water. In earlier times it was thought that the effects of ions on water structure were quite long range and would extend well beyond the first hydration layer [117]. Some ions were thus referred to as structure makers, others as structure breakers. However, recent experimental and theoretical work showed that for most ions the effect on the structure and dynamics of water is limited to only one or two hydration layers [118, 119, 120, 121, 122]. Only for specific combinations of ions, like Mg^{2+} and SO_4^{2-} , it was found that the water dynamics can be impeded over relatively long ranges [123].

The retardation of the dynamics of water molecules in the first solvation shell of anions is found to be quite generic [124, 125]. This is caused by the partial immobilization of the slightly positive hydroxyl groups that form a hydrogen-bond to the negatively charged ion. This explanation also supports the observation that anions with a higher surface charge density have a stronger immobilization effect on their surrounding water molecules. Those water molecules are not expected to remain in the anion solvation shell forever, but may exchange with the bulk. Recently this exchange was studied for aqueous solutions of NaBF_4 [126] and NaClO_4 [127, 3]. The time constant of the switching from the hydration shell of the anion to the bulk was found to be ~ 7 ps for BF_4^- and ~ 9 ps for ClO_4^- . Unfortunately, this time constant is very hard to measure for I^- , because the absorption bands of hydroxyl groups hydrogen bonded to either the anion and other water molecules are too strongly overlapping for these salt solutions. For ClO_4^- the absorption bands are quite well separated, thus allowing the measurement of the exchange rate between these components.

In this chapter we study in detail the short delay time behavior and exchange dynamics of water molecules in the anionic hydration shell of iodide and ClO_4^- . We measure the reorientation of the OD-stretch vibration of HDO molecules in solutions of isotopically diluted water and NaI or NaClO_4 . To this end we use polarization-resolved femtosecond infrared pump-probe spectroscopy. Thanks to the difference in vibrational lifetime and spectral response between the anion hydration shell on one hand and the bulk and the water molecules around the cation on the other hand, we can distinguish the orientational dynamics of water solvating the halide ions from the other water molecules.

8.2 EXPERIMENTAL

The experiments in this chapter were performed with the one-color setup described in section 3.1.1. The center frequency of the pump and probe spectra was for different experiments tuned between 2500 cm^{-1} and 2620 cm^{-1} . The solutions of NaI and NaClO_4 were made in isotopically diluted water (4% D_2O in H_2O) and prepared in a sample cell consisting of two CaF windows (2 mm thickness) pressed against each other with a teflon spacer of $25\text{ }\mu\text{m}$ in between. Linear spectra of 4 molal (mol/kg solvent) NaI and neat 4% D_2O in H_2O are shown in Fig. 8.1A.

8.3 RESULTS AND DISCUSSION

8.3.1 LINEAR SPECTRA

The linear spectra of iodide salts show a blue-shift of the OD-stretch vibration compared to that of neat 4% D_2O in H_2O that is independent of the cation (Fig. 8.1A). This blue-shift can be traced to the OD groups that are hydrogen-bonded to the anion ($\text{OD}\cdots\text{I}^-$), in contrast to OD groups that are hydrogen-bonded to other water molecules ($\text{OD}\cdots\text{O}$). The surface charge density of anions decreases with increasing anion size, which leads to a weakening of the $\text{OD}\cdots\text{I}^-$ hydrogen bond [128]. The anharmonic coupling of the hydrogen-bond to the OD stretch vibration results in such case to a blue-shift. In iodide solutions we thus can distinguish two different hydrogen-bonding species of OD oscillators. It is expected that the pump-induced absorption changes of these OD oscillators thus contribute to the transient spectra with a corresponding frequency shift. For iodide bound OD oscillators the blue-shift is 70 cm^{-1} , whereas for perchlorate bound OD oscillators the blue-shift is as much as 140 cm^{-1} .

8.3.2 VIBRATIONAL RELAXATION AND EXCHANGE

In Fig. 8.1B transient spectra at different delay-times are shown for a 4 molal solution of NaI, obtained with a pump-probe spectrum centered around 2500 cm^{-1} . At early delay times the spectrum shows a bleach due to the depletion of the ground state population and $\nu = 1 \rightarrow 0$ stimulated emission of the OD stretch vibration. This transient spectrum due to the vibrational excitation decays on a picosecond timescale. The transient spectrum at long delay-times is the thermal-difference spectrum resulting from the temperature rise due to the equilibrated pump-energy, as elaborated on in chapter 4. The blue side of the spectra decays more slowly than the red side, pointing to a difference in vibrational lifetime for the two OD oscillator species with different spectral response.

In previous work it was found that the vibrational relaxation dynamics of salt solutions containing Cl^- , Br^- , or I^- ions consists of two distinct components [129, 130]. One component is formed by OD groups that are hydrogen-bonded to the oxygen atom of another water molecule. This component comprises both

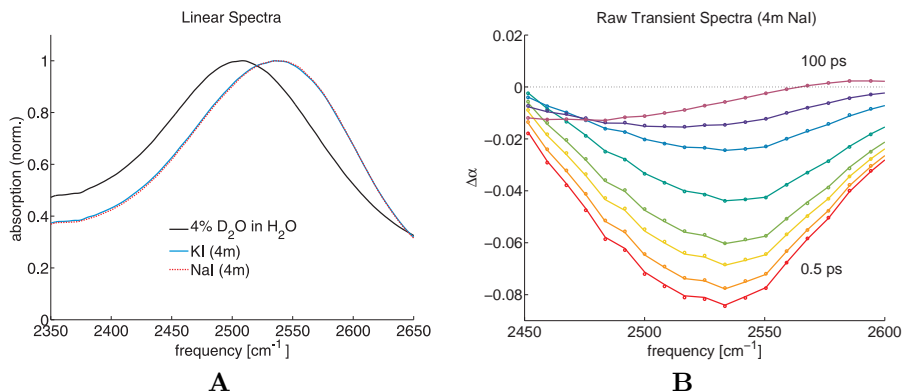


FIGURE 8.1. **(A)** Linear absorption spectra in the region of the OD-stretch vibration for a 4 molal solution of NaI and neat 4% D₂O in H₂O. The spectra of the KI and NaI solutions are nearly identical. **(B)** Transient spectra as measured for a 4 molal NaI solution for delay times of 0.5, 0.7, 1.1, 1.4, 2.5, 5.1, 8.1 and 100 ps.

the bulk water molecules and the water molecules in the hydration shells of the cations. These OD \cdots O groups absorb at about the same frequency as the OD groups in neat HDO:H₂O and have a vibrational lifetime T_1 of 1.8 ± 0.2 ps. The other component is formed by OD groups that are hydrogen bonded to the halogenic anion $A^- (=Cl^-, Br^- \text{ or } I^-)$. The excited OD $\cdots A^-$ vibrations have a vibrational lifetime of 3-6 ps [129, 130], substantially longer than the excited OD \cdots O oscillators. To take this blue-shifted contribution into account the kinetic model for neat HDO:H₂O is extended with a second excited state. The two excited states will exchange since the HDO molecules bound to an anion can rotate out of the anion-hydration shell and become OD \cdots O hydrogen-bonded and vice versa.

The kinetic model that is used to analyze the data is schematically displayed in Fig. 8.2 and elaborated on in section 4.4.3. We rewrite here equation Eq. (4.12) for the decomposition of the isotropic transient spectra $\Delta\alpha_{\text{iso}}(\nu, t)$ into the separate state contributions,

$$\Delta\alpha_{\text{iso}}(\nu, t) = \frac{\Delta\alpha_{\parallel}(\nu, t) + 2\Delta\alpha_{\perp}(\nu, t)}{3} = \sum_{i=1}^4 N_i(t)\sigma_i(\nu) \quad (8.1)$$

where $N_i(t)$ is the population dynamics and $\sigma_i(\nu)$ the associated transient spectrum of the i th species or state. In the analysis we neglect the effects of spectral diffusion within the OD \cdots O and OD $\cdots A^-$ bands. This is a good approximation as we use relatively broad-band excitation pulses (FWHM ~ 120 cm⁻¹) and because we only model the dynamics for delays ≥ 0.5 ps, for which the spectral diffusion is nearly complete [131, 130].

In view of the fact that the hydrogen bonds between water and the halogenic anions are stronger than those between water and $\text{BF}_4^-/\text{ClO}_4^-$, we expect the

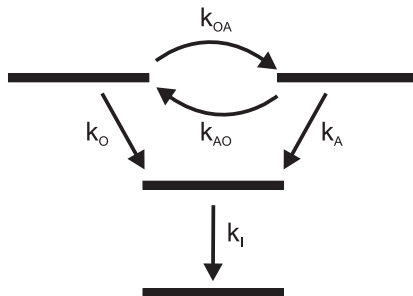


FIGURE 8.2. Schematics of the model used for fitting the vibrational decay processes. The two excited states are allowed to exchange from $\text{OD}\cdots\text{O}$ to $\text{OD}\cdots\text{A}^-$ (with rate constant k_{OA}) and vice versa (k_{AO}). The decay process of both states involves an intermediate state to which $\text{OD}\cdots\text{O}$ and $\text{OD}\cdots\text{A}^-$ oscillators decay with rates k_{O} and k_{A} respectively.

switching time for rotation out of the hydration shell of I^- to the bulk to be at least as large as observed for BF_4^- and ClO_4^- , i.e. $\tau_{\text{AO}} \leq 9$ ps. In the modeling we use a value of τ_{AO} of 9 ps. The value of τ_{OA} of the reverse process was chosen such that the number density of $\text{OD}\cdots\text{A}^-$ oscillators is conserved. Hence, $\tau_{\text{AO}}/\tau_{\text{OA}} = N_{\text{OD}\cdots\text{O}}/N_{\text{OD}\cdots\text{A}^-}$, meaning that τ_{OA} will decrease with increasing salt concentration.

Fig. 8.3A shows the spectra $\sigma_i(\nu)$ that result from a fit of the kinetic model to the data. We assign the spectrum around 2500 cm^{-1} to excited $\text{OD}\cdots\text{O}$ and the spectrum around 2550 cm^{-1} to excited $\text{OD}\cdots\text{I}^-$. Neither of the two spectral shapes changes significantly when the concentration or the nature of the cation is changed. The population dynamics $N_i(t)$ resulting from the fit are shown in Fig. 8.3B, from which it is clear that the $\text{OD}\cdots\text{I}^-$ spectrum decays much more slowly than the $\text{OD}\cdots\text{O}$ spectrum. These results demonstrate that we can distinguish between the two different species $\text{OD}\cdots\text{O}$ and $\text{OD}\cdots\text{I}^-$.

8.3.3 SEPARATION OF THE ANION-BOUND ANISOTROPY

The vibrational lifetime of the $\text{OD}\cdots\text{I}^-$ oscillators is longer than that of the $\text{OD}\cdots\text{O}$ oscillators. This implies that if Eq. (4.18) is used to calculate the anisotropy decay, the resulting dynamics would be dominated by the contribution of the $\text{OD}\cdots\text{I}^-$ oscillators for long delay times. For shorter delay times, the dynamics would have a mixed character with time-dependent weighting factors. To obtain the correct anisotropy dynamics, the anisotropy for both $\text{OD}\cdots\text{O}$ and $\text{OD}\cdots\text{A}^-$ species should thus be resolved separately. This is possible due to the spectral separation of their response and difference in vibrational lifetime. We therefore consider the difference signal $D(\nu, t)$, which can be written as,

$$D(\nu, t) = \frac{\Delta\alpha_{\parallel}(\nu, t) - \Delta\alpha_{\perp}(\nu, t)}{3} = \sum_{i=1}^4 R_i(t) N_i(t) \sigma_i(\nu) \quad (8.2)$$

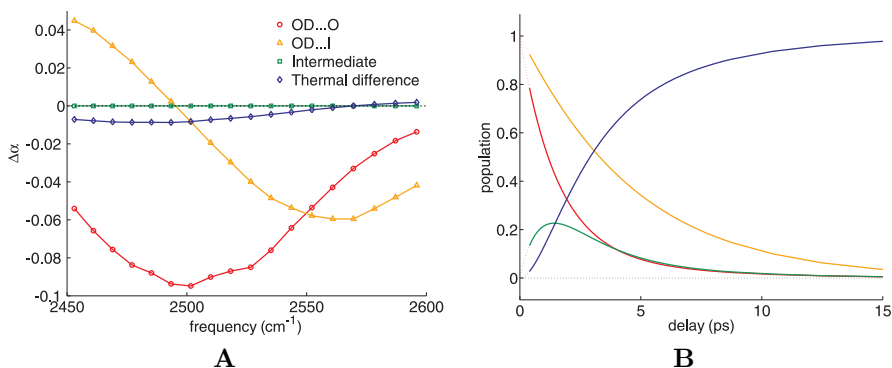


FIGURE 8.3. (A) Spectral components $\sigma_i(\nu)$ obtained from fitting the data of a 4 molal NaI solution. (B) Time dependence of the normalized populations $N_i(t)$ in the different states. At any given delay-time the total transient spectrum is the weighted sum of the spectra shown in A, the weight factors given by the population curves in B according to Eq. (8.1).

where $R_i(t)$ is the anisotropy decay of the i th species or state. The associated state spectra and population dynamics were already obtained from fitting the isotropic data and we thus can resolve from $D(\nu, t)$ the anisotropy dynamics for the independent states. This formalism implicitly assumes that the anisotropy decay within the absorption band of a certain species does not show any significant frequency dependence, as is the case for neat 4% D_2O in H_2O [22]. Since we assume the intermediate state to have a vanishing spectrum and the heat state to be isotropic (i.e. have a vanishing anisotropy), only the two excited states contribute to $D(\nu, t)$ and thus n equals 2. To resolve the $\text{OD}\cdots\text{O}$ anisotropy $R_{\text{OD}\cdots\text{O}}(t)$ and $\text{OD}\cdots\text{A}^-$ anisotropy $R_{\text{OD}\cdots\text{A}^-}(t)$ separately, we decompose the difference spectrum $D(\nu, t)$ at every delay-time t in the two excited state spectra $\sigma_i(\nu)$ obtained from the isotropic fit. The resulting time-dependent amplitudes both contain $N_i(t)$ and $R_i(t)$ and the latter is obtained through division by the fitted isotropic population dynamics. As implied by the kinetic model, $R_{\text{OD}\cdots\text{A}^-}(t)$ represents the reorientation of excited water molecules that keep their hydrogen bond with the anion intact or that have rotated from the bulk into the solvation shell. The dynamics of $R_{\text{OD}\cdots\text{A}^-}(t)$ thus includes both the effects of exchange and the intrinsic anisotropy decay of the anion-bound OD oscillators. In Fig. 8.4 a typical example of a decomposition for a 4 molal NaI solution is shown. The anisotropy decay of the $\text{OD}\cdots\text{O}$ component can be well fitted with a mono-exponential function with a time constant of ~ 2.6 ps, a behavior identical to that found for neat $\text{HDO}:\text{H}_2\text{O}$ [22]. The $\text{OD}\cdots\text{I}^-$ anisotropy decay is clearly not mono-exponential: after a fast relaxation, faster than in bulk water, the anisotropy decays via a much slower process.

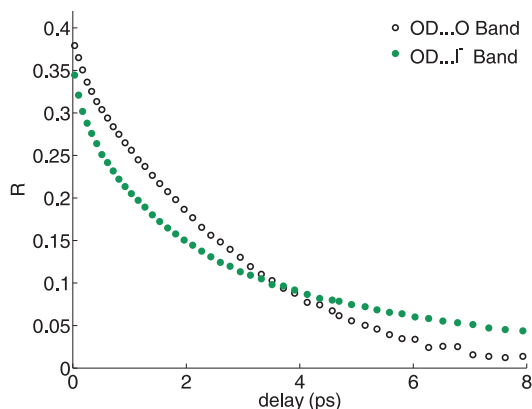


FIGURE 8.4. Results of a band decomposition on the data obtained for a 4 mol/kg NaI solution. The solid circles represent the orientational dynamics of OD groups bound to iodide, the open circles those of OD groups bound to other water molecules.

In contrast to previous femtosecond measurements on water reorientation in salt solutions, we resolved the dynamics of $\text{OD}\cdots\text{O}$ and $\text{OD}\cdots\text{A}^-$ groups separately. The $\text{OD}\cdots\text{I}^-$ curve shown in Fig. 8.4 therefore represents the orientation dynamics of OD-groups bound to iodide *only*. The features in the first 200 fs lie within the cross correlate of the pump and probe pulse and the effects of spectral diffusion are not negligible. Nonetheless, it is clear that an extremely rapid decay makes the anisotropy drop to about 0.3, which is 75% of its theoretical maximum of 0.4. This first drop is likely due to fast librational motions [132]. The behavior after 0.5 ps has a non-mono-exponential character with a fast decay component and a slower component at later delay times. The slow component corresponds to the slower dynamics of water that was previously found in aqueous solutions of halide salts [124, 125]. Its origin is explained by diffusion of OD-groups over the surface of the ion, and the reorientation of the complete hydration shell of the halogenic anion. The short delay time dynamics could not be resolved before. Chapter 9 will discuss the characteristics of the $\text{OD}\cdots\text{A}^-$ anisotropy decay in more detail, but before that we show in the next section that $R_{\text{OD}\cdots\text{I}^-}(t)$ contains a contribution that is not intrinsic to the reorientation of OD groups that keep their hydrogen bond to the anion intact.

8.3.4 CONTRIBUTION OF EXCHANGE TO THE ANISOTROPY

The data shown so far were obtained with the pump-probe spectrum centered at the $\text{OD}\cdots\text{O}$ resonance at 2500 cm^{-1} . Since the $\text{OD}\cdots\text{I}^-$ resonance peaks at 2570 cm^{-1} , the pump spectrum only partly overlaps with this band. One may thus wonder what effect different pump frequencies have on the results of the analysis presented above. To further investigate the nature of the $\text{OD}\cdots\text{I}^-$

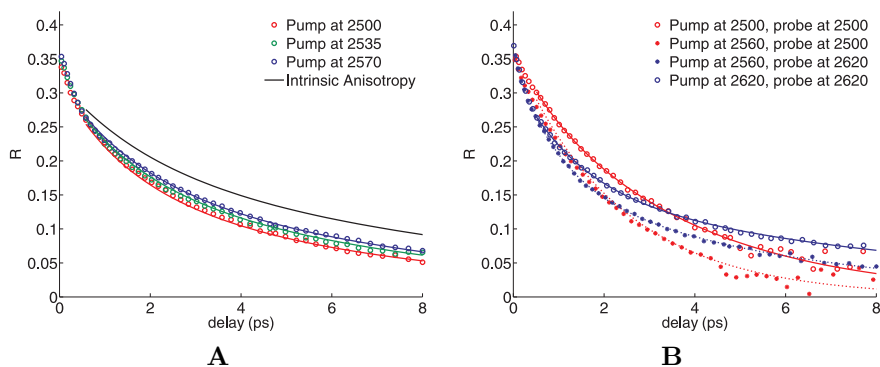


FIGURE 8.5. (A) Resolved anisotropy decays of anion-bound water for 4 molal NaI with different pump frequencies. If exchange is included in the anisotropy dynamics, the solid lines fitting the three measured anisotropy curves are obtained. (B) The total anisotropy decay of a 4 molal NaClO_4 solution at different frequencies for a pump spectrum centered around 2500, 2560 or 2620 cm^{-1} . If the pump and probe frequencies are not the same, exchange events make the anisotropy decay faster.

component we therefore shift the pump-probe spectrum to be centered around 2535 cm^{-1} and 2570 cm^{-1} to have an increasing overlap with the $\text{OD}\cdots\text{I}^-$ resonance. The resulting decomposed $\text{OD}\cdots\text{I}^-$ anisotropy decays of a 4 molal NaI solution are presented in Fig. 8.5A. The curves show a smaller initial decay when the pump has a better overlap with the iodide band.

The differences in $R_{\text{OD}\cdots\text{I}^-}(t)$ depending on the center frequency of the pump spectrum inspires to investigate solutions of NaClO_4 . A decomposition of the anisotropy is for this system not needed due to the large frequency shift of $\text{OD}\cdots\text{ClO}_4^-$ ($\sim 140 \text{ cm}^{-1}$), making it ideal for studying the effect of the pump frequency on the anion-bound anisotropy and a test case for our analysis. We repeat the previous experiments for solutions of NaClO_4 by tuning the center frequency of the pump to 2500, 2560 and 2620 cm^{-1} (Fig. 8.5B). In case the sample is pumped at 2560 cm^{-1} , the anisotropy probed at 2620 cm^{-1} shows a larger fast decaying component than when the sample is pumped at 2620 cm^{-1} . Similarly, with the pump at 2560 cm^{-1} the anisotropy decay at 2500 cm^{-1} shows a larger faster component compared to the case where the sample is both pumped and probed at 2500 cm^{-1} .

To model the vibrational relaxation we used a kinetic model that incorporates exchange events between water molecules in the anion hydration shell and water molecules hydrogen-bonded to other water molecules. These exchange events can account for part of the $\text{OD}\cdots\text{I}^-$ anisotropy decay shown in Fig. 8.4, and to treat the anisotropy data consistently we include these effects here as well. The way in which exchange affects the anisotropy can be understood as follows.

The rotation of excited OD-oscillators out of the anion hydration shell does not affect the decay of the $\text{OD}\cdots\text{A}^-$ anisotropy. These oscillators exchange their $\text{OD}\cdots\text{A}^-$ hydrogen bond for an $\text{OD}\cdots\text{O}$ hydrogen bond and thus no longer contribute to the $\text{OD}\cdots\text{A}^-$ spectral component $\sigma_{\text{OD}\cdots\text{A}^-}$. Therefore, the rotation out of the hydration shell will only lead to a decay of $N_{\text{OD}\cdots\text{A}^-}(t)$, but not to an additional decay of $R_{\text{OD}\cdots\text{A}^-}(t)$. However, there are also OD-groups that were excited as $\text{OD}\cdots\text{O}$ oscillators and have changed their orientation to become $\text{OD}\cdots\text{A}^-$ oscillators. These oscillators will contribute to the measured anisotropy of the $\text{OD}\cdots\text{A}^-$ spectral component. In fact it can be expected that these oscillators will decrease the anisotropy of the $\text{OD}\cdots\text{A}^-$ spectral component, because the angle of rotation in the exchange between the hydration shell and the bulk is ~ 55 degrees [2, 133, 134]. Since the time constants of the exchange are of the order of 10 ps the switching from the bulk to the hydration shell will mainly contribute to the slow component of the anisotropy decay.

The exchange explains the behavior of the anisotropy decay of anion-bound water for different pump frequencies. In the case of a pump spectrum centered around the $\text{OD}\cdots\text{O}$ resonance at 2500 cm^{-1} , relatively more water molecules *outside* the anion hydration shell are excited compared to an experiment with a blue-shifted pump spectrum. In both cases the anion band is probed, but exchange events with excited $\text{OD}\cdots\text{O}$ molecules will show a larger contribution to the decay of the measured $\text{OD}\cdots\text{I}^-$ anisotropy in the first situation.

The results for NaClO_4 presented in Fig. 8.5B show this effect very clearly. Here the two bands are well separated, allowing for excitation of almost exclusively $\text{OD}\cdots\text{ClO}_4^-$ or $\text{OD}\cdots\text{O}$ oscillators. Exclusive $\text{OD}\cdots\text{ClO}_4^-$ excitation is achieved with the pump-probe spectrum centered around 2620 cm^{-1} . The reorientation dynamics thus probed can only come from $\text{OD}\cdots\text{ClO}_4^-$ oscillators and shows a clear bi-exponential behavior. Only $\text{OD}\cdots\text{O}$ oscillators are excited with the pump-probe spectrum centered around 2500 cm^{-1} . The $R_{\text{OD}\cdots\text{O}}(t)$ anisotropy in this case decay with 2.5 ps similar to the reorientation dynamics in neat 4% D_2O in H_2O . However, when the pump spectrum is positioned in between the two bands around 2560 cm^{-1} , oscillators in both bands are excited. The exchange events then cause both the anisotropy probed at 2500 cm^{-1} and 2620 cm^{-1} to decay considerably faster compared to the previous situation in which the $\text{OD}\cdots\text{O}$ and $\text{OD}\cdots\text{ClO}_4^-$ bands were pumped separately at 2500 cm^{-1} and 2620 cm^{-1} , respectively.

To further formalize the exchange dynamics in the measured anisotropy decays, we fit all three anisotropy curves of Fig. 8.5A using the same model. We assume a single bi-exponential functional form for the intrinsic $\text{OD}\cdots\text{I}^-$ anisotropy decay ($R_{\text{intr}}(t)$) and then include exchange effects as follows. From the fitted vibrational decay constants and exchange rates we obtain the population dynamics of OD oscillators that remain $\text{OD}\cdots\text{A}^-$ bonded ($N_{\text{intr}}(t)$) and those that exchange from the bulk or the anion hydration shell ($N_{\text{ex}}(t)$). We can treat those two types of OD oscillators as different species. The exchanging species are now assumed to lose their orientation completely in the event ($R_{\text{ex}}(t) = 0$), which is a slight overestimation compared to a $\approx 75\%$ decrease associated with the jump angle found by Gaffney et al for perchlorate solutions [3].

The species that do not exchange are assumed to have the intrinsic reorientation dynamics. The total reorientation dynamics of $\text{OD}\cdots\text{I}^-$ oscillators is then given by the weighted sum of the two as follows,

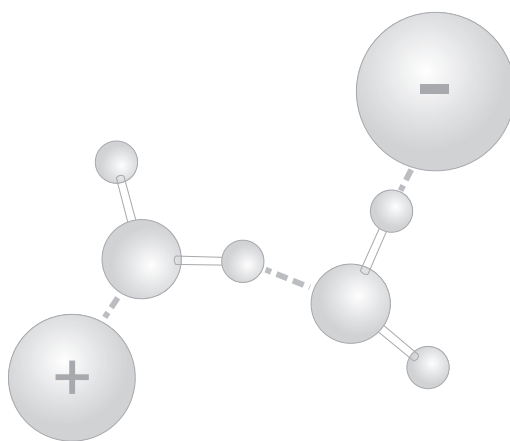
$$R_{\text{OD}\cdots\text{I}^-}(t) = \frac{N_{\text{intr}}(t)R_{\text{intr}}(t)}{N_{\text{intr}}(t) + N_{\text{ex}}(t)} \quad (8.3)$$

where the population dynamics depend on the initial populations and thus on the overlap of the pump spectrum with the $\text{OD}\cdots\text{I}^-$ band. The parameters of the intrinsic anisotropy are now varied to fit the total anisotropy curves including exchange to the curves obtained by the measurements with different pump frequencies simultaneously. The solid lines in Fig. 8.5A are the results of the fit, the black line is the intrinsic anisotropy if no exchange would occur. The single intrinsic anisotropy decay can indeed describe all three measurements, thus supporting our hypothesis that the differences between the data obtained with different pump frequencies were due to the exchange events.

8.4 CONCLUSIONS

By using the blue-shifted resonance frequency and slower vibrational decay time of OD-oscillators bound to iodide and perchlorate anions ($\text{OD}\cdots\text{A}^-$) we were able to separate the reorientation dynamics of the $\text{OD}\cdots\text{A}^-$ from those of bulk OD-oscillators ($\text{OD}\cdots\text{O}$). The $\text{OD}\cdots\text{A}^-$ anisotropy $R_{\text{OD}\cdots\text{A}^-}(t)$ is found to decay by a fast and a slow process. The relative amplitude of the two processes depend on the spectral position of the center frequency of the pump pulse. This can be readily understood by considering exchange events of excited $\text{OD}\cdots\text{O}$ that rotate into the anion hydration shell and become $\text{OD}\cdots\text{A}^-$. Such a rotation requires the OD-group to jump over an angle of about 55° , an event in which almost all orientation is lost. Exchange events thus result in an additional decrease of the $R_{\text{OD}\cdots\text{A}^-}(t)$. The magnitude of this decrease depends on the relative fraction of excited $\text{OD}\cdots\text{O}$ to $\text{OD}\cdots\text{A}^-$, which on its turn depends on the spectrum of the pump. In case the pump spectrum is tuned to have a better overlap with the $\text{OD}\cdots\text{O}$ resonance, relatively more $\text{OD}\cdots\text{O}$ than $\text{OD}\cdots\text{A}^-$ will be excited. The $\text{OD}\cdots\text{A}^-$ anisotropy will then represent more OD-oscillators that experienced a jump into the anion hydration shell and lost their orientation. In case the $\text{OD}\cdots\text{A}^-$ is exclusively pumped, the pure $\text{OD}\cdots\text{A}^-$ reorientation dynamics, or intrinsic anisotropy, is probed. The implementation of this model for exchange offers an excellent description of the observed pump-frequency dependent anisotropy decays.

Cooperative Effects in Ion Hydration



In the previous chapter we studied the solvation shell of anions in water. However, in salt solutions one also has to consider the cation. Its positive charge does not attract the OD-groups of water, but rather the lone electron pairs on the oxygen of the water molecules. As a result the solvation shell of a cation looks dramatically different, with the static dipoles of its water molecules sticking radially out. The OD-groups in the cation solvation shell are therefore hydrogen-bonded to the bulk surroundings and can fully participate in reorientation processes. **By using the technique described in the previous chapter we show in this chapter that the reorientation dynamics of OD-groups in the *anionic* hydration shell in fact are affected by the presence of the cation.** Anion-bound OD-groups have a freedom to wobble while keeping their hydrogen-bond intact. This wobbling motion is restricted in case cations with a sufficiently large surface charge density are co-solvated. This cooperative effect on the hydration of charged solutes is shown to be a generic feature that could play an important role in the process of denaturation of proteins by certain salts.

9.1 INTRODUCTION

Water plays an essential role in the determination of the spatial structure of (bio)molecules and (bio)molecular ions. Examples of this role of water are the hydrophobic collapse in the folding of proteins and the self-organized formation of cell membranes [135]. Concentrations of certain salts have been found to influence these processes. Over a century ago, Hofmeister arranged a number of salts to their ability to denature proteins, resulting in the so-called Hofmeister series [136]. In an attempt to explain this heuristic ordering of ions on a molecular level, the concepts of structure-making and structure-breaking were introduced [137]. It was thought that different ions either strengthen or weaken the hydrogen-bond network of water over long distances and that this effect would explain the observed (de)naturation effects. In the past decade, more evidence was found that the effect of ions on water does not extend much further than their first hydration shell [118, 119, 120, 121, 122]. These results imply that, rather than long range structuring effects, direct ion-protein and ion-membrane interactions are responsible for the influence of salts on the conformation of (bio)molecules.

More specifically, ions have been found to change the properties of a lipid membrane such as thickness, headgroup conformation and lateral diffusion [138, 139, 140, 141, 142, 143, 144, 145]. In a number of studies it was found that the tendency of anions to adsorb at the membrane surface follows the Hofmeister series: weakly hydrated anions (with a low surface charge density) such as iodide are attracted, while fluoride is repelled [141, 145]. For cations the effect is rather opposite: strongly hydrated ions (with a large surface charge density) such as Ca^{2+} and Na^{+} can penetrate into the interfacial region of the membrane and tend to form clusters with lipids by binding to their carbonyl and phosphate groups [138, 145, 142, 143, 146]. These results suggest a delicate balance of the interactions between the hydrophilic groups of the phospholipid headgroups, water and the co-solvated ions. For the understanding of membrane stability and protein denaturation, it is therefore crucial to have a proper knowledge on the details of ion hydration and water mediated interactions between ions and charged molecular groups.

In this chapter we investigate these interactions. To this end we study the orientational mobility of water molecules in a few selected electrolyte solutions. First we try to understand the influence of anions on their solvation shell by characterizing the reorientation of water molecules that are hydrogen bonded to either chloride or iodide. Subsequently, we address the influence of different co-solvated cations on the dynamics of the anion solvation shell. With this knowledge we look into two biologically important charged molecules in combination with different types of cations: 1) Phosphorylethanolamine, which forms the polar headgroup of a common class of membrane lipids (see structure formula in Fig. 9.1B) and 2) formate, which acts as a model system for carbonyl groups that are commonly encountered in proteins. We eventually draw the bigger picture of cooperative hydration that evolved out of a number of experiments in the last few years. Most results in this chapter were obtained using

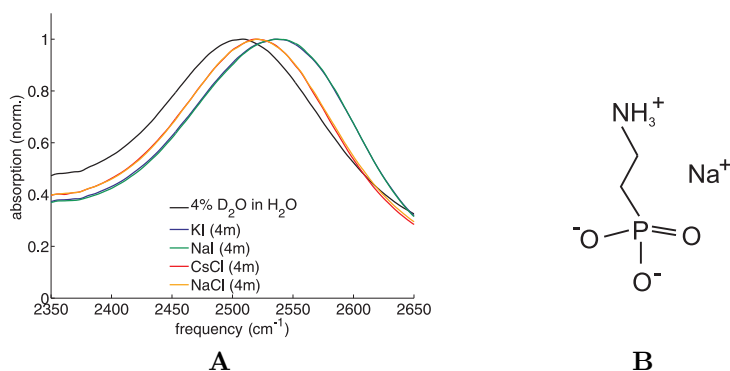


FIGURE 9.1. **A** Linear absorption spectra in the region of the OD stretch vibration for concentrated solutions of the measured alkali-halide salts and pure 4% D_2O in H_2O . The OD stretch spectrum is shifted depending on the nature of the anion. **B** Molecular structure formula of NaPE in water. PE^- is a zwitterion at neutral pH.

the one-color infrared setup described in section 3.1.1. Section 9.3.4 describes dielectric spectra that were obtained using the GHz dielectric relaxation setup described in section 3.3.

9.2 SAMPLES AND LINEAR SPECTRA

In the first part of this chapter we focus on simple aqueous solutions of alkali-halide salts. We chose NaCl, NaI, CsCl and KI for their high solubility and coverage of the moderately strong to weakly hydrating alkali and halide ion series [137]. The salts were purchased from Sigma Aldrich and were all of >99% purity. We dissolved the salts in solutions of 8% HDO in H_2O . Fig. 9.1A shows the linear spectra of 4 molal solutions of the thus obtained solutions in the region of the OD stretch vibration. As elaborated on in chapter 8, the hydrogen-bond between deuteroyl groups and halide ions is weaker than water-water hydrogen-bonds, resulting in a blue-shift of the OD stretch band. For the iodide salts this effect is stronger than for the chloride salts since iodide has a lower surface charge density than chloride. We will use the blue-shift of anion bound OD oscillators to study the reorientation dynamics of the anion solvation shell.

In subsequent sections we will study the reorientation dynamics of OD groups in solutions of the molecular anions phosphorylethanolamine (PE^-) and formate ($HCOO^-$) in combination with different cations $M=Cs^+$, K^+ , Na^+ , Ca^{2+} . PE^- forms a good model system for the hydrophilic headgroup of a very common class of phospholipids, the phosphatidylethanolamines. Phosphorylethanolamine (98% purity) was obtained in pure form from Sigma Aldrich. After dissolving PE in water (isotopically diluted or pure H_2O), a stoichiomet-

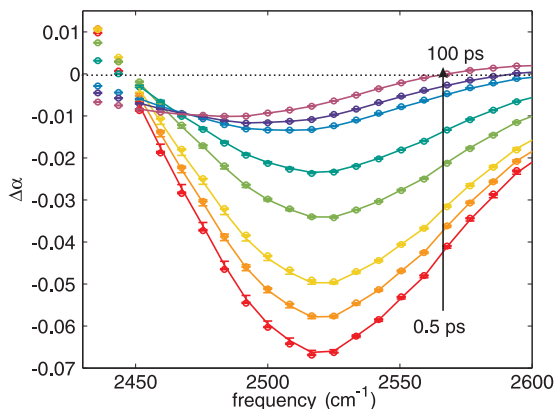


FIGURE 9.2. Transient absorption spectra at different delay times for a 4 molal NaCl solution. The solid lines are the results from the fit to the model described in the text.

ric amount of hydroxide with the appropriate cation was added to obtain the salt solution of interest. The solutions were brought to pH=8, at which pH the phosphate fragment is fully deprotonated and the ammonium group is positively charged [147], as illustrated in Fig. 9.1B. A small amount of D₂O was added to the samples used in the fs-IR experiments, such that the solvent consisted of 8% HDO:H₂O. For these salts, typically no blue-shift of the OD stretch vibration is observed. Samples for the dielectric experiments were prepared in volumetric flasks, in order to obtain well-defined molar concentrations of all components, required for the analysis of the dielectric data. Throughout the sections that cover the results on PE⁻ all concentrations mentioned will refer to the concentration of PE⁻, meaning that the amount of bivalent Ca²⁺ cations in a solution of CaPE is only half the amount of Na⁺ cations in a solution of NaPE of the same (PE) concentration. Formate is a model system for the carboxylate side group of the amino acids aspartic and glutamic acid and is also often present in the hydrophilic headgroup of certain types of membrane lipids.

9.3 RESULTS AND INTERPRETATION

9.3.1 REORIENTATION OF WATER IN THE ANION HYDRATION SHELL

Fig. 9.2 shows transient absorption spectra at different pump-probe delay times measured for a 4 molal NaCl solution. The negative absorption change (bleach) for short delay times results from the excitation ($\nu_s = 0 \rightarrow 1$) of the OD stretch vibration of a few percent of the HDO molecules. The excited state decays in a few picoseconds to a differential absorption spectrum that remains constant on the timescale of the experiment ($10 < t/ps < 100$). This differential

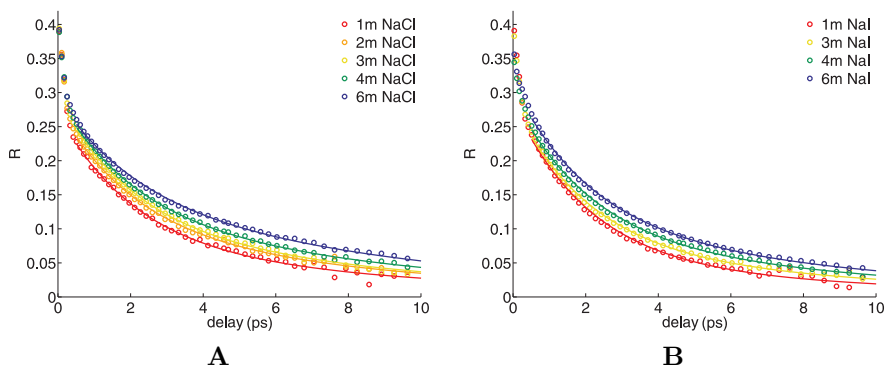


FIGURE 9.3. $\text{OD}\cdots\text{A}^-$ ($\text{A}^- = \text{Cl}^-, \text{I}^-$) anisotropy decay for different concentrations of NaCl (**A**) and NaI (**B**) solutions, including exchange effects. All curves show a fast and slow decay. The reorientation becomes slower for more concentrated solutions, in case of NaCl more so than for NaI.

absorption signal results from the increase of temperature after the excitation has completely equilibrated over all the bath modes and is referred to as the thermal difference spectrum (see section 4.3).

We analyze the data identically to the procedure described in section 4.4.3 and chapter 8, to which the reader is referred to for more details. In short, the isotropic spectra like those shown in Fig. 9.2 are described by a model of vibrational relaxation in which there are two different excited states, corresponding to the $|\nu_s = 1\rangle$ states of the $\text{OD}\cdots\text{O}$ and $\text{OD}\cdots\text{A}^-$ oscillators ($\text{A}^- = \text{Cl}^-, \text{I}^-$). In the kinetic modeling we included the effects of exchange between the anion hydration shell and the bulk (see for a graphical presentation of the model Fig. 4.7). Each of the states has a specific associated difference absorption spectrum with respect to the ground state absorption spectrum. The shapes of the difference spectra are fitted to the measured transient spectra at all delay times. The fitted difference spectra do not change in shape as a function of delay time, they only change in amplitude following the relaxation dynamics of the kinetic model. Using the thus obtained state spectra we obtain the reorientation dynamics of both the $\text{OD}\cdots\text{O}$ and $\text{OD}\cdots\text{A}^-$ oscillators by a spectral decomposition (see section 4.4.3). The $\text{OD}\cdots\text{A}^-$ anisotropy decays for various concentrations of both salts are shown in Fig. 9.3.

The anisotropy curves show a non-exponential decay with a fast and slow component. As described in chapter 8 these decay curves not only represent the reorientation dynamics of OD groups that remain hydrogen-bonded to the anion (the intrinsic anisotropy), but also include a contribution due to excited $\text{OD}\cdots\text{O}$ oscillators that rotated into the anion hydration shell. We model the anisotropy of the anion-bound water by assuming a bi-exponential form for the intrinsic anisotropy $R_{\text{OD}\cdots\text{A}^-}^{\text{intr}}(t)$, i.e. the anisotropy of the ion hydration shell

in case there would be *no* exchange [30]:

$$R_{OD\dots A^-}^{intr}(t) = R_0 \left[(1 - B_0)e^{-t/\tau_1^A} + B_0e^{-t/\tau_2^A} \right] \quad (9.1)$$

Here R_0 is the initial amplitude, B_0 a proportionality factor between the two exponentials and τ_1^A and τ_2^A the time constants of the reorientation processes. The initial drop due to librational motions is neglected here, as we only consider the data after 0.5 ps in the fit. We include the exchange effects as was described in section 4.4.3. It is not possible to determine the time constant of the exchange for chloride and iodide solutions from our experiments because the $OD\dots O$, $OD\dots Cl^-$ and $OD\dots I^-$ strongly overlap. Therefore we fixed the exchange time constant for all measurements to 9 ps, as found by Gaffney for perchlorate solutions [3]. The solid lines in Fig. 9.3 represent the results of the fit for the NaCl and NaI solutions including the exchange effects. For both NaCl and NaI we find $\tau_1^A = 2 \pm 0.3$ ps and $\tau_2^A = 9 \pm 1$ ps. The relative amplitudes of the 2 ps component are shown for all concentrations in Fig. 9.6A. For the iodide solutions this component larger than for the chloride solutions.

We assign the slow reorientation component of the intrinsic anisotropy decay to rotational diffusion of hydration shell water molecules on the charged anion surface, while keeping the $OD\dots A^-$ hydrogen bond intact [133]. The fitted timescale is 9 ± 1 ps, in good agreement with what was found previously for the long delay-time behavior of halide bound water [125, 132, 148]. For the fast component we found a time constant of 2.0 ± 0.3 ps that we assign to a wiggling motion of the OD bound to the anion. Since the iodide anion is substantially larger than a water molecule, the $OD\dots I^-$ bond is less directional than the $OD\dots O$ hydrogen-bond. The angle between the $O\dots I^-$ vector and the OD transition dipole moment $\vec{\mu}$ can therefore assume larger values than in bulk water, without significantly weakening this bond. The variation of this angle - while keeping the bond to the anion intact - will be influenced by the environment of the water molecule. In principle this contribution will therefore show a similar decay time as the bulk reorganisation/reorientation. We find a time constant that is somewhat faster than the bulk reorientation, which is possible since the wiggling within the anionic hydration shell does not necessarily require a completed bulk reorientation event. This mechanism was previously proposed for water solvating bromide ions in cationic micelles [149]. For small micelles the bromide concentration in the interior becomes extremely high and the total anisotropy will be dominated by the behavior of water solvating the anions. For this system, an initially rapidly decaying anisotropy was observed, assigned to the angular freedom of the $OD\dots Br^-$ hydrogen bond. With decreasing size of the anion from I^- to Cl^- , the amplitude of the fast process decreases (Fig. 9.6A). This is explained by the restricted angular freedom of motion that the smaller chloride ion allows for, which causes the anisotropy of chloride-bound water to drop less than that of iodide bound water (see also [89, 150]).

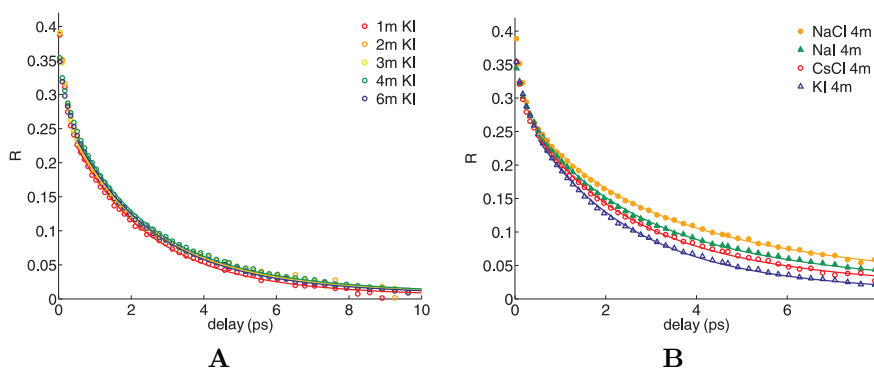


FIGURE 9.4. (A) Anion-bound anisotropy decays for different concentrations of KI solutions, with the pump-spectrum centered around 2500 cm^{-1} . With K^+ instead of Na^+ as the counterion (see Fig. 9.3) the reorientation dynamics have only a very small slow component, which does not depend on the concentration. (B) Orientational dynamics of anion-bound water compared for 4 molal solutions of four different salts. The curves represent the orientational dynamics of the OD hydrogen-bonded to the anion only, but the amplitude of the slow decay process is dependent on the nature of the cation as well as the anion.

9.3.2 EFFECT OF CATIONS ON THE ANION HYDRATION SHELL

Fig. 9.4A presents the $\text{OD}\cdots\text{I}^-$ anisotropy for different concentrations of KI. The curves show no change up to 6 molal. This is in stark contrast to the results on NaI that were shown in Fig. 9.3B, while only the *cation* was replaced. Fig. 9.4B shows a collection of $\text{OD}\cdots\text{A}^-$ anisotropy curves obtained from 4 molal solutions of four different salts, all obtained with the pump-spectrum centered around 2500 cm^{-1} . Although $R_{\text{OD}\cdots\text{A}^-}(t)$ only represents the reorientation of anion bound OD groups, it not only depends on the nature of the anion but also on the nature of the cation. It is excluded that the slower reorientation in $R_{\text{OD}\cdots\text{A}^-}(t)$ can be assigned to direct interaction of Na^+ with OD groups: Not only assures the spectral decomposition the contribution of anion bound OD groups only, the vibrational lifetime of $\text{OD}\cdots\text{O}$ oscillators around Na^+ is much shorter than the $\text{OD}\cdots\text{A}^-$ vibrational lifetime. The reorientation dynamics are thus dominated by the anion-bound oscillators for long delay times. We performed the same analysis of the anisotropy curves as was done in the previous section to obtain the relative amplitude of the fast relaxation process of the intrinsic anisotropy (Fig. 9.6A). The large cations K^+ and Cs^+ induce a large fast decay component of the anisotropy decay of OD groups that are hydrogen-bonded to the anion, while the smaller Na^+ cation restricts the fast decay component.

Dielectric relaxation spectroscopy measurements showed that the moderately strongly hydrated sodium ion has no effect on the reorientation of water

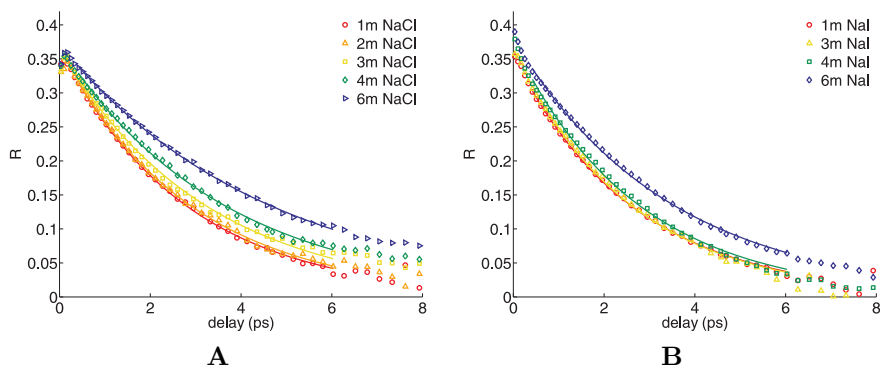


FIGURE 9.5. OD \cdots O anisotropy decay for different concentrations of NaCl (**A**) and NaI (**B**) solutions. The reorientation becomes slower for more concentrated solutions, in case of NaI this occurs at higher concentration compared to NaCl.

molecules beyond its own hydration shell [151]. In this work we distinguish the anisotropy dynamics of the anion-bound water molecules from other water molecules and focus on the anion hydration shell. Surprisingly, we find that moderately hydrated cations like sodium in fact do influence water reorientation in the solvation shell of its counterion depending on the size and concentration of the cation. From the faster OD \cdots I $^-$ anisotropy decay for KI compared to NaI solutions, it is clear that the orientational relaxation of water molecules around the *anions* depends on the nature of the *cations*. The sodium induces a decrease in the amplitude of the fast relaxation process, which is absent for the larger cations (Fig. 9.4A). We explain this observation from the electric field between cations and anions, which is larger in the case of smaller ions with a larger surface charge density. If the field around the cation is strong enough it partly aligns the static dipole of the water molecules around the anion, hindering the fast reorientation process by decreasing the angle of the cone over which the OD can wiggle. Fig. 9.6A shows that the amplitudes of the fast process is diminished by the presence of the stronger hydrated sodium for all measured concentrations of iodide and chloride salts.

From the decomposition we also obtain the OD \cdots O anisotropy curves, which are shown for the two sodium salts in Fig. 9.5. For low concentrations the curves can be fitted well with a mono-exponential function with a time constant of ~ 2.5 ps and thus resembles the dynamics observed for pure HDO:H $_2$ O [22]. The fitted reorientation times of the OD \cdots O anisotropy of all salts are shown in Fig. 9.6B. For the more concentrated solutions the reorientation slows down, the onset of this slowing down occurring at a higher concentration for NaI than for NaCl. In contrast, the OD \cdots O anisotropy decays for the KI and CsCl solutions behave like neat HDO:H $_2$ O up to the highest concentration measured.

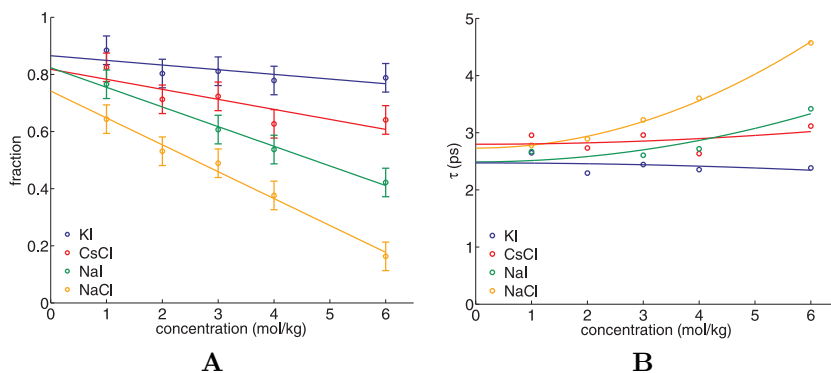


FIGURE 9.6. (A) The fraction of the fast component in the anisotropy decay of OD hydrogen-bonded to the anion (solid lines are guides to the eye). The results are from a global fit on all the measured concentrations of all salts, with the fast and slow reorientation times as global parameters. (B) Reorientation times fitted to the decomposed anisotropy decay of OD \cdots O water.

It should be noted that $R_{OD\cdots O}(t)$ also contains the dynamics of the water molecules in the hydration shell of the cations.

The anisotropy decays obtained from the OD \cdots O band show hardly any difference from the reorientation dynamics of OD groups in neat HDO:H₂O, except for the higher concentrations of the sodium salts (Fig. 9.5). This implies that up to concentrations of 3 molal the cation does not affect the reorientation of the hydroxyl groups of water molecules in its solvation shell, which was shown before to be the case even for strongly hydrated cations like Mg²⁺ [118, 123]. The solutions containing a high concentration of sodium ions (≥ 4 molal) do show a somewhat slower reorientation of the OD \cdots O groups, and this effect is more pronounced for NaCl than for NaI. The difference between NaI and NaCl indicates that the hydration shell dynamics of the cation is dependent on the nature of the counterion. For the weaker hydrated Cs⁺ and K⁺ cations we observe no strong dependence on concentration and/or the nature of the anion, from which we conclude that the slowing down of the reorientation of the OD \cdots O groups increases with both the cation and the anion hydration strength.

9.3.3 COOPERATIVE EFFECTS OF CATIONS COMBINED WITH FORMATES OR PHOSPHORYLETHANOLAMINE

In the past two sections we have shown that in solutions of alkali-halide salts the reorientation of water depends on the hydration strength (or surface charge density) of both the cation and the anion. Many biologically relevant molecules possess charged groups and in this section we investigate whether similar co-

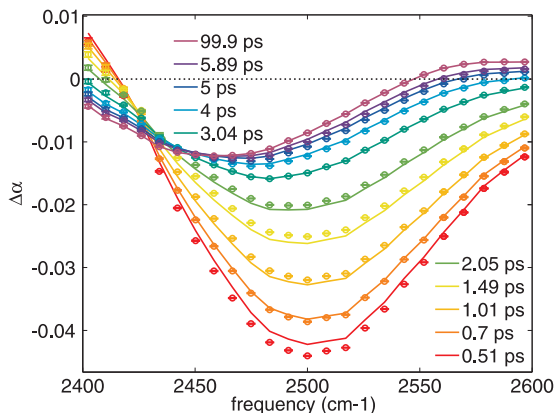


FIGURE 9.7. Transient absorption spectra at different delay times for a 1 molal solution of KPE. The solid lines are the results of a fit to the data of the kinetic model described in the text.

operative effects occur in solutions of such molecules and cations of various hydration strengths.

Fig. 9.7 shows transient differential absorption spectra for ten pump-probe delay times for a 1 molal solution of KPE. Since the linear spectra of PE solutions do not show a spectral blue-shift of the OD stretch absorption band, we assume that there are no different species of OD oscillators that are spectrally distinguishable. We therefore fit a kinetic model to the data in which only one excited state relaxes to the thermalized, hot ground state (for details see section 4.2.2). The solid lines in Fig. 9.7 represent the fit of the model to the 1 molal KPE data. For all the different salts and concentrations the vibrational relaxation times obtained from the fits are very close to the value of 1.7 ± 0.1 ps obtained for neat 8% HDO:H₂O with the same model [22]. Similar results were obtained for solutions of PE⁻ with different cations and for solutions of various formate salts. The finding that the model parameters are nearly independent on the type of salt and concentration is a sign that all OD oscillators in the solutions have a similar distribution of hydrogen-bond strengths as in bulk water.

Using the results of the fit of the kinetic model we subtract the contribution of the thermalized ground state at all delay times from both the parallel and perpendicular probed signals to obtain the polarization dependent absorption changes that only result from the excited OD oscillators. From these signals we obtain the anisotropy of the excited OD oscillators using Eq. (4.3). The anisotropy decay for different concentrations of NaHCOO and KHCOO are presented in Fig. 9.8. Since we could not discriminate the reorientation dynamics of OD groups in the ion solvation shells from those in the bulk, the anisotropy curves shown here represent the averaged dynamics of all OD oscillators in the solution. The reorientation dynamics of neat 8% HDO:H₂O shows a mono-exponential decay with a time constant of 2.5 ± 0.1 ps, similar to what

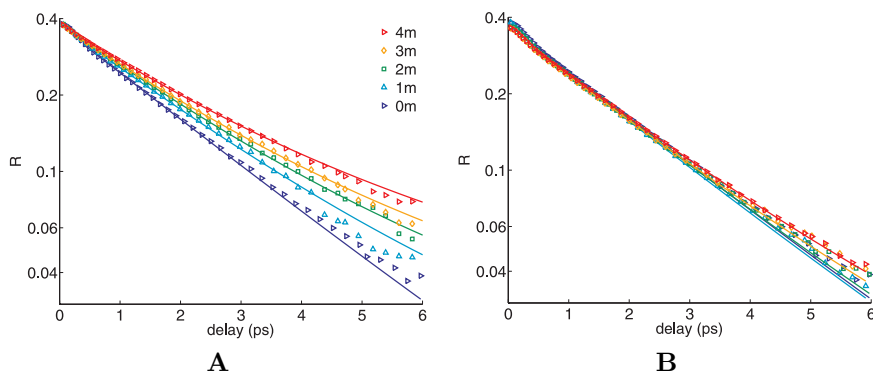


FIGURE 9.8. Logarithmic plot of the anisotropy decay of the OD stretch vibration in solutions of NaHCOO (A) and KHCOO (B). For increasing concentrations of the sodium salt the anisotropy becomes slower, which effect is absent in the potassium salt solutions.

was found in previous work [22]. For increasing concentrations of NaHCOO, the anisotropy decay becomes slower, while the addition of KHCOO has little to no effect on the reorientation dynamics of water.

Fig. 9.9A shows the anisotropy decays obtained for 1 molal solutions of NaPE and KPE. For comparison, the OD \cdots O anisotropy obtained for solutions of NaI and KI in the previous section are plotted in Fig. 9.9B. Like in the formate solutions, the reorientation dynamics in the PE solutions becomes slower upon replacing potassium by sodium as the counterion. In contrast to KHCOO, the reorientation dynamics in the KPE solutions is slower than in bulk water, although not as much as for the NaPE solutions.

The curves in the logarithmic plot of Fig. 9.9 clearly show that the decay is not single exponential. The anisotropy decay of all measured salts and concentrations are very well described by a bi-exponential function with a fast and a slow component like Eq. (9.1). Previous work on aqueous solutions of osmolytes also found a bi-exponential behavior of the anisotropy dynamics of water [28, 24, 152]. It was shown that even in concentrated solutions a fast relaxation component persists with a time constant similar to the bulk water reorientation time. For such concentrated solutions it is very unlikely that there are many water molecules in an environment that is like bulk water. However, concerning the dynamics of water, apparently even at high solute concentrations there is still a considerable amount of OD groups that have the freedom to reorient on a timescale like in bulk water.

We thus associate the fast component in our measurements to OD-groups that reorient in a bulk-like fashion, that is, on a similar time scale as bulk water, and we accordingly fix the time constant of this component to 2.5 ps. The slow component represents OD-groups for which the reorientation is severely

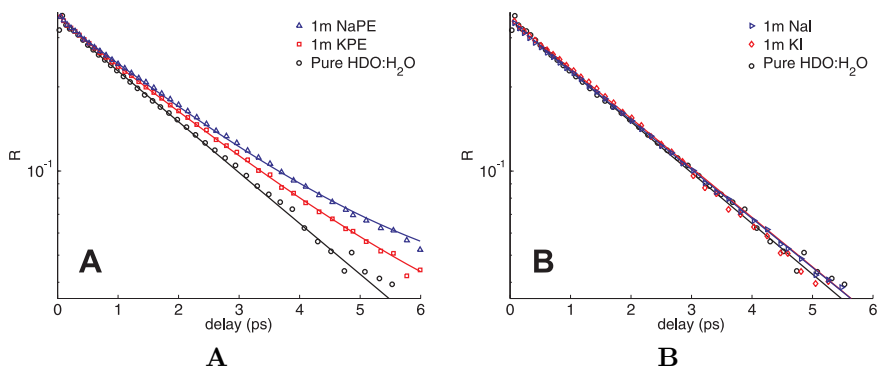


FIGURE 9.9. Comparison of the anisotropy decay of different salt solutions, all at a concentration of 1 molal. **(A)** NaPE has a stronger effect of immobilization of water molecules than KPE. **(B)** This difference is absent in the case of the corresponding iodide salts and therefore finds its origin in a cooperative effect between the cation and the PE^- ion.

hindered. Due to the fact that we can only probe the anisotropy over a time interval of 8 ps, the time constant of this component cannot be determined accurately. For all concentrations we fix this time constant to 20 ps. This value is an average value obtained from a bi-exponential fit to the 2 molal anisotropy decays of KPE and NaPE, with the notion that the error margin on the fitted time constants is quite large. The fraction of slowly reorienting water $f_{slow} = A_{slow}/(A_{slow} + A_{fast})$ follows from the fitted amplitudes of the fast and slow reorientation processes, A_{fast} and A_{slow} respectively. The bi-exponential fits are represented by the solid lines in Fig. 9.8 and Fig. 9.9. The slow water fraction f_{slow} is shown in Fig. 9.10 for all data (salt solutions and concentrations). We obtain the hydration number Z from the slope of a straight line fitted through the data points (solid lines in Fig. 9.10). Z is the number of slow OD-groups per solute molecule in the solution. We find that the hydration number decreases in the cation series $\text{Ca}^{2+} > \text{Na}^+ > \text{K}^+ \approx \text{Cs}^+$.

The hydration numbers obtained from the analysis of our fs-IR data for solutions with low charge density cations like K^+ , Cs^+ are $Z = 2 \pm 1$ for the formate solutions and $Z = 7 \pm 1$ for the PE solutions. In the previous section we concluded that these cations have a low surface charge density, what suggests that the hydration number of the potassium and caesium salts is entirely due to the solvation of the (formate or PE^-) anion. In the case of PE^- this hydration water likely corresponds to water molecules that are hydrogen-bonded to the phosphate group or are contained in the hydrophobic hydration shell of the C_2H_4 backbone of PE^- .

Fig. 9.10 shows that a marked difference in hydration number exists between the potassium salts and the sodium salts. For both anions the replacement of

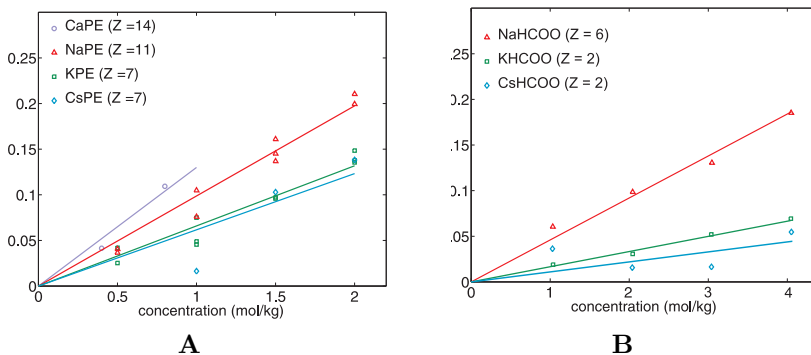


FIGURE 9.10. Slow fraction of water ($\tau_{slow} = 20$ ps) for PE solutions (A) and formate solutions (B) with different cations, as inferred from fs-IR experiments. The hydration number Z is the slope of the straight line fitted through the data points. Cations with a larger surface charge density are observed to slow down a larger number of water molecules.

potassium by sodium results in an increase of Z by four OD groups with slower reorientation. This suggests that for NaHCOO and NaPE not only the anion, but also the cation is responsible for the slower dynamics of water. However, the OD \cdots O reorientation dynamics in solutions of NaI and KI in Fig. 9.9B are contradicting the hypothesis that the stronger retardation around NaPE/NaHCOO compared to KPE/KHCOO is just caused by the cation. Like we found in the previous section, the difference between the sodium and potassium salts implies a cooperative effect that is present between sodium and the anion, but is absent for potassium. This cooperative effect is indicative of the formation of weak solvent separated ions pairs. In case the cation is Ca^{2+} , with a yet higher surface charge density than Na^+ , the effect is even more pronounced ($Z = 14 \pm 2$ for CaPE). It should be noted that Z is this large even though the number density of cations in solutions of CaPE is twice as low as that in solutions of NaPE.

9.3.4 LIFETIME OF THE PE-NA AND PE-CA ION-PAIRS

Fig. 9.11 shows the real (blue, circles) and imaginary (red, squares) part of the dielectric function for different concentrations of NaPE. From the raw data it is apparent that the spectra contain an intense relaxation mode (peak in ϵ'' and accompanying dispersion in ϵ') at frequencies ~ 0.3 to 1 GHz. Its amplitude increases with concentration, apparent from the increase of the peak in the dielectric loss upon the addition of solute. The electronic structure of the PE^- anion is such that the negative charge is located at the phosphate group and the positive charge is centered at the ammonium fragment. This charge separation leads to an intrinsically large dipole moment and the observed lower frequency relaxation can thus be assigned to the rotation of the PE^- ion.

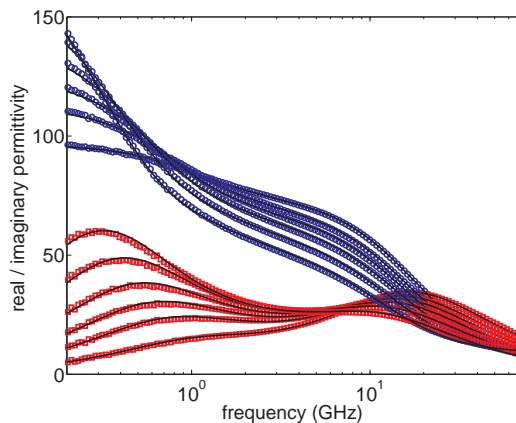


FIGURE 9.11. The real (blue, circles) and imaginary (red, squares) part of the dielectric function for solutions of 0.24, 0.48, 0.71 0.93 1.33 and 1.75 molal of NaPE in water. The bulk water mode at 20 GHz is decreasing with concentration and a mode at low frequencies grows in with concentration. The latter mode is assigned to the reorientation of the zwitterion PE^- .

The observed frequency corresponds to a reorientation time of the solute on the order of 200 ps, increasing with increasing solute concentration to over 400 ps. We derive the effective dipole μ_{eff} of the PE^- ions from the fitted mode amplitudes using the Cavell equation (Eq. (4.43)). For all salt solutions except CaPE the effective dipole is independent of both cation type and its concentration (Fig. 9.12). The obtained dipole moments of 25 ± 1 Debye correspond well to the results of an *ab initio* calculation of a PE^- zwitterion in a dielectric continuum ^a. Interestingly, the effective dipole of PE^- in solutions of CaPE shows a significant decrease with concentration.

The data in Fig. 9.11 shows another relaxation mode that is centered at ~ 20 GHz. The amplitude of this relaxation decreases with increasing concentration and can be readily assigned to the reorientation of bulk-like water [31].

From the fs-IR data it is apparent that not all water molecules show bulk-like dynamics, and that a subensemble of water molecules exhibits distinctively slower rotational dynamics. Accordingly, we fit a superposition of three Debye modes to the experimental permittivity spectra, representing the solute rotation, the relaxation of slow water molecules, and the orientational relaxation of

^aQuantum mechanical geometry optimizations for several conformers of the PE^- anion were performed using density functional theory (B3LYP [153, 154] and PBE [155, 156]) as provided by the ORCA program package [157]. For all calculations, the TZVPP basis set [158, 159] was used within the resolution of identity [160, 161]. Solvation effects were taken into account by the COSMO model [162] taking the dielectric constant of water $\epsilon_s = 80$ as the permittivity of the medium. Dipole moments were calculated assuming the geometric center as the pivot. These calculations give values for $\mu_{\text{eff}}=24\text{-}33$ D, depending on the conformation.

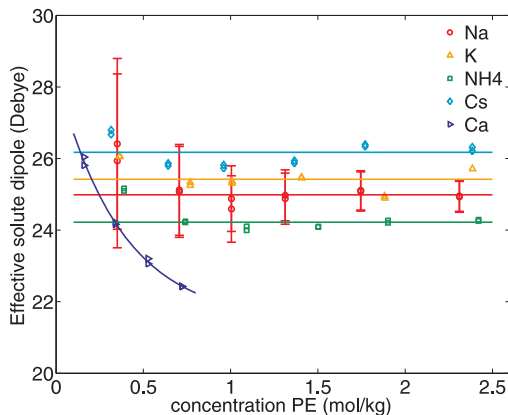


FIGURE 9.12. The effective dipole moment μ_{eff} of PE^- as obtained from the amplitude of the low frequency mode using the Cavell equation (Eq. (4.43)). The obtained values are in good agreement with an ab initio calculation of the PE^- dipole in a constant medium, which gives $\mu_{\text{eff}}=24\text{--}33\text{D}$, depending on the conformation. The error bars for the NaPE data points are exemplary, the error bars for the other data points are of similar magnitude. The dipole moments of PE^- thus show no significant dependence on concentration, except if Ca^{2+} forms the counterion.

bulk-like water molecules,

$$\hat{\epsilon}(\nu) = \frac{S_{PE}}{1 + 2\pi i\nu\tau_{PE}} + \frac{S_{slow}}{1 + 2\pi i\nu\tau_{slow}} + \frac{S_{bulk}}{1 + 2\pi i\nu\tau_{bulk}} - \frac{i\sigma}{2\pi\nu\epsilon_0} + \epsilon_\infty, \quad (9.2)$$

where σ is the conductivity of the sample (see also section 4.5). As the relaxation of the slow water sub-ensemble is located in the spectrum between the intense bulk water relaxation and the lower frequency solute mode, it is difficult to unambiguously determine its amplitude and central frequency. Thus, we reduce the number of adjustable parameters and fix the fraction of slow water molecules in these fits to that obtained from our fs-IR experiments. GHz-DR measures the first order correlation function of the macroscopic polarization, whereas fs-IR measures the second order correlation function of the transition dipole moments of the OD stretch vibration. The rotational correlation times of the two different experiments are found to be related to each other by a factor of 3.4 [35]. We therefore further assume the relaxation time of the slow water molecules to be $\tau_{slow} = 68$ ps, corresponding to the value of 20 ps used in our fs-IR analysis. As can be seen in Fig. 9.11 such fits are in excellent agreement with our experimental spectra. The good quality of the spectral decomposition into the three Debye modes is exemplified in Fig. 9.13 for the spectrum of a 1.75 molal solution of NaPE.

After correction for kinetic depolarization [38] the sum of the amplitudes of the two water relaxation modes (slow water + bulk-like water) reproduce the total analytical water concentrations for KPE and CsPE within experimental accuracy. For the samples with Ca^{2+} and Na^+ as counterions, the water con-

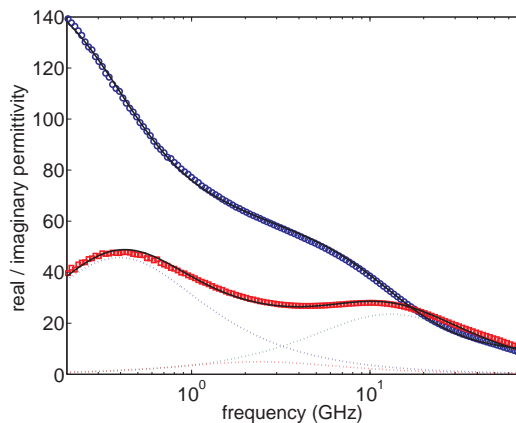


FIGURE 9.13. The results of a fit (solid line) of three Debye modes to the real (blue, circles) and imaginary (red, squares) part of the dielectric function of a 1.75 molal solution of NaPE in water. The dotted lines represent the imaginary part of the three resolved modes. The amplitude and time constant of the slow water mode (middle) are obtained from the fs-IR experiments.

centration extracted from the sum of the amplitudes of the two water relaxation modes, is lower than the analytical water concentration, indicative of the presence of irrotationally bound water molecules within the hydration shell shells of those cations [38].

In the previous section we found strong evidence for the formation of solvent separated ion pairs for NaPE and $\text{Ca}(\text{PE})_2$ solutions. Dielectric spectroscopy is in particular powerful in detecting such ion pair species, since an ion aggregate possesses an intrinsic electrical dipole moment. In case the lifetime of such an ion aggregate is comparable or longer than its rotational correlation time, the rotation of the aggregate will be observed as a strong low frequency relaxation in the DR spectrum [163].

In the present case the PE^- anion itself has an electrical dipole owing to its zwitterionic chemical structure. The formation of an ion-pair via interaction of the cation with the negatively charged phosphate group of PE would balance part of the negative charge located at the phosphate group. An M^+PE^- ion pair would therefore have a smaller electrical dipole than the PE^- anion itself.

For all studied samples (except for Ca^{2+}), we observe μ_{eff} to be constant at all studied concentrations. This observation implies that ion pairs between PE^- and the monovalent alkali-metal ions (including Na^+) are too short-lived ($< 200\text{ps}$) to be detected with DRS. Only for Ca^{2+} we observe μ_{eff} to decrease with increasing concentration. This indicates that only for Ca^{2+} the solvent separated ion pair exists longer than 200ps. Apparently, the formation probability or lifetime depends on concentration.

It is noteworthy that we observe the rotation time of water molecules located

between the phosphate group and the cation of the solvent separated ion-pair to be in the order of 20 ps. This time constant implies that the life time of the PE-Na ion-pairs must exceed 20 ps in order to observe a noticeable retardation of the water dynamics. The DRS results provide the upper boundary for the persistence times of the PE-Na contacts of 200 ps.

9.4 COOPERATIVE ION HYDRATION: THE BROAD PICTURE

Various salts have quite a different impact on properties of water that can be detected macroscopically. Examples are the viscosity, or the ability to salt out proteins, the latter of which led Hofmeister already in 1888 to formulate an empirical ordering of salts [136]. In spite of their relevance for many processes, still no consensus has been reached about the microscopic origins of such effects. A parameter of importance that follows from the Hofmeister series is the surface charge density of ions, which is determining the strength of the interaction of the ion with the polar water molecules. Most current disagreements concern the extent over which ions affect their environment and whether the influence of ions on their environment is additive or not [118, 164, 137, 165, 166]. In discussing these issues, the definition of terms should be taken with care. The influence sphere of an ion is often called its hydration shell. However, there can be quite a difference in the size of this hydration shell depending on the measurement technique [137, 123].

Here we find that for salt solutions the orientational dynamics of the water molecules often depend on both the nature of the cation and the anion, in agreement with other work [123, 37, 29]. In addition to previous work, we identified the separate contributions of the cations and anions to the reorientation dynamics. We found that both ions have their own characteristic influence on the reorientation of water and that these effects are often non-additive. The combination of a cation and anion with both a large surface charge density has a substantially larger deceleration effect on the water dynamics than the sum of the effects of both ions when they are combined with counterions with a much lower surface charge density.

It has been argued that some of such combined effects of ions on the water dynamics can be explained by the speed up of water reorientation by ions with a low surface charge density [166]. NMR experiments showed that for solutions of a few molal NaClO_4 the average reorientation time increases slightly (3%) with respect to that of bulk water [167], assigned to water solvating the perchlorate anions. In previous NMR, dielectric relaxation spectroscopy and fs-IR experiments, only the average reorientation time of all water molecules in the solution was measured, meaning that this claim could not be tested. By separating the response of OD groups solvating anions ($\text{OD}\cdots\text{A}^-$) and that of OD groups solvating other water molecules ($\text{OD}\cdots\text{O}$), we were able to show that the water solvating the anion can indeed possess a reorientation component that is faster than bulk liquid water [30] (Fig. 8.5). This fast component can be assigned

to a wobbling motion of the OD group while keeping its hydrogen-bond to the anion intact [149]. The OD group can wobble over a relatively large cone due to the large size of the anion in comparison to the $\text{OD}\cdots\text{A}^-$ bond length. This assignment is supported by the observation that the fast wobbling component is larger for anions that are bigger and that have a lower surface charge density (Fig. 9.6A). Classical MD simulations found that a high surface charge anion Cl^- much more aligns the transition dipole of a solvating OH group than I^- does. ClO_4^- has a very low surface charge density [128], and for solutions of NaClO_4 this component is apparently large enough to suppress the average reorientation time of all water molecules as observed by NMR [167]. At high concentrations, matters become different as we will discuss in a moment.

The reorientation of the $\text{OD}\cdots\text{O}$ groups at relatively low concentrations is identical to that of bulk water [30] (Fig. 8.5). Since the $\text{OD}\cdots\text{O}$ component contains the water molecules solvating the cations, this observation implies that at low concentrations Na^+ does not affect the reorientation of OD groups in its solvation shell. This is consistent with previous findings [118]. In analogy to water solvating anions, it was predicted that the reorientation of water molecules solvating cations with a low surface charge density also speeds up [166]. However, this is not what we observe: Fig. 9.6B shows that the $\text{OD}\cdots\text{O}$ reorientation in solutions of CsCl is not faster but identical to that of bulk water. The Cs^+ cations thus leave the reorientation of OD groups merely unaffected.

The identification of two different species with different orientational relaxation dynamics was recently challenged [29]. In this work it was suggested that the reorientation of water is highly concerted and a separation between OD groups solvating ions and OD groups hydrogen-bonded to other water molecules is invalid for this observable at the concentrations studied. The argument used was that the *total* anisotropy for MgBr_2 did not show a noticeable dependence on frequency as the $\text{OD}\cdots\text{O}$ and $\text{OD}\cdots\text{Br}^-$ oscillators have a different linear absorption spectrum. A difference in reorientation dynamics should have led to a frequency dependence of the overall anisotropy decay. There are a number of points missing in this argumentation. First, the discussion does not address the influence of the population dynamics on the total anisotropy. Since the stretch vibrations of $\text{OD}\cdots\text{Br}^-$ oscillators have a considerably longer lifetime, their relative contribution to the total anisotropy does not only depend on the distributions in the linear spectrum. At short delay times the anisotropy is dominated by the orientation of $\text{OD}\cdots\text{O}$ oscillators, while at 8 ps delay time the anisotropy is almost exclusively representing the orientation of $\text{OD}\cdots\text{Br}^-$ oscillators [133], irrespective of the probe frequency (see also Fig. 8.3 in the previous chapter). Hence, the lack of frequency dependence in the overall anisotropy dynamics of Ref. [29] is mostly due to the fact that at later delays only the $\text{OD}\cdots\text{Br}^-$ dynamics are observed. In case both species have highly different reorientation dynamics, a large frequency separation of their resonances, and not too different lifetimes, as is the case for the core and shell water of reverse micelles [27], the total anisotropy dynamics clearly shows a frequency dependence. This is also the case for NaClO_4 solutions, for which also a strong frequency dependence of the total anisotropy dynamics was found [30]. For systems with a smaller spec-

tral separation of the two species, a spectral decomposition as was performed in this chapter yields a more accurate method to obtain the reorientation dynamics of the different water species. Would the proposition of Ref. [29] be correct, then the decomposed anisotropy dynamics of both species would be equal. This is clearly not what we observe.

For increasing concentrations, some cations can have a pronounced effect on the reorientation of OD groups in the anion solvation shell (Fig. 9.4B and Fig. 9.6A). Cations with a larger surface charge density like Na^+ induce a decrease of the fast wobbling component. Since we associated this component with an alignment of the $\text{OD}\cdots\text{A}^-$ hydrogen-bonds, this observation implies that Na^+ enhances this alignment and eg. Cs^+ does not. The fast wobbling component thus depends on both the anion and the cation and represents a non-additive or cooperative contribution to the reorientation of water in ion-solutions. At a certain concentration also the dynamics in the $\text{OD}\cdots\text{O}$ becomes slower (Fig. 9.6B). The origin for this effect is likely to be found in crowding effects, the overlap of hydration shells of the ions. Important to notice here is that the critical threshold for this effect to happen is different for different ion-combinations and again depends on both the cation and the anion.

An extrapolation of the results of this chapter can be made to the observations in solutions where both ions have a very high surface charge density, like MgSO_4 [123, 37]. OD groups that are hydrogen-bonded to SO_4^{2-} experience a strong limitation of their wobbling motion due to the ions very large surface charge density. The addition of a weakly hydrated counterion like Cs^+ does not restrict this wobbling motion any further, while Mg^{2+} does. In addition, the strong field between SO_4^{2-} and Mg^{2+} further hinders the rotation of water molecules in the Mg^{2+} solvation shell [123, 168]. Since the reorientation of water solvating Mg^{2+} is hardly affected in solutions of MgClO_4 [118], the observations for the water dynamics in MgSO_4 solutions form a clear example of a non-additive ion-effect.

Recent classical MD simulations argued that there are no cooperative effects for ions with high surface charge density (like MgSO_4 and Na_2SO_4) and that the slow down of the water reorientation is due to a dominant contribution of slower frame reorientation, related to the increased viscosity of such solutions [166]. This conclusion disregards the fact that cooperative effects were already observed for concentrations of MgSO_4 and MgCl_2 lower than 0.5 molal [123], at which concentration no crowding effects are expected by the same classical MD study [166]. Moreover, a slower frame reorientation and a higher viscosity are not at all at odds with the formation of cooperative solvent-separated ion-pairs. In fact, the slower frame reorientation and higher viscosity are likely (macroscopic) consequences of the formation of solvent separated ion-pairs. Unfortunately, in this MD study [166], the dynamics of water were only compared in solutions of Na_2SO_4 and NaClO_4 , and not to those in a solution of CsSO_4 . A comparison in which the strongly hydrating ions (Mg^{2+} , Na^+ , SO_4^{2-}) are combined with much more weakly hydrating counterions (ClO_4^- , Cs^+) could truly have provided more insight in the cooperative effects of particular ion

combinations on the dynamics of water.

At infinite dilution, cooperative effects can only arise in case the ions show some affinity for each other. In such a case a subtle balance exists: the salt is not precipitating yet, although pairs of ions of opposite charge are formed. In case no water percolates in between the ions, such a formation is called a contact ion-pair (CIP). Sometimes stable configurations are formed with one or two layers of water in between the ions, called solvent shared ion-pairs (SSIP) or solvent separated ion-pairs (2SIP), respectively. In concentrated solutions these concepts start to break down, as the water-ion ratio becomes such that most hydration shells necessarily start to overlap. Since most monovalent ions have 6-8 water molecules in their hydration shell [137], extensive overlap of hydration shells due to crowding is expected to happen at concentrations exceeding 3 molal. For bivalent ion combinations like Na_2SO_4 the threshold is rather around 1 molal [166].

At the concentrations for which cooperative ion effects are found in this chapter, as well as for MgSO_4 [123], it is thus likely that the ions engage in SSIP or 2SIP rather than that crowding effects play a role. Dielectric relaxation spectroscopy (DRS) measurements did indeed find Na_2SO_4 ion-pairs [151, 36]. Since DRS can only probe ion-pairs of which the lifetime exceeds the rotational correlation time of the complete pair, the lifetime must be at least 100 ps. These results thus appear to be in contradiction with the lifetimes shorter than 10 ps of such ion-pairs that were found by classical MD simulations [166]. The DRS results thus do not support the argument based on classical MD simulations that ion-pairs cannot play a dominant role in the observed retardation. The formation of ion-pairs is clearly a very subtle balance and difficult to capture by classical MD simulations [169, 170, 171, 172], as was also mentioned in other studies [168].

Due to the difficulties in capturing the formation of ion-pairs, other work specifically studied the differences in hydration dynamics for fixed anion-cation distances [168]. In this work, a clear additional retardation effect on solvating water molecules was found in case a Mg^{2+} and SO_4^{-2} ion were close enough to each other. The retardation was found to depend on the surface charge density of the ions: The water dynamics of a similar configuration with Cs^+ and Cl^- ions was found to have a significantly smaller additional retardation effect. At larger ion distances (12 Å), only a small additional retardation effect was observed outside the hydration shells of both ions. These findings let the authors to conclude that cooperative effects are small beyond the ions first solvation shell and mainly affect the reorientation time and not the number of slower water molecules.

So far, we only considered simple inorganic salt solutions. Biologically relevant Hofmeister effects however concern the influence of salts on the conformation of proteins and lipid membranes. It is easy to picture ions to have water mediated interaction with charged groups of proteins similar to the effects described above. To test this, we studied the reorientation of water in solutions that contain simple molecules with negatively charged groups as a model for

biologically relevant systems with different types of cations. As model systems we used phosphorylethanolamine (PE^-) and formate.

The results on these solutions are easily viewed in the same context as described above. We cannot resolve the reorientation dynamics of OD oscillators hydrogen-bonded to the phosphate group separately, since those oscillators lack a different spectral response like for the halide anions. The reorientation dynamics that we obtain thus represent all OD groups in the solution. It is however likely that the reorientation of OD oscillators bound to the negatively charged phosphate group of PE^- or the carboxyl group of formate involves a similar wobbling motion as we observed for the halide anions. In perfect analogy to what was discussed above, co-solvated K^+ or Cs^+ have a low surface charge density and have no influence on these dynamics. In contrast, the electric fields around $\text{Na}^+/\text{Ca}^{2+}$ are high enough to align a number of OD groups in a water complex with phosphate/carboxyl. Since we find these effects already for relatively low concentrations, the close vicinity between the ions that is needed for such an alinement can be explained by the formation of solvent separated ion pairs.

With DRS we observed PE-Ca ion-pairs but no PE-Na ion-pairs. These results put an upper boundary on the lifetime of the PE-Na ion pairs (< 200 ps): They must be formed and broken only fleetingly. Since the fs-IR experiment is capable of measuring the reorientation of water molecules on a much shorter timescale, we are able to probe the slower dynamics caused by those short living ion-pairs. For Ca^{2+} it has been found that the residence time of water molecules in its solvation shell can be as long as 700 ps [173], while for Na^+ this value is only 22 ps. The rigidity of the Ca^+ hydration shell could explain why the PE-Ca ion pair is much longer lived than the PE-Na ion pair.

Our findings agree with previous theoretical work and molecular dynamics simulations that showed that the interaction between membrane lipids and co-solvated ions is highly dependent on the charge density of the ions. Cations with a high surface charge density like sodium and calcium were found to have a higher propensity at the lipid surface [141, 145, 146]. The binding of Na^+ and Ca^{2+} to particular anionic groups may also play a role in the denaturation of biomolecules (e.g. proteins and DNA), as cations with a higher surface charge density typically destabilize protein conformation [137]. To explain denaturation effects, most recent work favors the picture of direct ion-protein interaction rather than a long-range structure making or breaking effect on water [174, 119, 120, 175, 121, 122]. Our observation of the existence of solvent separated ion pairs between phosphate and Na^+ or Ca^{2+} , forms strong support for the important role of direct ion-protein interaction.

9.5 SUMMARY

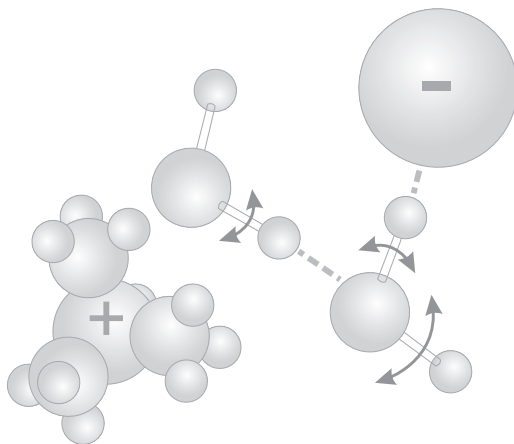
We studied the reorientation dynamics of water in electrolyte solutions of different types of cations and halide ions, phosphorylethanolamine (PE^-) and formate. Using the spectral blue-shift of the OD-stretch resonance frequency of

halide bound water molecules, we were able to specifically isolate the response of these water molecules. We find that the reorientation of OD groups in the anion hydration shell happens by a fast and slow process (2.0 ± 0.3 ps and 9 ± 1 ps). The amplitude of the fast component was found to decrease for smaller anions and for smaller cations. The fast component is associated with the wiggling motion of the OD groups that keep their hydrogen-bond to the anions intact. An anion with a smaller radius and higher surface charge density exerts a stronger restriction on the angle of the cone it is allowed to wiggle, explaining the decrease of the amplitude of this process for smaller anions. We found that a strongly hydrating cation like Na^+ has the tendency to align the water molecules in the anion hydration shell, thereby restricting the angular cone even further.

In the case of stronger hydrating cations, the dynamics of water molecules that are hydrogen-bonded to other water molecules are also found to have slower dynamics but only at relatively high concentrations. These molecules are likely hydrating the cation and are restricted in their reorientation by the influence of the anion. This effect is more pronounced in the case of a stronger hydrating anion and can be seen as the onset of the formation of the locked water complexes that were recently observed for strongly hydrating cations and anions like Mg^{2+} and SO_4^{2-} .

Cooperative effects as described above are a general phenomenon and may play an important role in the ion-specific Hofmeister effects on protein conformation that have been observed. To investigate this, we also studied water reorientation and ion-pair formation in solutions of formate or phosphorylethanolamine with different types of cations. In line with the results on inorganic salts, we find that cations with a large surface charge density like sodium and calcium form solvent separated ion pairs with the phosphate group of PE^- and the carboxyl group of formate. For larger cations like potassium or cesium such ion pairs are not observed. The dielectric spectra in the region of 200 MHz to 70 GHz are consistent with these results. In these spectra we find a low frequency mode that we assign to the reorientation of the PE^- ion. From this mode we determined the effective dipole moment of PE^- to be 25 ± 1 Debye, consistent with ab initio calculations. The effective dipole shows a concentration dependence in the case of Ca^{2+} as counterion, which is indicative of the formation of ion pairs with life-times exceeding 200 ps. Since such a long-living ion-pair is not observed in the DRS studies of NaPE , while the fs-IR results do provide evidence for the formation of ion pairs nonetheless, the lifetime of Na^+ - PE^- complexes must be in the range 20-200 ps.

Hydrophobic and Coulomb Interactions Disentangled



In the previous two chapters we investigated the effect of charges on the reorientation dynamics of water: Positive charges align a different vector in the water molecules than negative charges. If they do so strongly enough, their combined effect may lead to a locked water complex in which the reorientation of water molecules is severely hindered. In chapter 7 we saw that hydrophobic groups have a pronounced effect on the dynamics of water as well, for a very different reason. **Many molecular systems in nature involve both hydrophobic groups and electric charges and the purpose of this chapter is to reveal their combined effects on the dynamics of water.** To that end we used salts of which the cation has hydrophobic alkyl chains. By varying the length of the alkyl chains we can tune the hydrophobicity of the cation. We find that not only the reorientation dynamics of water molecules around the hydrophobic groups are strongly retarded, also the OD-groups that are hydrogen-bonded to the anion have a much slower reorientation dynamics. The wobbling component that was found in chapter 9 becomes much slower. This observation shows that the wobbling motion is governed by the reorientation of the hydrogen-bond network outside the anion hydration shell.

10.1 INTRODUCTION

Many processes in biological systems involve a subtle interplay between hydrophilic and hydrophobic molecular groups and water. The aggregation of hydrophobic side groups of amino acids in proteins for example is a driving force for proteins to assume their native conformation in water. Charged side groups can form salt bridges to enforce the thus formed structure. A detailed understanding of the effect of hydrophobes and charges on water is therefore crucial to understand processes like protein folding and membrane formation.

Symmetrical tetra- n -alkylammonium (TAA, $N(C_nH_{2n+1})_4^+$) salts are good model systems for hydrophobic hydration since they are often well soluble in water and their hydrophobicity is easily increased by increasing n . Moreover, tetramethylammonium (Me_4N^+) is ubiquitous in biological systems as it forms the positively charged moiety in polar head groups of a common class of phospholipids. Frank and Evans used TAA salts in their famous work in which they proposed so-called iceberg formation around hydrophobes, thereby explaining the counter-intuitive thermodynamic behavior that is common for hydrophobic solutions [96]. The formation of more structured ice-like water around hydrophobic moieties provided an explanation for the increased heat capacity of solutions containing amphiphiles. In later work the iceberg theory was disputed, as hardly any changes in the hydrogen-bond structure of water were observed upon the addition of amphiphilic solutes [97]. However, recent Raman spectroscopy studies did find a more ordered hydration structure around hydrophobic groups [98]. In other work the *dynamics* rather than the structure of water were found to be affected: water molecules are observed to reorient much more slowly in solutions containing amphiphilic molecules [28, 110, 17].

The ionic nature of TAA salts offers an interesting opportunity to study the combination of coulomb and hydrophobic effects. Not only does the cation carry both charge and hydrophobic groups in different ratios depending on the length of the alkyl chains, the system also necessarily includes counter ions. The combined ionic and hydrophobic character of the TAA cations is often used to explain their influence on the conformation of proteins in terms of the concepts of structure making and breaking [176, 177, 137, 178]. The $n = 1$ salts were found to be structure breakers, the $n \geq 3$ salts structure makers, and the $n = 2$ salts neutral intermediates [176]. This change in character with increasing alkyl length is believed to result from the competition between coulomb and hydrophobic interactions [178, 103]. Some recent studies suggested that the water structure around the TAA hydrophobic moieties is enhanced [98], and that this is less the case for Me_4NBr and Et_4NBr compared to Pr_4NBr and Bu_4NBr [97, 178].

In this chapter we study the reorientation of water in solutions of $TAABr$ salts for four different chain lengths ($n = 1, 2, 3, 4$) using polarization-resolved femtosecond pump-probe spectroscopy. In line with what was shown in the previous chapters we will demonstrate that this technique also allows to disentangle the effects of the hydrophobic cation on water from those of the anion. We compare the data with results on solutions of $NaBr$, for which the coulomb effects will dominate.

10.2 EXPERIMENT

For our experiments we use the one-color setup described in section 3.1.1. The pump-probe spectrum was centered around 2525 cm^{-1} . We prepared solutions containing different concentrations (0.25, 0.5, 1, 2, 3, 4 and 6 molal, mol/kg solvent) of tetra-*n*-alkylammonium bromide in isotopically diluted water (4% D_2O in H_2O). We used bromide salts with tetra-*n*-alkylammonium cations with four different alkyl chain lengths: 4-methylammonium (Me_4NBr), 4-ethylammonium (Et_4NBr), 4-propylammonium (Pr_4NBr) and 4-butylammonium (Bu_4NBr). We use solutions of NaBr as a reference, since the sodium cation has no hydrophobicity and we expect only coulomb interactions in its hydration shell. We did not choose the ammonium salt as a reference since the protons of the ammonium cation exchange with the deuterium in the solvent. The thus formed ND-groups absorb at nearly the same frequency as the OD-groups in the solvent. As a result, the observed dynamics would no longer exclusively represent the dynamics of the water molecules. All salts were purchased from Sigma Aldrich and had a purity of $\geq 98\%$. The sample cell consisted of two calcium fluoride windows (dimensions $\text{W}\times\text{H}\times\text{D}$ $20\times 39\times 4\text{ mm}^3$) pressed against each other with a teflon spacer in between. The thickness of the spacer was varied between $25\text{ }\mu\text{m}$ and $100\text{ }\mu\text{m}$ for different compounds and concentrations to obtain about 10% transmission in the OD stretch region in all measurements. To prevent heat accumulation during the measurements the sample cell was slowly moved up and down with an oscillation period of a few seconds.

10.3 RESULTS AND ANALYSIS

10.3.1 EXPERIMENTAL RESULTS

Fig. 10.1A displays linear spectra of the OD-stretch absorption band of neat 4% D_2O in H_2O and 4 molal solutions of the different salts. The TAA salt solutions show a blue-shift with respect to neat $\text{HDO}:\text{H}_2\text{O}$, without any clear dependence on the nature of the cation. The blue-shift increases with concentration. Analog to what was discussed in the previous chapter, we can assign this blue-shift to the OD oscillators of HDO molecules that are hydrogen-bonded to the anions ($\text{OD}\cdots\text{Br}^-$) [128]. Since this bond is weaker than water-water hydrogen bonds ($\text{OD}\cdots\text{O}$), the coupled OD-stretch resonance frequency is blue-shifted. We centered the pump and probe spectrum in our experiment at 2525 cm^{-1} to have them optimally overlapping with both contributions to the absorption band. The linear spectrum of the same concentration NaBr shows a significantly larger blue-shift of the OD-stretch compared to the TAA salt solutions. We will come back to this observation in the discussion section of this chapter.

Fig. 10.1B shows transient spectra at different pump-probe delay times for a 2 molal solution of Bu_4NBr . For early delays, a bleach due to the depleted ground state and stimulated emission is observed in the center and at the blue side of the spectrum. The positive feature at lower frequencies is the onset of the induced absorption $\nu = 1 \rightarrow 2$. For increasing delay times, the absorption changes decay to a spectral feature that remains constant on the timescale of the

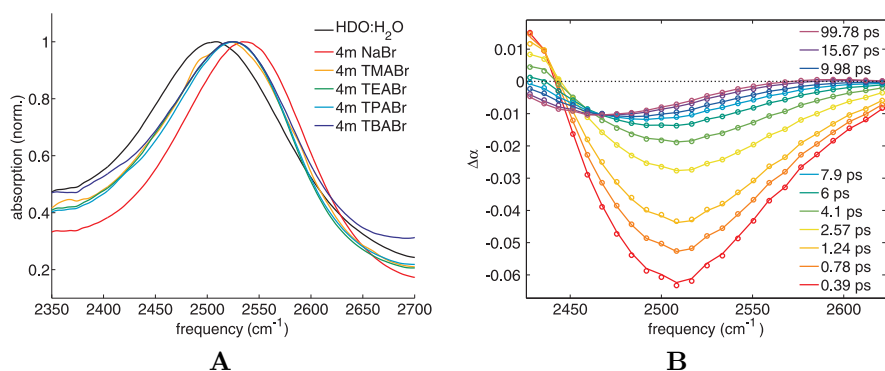


FIGURE 10.1. **A** Comparison of the linear spectra of 4 molal TAABr solutions in the OD-stretch region in isotopically diluted water (4% D₂O in H₂O). The spectra are blue-shifted compared to neat 4% D₂O in H₂O due to the bromide ions, but not as much as for 4 molal NaBr. Panel **B** shows the transient spectra measured for different delay times for a 2 molal solution of Bu₄NBr. The solid lines represent a fit of the kinetic model described in section 10.3.2.

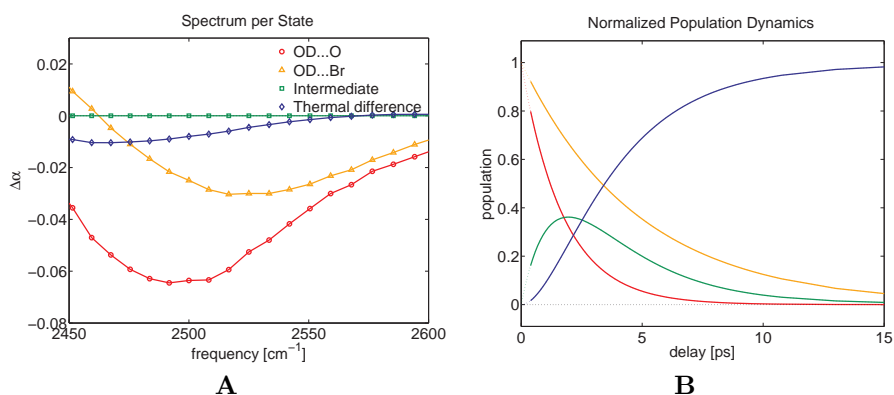


FIGURE 10.2. The results of a fit of the kinetic model described in the text to the data obtained for a 2 molal solution of TBABr. Panel **A** shows the fitted state spectra and panel **B** the fitted population dynamics. The vibrational decay is very slow and has at 15 ps not yet come to a complete end.

experiment (<100 ps). This final spectrum is a thermal-difference spectrum that results from the heating of the sample by a few degrees due to the thermalization of the excitation energy [179]. To calculate the anisotropy dynamics of the excited OD oscillators we subtract this thermal contribution by fitting a kinetic model for the vibrational decay to the isotropic data.

10.3.2 MODELING

Analogous to what we found for the alkali-halide solutions in chapters 8 and 9 we expect that the transient spectra contain contributions of OD \cdots O and OD \cdots Br $^-$ oscillators that are spectrally shifted with respect to each other. We therefore assume the same kinetic model as brought forward in section 4.3.1, in which the two contributions are fitted as separate excited states. In this chapter we neglect the exchange discussed in chapter 8, as these effects are very small.

Both OD \cdots O and OD \cdots Br $^-$ oscillators have different reorientation dynamics [30] and therefore we assume a functional form for the anisotropy decays of these two species. Several studies showed that in solutions containing amphiphilic solute molecules the reorientation of water takes place on two different timescales [103, 28, 17]. The fast timescale is associated with OD-groups that have bulk-like reorientation dynamics and the slow timescale with OD-groups hydrating the hydrophobic group of the solute. We thus model the OD \cdots O anisotropy decay by,

$$R_{OD\cdots O}(t) = A_f e^{-t/\tau_f^O} + A_s e^{-t/\tau_s^O} \quad (10.1)$$

where A_f and A_s are the relative amplitudes of the fast and slow relaxation processes and τ_f^O and τ_s^O are the fast and slow relaxation time constants.

In other work, the anisotropy of OD groups bound to anions was found to decay by a number of processes [132, 150, 104]: (1) a very fast decay due to librational motions (~ 150 fs), (2) a contribution due to a wobbling motion that is caused by the reorganization of the hydrogen-bond network outside the first solvation shell (~ 2 ps) and (3) a much slower decay due to rotational diffusion of the solvating water over the anion surface or frame reorientation (~ 10 ps). Therefore, we choose the following functional form for the OD \cdots Br $^-$ anisotropy decay,

$$R_{OD\cdots Br^-}(t) = B_f \left(C e^{-t/\tau_{lib}^{Br}} + (1 - C) e^{-t/\tau_f^{Br}} \right) + B_s e^{-t/\tau_s^{Br}} \quad (10.2)$$

where B_f and B_s are the relative amplitudes of the fast and slow orientational relaxation processes described above and τ_{lib}^{Br} , τ_f^{Br} and τ_s^{Br} are their corresponding time constants. The anisotropy dynamics in (10.2) thus contains a fast decaying part and a slow decaying part analogous to the OD \cdots O anisotropy decay in equation (10.1). Both the librational decay and wobbling motion are included in the fraction of the fast decaying part, with relative weighting given by the parameter C .

Both the kinetic model for the vibrational decay and the functions for the two excited state anisotropy decays are fitted to the data simultaneously in a self-consistent fit (see also section 4.4.2). To limit the freedom in the fit we fix several parameters entering Eq. (10.1) and Eq. (10.2). Since the vibrational lifetime of OD \cdots O oscillators in pure HDO:H $_2$ O is 1.8 ps [22], the OD \cdots O anisotropy can only be measured accurately up to about 10 ps. The long delay time dynamics of the OD \cdots O anisotropy in the TAA solutions is even more obscured by the response of the OD \cdots Br $^-$ oscillators that have a much longer

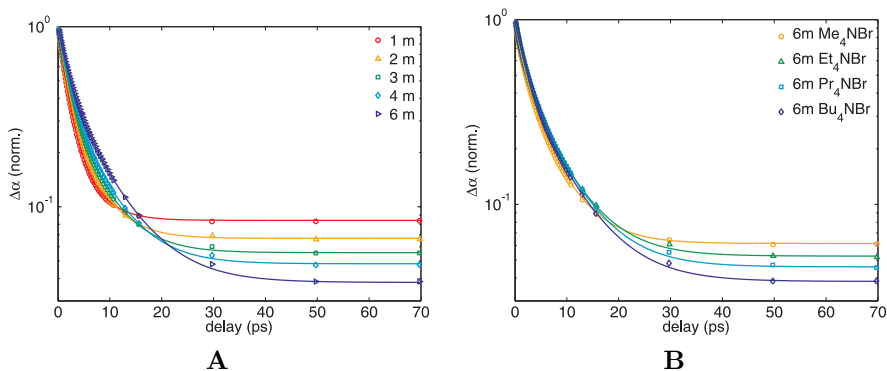


FIGURE 10.3. The vibrational decay dynamics become slower for increasing concentrations of Bu_4NBr (**A**) and for increasing chain lengths (**B**). The delay traces shown are taken at 2525 cm^{-1} . The solid lines in the figures are the fits of the kinetic model described in the text to the data.

vibrational lifetime. We therefore model the slow component of the $\text{OD}\cdots\text{O}$ reorientation as an endlevel of the anisotropy, i.e. we set the slow time constant to $\tau_s^O = \infty$ ps. In previous work on solutions of amphiphiles in water it was found that up to high concentrations a fast reorientation process is present in $R_{\text{OD}\cdots\text{O}}(t)$ with a time constant of $\tau_f^O = 2.5$ ps [24]. Similarly it was found in aqueous solutions of alkali-halide salts that a fast reorientation process is present in the anion-bound reorientation dynamics with a time constant of $\tau_f^{Br} = 2$ ps [30]. In our fit we fix those constants accordingly. Finally, the time resolution of our experiment is limited to the cross correlate of the pump and probe pulses (~ 250 fs). For this reason we fix the amplitude $C = 0.25$ and the time constant of the librational decay $\tau_{lib}^{Br} = 170$ fs, corresponding to the values found in previous work on alkali halide solutions [104]. The freely fitted parameters are thus the parameters of the kinetic model describing the isotropic decay, the amplitudes A_f , A_s , B_f and B_s and the slow reorientation time τ_s^{Br} of bromide bound water.

10.3.3 MODELING RESULTS

The solid lines in Fig. 10.1B represent the isotropic results of a fit of the model to the data obtained for a 2 molal Bu_4NBr solution. Fig. 10.2A presents the fitted state spectra $\sigma_i(\omega)$ and the corresponding population dynamics $N_i(t)$ are shown in Fig. 10.2B. The excited $\text{OD}\cdots\text{Br}^-$ spectrum shows a blue-shift of about 30 cm^{-1} with respect to the excited $\text{OD}\cdots\text{O}$ spectrum, significantly smaller than the value of 50 cm^{-1} that was found for alkali bromide salts [128]. The vibrational decay time of the $\text{OD}\cdots\text{Br}^-$ is slow, as is the decay of the intermediate state, leading to a long delay of the heat ingrowth. Delay traces show that the vibrational decay becomes slower with increasing concentration

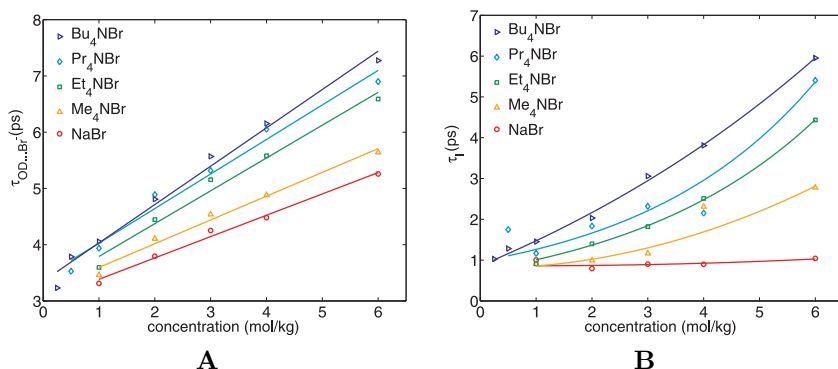


FIGURE 10.4. For all measured salts and concentrations the vibrational decay time of the OD \cdots Br $^-$ oscillators (**A**) and the decay time of the intermediate state (**B**). The vibrational lifetime of bromide-bound water becomes very slow for high concentrations of the salts with longer alkyl chains. The solid lines are guides to the eye.

(Fig. 10.3). Equal concentrations of different TAA salts show the same trends.

The fit results of the isotropic model are summarized for all measured data sets in Fig. 10.4. The vibrational lifetime of OD \cdots Br $^-$ increases both with TAABr salt concentration and with alkyl chain length and becomes as long as 7.3 ± 3 ps for the highest concentration of Bu₄NBr. The dynamics of the ingrowing heat strongly depends on the decay time of the intermediate state, which is found to increase strongly for increasing concentrations and longer alkyl chain lengths. The right panel shows the population of OD \cdots Br $^-$ relative to that of OD \cdots O. When calculating these values we took into account that the cross section of OD \cdots Br $^-$ is ~ 1.5 times higher than the cross section of OD \cdots O. This ratio is obtained from an analysis of the linear absorption spectra. From the slope we determine a hydration number of 7 ± 2 , consistent with earlier work [150, 180], and without clear dependence on the nature of the counterion (Fig. 10.2C). For the 3 molal solutions all fitted spectra are shown in Fig. 10.5. The blue-shift of the OD \cdots Br $^-$ spectrum clearly depends on the nature of the cation, while the OD \cdots O spectrum is the same for all cations. This is surprising since the linear spectra of the solutions do not show a clear dependence on the length of the alkyl chains.

Fig. 10.6 shows the OD \cdots O and OD \cdots Br $^-$ anisotropy decays and corresponding fits for different concentrations of Bu₄NBr (a detailed description of how the data-points of the anisotropy decays were obtained can be found in section 4.4.2). Both $R_{OD...O}(t)$ and $R_{OD...Br^-}(t)$ show a bi-exponential behavior with a slow component of which the amplitude increases with increasing concentration. The fraction of this component is determined from the fitted amplitudes. More specifically, we determine the fraction of slow OD-groups $f_A = A_s / (A_f + A_s)$ in the case of OD \cdots O. For the OD \cdots Br $^-$ anisotropy de-

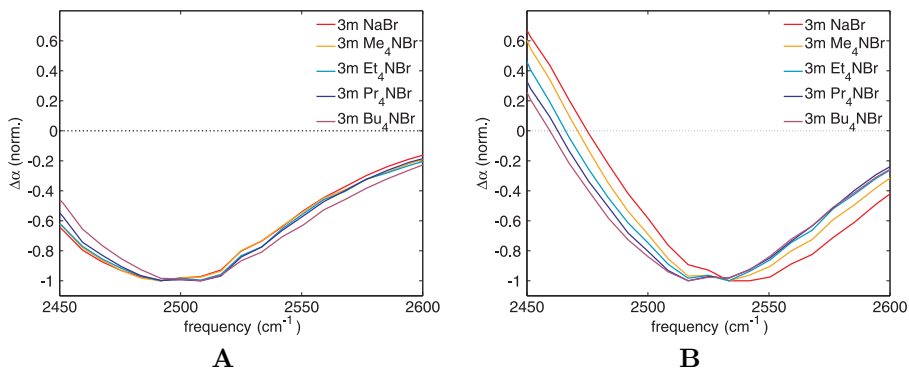


FIGURE 10.5. The spectra of OD···O (**A**) and OD···Br⁻ (**B**) oscillators obtained by fitting the kinetic model to all 3 molal solutions. Depending on the alkyl chain length the resonance frequency of the bromide-bound oscillators blue-shifts less compared to that of aqueous NaBr.

say the fraction $f_B = B_s / (B_f + B_s)$ represents the part of the anisotropy that decays by the slow process. The fractions are plotted for all measured data in Fig. 10.7. f_A and f_B increase with increasing alkyl chain length and with concentration. Towards infinite dilution, the OD···Br⁻ slow fraction extrapolates to a non-zero value that is roughly 0.25 for all salts. In Fig. 10.9 f_A and f_B are plotted against the number of carbons in the cation alkyl chains for two concentrations. The increase of the alkyl chains is shown to increase the fraction of water with slower dynamics, both for the OD···O and the OD···Br⁻ oscillators.

The time constant τ_s^{Br} was a free parameter in the model and its fitted values are shown in Fig. 10.8. The slow reorientation time of water bound to bromide is 14 ± 2 ps for Me₄NBr, independent of the concentration. This time constant can be well determined thanks to the very slow vibrational relaxation of the OD···Br⁻ oscillators (T_1 up to 5.5 ps for the highest concentration of Me₄NBr). The value of τ_s^{Br} for Et₄NBr τ_s^{Br} depends strongly on the concentration, increasing from 20 ± 2 ps for the lowest concentrations up to 41 ± 13 ps for the highest concentration. In the case of the cations with the longest alkyl chains (Pr₄NBr and Bu₄NBr) the slow reorientation time exceeds 40 ps already at low concentrations.

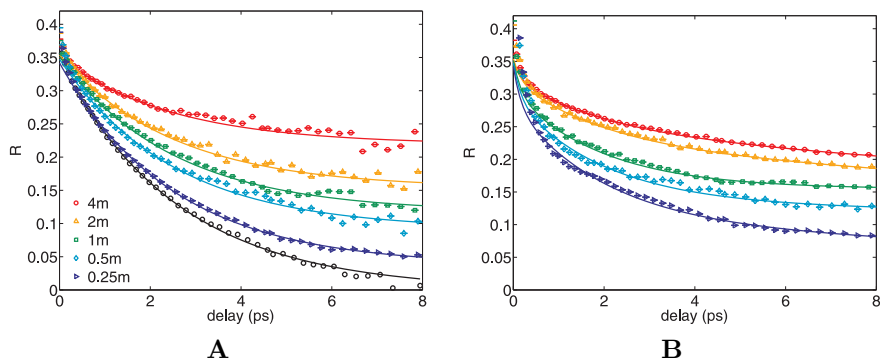


FIGURE 10.6. The anisotropy decay in solutions of different concentrations Bu_4NBr , decomposed in its components $\text{OD}\cdots\text{O}$ (A) and $\text{OD}\cdots\text{Br}^-$ (B). Already for 250 mmolal Bu_4NBr the anisotropy decay shows a substantial slow component compared that of neat water (black circles). The $\text{OD}\cdots\text{Br}^-$ anisotropy decay shows a saturation effect for the higher concentrations.

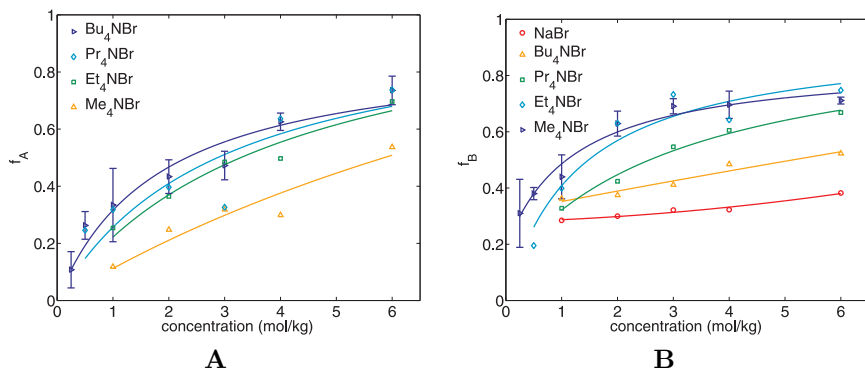


FIGURE 10.7. The fractions of OD-groups with slow reorientation for $\text{OD}\cdots\text{O}$ (A) and $\text{OD}\cdots\text{Br}^-$ (B) oscillators. Bromide-bound OD-groups have an intrinsic slow fraction, which becomes more retarded in solutions with many or large hydrophobic cations. The solid lines are guides to the eye.

10.4 DISCUSSION

10.4.1 HYDROPHOBIC EFFECTS ON THE ANION HYDRATION SHELL

The blue-shift of $\text{OD}\cdots\text{Br}^-$ oscillators relative to $\text{OD}\cdots\text{O}$ oscillators enables us to disentangle the anisotropy dynamics of these two species, similar to our

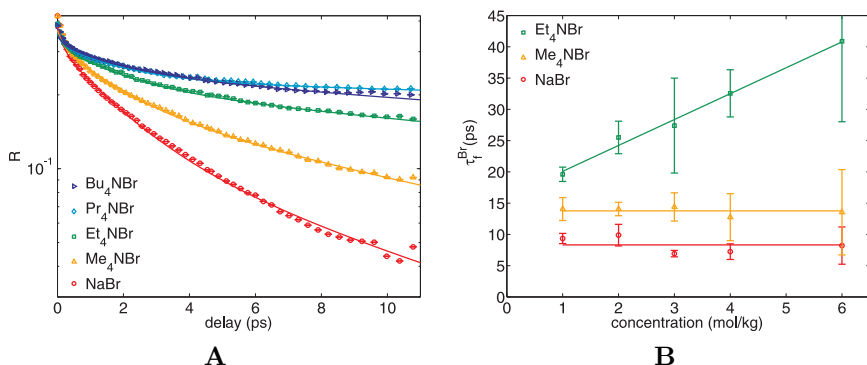


FIGURE 10.8. **(A)** A comparison of the anisotropy decay of bromide-bound OD-groups for salts with different alkyl chain lengths. The vertical axis is logarithmic. **(B)** The slow reorientation time becomes slower for higher concentrations of Et_4NBr . All fitted time constants for Pr_4NBr and Bu_4NBr were longer than 40 ps (data-points not shown). At such long timescale our experiment is not sensitive enough to determine this time constant accurately.

analysis in the previous two chapters. The dynamics of water around the TAA cations, included in the $\text{OD}\cdots\text{O}$ component, is strongly perturbed (Fig. 10.7A). With increasing alkyl length the number of retarded OD groups increases from 12 for Me_4NBr up to 34 for the lower concentrations of Bu_4NBr . For Pr_4NBr and Bu_4NBr these numbers are in good agreement with the estimated number of water molecules in the hydration shells of these ions as obtained from GHz dielectric relaxation spectroscopy [103] and molecular volumes [181]. The fact that the slow water fraction for the lower concentrations scales nearly linearly with the number of CH_n ($n=2,3$) groups in the solution evidences that the retardation is caused by a hydrophobic effect. This is in line with previous studies on amphiphilic molecules in water, where a similar retardation was found of about three water molecules per methyl group [28, 110]. It may be expected that such a distortion of the dynamics of the hydrogen-bond network is accompanied by structural changes, and indeed it was shown in recent work that the hydrophobic solvation shell is slightly more ordered compared to bulk water [98].

The slow fraction of water around the bromide ion f_B (Fig. 10.7B) shows the same qualitative behavior compared to water outside the bromide hydration shell. Extrapolation of f_B towards infinite dilution suggests that there is an intrinsic effect of the bromide on the reorientation dynamics. This fits the picture sketched in chapter 9, where the reorientation dynamics of OD-groups bound to an anion were found to have two main contributions on a fast and slow timescale. A fast decay process (~ 2 ps) is caused by the wobbling motion of a water molecule while keeping its hydrogen bond to the anion intact. As

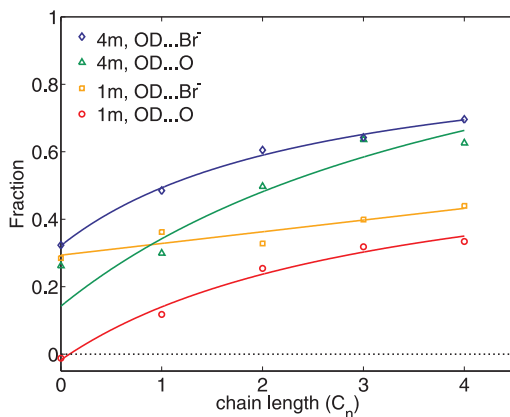


FIGURE 10.9. The fraction of slow water for different alkyl chain lengths decomposed in its components for 1 molal and 4 molal solutions. The solid lines are guides to the eye.

the anion restricts the wobbling motion to a certain angle, this process does not lead to a full decay of the anisotropy and the remaining part decays by the much slower process of rotational diffusion of the molecules over the anionic surface [149, 30]. The latter slow component is the intrinsic anionic effect that is present in Fig. 10.7B. For increasing alkyl chain lengths and concentrations the amplitude of the slow process becomes larger (see also Fig. 10.9). $R_{OD\cdots Br}(t)$ must therefore be interpreted as a combination of an anionic effect and a hydrophobic effect and the latter can be understood as follows. The wobbling motion of an OD group bound to the bromide anion is caused by the reorganization of the hydrogen-bond network outside the first solvation shell. For this reason, the wobbling reorientation time (~ 2 ps) is close to that of normal hydrogen-bond network reorganization (~ 2.5 ps). In the TAABr solutions, the dynamics of the hydrogen-bond network is dramatically retarded by the presence of the hydrophobic cations. This decreased mobility is reflected in the dynamics of the OD-groups that are hydrogen bonded to the bromide ion. The $OD\cdots Br^-$ wobbling motion thus becomes slower for increasing alkyl chain lengths and concentrations.

The vibrational lifetime of the OD-stretching mode of anion bound water is in general observed to be longer than for bulk water [182, 183]. It depends on the salt concentration and was reported to be as long as 4.8 ps for a 6 molal NaBr solution [130], in agreement with our current findings (Fig. 10.4). The increased vibrational lifetime is generally caused by a decrease of the hydrogen bond interaction [182]. Typically we observe that the vibrational lifetime becomes slower with increasing concentration. This dependence may in part be due to exchange events between $OD\cdots Br^-$ and $OD\cdots O$ species [184]. An initially excited $OD\cdots Br^-$ oscillator can rotate out of the solvation shell and become

OD \cdots O, thereby decreasing the effective vibrational lifetime. We have seen in chapter 8 that in salt solutions these exchange effects take place on a timescale of ~ 10 ps depending on concentration [126, 127]. For the TAABr salts, the OD \cdots Br $^-$ vibrational lifetime becomes even longer than for NaBr, up to 7.3 ps for a 6 molal concentration of Bu $_4$ NBr (Fig. 10.4). We interpret this long lifetime as a result of a considerably slower exchange rate out of the bromide solvation shell in solutions with big hydrophobic cations. This picture is consistent with the decreased mobility of the OD \cdots Br $^-$ wobbling component: a more slowly wobbling OD-group will jump out of the solvation shell at a lower rate.

For all solutions we observe that the thermalization is delayed with respect to the vibrational relaxation. This delay is ~ 800 fs in pure water and was interpreted to reflect the adaptation of the hydrogen-bond network to the new energy distribution after vibrational relaxation [185, 22]. Fig. 10.4B shows that the thermalization dynamics, expressed in the decay time of the intermediate state, becomes very slow upon the addition of Bu $_4$ NBr. Apparently, at high concentrations the hydrogen bond network is less capable of adapting to the new energy distribution after the vibrational excitation has relaxed into thermal modes. The effect is weaker for the shorter alkyl chains, indicating that this effect is correlated with the hydrophobicity in the solution.

The OD \cdots Br $^-$ oscillators shows a smaller blue-shift in solutions of TAABr than in solutions of NaBr as seen in both the linear spectra (Fig. 10.1) and the transient spectra (Fig. 10.5). A smaller blue-shift means relatively stronger OD \cdots Br $^-$ hydrogen-bonds, which in this case appears to be induced by the presence of the hydrophobic cations. The stronger OD \cdots Br $^-$ interaction can be explained if on average less OD groups are hydrogen-bonded to bromide per anion, as the anion charge is in such case less screened. The depletion of the bromide solvation shell can be caused by the large hydrophobic chains of the cations that stick into the bromide solvation shell. This explanation is supported by the OD \cdots Br $^-$ populations that show that the number of OD groups in the bromide solvation shell is systematically lower in solutions of TAABr than in solutions of NaBr. This interpretation is also in agreement with recent findings of a tendency of weaker hydrated halide anions to form ion pairs with TAA cations [186].

10.4.2 FORMATION OF AGGREGATED ION CLUSTERS

The fraction of slow water f_A in Fig. 10.7 saturates for increasing concentrations Et $_4$ NBr, Pr $_4$ NBr and Bu $_4$ NBr, which means that there is a decreasing number of slow OD groups per solute molecule. This can partly be explained by overlapping hydration shells: with 34 OD groups per Bu $_4$ N $^+$ solvation shell this overlap is bound to happen already at concentrations of 2 molal. In addition, MD simulations and neutron diffraction experiments show that large hydrophobic cations tend to aggregate strongly [187, 177]. The aggregation leads to a reduced hydrophobic surface that is exposed to water and hence effectively decreases the slow fraction. Me $_4$ NBr does not seem to aggregate much, which was also predicted by MD simulations [188]. A very similar situation occurs when aqueous

solutions of TMU or TBA are compared to solutions of TMAO. TMU and TBA show saturation behavior due to aggregation starting at concentrations of 3 molal [189]. The very polar TMAO molecule, on the contrary, has little tendency to aggregate and the slow water fraction for TMAO solutions is accordingly observed to saturate only at very high concentrations (>8 molal) due to inevitable overlap of the hydration shells at these high concentrations [189, 152]. The lack of aggregation for Me_4NBr solutions is therefore attributed to the charged nature of the Me_4N^+ cation. In spite of this charged nature, we observe a fraction of slowly reorienting water molecules around the Me_4N^+ that we associate with the hydration of the hydrophobic methyl groups. This observation agrees with the results of NMR studies in which it was found that Me_4N^+ , other than Na^+ , is not capable of aligning the static dipoles of its solvating water molecules, in agreement with its qualification as a hydrophobe [176, 190, 100, 191].

We observe that the slow reorientation time of $\text{OD}\cdots\text{Br}^-$ (τ_s^{Br}) has a constant value of 14 ± 2 ps for all measured concentrations of Me_4NBr , while for Et_4NBr τ_s^{Br} increases from 20 ps to more than 40 ps (Fig. 10.8). The reorientation time constants τ_s^{Br} of Pr_4NBr and Bu_4NBr are longer than 40 ps for all concentrations. For alkali-halide salts the slow reorientation was found to occur with a time-constant of ~ 10 ps and is primarily due to rotational diffusion of OD-groups over the anionic surface while keeping their $\text{OD}\cdots\text{Br}^-$ hydrogen-bond intact [125, 30]. The exchange of water between the hydration shell and the bulk can also contribute to the anisotropy dynamics, but this will be a minor contribution [30]. The exchange mainly affects the amplitude of the anion-bound spectral component, i.e. the T_1 time constant. We observe that the presence of the hydrophobic cations leads to a severe retardation effect in the anisotropy dynamics. Rotational diffusion over the anionic surface requires the reorganization of the hydrogen bond network outside the solvation shell. The hydrophobic cations appear to slow down this reorganization and thereby slow down the rotational diffusion.

The results for Me_4NBr are distinct from the other TAABr salts in the sense that no concentration dependence for the slow reorientation time of $\text{OD}\cdots\text{Br}^-$ is found. This is related to the previous observation that Me_4NBr has no tendency to aggregate. From classical MD simulations it was shown that whether amphiphilic solute molecules tend to aggregate or not has a strong effect on the dynamics of the solvating water molecules [107]. Weakly aggregating molecules like TMAO mix better with the solvent, resulting in water molecules confined in thin films in between the big solute molecules. Aggregating molecules like TMU form clusters at higher concentrations, with nanopools of bulk-like water in between. In the case of water films around TMAO, the reorientation time is further slowed down due to the nano-confinement in addition to a hydrophobic effect. With this in mind we can interpret our results on τ_s^{Br} as follows. For increasing concentrations of Et_4NBr the slow water fraction saturates, which points towards a decrease in the exposed hydrophobic surface and hence aggregation. At the same time we find increasing values of τ_s^{Br} , which point towards an increasingly slower reorientation of the hydrogen-bond network around the anions. The distortion of the hydrogen-bond network can

be caused by nano-confinement of the solvating water in between the clustering cations. In concentrated solutions of Et_4NBr domains are likely formed in which bromide anions and Et_4N^+ cations cluster together with a restricted number of water molecules in between. For Pr_4NBr and Bu_4NBr this type of clustering already happens at the lowest concentrations measured. The affinity of large halide anions for TAA cations was shown in MD simulations [186]. In the case of Me_4NBr there is no decrease in the exposed hydrophobic surface and hence no aggregation. The values of τ_s^{Br} remain constant up to 6 molal, similar to the results for NaBr , indicating that aggregation and confinement does not play a role. The Me_4N^+ cation is thus unique in the sense that the coulomb interactions are strong enough to prevent it from aggregating, but the hydrophobic nature is still slowing down the reorientation of the water molecules hydrating the methyl groups. The reason why even at low concentrations the slow reorientation time of bromide bound OD groups is affected by the cations may find its origin in ion-pair formation, which is indeed observed for these solutions [103, 186].

10.5 CONCLUSIONS

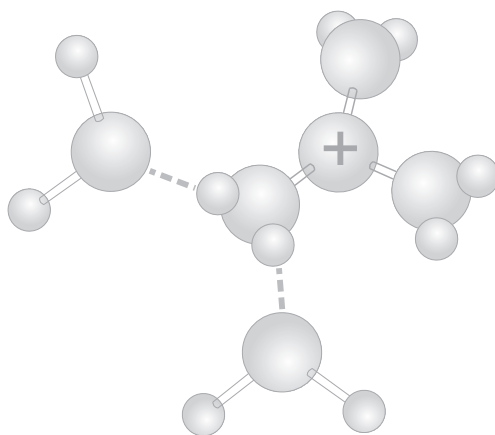
We studied the dynamics of water in aqueous tetra-*n*-alkylammonium bromide solutions for different lengths of the alkyl chains (Me_4NBr , Et_4NBr , Pr_4NBr and Bu_4NBr). Using the blue-shift of the OD stretch resonance of HDO molecules bound to bromide ($\text{OD}\cdots\text{Br}^-$), we can distinguish the dynamics of the bromide solvation shell from the bulk water dynamics ($\text{OD}\cdots\text{O}$). The number of slow water molecules increases with the length of the alkyl chains and corresponds to the solvation numbers of these ions found in other work. For Me_4NBr we find that about 12 OD-groups per cation have slower dynamics, consistent with the picture of hydrophobic hydration. This means that not the charged nature but the hydrophobic nature of the cation governs the water dynamics of its solvation shell. For the larger tetra-*n*-alkylammonium ions this dominance of the hydrophobic effect is even stronger.

The slower dynamics of the hydrogen bond network is reflected in the solvation shell of the bromide anion as well. The dynamics of OD-groups that remain hydrogen bonded to bromide is partially governed by a wobbling motion that roughly follows the reorganization of the hydrogen bond network outside the solvation shell. We find that this wobbling motion acquires a slow component due to the presence of the hydrophobic cations. We also find that the blue-shift of both the linear and transient spectra of $\text{OD}\cdots\text{Br}^-$ compared to $\text{OD}\cdots\text{O}$ is much smaller for solutions of TAABr compared to NaBr solutions. This observation can be explained from the partial hydration of the Br^- hydration shell by the protruding hydrophobic chains of the TAA cations. This picture also explains the increase of the vibrational lifetime for the OD-stretch excitation of $\text{OD}\cdots\text{Br}^-$ with increasing TAA concentration and increasing alkyl chain length: For alkali-halide salt solutions this lifetime is partly determined by exchange events between OD groups bound to bromide and water outside

the solvation shell. These exchange events typically take place on a timescale of ~ 10 ps, but will be much slower in concentrated TAABr solutions due to the effect of the nearby hydrophobic TAA cations on the dynamics of the surrounding liquid.

From the saturation behavior of the fraction of water decaying by the slow process and the increasing reorientation time of $\text{OD}\cdots\text{Br}^-$ oscillators we infer that cations with long alkyl chains form clusters with bromide ions and water molecules. The clustering effectively decreases the total exposed hydrophobic surface which leads to a saturation effect in the observed slow water fraction. The water molecules inside these clusters are highly confined, causing the reorientation of OD groups bound to the bromide ions that penetrated such a cluster to become even slower than 30 ps. Normally such slow reorientation processes are difficult to probe in this type of experiments due to the short lifetime of the OD-stretch vibration. However, the long $\text{OD}\cdots\text{Br}^-$ vibrational lifetime allows for an accurate determination of such long reorientation time constants. The aggregation effect is not observed for Me_4NBr even at concentrations of 6 molal, probably because for this ion the repulsive coulomb interaction is just strong enough to prevent the formation of large aggregated ion clusters.

Osmolytes and Denaturation



Some of the work in previous chapters was considered in the context of protein denaturation. In chapter 9 we saw that cations with a large surface charge density have a preference to form hydration complexes with strongly hydrated anionic groups. Weakly hydrated anions, on the other hand, like to pair-up with weakly hydrated cationic groups. In proteins most cationic groups are weakly hydrated and most anionic groups are strongly hydrated, explaining the Hofmeister series in which most denaturing power is assigned to a combination of a weak cation and strong anion. However, there exist also non-ionic osmolytes that are able to denature proteins, like urea and tetramethylurea (TMU). **In this chapter we investigate the hydration dynamics around guanidinium chloride and tetramethylguanidinium chloride and compare their properties to those of urea and TMU.** The replacement of four protons in guanidinium and urea by methyl groups (yielding tetramethylguanidinium and TMU, respectively), has a strong effect on the reorientation dynamics of their solvating water molecules. We find that guanidinium chloride is the strongest denaturant and urea the weakest, but the methyl substitution puts them both in the middle. These results suggest a different mechanism of denaturation for the denaturants containing hydrophobic groups.

11.1 INTRODUCTION

The conformation of macromolecules in aqueous media is crucial for their functioning in biological systems. Many studies have been devoted to the understanding of how these structures are formed and how this formation can be influenced by co-solutes like salts and sugars. These studies go back to the pioneering work of Franz Hofmeister [136]. In his 1888 paper Hofmeister discussed the influence of different salts on the precipitation of proteins, a process called salting out. Currently, the well known Hofmeister series comprises two series of cations and anions, ordered by their ability to salt out proteins. It has been argued that salts affect the conformation of proteins by changing the denaturants work indirectly by affecting the properties of water [192, 193, 194]. This effect has been assigned to structure-making and structure-breaking concepts [137], i.e. a presumed ion-induced strengthening or weakening of the hydrogen-bond network of water over long distances. Although these concepts offer an explanation of the observed (de)naturation effects according to the Hofmeister series, experimentally no evidence was found of the supposed long range structuring influence of ions on water [119, 120, 121, 122]. Most ions influence the structure and dynamics of only their first solvation shell [118] and only in the (rare) case of very strongly hydrated ions, water molecules were found to be affected over a somewhat larger distance [123]. A more detailed consideration of ion-water interaction and its possible relation to denaturation and the stabilization of conformations can be found in chapter 9.

The guanidinium cation (see inset Fig. 11.1) is on the far end of the Hofmeister series. Its chloride salt (GndCl) is among the strongest denaturants known, causing almost all proteins to unfold completely at a concentration of 6 mol/l [195]. There is an ongoing debate about the underlying microscopic principles of its working mechanism. Dielectric relaxation spectroscopy and neutron diffraction studies on the water structure around the guanidinium ion suggest that the ion lacks a significant hydration shell [196, 174]. From these results it was concluded that the denaturation process likely involves a direct interaction with proteins, as has been proposed for urea [174, 175]. However, molecular dynamics (MD) simulations show surprising differences between urea and guanidinium chloride [197, 192, 193, 198]: it was found that urea binds to peptide groups but guanidinium does not [193]. In line with this finding, it was shown in other studies that the interaction between guanidinium and water might be crucial in understanding its denaturing properties [194]. Finally, it should be noted that both microscopic mechanisms for denaturation are not mutually exclusive and might in fact both be active [199].

The substitution of the hydrogen atoms of urea by methyl groups yields the osmolyte tetra-methyl urea (TMU). Compared to urea, TMU is an even more effective denaturant [200] and shows a profound (hydrophobic) effect on the water dynamics of its solvation shell [17]. It is therefore not surprising that previous work indicated that denaturation induced by TMU may have another microscopic origin than urea [200]. Given the fundamental differences in the nature of guanidinium chloride and urea it is interesting to study the effects

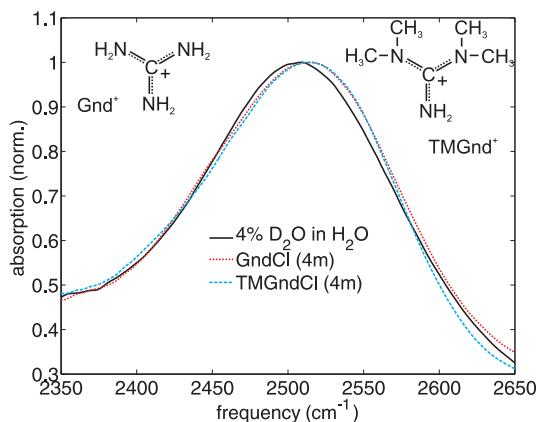


FIGURE 11.1. Linear absorption spectra in the region of the OD stretch vibration for concentrated solutions of the measured salts and neat 4% D₂O in H₂O. The addition of the salts cause the spectrum to slightly blue-shift.

of the substitution of the hydrogen atoms of the guanidinium ion by methyl groups on the molecular properties of water and the denaturation of proteins.

In this chapter we use THz-DR and fs-IR to study the effects of electrostatic and hydrophobic interactions on the dynamics of water. We compare solutions of the strong denaturing salts guanidinium chloride and tetramethyl guanidinium chloride. To relate the results to denaturation, we compare the effectiveness of guanidinium chloride, tetramethylguanidinium chloride, urea and TMU in the denaturation of the model protein Photoactive Yellow Protein.

11.2 EXPERIMENTAL

The fs-IR measurements were performed using the one color pump-probe setup that was described in section 3.1.1. The measurements were performed on the OD-stretch vibration in isotopically diluted water (4% D₂O in H₂O). We tuned the pump and probe spectrum to be centered around 2525 cm⁻¹. The dielectric spectra were measured with the THz dielectric relaxation setup described in section 3.3.

Guanidinium chloride (GndCl) and 1,1,3,3-tetramethylguanidine (TMG) were purchased from Sigma Aldrich. TMG is a strong base ($pK_a = 13.6$) and was neutralized by adding a stoichiometric amount of hydrochloric acid to create the tetramethylguanidinium chloride (TMGndCl) salt. Fig. 11.1 shows a graphical representation of the (tetramethyl)guanidinium cation. Solutions at different concentrations were prepared with a mixture of 4% D₂O in H₂O (Sigma Aldrich) as the solvent. The measured concentrations range from 0.25 to 4 molal (mol/kg solvent) for the THz-DR experiment, and from 1 to 6 molal for the fs-IR experiments. The deuterium atoms of D₂O exchange both with water

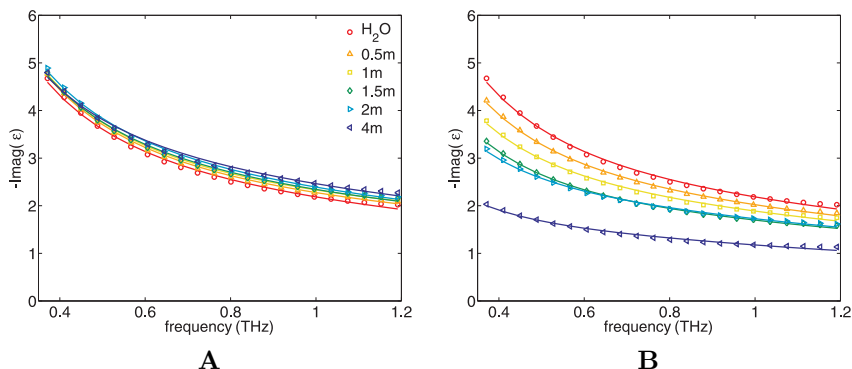


FIGURE 11.2. The imaginary part of the dielectric function of (A) GndCl and (B) TMGndCl solutions of different concentrations. The decrease of the spectrum for increasing concentrations is called depolarization. The depolarization in solutions of TMGndCl is clearly much larger than that in solutions of GndCl.

to form HDO molecules and with the NH_2 groups of the guanidinium salts to form NHD. The resonance frequency of the thus formed ND is very close to that of the OD, but its cross section - which is entering quadratically in the pump-probe signal - is twice as small. In addition, for a 4 m GndCl solution the concentration of ND is 3 times lower than the OD concentration. Therefore the contribution of the NHD groups to the pump probe signal will be small and is neglected. In the THz-DR experiment an Infrasil quartz cuvette was used with a pathlength of $103 \pm 0.5 \mu\text{m}$. In the fs-IR measurements we used two square CaF_2 windows (thickness 4 mm) with a 50 or 100 μm spacer in between. The concentrations of H_2O in the solutions are determined using a density meter (Mettler Toledo DM40).

11.3 RESULTS

11.3.1 THZ DIELECTRIC RELAXATION

In Fig. 11.2 we show the imaginary part of the dielectric function $\varepsilon(\nu)$ measured for different concentrations of GndCl and TMGndCl. A decrease of $\varepsilon(\nu)$ is indicative for a decreased polarization response of water molecules with bulk-like reorientation and is called depolarization. There are a number of effects causing depolarization. In the first place there is the effect of dilution due to the decrease in the number of water molecules in a constant volume contributing to the signal when a solute is added. This is corrected for using the densities of the measured solutions. Second, there is the effect of kinetic depolarization that results from the movement of charges in an electric field. Water molecules close to the moving ion will align preferentially to the local field of the ion

instead of the externally applied field, leading to a depolarization effect when rotating against this external field. This contribution can also be accounted for [37]. The conductivities of the GndCl solutions required to calculate the kinetic depolarization effect were obtained by interpolation from the data of ref. [196]. Thirdly, the water molecules that weakly bind to the ions may no longer reorient in the applied electric field and therefore no longer contribute to $\hat{\epsilon}(\nu)$. And finally, the reorientation time of the dipoles may increase, thereby shifting the imaginary response to lower frequencies and therefore out of the THz measurement window.

TMGndCl shows a much stronger depolarization effect than GndCl. This cannot be due to electrostatic alignment of the water molecules in the solvation shell of the cation, since the electric field exerted by the TMGnd⁺ cation is not stronger than the field exerted by the Gnd⁺ cation. More likely, a large fraction of water in TMGndCl solutions reorients slowly because of the presence of the hydrophobic methyl groups, as has been observed before for other amphiphilic solutes [103, 17] and was elaborated on in chapters 7 and 10 in this thesis. For these water molecules the frequency response has shifted to lower frequencies. In addition to the two Debye modes for pure water (described in section 4.5) we therefore add another Debye mode for the slowly reorienting water to the model. Including the term for conductivity the model function can thus be written as,

$$\hat{\epsilon}(\nu) = \frac{S_{slow}}{1 + 2\pi i\nu\tau_{slow}} + \frac{S_{bulk}}{1 + 2\pi i\nu\tau_{bulk}} + \frac{S_{fast}}{1 + 2\pi i\nu\tau_{fast}} + \frac{\sigma}{2\pi i\epsilon_0\nu} + \epsilon_\infty. \quad (11.1)$$

As pointed out in section 4.5, the THz-DR experiment is not very sensitive to the frequency dependence of the dielectric relaxation modes that peak at much lower frequencies. These modes are rather present as a decrease in the amplitude. Hence in fitting the observed dielectric response of the TMGndCl, we fix the values for τ_{slow} of the slow water mode and τ_{bulk} of the bulk water to the parameters found for TMU in the GHz regime [17]. The fits to the data are presented as the solid lines in Figs. 11.2.

After correcting for dilution effects and the kinetic depolarization, we obtain the values of the slow water fractions for the different solutions, shown in Fig. 11.3A. For comparison we also show the slow fractions observed for TMU from Ref. [17].

11.3.2 FS-IR PUMP-PROBE

Chapters 8, 9 and 10 already extensively elaborated on how to treat fs-IR pump-probe data of aqueous halide salt solutions. Also for the chloride salts studied in this chapter we expect that two separate bands can be resolved with different dynamics. The transient spectra of GndCl in fact showed the presence of a third spectral component (in addition to the OD \cdots O and OD \cdots Cl⁻ components) on the red side of the OD \cdots O spectrum ($<2470\text{ cm}^{-1}$) with a very fast vibrational decay. This fast relaxing mode is possibly due to coupling of the OD-stretch vibration to vibrational modes in the guanidinium cation [194, 201]. We minimize

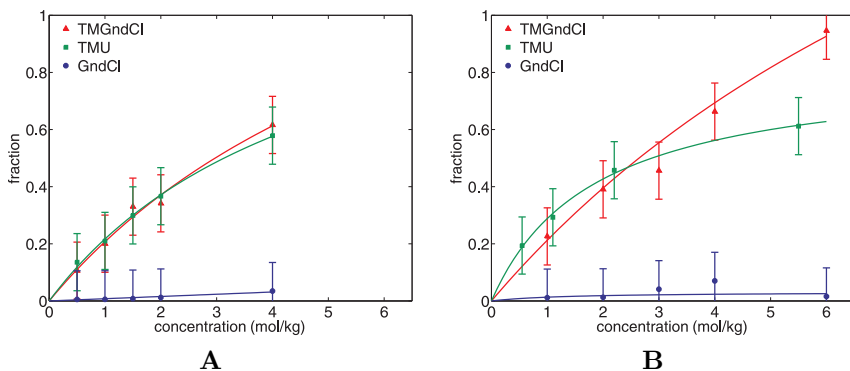


FIGURE 11.3. **(A)** Slow water fractions obtained from the THz-DR measurements. For both experiments hardly any effect is seen for GndCl, while the effects for TMGndCl and TMU are almost identical. The slow water fractions for GndCl and TMU were calculated with data from [196] and [17] respectively. **(B)** Slow water fractions of the OD \cdots O anisotropy decays obtained from the fs-IR measurements. The data for TMU are taken from ref. [24].

the contribution of this fast component by tuning the pump-probe spectrum to have a center frequency around 2525 cm^{-1} , slightly blue-shifted from the OD-stretch absorption band. The transient spectra measured for a 4 molal solution of GndCl are presented in Fig. 11.4.

The data is modeled following the same approach as was used for solutions of tetra-*n*-alkylammonium salts in chapter 10. We assumed a kinetic model for the vibrational decay that includes two excited states that decay with different time constants to an intermediate state. The intermediate state subsequently decays to the thermalized ground state. A graphical representation of this model was presented in Fig. 4.7. For the anisotropy data we assume the functional forms of (10.1) and (10.2), for which all made assumptions were the same except for the slow reorientation time τ_s^O in the OD \cdots O component. The values for τ_s^O were fixed to the reorientation times that were found for solutions of TMU using GHz dielectric relaxation [17]. We performed a self-consistent fit in which both the kinetic model and the functional forms of the OD \cdots O and OD \cdots Cl $^-$ reorientation dynamics are simultaneously fitted to the isotropic data and the anisotropy data, respectively.

Fig. 11.5 shows the total anisotropy measured for solutions of GndCl and TMGndCl of different concentrations. The curves shown in Fig. 11.5 represent the averaged reorientation behavior of all OD \cdots O and OD \cdots Cl $^-$ groups in solution, weighted by their respective time-dependent populations. For the GndCl solutions the anisotropy decays are observed to be only slightly different from the anisotropy decays of pure HDO:H $_2$ O. In contrast, the anisotropy curves of the TMGndCl solutions show a much slower decay, indicating that a large

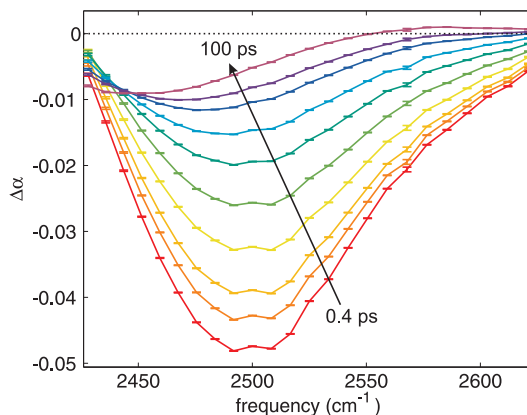


FIGURE 11.4. Transient absorption spectra measured for a 4 molal GndCl solution. For increasing pump-probe delay times the transient absorption spectra decay to the thermal difference spectrum (blue).

amount of the water molecules have very slow orientational dynamics. The retardation effect strongly increases with concentration.

From the fitting results we reconstruct the reorientation dynamics of the OD \cdots O and OD \cdots Cl $^-$ components separately. The results for TMGndCl are shown in Fig. 11.6, the solid lines are the results of the fits. In both components a strong retardation effect of the reorientation dynamics is present. The slower anisotropy dynamics in the OD \cdots Cl $^-$ component is an indirect result of the hydrophobic groups of the cation. Anion-bound OD groups display a wobbling motion that leads to a fast (~ 2 ps) anisotropy decay (see chapter 9). This wobbling motion is hindered by the hydrophobic cation, causing the dynamics of the hydrogen-bond network surrounding the anion solvation shell to become slower (10). In this chapter we mainly on the OD \cdots O component. The fraction of water molecules with slower dynamics is calculated from the fitted amplitudes A_f and A_s in $R_{OD\cdots O}(t)$ and plotted for different concentrations in Fig. 11.3B. The slow water fractions for TMGndCl are a bit higher than what we found for tetramethylammonium bromide, as presented in chapter 10. This is mainly caused by a different choice of the slow water reorientation time τ_s^O : Here we assumed τ_s^O of TMGndCl to be equal to τ_s^O of TMU, whereas in the analysis of the data obtained for different tetra- n -alkylammoniumbromide solutions, we set τ_s^O equal to infinity. This latter choice was based on the fact that we observed quite different behavior for tetra- n -alkylammoniumbromide salts with $n = 2, 3, 4$. Since we have a good estimate of τ_s^O for TMGndCl from GHz-DR data on TMU [17], this time constant was not set to infinity. This finite values of τ_s^O yield slightly higher values for the slow water fractions.

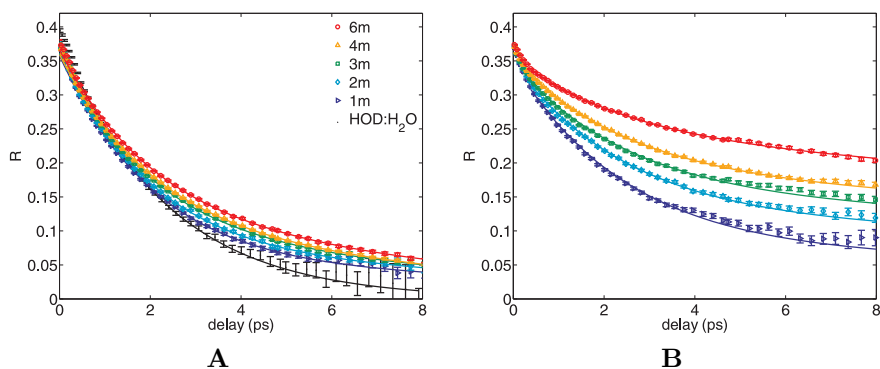


FIGURE 11.5. The total anisotropy decay for solutions containing different concentrations of GndCl (**A**) and TMGndCl (**B**). The substitution of hydrogen atoms by methyl group has a dramatic slowing down effect on the anisotropy decay.

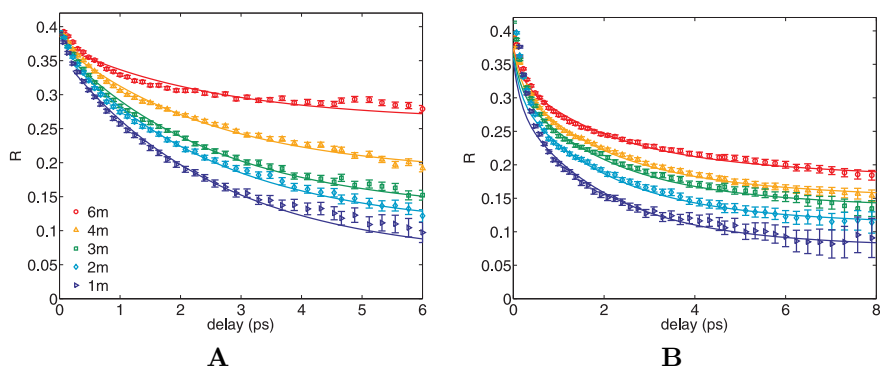


FIGURE 11.6. Anisotropy decays of OD...O (**A**) and OD...Cl⁻ (**B**) for different concentrations of TMGndCl. The hydrophobic groups of the cation slow down the dynamics of the water hydrogen-bond network outside the anion hydration shell, and thereby also decelerate the wobbling motion of the chloride bound OD groups.

11.4 DISCUSSION

The addition of GndCl to water is observed to have a very small effect on the reorientation dynamics of the water molecules. Guanidinium is a relatively large cation which means that the charge density of the positive charge will be rather low. As previously discussed (chapter 9), the electrostatic interaction between water and this ion will thus be weak. The interaction of water with guanidinium will thus be dominated by hydrogen bonding to the NH₂

groups. These hydrogen-bond interactions are quite similar to the hydrogen bonds between water molecules [174, 196]. An analog can be drawn here with aqueous solutions of urea ($\text{CH}_4\text{N}_2\text{O}$). Hydrogen-bonds between water and urea are also quite like water-water hydrogen-bonds, and the reorientation dynamics of water in such solutions was observed to be largely unaffected by the presence of urea [111]. Apparently, urea and guanidinium both fit very well in the hydrogen-bond structure of water, allowing the water molecules to reorient with a similar rate as is observed in bulk liquid water. The small slowing down of the total anisotropy decay observed for solutions of GndCl , as shown in Fig. 11.5A, can be fully assigned to the presence of the chloride anion. Water molecules solvate the Cl^- anions by forming a $\text{OD}/\text{OH}\cdots\text{Cl}^-$ hydrogen-bond. This limits the reorientation freedom of those hydroxyl groups, whereas the *static* dipole moments of these water molecules remain quite free in their reorientation. The reorientation of the static dipoles of the water molecules is measured in the THz-DR experiment (Fig. 11.3A). This notion explains why the THz-DR measurements show no difference in water dynamics between solutions of GndCl and bulk water. This effect is more extensively discussed in chapter 9.

We observe that TMGndCl has a large effect on the dynamics of water in both the THz-DR and in the fs-IR experiments. The fs-IR measurements show a strong retardation effect of the water dynamics in both the $\text{OD}\cdots\text{O}$ and the $\text{OD}\cdots\text{Cl}^-$ component (Fig. 11.6). The slower dynamics in the $\text{OD}\cdots\text{O}$ component are due to water molecules in the hydrophobic solvation shell of the TMGnd^+ cation similar to the effect of TMU on water dynamics [28]. With regard to the water dynamics, the hydrophobic nature of the TMGnd^+ cation is thus dominant over its charged nature, as was also found for tetramethylammonium bromide. We also see a strong increase of the slow fraction of the $\text{OD}\cdots\text{Cl}^-$ component of TMGndCl compared to that of GndCl . This increase can be assigned to the effects of the hydrophobic molecular groups of TMGnd^+ on the dynamics of the wobbling component of the chloride-bound OD groups. This is analogous to the results for tetra-*n*-methylammonium bromide that were presented in chapter 10.

The THz-DR results also show a slowing down effect of the water dynamics (Fig. 11.2). The fact that slower reorientation dynamics is observed in both experiments implies that the TMGnd^+ cation affects the dynamics of the OD groups and the water dipole moments in a similar manner. For solutions of TMU it was also observed that the slowing down effect is quite similar in dielectric relaxation and in femtosecond mid-infrared measurements [17]. It is illustrative to compare the results obtained for TMGndCl with the results obtained for solutions of TMU at similar concentrations, as TMU also possesses four methyl groups in a similar configuration as the TMGnd^+ cation. The THz-DR data of TMGndCl agree very well with the results of TMU (Fig. 11.3). This agreement strongly supports the interpretation that the effects of TMGnd^+ and TMU on the dynamics of water are completely dominated by the methyl groups and their hydrophylic group or charged nature is less relevant.

In NMR studies it is also observed that hydrophobic molecular groups have a strong effect on the reorientation dynamics of liquid water that increases with

increasing size of the hydrophobic group [99, 100, 101, 102]. For instance, in the NMR study by Shimizu et al. [101], the slowing down of the water reorientation dynamics was found to scale with the number of substituted methyl groups of the urea molecule, urea showing only a negligible effect and TMU the strongest effect. In the same study GndCl was also found to have a negligible effect on the reorientation dynamics of water [101], in line with the present observations.

In order to relate the effects of GndCl and TMGndCl on the dynamics of water to their role in the denaturation of proteins, we measured the fraction of unfolded Photoactive Yellow Protein (PYP) as a function of concentration GndCl, TMGndCl, urea and TMU. The measurements, of which the results are shown in Fig. 11.7, were performed according to the procedure described in Ref. [202] at pH 7 (using a potassium phosphate buffer). GndCl is clearly most effective, as it completely unfolds all PYP at a concentration of 3.5 mol/l. Urea is by far the least effective.

TMU completely denatures PYP at much lower concentrations compared to urea. Apparently, the substitution of the four hydrogen atoms of urea by methyl groups enhances the effectiveness of the denaturant. One may expect a similar enhancement for TMGndCl relative to GndCl, but TMGndCl is in fact less effective than GndCl. TMGndCl rather shows a similar denaturation behavior as TMU. The denaturation mechanisms of urea and GndCl compounds appear to be completely replaced by denaturation effects associated with the methyl groups of TMU and TMGndCl. We also found that TMGndCl and TMU show a quite similar retardation effect on the dynamics of water. Both observations can be explained by the limiting effect of the methyl groups on the configurational space of the solvating water. As a result, the entropy of the solution is decreased and the reorientation dynamics slows down. Entropy changes are believed to be the main driving force for the denaturation of proteins by TMU. Both the denaturation effects and the retardation of water dynamics thus both find a common origin in the hydrophobic moieties of TMU and TMGndCl.

11.5 CONCLUSIONS

We studied the effects of guanidinium chloride (GndCl) and tetramethylguanidinium chloride (TMGndCl) on the reorientation dynamics of water using THz dielectric relaxation (THz-DR) and polarization-resolved femtosecond mid-infrared spectroscopy (fs-IR). THz-DR probes the reorientation of the water dipole moments while fs-IR probes the reorientation of the water OH/OD groups.

For GndCl solutions there is a small slow component in the reorientation dynamics associated with water molecules that are hydrogen bonded to the Cl^- anion. The guanidinium ion has no effect on the reorientation dynamics of water. In the case of TMGndCl the effect on the dynamics of water are dominated by the hydrophobic methyl groups of the TMGnd cation. The four methyl groups of TMGnd^+ lead to a strong slowing down of the reorientation

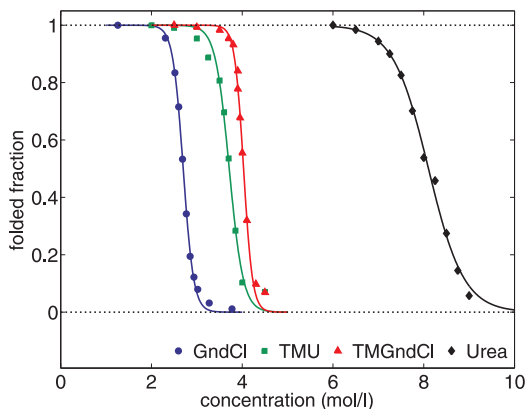


FIGURE 11.7. Fraction of folded protein PYP as a function of denaturant concentration for different denaturants. The measurements were performed for a buffered solution at pH 7.

dynamics of water, that is quite similar to what is observed for solutions of tetramethylurea (TMU). The water molecules that form hydrogen bonds to Cl^- show a strong slowing down of their wobbling motion due to the nearby presence of the hydrophobic TMGnd^+ cations.

Finally, we put these results in the perspective of the capabilities of GndCl, TMGndCl, urea and TMU to denature proteins. While urea and GndCl differ strongly in their effectiveness of denaturation, TMGndCl and TMU both show very similar behavior. The denaturation mechanism of TMGndCl and TMU may thus well be associated with their hydrophobic moieties.

Bibliography

1. M. Chaplin. Anomalous properties of water (<http://www.lsbu.ac.uk/water/anmlies.html>), October 2013.
2. D. Laage and J. T. Hynes. A molecular jump mechanism of water reorientation. *Science*, 311:832–835, 2006.
3. K.J. Gaffney, M. Ji, M. Odellius, S. Park, and Z. Sun. H-bond switching and ligand exchange dynamics in aqueous ionic solutions. *Chem. Phys. Lett.*, 504:1–6, 2011.
4. K. Ramasesha, S.T. Roberts, A. Nicodemus, R.A. Mandal, and A. Tokmakoff. Ultrafast 2d ir anisotropy of water reveals reorientation during hydrogen-bond switching. *J. Chem. Phys.*, 135:054509, 2011.
5. J. D. Bernal and R. H. Fowler. A theory of water and ionic solution, with particular reference to hydrogen and hydroxyl ions. *J. Chem. Phys.*, 1(8):515–548, 1933.
6. C. J. T. de Grotthuis. Sur la decomposition de l'eau et des corps qu'elle tient en dissolution l'aide de l'electricit galvanique. *Ann. Chim.*, 58:54–74, 1806.
7. H. J. Bakker and J. L. Skinner. Vibrational spectroscopy as a probe of structure and dynamics in liquid water. *Chem. Rev.*, 110:1498–1514, 2010.
8. Alexander Y. Zaslavsky. Dielectric relaxation in liquidwater: Two fractions or two dynamics? *Phys. Rev. Lett.*, 107:117601, 2011.
9. K. Ramasesha, L. De Marco, A. Mandal, and A. Tokmakoff. Water vibrations have strongly mixed intra- and intermolecular character. *Nature Chem.*, 5:935940, 2013.
10. J. Barthel, K. Bachhuber, R. Buchner, and H. Hetzenauer. Dielectric spectra of some common solvents in the microwave region. water and lower alcohols. *Chem. Phys. Lett.*, 165(4):369–373, January 1990.

11. D. Chandler. Interfaces and the driving force of hydrophobic assembly. *Nature*, 437:640, 2005.
12. Scott Prahl. Optical absorption of water. <http://omlc.ogi.edu/spectra/water/index.html>, july 2009.
13. E.M. Heatwole and O.V. Prezhdo. Analytic dynamics of the morse oscillator derived by semiclassical closures. *J. Chem. Phys.*, 130:244111, 2009.
14. E.R. Lippincott and R. Schroeder. One-dimensional model of the hydrogen-bond. *J. Chem. Phys.*, 23:1099–1106, 1955.
15. J. R. Schmidt, S. A. Corcelli, and J. L. Skinner. Pronounced non-condon effects in the ultrafast infrared spectroscopy of water. *J. Chem. Phys.*, 123(4):044513, 2005.
16. Eugene Hecht. *Optics, Fourth Edition*. Addison Wesley, 2002.
17. K.-J. Tielrooij, J. Hunger, R. Buchner, M. Bonn, and H.J. Bakker. Influence of concentration and temperature on the dynamics of water in the hydrophobic hydration shell of tetramethylurea. *J. Am. Chem. Soc.*, 132:15671–15678, 2010.
18. O. Gottmann, U. Kaatze, and P. Petong. Coaxial to circular waveguide transition as high-precision easy-to-handle measuring cell for the broad band dielectric spectrometry of liquids. *Measurement Science and Technology*, 7:525–534, 1996.
19. W. Ensing, J. Hunger, N. Ottosson, and H.J. Bakker. On the orientational mobility of water molecules in proton and sodium terminated nafion membranes. *J. Phys. Chem. C*, 117:12930–12935, 2013.
20. D.V. Blackham and R.D. Pollard. An improved technique for permittivity measurements using a coaxial probe. *IEEE Trans. on Instrumentation and Measurement*, 46:1093–1099, 1997.
21. M. J. Tauber, R. A. Mathies, X. Chen, and S. E. Bradforth. Flowing liquid sample jet for resonance raman and ultrafast optical spectroscopy. *Rev. Sci. Instr.*, 74:4958, 2003.
22. Y. L. A. Rezus and H. J. Bakker. On the orientational relaxation of HDO in liquid water. *J. Chem. Phys.*, 123:114502, 1–7, 2005.
23. A. J. Lock, S. Woutersen, and H. J. Bakker. Ultrafast energy equilibration in hydrogen-bonded liquids. *J. Phys. Chem. A*, 105:1238–1243, 2001.
24. Y. L. A. Rezus and H. J. Bakker. Strong slowing down of water reorientation in mixtures of water and tetramethylurea. *J. Phys. Chem. A*, 112:2355–2361, 2008.

25. G. Lipari and A. Szabo. Effect of librational motion on fluorescence depolarization and nuclear magnetic resonance relaxation in biomolecules and membranes. *Biophys. J.*, 30:489–506, 1980.
26. L. Piatkowski, K. B. Eisenthal, and H. J. Bakker. Ultrafast intermolecular energy transfer in heavy water. *Phys. Chem. Chem. Phys.*, 11:9033–9038, 2009.
27. A. Dokter, S. Woutersen, and H.J. Bakker. Inhomogeneous dynamics in confined water nanodroplets. *PNAS*, 103:15355–15358, 2006.
28. Y. L. A. Rezus and H. J. Bakker. Observation of immobilized water molecules around hydrophobic groups. *Phys. Rev. Lett.*, 99:148301, 1–4, 2007.
29. C.H. Giammanco, D.B. Wong, and M.D. Fayer. Water dynamics in divalent and monovalent concentrated salt solutions. *J. Phys. Chem. B*, 116:13781–13792, 2012.
30. S.T. van der Post and H.J. Bakker. The combined effect of cations and anions on the dynamics of water. *Phys. Chem. Chem. Phys.*, 14:6280–6288, 2012.
31. T. Fukasawa, T. Sato, J. Watanabe, Y. Hama, W. Kunz, and R. Buchner. Relation between dielectric and low-frequency raman spectra of hydrogen-bond liquids. *Phys. Rev. Lett.*, 95:197802, 2005.
32. H. Yada, M. Nagai, and K. Tanaka. Origin of the fast relaxation component of water and heavy water revealed by terahertz time-domain attenuated total reflection spectroscopy. *Chem. Phys. Lett*, 464:166–170, 2008.
33. C.J. Fecko, J.D. Eaves, and A.J. Tokmakoff. Isotropic and anisotropic raman scattering from molecular liquids measured by spatially masked optical kerr effect spectroscopy. *J. Chem. Phys*, 117:1139–1154, 2002.
34. D.A. Turton, J. Hunger, G. Hefter, R. Buchner, and K. Wynne. Glasslike behavior in aqueous electrolyte solutions. *J. Chem. Phys*, 128:161102, 2008.
35. K. J. Tielrooij, C. Petersen, Y. L. A. Rezus, and H. J. Bakker. Reorientation of hdo in liquid h2o at different temperatures: Comparison of first and second order correlation functions. *Chem. Phys. Lett*, 471:71–74, 2009.
36. R. Buchner, T. Chen, and G. Hefter. Complexity in "simple" electrolyte solutions: Ion pairing in mgso4(aq). *J. Phys. Chem. B*, 108:2365–2375, 2004.
37. K.-J. Tielrooij, S.T. van der Post, J. Hunger, M. Bonn, and H.J. Bakker. Anisotropic water reorientation around ions. *J. Phys. Chem. B*, 115:12638–12647, 2011.

38. Richard Buchner, Glenn T. Hefter, and Peter M. May. Dielectric relaxation of aqueous nacl solutions. *J. Phys. Chem. A*, 103, 1999.
39. U. Kaatze. The dielectric properties of water in its different states of interaction. *Journal of Solution Chemistry*, 26:1049–1112, 1997.
40. D. Cringus, T. I. C. Jansen, M. S. Pshenichnikov, and D. A. Wiersma. Ultrafast anisotropy dynamics of water molecules dissolved in acetonitrile. *J. Chem. Phys*, 127:084507, 2007.
41. D. Kraemer, Cowan. M. L., A. Paarmann, N. Huse, E. T. J. Nibbering, T. Elsaesser, and R. J. Dwayne Miller. Temperature dependence of the two-dimensional infrared spectrum of liquid h₂o. *PNAS*, 105:437–442, 2008.
42. T.L.C. Jansen, B.M. Auer, M. Yang, and J.L. Skinner. Two-dimensional infrared spectroscopy and ultrafast anisotropy decay of water. *J. Chem. Phys*, 132:224503, 2010.
43. D.E. Rosenfeld and M.D. Fayer. Excitation transfer induced spectral diffusion and the influence of structural spectral diffusion. *J. Chem. Phys*, 137:064109, 2012.
44. J. Lindner, P. Vohringer, M. S. Pshenichnikov, D. Cringus, D. A. Wiersma, and M. Mostovoy. Vibrational relaxation of pure liquid water. *Chem. Phys. Lett*, 421:329–333, 2006.
45. V.H. Segtnan, S. Sasic, T. Isaksson, and Y. Ozaki. Studies on the structure of water using two-dimensional near-infrared correlation spectroscopy and principal component analysis. *Anal. Chem.*, 73:3153–3161, 2001.
46. S. Ashihara, N. Huse, A. Espagne, E. T. J. Nibbering, and T. Elsaesser. Vibrational couplings and ultrafast relaxation of the O-H bending mode in liquid H₂O. *Chem. Phys. Lett*, 424:66, 2006.
47. M. Sovago, R.K. Campen, G.W.H. Wurpel, M. Müller, H.J. Bakker, and M. Bonn. Vibrational response of hydrogen-bonded interfacial water is dominated by intramolecular coupling. *Phys. Rev. Lett.*, 100:173901, 2008.
48. J. C. Deak, S. T. Rhea, L. K. Iwaki, and D. D. Dlott. Vibrational energy relaxation and spectral diffusion in water and deuterated water. *J. Phys. Chem. A*, 104:4866–4875, 2000.
49. T.L.C. Jansen, D. Cringus, and M.S. Pshenichnikov. Dissimilar dynamics of coupled water vibrations. *J. Phys. Chem. A*, 113:6260–6265, 2009.
50. M.G. Sceats, M. Stavola, and S.A. Rice. On the role of fermi resonance in the spectrum of water in its condensed phases. *J. Chem. Phys*, 71:983, 1979.

51. Glen Nielson and Stuart A. Rice. An improved analysis of the oh stretching spectrum of amorphous solid water. *J. Chem. Phys.*, 78:4824, 1983.
52. K. Belsley and M.G. Sceats. The overtone oh stretching raman spectrum of liquid water. *Chem. Phys. Lett.*, 70:504, 1980.
53. G.E. Walrafen and E. Pugh. Raman combinations and stretching overtones from water, heavy water and nacl in water at shifts to ca. 7000 cm⁻¹. *J. Solution Chem.*, 33:81–97, 2004.
54. M.G. Sceats and K. Belsley. A conjecture on the overtone oh stretching spectrum of hdo in liquid water. *Mol. Phys.*, 40:1389–1400, 1980.
55. G.R. Choppin and M.R. Violante. Nearinfrared studies of the structure of water iii. mixed solvent systems. *J. Chem. Phys.*, 56:5890, 1972.
56. J.D. Worley and I.M. Klotz. Near-infrared spectra of h₂o-d₂o solutions. *J. Chem. Phys.*, 45:2868–2871, 1966.
57. T. Forster. Experimentelle und theoretische untersuchung des zwischenmolekularen uberangs von elektronenanregungsenergie. *Z.Naturforsch.*, 4:821–827, 1940.
58. P. J. Flory. *Statistical Mechanics of Chain Molecules*. Interscience: New York, 1969.
59. M. Morin, P. Jakob, N. J. Levinos, Y. J. Chabal, and A. L. Harris. Vibrational energy transfer on hydrogen-terminated vicinal si(111) surfaces: Interadsorbate energy flow. *J. Chem. Phys.*, 96(8):6203–6212, 1992.
60. C. J. Fecko, J. D. Eaves, J. J. Loparo, A. Tokmakoff, and P. L. Geissler. Ultrafast hydrogen-bond dynamics in the infrared spectroscopy of water. *Science*, 301:1698–1701, 2003.
61. J. D. Eaves, J. J. Loparo, C. J. Fecko, S. T. Roberts, A. Tokmakoff, and P. L. Geissler. Hydrogen bonds in liquid water are broken only fleetingly. *PNAS*, 102:13019–13022, 2005.
62. C. J. Fecko, J. J. Loparo, S. T. Roberts, and A. Tokmakoff. Local hydrogen bonding dynamics and collective reorganization in water: Ultrafast infrared spectroscopy of hod/d₂o. *J. Chem. Phys.*, 122:054506, 2005.
63. Sander Woutersen and Huib J. Bakker. Hydrogen bond in liquid water as a brownian oscillator. *Phys. Rev. Lett.*, 83(10):2077–2080, September 1999.
64. G. M. Gale, G. Gallot, F. Hache, N. Lascoux, S. Bratos, and J-Cl. Leicknam. Femtosecond dynamics of hydrogen bonds in liquid water: A real time study. *Phys. Rev. Lett.*, 82:1068–1071, 1999.

65. J. Stenger, D. Madsen, P. Hamm, E. T. J. Nibbering, and T. Elsaesser. Ultrafast vibrational dephasing of liquid water. *Phys. Rev. Lett.*, 87:027401, 2001.
66. Sergey Yeremenko, Maxim S. Pshenichnikov, and Douwe A. Wiersma. Hydrogen-bond dynamics in water explored by heterodyne-detected photon echo. *Chem. Phys. Lett*, 369(1-2):107–113, February 2003.
67. C. P. Lawrence and J. L. Skinner. Vibrational spectroscopy of HOD in liquid D₂O. VII. temperature and frequency dependence of the OH stretch lifetime. *J. Chem. Phys.*, 119:3840–3848, 2003.
68. Joseph J. Loparo, Sean T. Roberts, and Andrei Tokmakoff. Multidimensional infrared spectroscopy of water. ii. hydrogen bond switching dynamics. *J. Chem. Phys.*, 125:194522, 2006.
69. S. Woutersen and H. J. Bakker. Resonant intermolecular transfer of vibrational energy in liquid water. *Nature*, 402:507–509, 1999.
70. K. Weidlich G. Seifert and H. Graener. Anharmonic bendstretch coupling in neat liquid water. *Phys. Rev. B*, 56:14231, 1997.
71. Adriaan M. Dokter and Huib J. Bakker. Transient absorption of vibrationally excited ice ih. *J. Chem. Phys.*, 128(2):024502, 2008.
72. F. Perakis, S. Widmer, and P. Hamm. Two-dimensional infrared spectroscopy of isotope-diluted ice lh. *J. Chem. Phys.*, 134:204505, 2011.
73. M. L. Cowan, B. D. Bruner, N. Huse, J. R. Dwyer, B. Chugh, E. T. J. Nibbering, T. Elsaesser, and R. J. D. Miller. Ultrafast memory loss and energy redistribution in the hydrogen bond network of liquid H₂O. *Nature*, 434:199, 2005.
74. A. J. Lock and H. J. Bakker. Temperature dependence of vibrational relaxation in liquid H₂O. *J. Chem. Phys.*, 117(4):1708–1713, 2002.
75. S. Ashihara, N. Huse, A. Espagne, E. T. J. Nibbering, and T. Elsaesser. Ultrafast structural dynamics of water induced by dissipation of vibrational energy. *J. Phys. Chem. A*, 111:743, 2007.
76. Buijs K. and Chopin G.R. Near-infrared studies of the structure of water. i. pure water. *Chem. Phys.*, 39:2035, 1963.
77. W.L. Jorgensen and J.D. Madura. Temperature and size dependence for monte carlo simulations of tip4p water. *Mol. Phys.*, 56:1381, 1985.
78. Sungho Han, Pradeep Kumar, , and H. Eugene Stanley. Hydrogen-bond dynamics of water in a quasi-two-dimensional hydrophobic nanopore slit. *Physical Review E*, 79:041202, 2009.

-
79. B. Auer, R. Kumar, J. R. Schmidt, and J. L. Skinner. Hydrogen bonding and raman, ir, and 2d-ir spectroscopy of dilute hod in liquid d2o. *PNAS*, 104(36):14215–14220, September 2007.
80. J. Lindner, D. Cringus, M.S. Pshenichnikov, and P. Vöhringer. Anharmonic bend-stretch coupling in neat liquid water. *Chem. Phys.*, 341:326–335, 2007.
81. A. I. Burshtein and V S. Malinovsky. Free-induction decay in the framework of sudden-modulation theory. *J. Opt. Soc. Am. B*, 8(5):1098–1113, May 1991.
82. S.T. Roberts, K. Ramasesha, and A. Tokmakoff. Structural rearrangements in water viewed through two-dimensional infrared spectroscopy. *Accounts of Chemical Research*, 42:1239–1249, 2009.
83. R. Ludwig, F. Weinhold, and T.C. Farrar. Experimental and theoretical determination of the temperature dependence of deuteron and oxygen quadrupole coupling-constants of liquid water. *J. Chem. Phys*, 103:6941, 1995.
84. C. Rønne, L. Thrane, P. O. Astrand, A. Wallqvist, K. V. Mikkelsen, and S. R. Keiding. Investigation of the temperature dependence of dielectric relaxation in liquid water by THz reflection spectroscopy and molecular dynamics simulation. *J. Chem. Phys*, 107(14):5319–5331, 1997.
85. H.-K. Nienhuys, R. A. Van Santen, and H. J. Bakker. Orientational relaxation of liquid water molecules as an activated process. *J. Chem. Phys*, 112:8487–8494, 2000.
86. D. Laage and J. T. Hynes. On the molecular mechanism of water reorientation. *J. Phys. Chem. B*, 112:14230, 2008.
87. R.A. Nicodemus, K. Ramasesha, S.T. Roberts, and A. Tokmakoff. Hydrogen bond rearrangements in water probed with temperature-dependent 2d ir. *Journal of Phys. Chem. Letters*, 1:1068–1072, 2010.
88. R.A. Nicodemus, S.A. Corcelli, J.L. Skinner, and A. Tokmakoff. Collective hydrogen bond reorganization in water studied with temperature-dependent ultrafast infrared spectroscopy. *J. Phys. Chem. B*, 115:5604–5616, 2011.
89. A. D. Laage and J. T. Hynes. Do more strongly hydrogen-bonded water molecules reorient more slowly? *Chem. Phys. Lett*, 433:80–85, 2006.
90. H. J. Bakker, Y. L. A. Rezus, and R. L. A. Timmer. Molecular reorientation of liquid water studied with femtosecond midinfrared spectroscopy. *J. Phys. Chem. A*, 112:11523–11534, 2008.

91. D. E. Moilanen, E. E. Fenn, Y. Lin, J. L. Skinner, B. Bagchi, and M. D. Fayer. Water inertial reorientation: Hydrogen bond strength and the angular potential. *PNAS*, 105:5295, 2008.
92. F.H. Stillinger. Structure in aqueous solutions of nonpolar solutes from the standpoint of scaled-particle theory. *Journal of Solution Chem.*, 2:141–158, 1973.
93. K. P. Murphy, P. L. Privalov, and S. J. Gill. Common features of protein unfolding and dissolution of hydrophobic compounds. *Science*, 247:559, 1990.
94. Shekhar Garde, Gerhard Hummer, Angel E. García, Michael E. Paulaitis, and Lawrence R. Pratt. Origin of entropy convergence in hydrophobic hydration and protein folding. *Phys. Rev. Lett.*, 77(24):4966–4968, Dec 1996.
95. David M. Huang and David Chandler. Temperature and length scale dependence of hydrophobic effects and their possible implications for protein folding. *PNAS*, 97(15):8324–8327, 2000.
96. H. S. Frank and M. W. Evans. Free volume and entropy in condensed systems iii. entropy in binary liquid mixtures; partial molal entropy in dilute solutions; structure and thermodynamics in aqueous electrolytes. *J. Chem. Phys.*, 13:507–532, 1945.
97. J.T. Slusher and P.T. Cummings. Molecular simulation study of tetraalkylammonium halides: 1. solvation structure and hydrogen bonding in aqueous solutions. *J. Phys. Chem. B*, 101:3818–3826, 1997.
98. J.G. Davis, K.P. Gierszal, P. Wang, and D. Ben-Amotz. Water structural transformation at molecular hydrophobic interfaces. *Nature*, 491:582–585, 2012.
99. Y. Ishihara, S. Okouchi, and H. Uedaira. Dynamics of hydration of alcohols and diols in aqueous solution. *J. Chem. Soc. Faraday Trans.*, 93:3337–3342, 1997.
100. Koichi Fumino, Kenichi Yukiyasu, Akio Shimizu, and Yoshihiro Taniguchi. Nmr studies on dynamic behavior of water molecules in tetraalkylammonium bromide-d₂o solutions at 5–25 c. *J. Mol. Liq.*, 75:1–12, 1998.
101. A. Shimizu, K. Fumino, K. Yukiyasu, and Y. Taniguchi. NMR studies on dynamic behavior of water molecule in aqueous denaturant solutions at 25 degrees c: Effects of guanidine hydrochloride, urea and alkylated ureas. *J. Mol. Liq.*, 85:269–278, 2000.
102. J. Qvist and B. Halle. Thermal signature of hydrophobic hydration dynamics. *J. Am. Chem. Soc.*, 130:10345, 2008.

103. R. Buchner, C. Hölzl, J. Stauber, and J. Barthel. Dielectric spectroscopy of ion-pairing and hydration in aqueous tetra-n-alkylammonium halide solutions. *Phys. Chem. Chem. Phys.*, 4:2169–2179, 2002.
104. S.T. van der Post, K.-J. Tielrooij, J. Hunger, E.H.G. Backus, and H.J. Bakker. Femtosecond study of the effects of ions and hydrophobes on the dynamics of water. *Faraday Discuss.*, 160:171–189, 2013.
105. Damien Laage, Guillaume Stirnemann, and James T. Hynes. Why water reorientation slows without iceberg formation around hydrophobic solutes. *J. Phys. Chem. B*, 113:2428–2435, 2009.
106. G. Stirnemann, J.T. Hynes, and D. Laage. Water hydrogen bond dynamics in aqueous solutions of amphiphiles. *J. Phys. Chem. B*, 114:3052–3059, 2010.
107. G. Stirnemann, F. Sterpone, and D. Laage. Dynamics of water in concentrated solutions of amphiphiles: Key roles of local structure and aggregation. *J. Phys. Chem. B*, 115:3254–3262, 2011.
108. J.T. Titantah and M. Karttunen. Long-time correlations and hydrophobe-modified hydrogen-bonding dynamics in hydrophobic hydration. *J. Am. Chem. Soc.*, 134:9362–9368, 2012.
109. Artem A. Bakulin, C. Liang, T. la Cour Jansen, D. A. Wiersma, H. J. Bakker, and M. S. Pshenichnikov. Hydrophobic solvation: A 2d ir spectroscopic inquest. *Accounts of Chemical Research*, 42:1229–1238, 2009.
110. A.A. Bakulin, M.S. Pshenichnikov, H.J. Bakker, and C. Petersen. Hydrophobic molecules slow down the hydrogen-bond dynamics of water. *J. Phys. Chem. A*, 115:1821–1829, 2011.
111. Y. L. A. Rezus and H. J. Bakker. Effect of urea on the structural dynamics of water. *PNAS*, 103:18417–20, 2006.
112. Pier Luigi Silvestrelli. Are there immobilized water molecules around hydrophobic groups? aqueous solvation of methanol from first principles. *J. Phys. Chem. B*, 0:0, 2009.
113. L. Almasy, A. Lenb, N.K. Szekelyb, and J. Pletilc. Solute aggregation in dilute aqueous solutions of tetramethylurea. *Fluid Phase Equilibria*, 257:114–119, 2007.
114. W. Homsí Brandeburgo and E.J. Meijer. To be published.
115. I. Ohmine and H. Tanaka. Fluctuation, relaxations, and hydration in liquid water - hydrogen-bond rearrangement dynamics. *Chemical Reviews*, 93:2545–2566, 1993.

116. C. Petersen, K.-J. Tielrooij, and H. J. Bakker. Strong temperature dependence of water reorientation in hydrophobic hydration shells. *J. Chem. Phys.*, 130(21):214511, 2009.
117. W.M. Cox and J.H. Wolfenden. *Proc. R. Soc. London, Ser. A*, 145:486, 1934.
118. A. W. Omta, M. F. Kropman, S. Woutersen, and H. J. Bakker. Negligible effect of ions on the hydrogen-bond structure in liquid water. *Science*, 301:347–349, 2003.
119. J.D. Smith, R.J. Saykally, and P.L. Geissler. The effects of dissolved halide anions on hydrogen bonding in liquid water. *J. Am. Chem. Soc.*, 129:13847–13856, 2007.
120. R. Mancinelli, A. Botti, F. Bruni, M.A. Ricci, and A.K. Soper. Hydration of sodium, potassium, and chloride ions in solution and the concept of structure maker/breaker. *J. Phys. Chem. B*, 111:13570–13577, 2007.
121. Diedrich A. Schmidt, Oezguer Birer, Stefan Funkner, Benjamin P. Born, Ramachandran Gnanasekaran, Gerhard W. Schwaab, David M. Leitner, and Martina Havenith. Rattling in the cage: Ions as probes of subpicosecond water network dynamics. *J. Am. Chem. Soc.*, 131:18512–18517, 2009.
122. Y.A. Lin, B.M. Auer, and J.L. Skinner. Water structure, dynamics, and vibrational spectroscopy in sodium bromide solutions. *J. Chem. Phys.*, 131:144511, 2009.
123. K.-J. Tielrooij, N. Garcia-Araez, M. Bonn, and H.J. Bakker. Cooperativity in ion hydration. *Science*, 328:1006–1009, 2010.
124. M. F. Kropman and H. J. Bakker. Dynamics of water molecules in aqueous solvation shells. *Science*, 291:2118–2120, 2001.
125. M. F. Kropman, H.-K. Nienhuys, and H. J. Bakker. Real-time measurement of the orientational dynamics of aqueous solvation shells in bulk liquid water. *Phys. Rev. Lett.*, 88:077601, 1–4, 2002.
126. David E. Moilanen, Daryl Wong, Daniel E. Rosenfeld, Emily E. Fenn, and M. D. Fayer. Ion-water hydrogen-bond switching observed with 2d ir vibrational echo chemical exchange spectroscopy. *PNAS*, 106(2):375–380, January 2009.
127. M. Ji, M. Odellius, and K.J. Gaffney. Large angular jump mechanism observed for hydrogen bond exchange in aqueous perchlorate solution. *Science*, 328:1003–1005, 2010.
128. Pehr Aake Bergstrom, Jan Lindgren, and Olof Kristiansson. An ir study of the hydration of perchlorate, nitrate, iodide, bromide, chloride and sulfate anions in aqueous solution. *J. Phys. Chem.*, 95:8575–8580, 1991.

129. M. F. Kropman and H. J. Bakker. Femtosecond mid-infrared spectroscopy of aqueous solvation shells. *J. Chem. Phys.*, 115(19):8942–8948, 2001.
130. Sungnam Park and M. D. Fayer. Hydrogen bond dynamics in aqueous nabr solutions. *PNAS*, 104:16731–16738, 2007.
131. Sean T. Roberts, Joseph J. Loparo, and Andrei Tokmakoff. Characterization of spectral diffusion from two-dimensional line shapes. *J. Chem. Phys.*, 125:084502, 2006.
132. B. Nigro, S. Re, D. Laage, R. Rey, and J.T. Hynes. On the ultrafast infrared spectroscopy of anion hydration shell hydrogen bond dynamics. *J. Phys. Chem. A*, 110:11237–11243, 2006.
133. D. Laage and J. T. Hynes. Reorientational dynamics of water molecules in anionic hydration shells. *PNAS*, 104:11167, 2007.
134. D. Laage and J.T. Hynes. On the residence time for water in a solute hydration shell: Application to aqueous halide solutions. *J. Phys. Chem. B*, 112:7697–7701, 2008.
135. Anthony G Lee. How lipids affect the activities of integral membrane proteins. *Biochim. Biophys. Acta*, 1666:62–87, 2004.
136. F. Hofmeister. Zur lehre von der wirkung der salze. *Arch. Exp. Pathol. Pharmacol.*, 24:247–260, 1888.
137. Y. Marcus. Effect of ions on the structure of water: Structure making and breaking. *Chem. Rev.*, 109:1346–1370, 2009.
138. R.J. Clarke and C. Lupfert. Influence of anions and cations on the dipole potential of phosphatidylcholine vesicles: A basis for the hofmeister effect. *Biophys. J.*, 76:2614–2624, 1999.
139. Rainer A. Böckmann, Agnieszka Hac, and Helmut Grubmüller. Effect of sodium chloride on a lipid bilayer. *Biophys. J.*, 85:16471655, 2003.
140. M.L. Berkowitz, D.L. Bostick, and S. Pandit. Aqueous solutions next to phospholipid membrane surfaces: Insights from simulations. *Chem. Rev.*, 106:1527–1539, 2006.
141. Juan J. Garcia-Celma, Lina Hatahet, Werner Kunz, and Klaus Fendler. Specific anion and cation binding to lipid membranes investigated on a solid supported membrane. *Langmuir*, 23:1007410080, 2007.
142. E. Leontidis, A. Aroti, and L. Belloni. Liquid expanded monolayers of lipids as model systems to understand the anionic hofmeister series: 1. a tale of models. *J. Phys. Chem. B*, 113:14471459, 2009.
143. E. Leontidis and A. Aroti. Liquid expanded monolayers of lipids as model systems to understand the anionic hofmeister series: 2. ion partitioning is mostly a matter of size. *J. Phys. Chem. B*, 113:14601467, 2009.

144. N.N. Casillas-Ituarte, X.K. Chen, H. Castada, and H.C. Allen. Na⁺ and Ca²⁺ effect on the hydration and orientation of the phosphate group of DPPC at air-water and air-hydrated silica interfaces. *J. Phys. Chem. B*, 114:9485–9495, 2010.
145. R. Vacha, P. Jurkiewicz, M. Petrov, M.L. Berkowitz, R.A. Bockmann, J. Barucha-Kraszewska, M. Hof, and P. Jungwirth. Mechanism of interaction of monovalent ions with phosphatidylcholine lipid membranes. *J. Phys. Chem. B*, 114:9504–9509, 2010.
146. P. Jurkiewicz, L. Cwiklik, A. Vojtiskova, P. Jungwirth, and M. Hof. Structure, dynamics, and hydration of POPC/POPE bilayers suspended in NaCl, KCl, and CsCl solutions. *Biochim. Biophys. Acta-Biomembr.*, 1818:609–616, 2012.
147. A.T. Myller, J.J. Karhe, and T.T. Pakkanen. Preparation of aminofunctionalized TiO₂ surfaces by binding of organophosphates. *Appl. Surf. Sci.*, 257:1616–1622, 2010.
148. Jean Boisson, Guillaume Stirnemann, Damien Laage, and James T. Hynes. Water reorientation dynamics in the first hydration shells of F- and I-. *Phys. Chem. Chem. Phys.*, 13:19895–19901, 2011.
149. A.M. Dokter, S. Woutersen, and H.J. Bakker. Ultrafast dynamics of water in cationic micelles. *J. Chem. Phys.*, 126:124507, 1–7, 2007.
150. A.K. Soper and K. Weckström. Ions solvation and water structure in potassium halide aqueous solutions. *Biophys. Chem.*, 124:180–191, 2006.
151. R. Buchner, S.G. Capewell, G. Hefter, and P.M. May. Ion-pair and solvent relaxation processes in aqueous Na₂SO₄ solutions. *J. Phys. Chem. B*, 103:1185–1192, 1999.
152. Christian Petersen, Artem A. Bakulin, Vlad G. Pavelyev, Maxim S. Pshenichnikov, and Huib J. Bakker. Femtosecond midinfrared study of aggregation behavior in aqueous solutions of amphiphilic molecules. *J. Chem. Phys.*, 133:164514, 1–8, 2010.
153. A.D. Becke. *J. Chem. Phys.*, 98:5648, 1993.
154. P.J. Stephens, F.J. Devlin, C.F. Chabalowski, and M.J. Frisch. *J. Phys. Chem.*, 98:11623, 1994.
155. J.P. Perdew and Y. Wang. *Phys. Rev. B*, 45:13244, 1992.
156. J.P. Perdew, K. Burke, and M. Ernzerhof. *Phys. Rev. Lett.*, 77:3865, 1996.
157. F. Neese. *Wiley Interdiscip. Rev.: Comput. Mol. Sci.*, 2:73, 2012.
158. A. Schafer, H. Horn, and R. Ahlrichs. *J. Chem. Phys.*, 97:2571, 1992.

-
159. F. Weigend and R. Ahlrichs. *Phys. Chem. Chem. Phys.*, 7:3297, 2005.
 160. O. Vahtras, J. Almlöf, and M.W. Feyereisen. *Chem. Phys. Lett*, 213:514, 1993.
 161. F.J. Nesse. *Comput. Chem.*, 97:2571, 2003.
 162. S. Sinnecker, A. Rajendran, A. Klamt, M. Diedenhofen, and F. Nesse. *J. Phys. Chem. A*, 110:2235, 2006.
 163. Glenn Buchner, Richard; Hefter. Interactions and dynamics in electrolyte solutions by dielectric spectroscopy. *Phys. Chem. Chem. Phys.*, 11:8984–8999, 2009.
 164. W. Wachter, W. Kunz, and R. Buchner. Is there an anionic Hofmeister effect on water dynamics? dielectric spectroscopy of aqueous solutions of NaBr, NaI, NaNO₃, NaClO₄, and NaSCN. *J. Phys. Chem. A*, 109:8675–8683, 2005.
 165. S. Funkner, G. Niehues, D.A. Schmidt, M. Heyden, G. Schwaab, K.M. Callahan, D.J. Tobias, and M. Havenith. Watching the low-frequency motions in aqueous salt solutions: The terahertz vibrational signatures of hydrated ions. *J. Am. Chem. Soc.*, 134:1030–1035, 2012.
 166. G. Stirnemann, E. Wernersson, P. Jungwirth, and D. Laage. Mechanisms of acceleration and retardation of water dynamics by ions. *J. Am. Chem. Soc.*, 135:11824–11831, 2013.
 167. G. Engel and H.G. Hertz. On the negative hydration. a nuclear magnetic relaxation study. *Ber. Bunsen-Ges. Phys. Chem.*, 72:808–834, 1968.
 168. Ana Vila Verde and Reinhard Lipowsky. Cooperative slowdown of water rotation near densely charged ions is intense but short-ranged. *J. Phys. Chem. B*, 117:10556–10566, 2013.
 169. M. Fyta, I. Kalcher, J. Dzubiella, L. Vrbka, and R.R. Netz. Ionic force field optimization based on single-ion and ion-pair solvation properties. *J. Chem. Phys.*, 132:024911, 2010.
 170. K.M. Callahan, N.N. Casillas-Ituarte, M. Roeselova, H.C. Allen, and D.J. Tobias. Solvation of magnesium dication: Molecular dynamics simulation and vibrational spectroscopic study of magnesium chloride in aqueous solutions. *J. Chem. Phys.*, 114:5141–5148, 2010.
 171. Maria Fyta and Roland R. Netz. Ionic force field optimization based on single-ion and ion-pair solvation properties: Going beyond standard mixing rules. *J. Chem. Phys.*, 136:124103, 2012.
 172. Y. Luo, W. Jiang, H. Yu, A.D. MacKerell, and B. Roux. Simulation study of ion pairing in concentrated aqueous salt solutions with a polarizable force field. *Faraday Discuss.*, 160:135–149, 2013.

173. S. Koneshan, J.C. Rasaiah, R.M. Lynden-Bell, and S.H. Lee. Solvent structure, dynamics, and ion mobility in aqueous solutions at 25 deg c. *J. Phys. Chem. B*, 102:4193–4204, 1998.
174. P.E. Mason, G.W. Neilson, C.E. Dempsey, A.C. Barnes, and J.M. Cruickshank. The hydration structure of guanidinium and thiocyanate ions: Implications for protein stability in aqueous solution. *PNAS*, 100:4557–4561, 2003.
175. Atanu Das and Chaitali Mukhopadhyay. Urea-mediated protein denaturation: A consensus view. *J. Phys. Chem. B*, 113:12816–12824, 2009.
176. A. Shimizu and Y. Taniguchi. Nmr studies on reorientational motion of hydrated d2o molecules in tetraalkylammonium bromide dilute aqueous solutions. *Bull. of the Chem. Soc. of Japan*, 63:3255–3259, 1990.
177. Y. Marcus. Tetraalkylammonium ions in aqueous and non-aqueous solutions. *J. Solutions Chem.*, 37:1071–1098, 2008.
178. Ningdong Huang, Daniel Schlesinger, Dennis Nordlund, Congcong Huang, Tolek Tyliczszak, Thomas M. Weiss, Yves Acremann, Lars G.M. Pettersson, and Anders Nilsson. Microscopic probing of the size dependence in hydrophobic solvation. *J. Chem. Phys*, 136:074507, 1–7, 2012.
179. T. Steinel, J. B. Asbury, J. Zheng, and M. D. Fayer. Watching hydrogen bonds break: A transient absorption study of water. *J. Phys. Chem. A*, 108:10957–10964, 2004.
180. C. Krekeler, B. Hess, and L. Delle Site. Density functional study of ion hydration for the alkali metal ions (li+,na+,k+) and the halide ions (f-,br-,cl-). *J. Chem. Phys*, 125:054305, 1–7, 2006.
181. P.O. Eriksson, G. Lindblom, E.E. Burnell, and G.J.T. Tiddy. Influence of organic solutes on the self-diffusion of water as studied by nuclear magnetic-resonance spectroscopy. *Journal of the Chemical Society-Faraday Transactions*, 84:3129–3139, 1988.
182. M.F. Kropman and H.J. Bakker. Vibrational relaxation of liquid water in ionic solvation shells. *Chem. Phys. Lett*, 370:741–746, 2003.
183. Michel F. Kropman and Huib J. Bakker. Effect of ions on the vibrational relaxation of liquid water. *J. Am. Chem. Soc.*, 126(29):9135–9141, July 2004.
184. H. J. Bakker. Structural dynamics of aqueous salt solutions. *Chem. Rev.*, 108(4):1456–1473, 2008.
185. H.J. Bakker, A.J. Lock, and D. Madsen. Strong feedback effect in the vibrational relaxation of liquid water. *Chem. Phys. Lett*, 384:236–241, 2004.

186. Jan Heyda, Mikael Lund, Milan Oncak, Petr Slavicek, and Pavel Jungwirth. Reversal of hofmeister ordering for pairing of nh_4^+ vs alkylated ammonium cations with halide anions in water. *J. Phys. Chem. B*, 114:10843–10852, 2010.
187. N.G. Polydorou, J.D. Wicks, and J.Z. Turner. Hydrophobic interaction of tetrapropylammonium ions in water: A neutron diffraction and reverse monte carlo study. *J. Chem. Phys.*, 107:197–204, 1997.
188. H. Krienke, V. Vlachy, G. Ahn-Ercan, and I. Bako. Modeling tetraalkylammonium halide salts in water: How hydrophobic and electrostatic interactions shape the thermodynamic properties. *J. Phys. Chem. B*, 113:4360–4371, 2009.
189. Y. L. A. Rezus and H. J. Bakker. Femtosecond spectroscopic study of the solvation of amphiphilic molecules by water. *Chem. Phys.*, 350:87 – 93, 2008.
190. J.Z. Turner, A. K. Soper, and J.L. Finney. Ionic versus apolar behavior of the tetramethylammonium ion in water. *J. Chem. Phys.*, 102:5438–5443, 1995.
191. A. K. Soper, L. Dougan, J. Crain, and J. L. Finney. Excess entropy in alcohol-water solutions : A simple clustering explanation. *J. Phys. Chem. B*, 110:3472, 2006.
192. C. Camilloni, A. G. Rocco, I. Eberini, E. Gianazza, R. A. Broglia, and G. Tiana. Urea and guanidinium chloride denature protein l in different ways in molecular dynamics simulations. *Biophys. J.*, 94:4654–4661, 2008.
193. W.K. Lim, J. Rosgen, and S.W. Englander. Urea, but not guanidinium, destabilizes proteins by forming hydrogen bonds to the peptide group. *PNAS*, 106:2595–2600, 2009.
194. J. Scott, N.V. Nucci, and J.M. Vanderkooi. Changes in water structure induced by the guanidinium cation and implications for protein denaturation. *J. Phys. Chem. A*, 112:10939–10948, 2008.
195. F. Rashid, S. Sharma, and B. Bano. Comparison of guanidine hydrochloride (gdnhcl) and urea denaturation on inactivation of hpc. *The Protein Journal*, 24:283–292, 2005.
196. J. Hunger, S. Niedermayer, R. Buchner, and G. Hefter. Are nanoscale ion aggregates present in aqueous solutions of guanidinium salts? *J. Phys. Chem. B*, 114:13617–13627, 2010.
197. P.A. Mason, J.W Brady, G.W. Neilson, and C.E. Dempsey. The interaction of guanidinium ions with a model peptide. *Biophys. J.*, 93:L4–L6, 2007.

198. J. Heyda, M. Kozsek, L. Bednarova, G. Thompson, J. Konvalinka, J. Vondrasek, and P. Jungwirth. Urea and guanidinium induced denaturation of a trp-cage miniprotein. *J. Phys. Chem. B*, 115:8910–8924, 2011.
199. M.C. Stumpe and H. Grubmuller. Interaction of urea with amino acids: Implications for urea-induced protein denaturation. *J. Am. Chem. Soc.*, 129:16126–16131, 2007.
200. H. Wei, Y. Fan, and Y.Q. Gao. Effects of urea, tetramethyl urea and trimethylamine n-oxide on aqueous solution structure and solvation of protein backbones: A molecular dynamics simulation study. *J. Phys. Chem. B*, 114:557–568, 2010.
201. D.Y. Vorobyev, C.-H. Kuo, D.G. Kuroda, J.N. Scott, J.M. Vanderkooi, and R.M. Hochstrasser. Water-induced relaxation of a degenerate vibration of guanidinium using 2d ir echo spectroscopy. *J. Phys. Chem. B*, 114:2944–2953, 2010.
202. B.C. Lee, M. Kumauchi, and W.D. Hoff. Modulating native-like residual structure in the fully denatured state of photoactive yellow protein affects its refolding. *Journal of Biological Chemistry*, 285:12579–12586, 2010.

Summary

Water molecules are deceptively simple considering their importance to many (biological) processes. Since a number of decades it has become clear that the interesting properties of water and its role in these processes can be attributed to the ability of water molecules to form up to four hydrogen-bonds. Key aspects to consider in this context are the characteristics of water in the vicinity of electric charges and hydrophobic groups. In this thesis we describe a number of studies on the vibrational relaxation and reorientation dynamics of water molecules in aqueous solutions. These processes take place on a picosecond timescale and have been found to be sensitive probes of the hydrogen-bond network. The experimental technique that we used is polarization resolved femtosecond infrared pump-probe spectroscopy. This technique uses extremely short laser pulses (100 femtoseconds) to excite a molecular vibration in a small subset of the water molecules. The excited molecules have a different absorption spectrum than those in the ground state and this transient absorption difference is probed by a second laser pulse. By varying the waiting time between the pump and probe pulses, the time dependent behavior of the transient absorption differences are obtained. These time dependent data provide information on dynamical parameters of the system like hydrogen-bond dynamics and molecular reorientation. In the following paragraphs we summarize our findings on the structure and dynamics of water in solutions of salts and amphiphilic molecules that we obtained with this technique.

VIBRATIONAL DECAY IN PURE WATER In chapter 5 we demonstrated that the vibrational relaxation time T_1 of the OH stretch vibration in pure liquid water depends on the strength of the local hydrogen-bond interaction. The resonance frequency of weakly hydrogen-bonded OH groups of water is blue-shifted with respect to that of strongly hydrogen-bonded OH groups. By varying the spectrum of the pump pulse we could thus selectively excite a subset of OH groups that donate hydrogen-bonds of a certain strength. We found that the T_1 lifetime shows a smooth transition between $T_1 = 220$ fs for strongly hydrogen-bonded OH groups to $T_1 = 560$ fs for weakly hydrogen-bonded OH groups. These values were found to be consistent with a kinetic model including spectral diffusion, Förster transfer, and vibrational relaxation via energy transfer to the overtone

of the H₂O-bending mode. In addition, we showed that the OH stretch overtone absorption band mainly represents weakly hydrogen-bonded OH groups due to an interference effect of the electrical and mechanical anharmonicities of the OH vibration. After excitation, the overtone decays extremely rapidly to the first excited state. The subsequent decay to the ground state shows the same characteristics as found after direct excitation of weakly hydrogen-bonded OH groups.

JUMP REORIENTATION OF WATER In chapter 6 we studied the reorientation dynamics of water. To avoid certain experimental difficulties, these experiments were performed by exciting the OD stretch vibration of HDO molecules in isotopically diluted water (8% HDO in H₂O) instead of using pure H₂O. After excitation the transient absorption changes were monitored with a probe pulse that is polarized either parallel or perpendicular to the pump polarization. From these two signals, a parameter can be constructed that exclusively represents the reorientation dynamics of the excited OD groups. It was predicted by molecular dynamics simulations that water molecules do not rotate in a diffusive fashion, but rather make small rotational jumps in which a hydrogen-bond is broken and a new hydrogen-bond is formed with another water molecule. We excited a subset of OD groups that donate a very weak hydrogen-bond and have a large probability to be close to a jump. The reorientation dynamics that we obtained were fully consistent with the jump model of reorientation. In addition, we found that for increasing temperatures the rate of jumps increases. From these results we derived that the activation energy of the jumping mechanism is 11 kJ/mol.

SLOW WATER AROUND HYDROPHOBIC GROUPS In chapter 7 we studied the reorientation dynamics of water in a concentrated solution of tetramethylurea (TMU) in isotopically diluted water. TMU contains four methyl groups and has shown to be an ideal model system to study hydrophobic hydration. We found that both the reorientation dynamics and spectral diffusion of water molecules are much slower in the TMU solution than in neat water. Our results show that the translational motion of water molecules around hydrophobic groups is hindered. As a result, it is harder for a water molecule to increase the distance to its hydrogen-bonding partners and to allow a possible new partner to approach. Such a configurational change is needed to enable a reorientational jump. The slow reorientational dynamics thus follow directly from the slower structural diffusion. With increasing temperature we found that both the structural diffusion and the reorientation dynamics speed up, consistent with previous findings that show that the effects of hydrophobes on the dynamics of water strongly decreases at higher temperatures.

COOPERATIVE EFFECTS IN ION HYDRATION In chapters 8 and 9 we studied the reorientation dynamics of water molecules in (halide) salt solutions using a similar experiment as described above. The spectral blue-shift of the OD-stretch resonance frequency of halide bound water molecules enabled us to specifically isolate the response of these water molecules. We found a number of contribu-

tions to the observed dynamics: 1) a wobbling motion with a time constant of 2.0 ± 0.3 ps, 2) a slow motion with a time constant of 9 ± 1 ps that we associate with the rotational diffusion of the water molecule over the anion surface and 3) a component due to the exchange of water molecules inside and outside the anion solvation shell. Anions with a smaller radius interact more strongly with their solvation shell and thus have a larger restricting effect on the wobbling motion. We found that the nature of the cation can limit the freedom of the wobbling motion even further, but only if its surface charge density is sufficiently high. Highly charged anions and cations (or ionic molecular groups) were found to participate in a water complex, in which the solvating water molecules are severely hindered in their reorientation due to the combined effect of the cation and the anion.

COMBINED EFFECTS OF HYDROPHOBES AND IONS Cations of the class of tetra-*n*-alkylammonium (TAA) salts contain hydrophobic groups in the form of four alkyl chains. For such systems the question arises whether the charged nature or the hydrophobic nature is more dominant in the hydration properties. In chapter 10 we studied TAABr salts with various alkyl lengths and thus hydrophobicity using the same analysis techniques as for the halide salts in previous chapters. We find that even for the shortest alkyl chains (Me_4NBr), the reorientation dynamics of the water solvating the cation is slower than in bulk water, consistent with the picture of hydrophobic hydration. In addition, at high concentrations the wobbling component of OD groups hydrogen-bonded to halide ions that we found in previous chapters was found to be severely hindered by the presence of the hydrophobic cations. The cations with long alkyl chains (Et_4NBr , Pr_4NBr , Bu_4NBr) form clusters with bromide ions and water molecules. The water molecules inside these clusters are highly confined, causing the reorientation of OD groups bound to the bromide ions that penetrated such a cluster to become even slower than 30 ps. For Me_4NBr such aggregation effects are not observed, probably because for this ion the repulsive coulomb interaction is strong enough to prevent the formation of large aggregated ion clusters. Continuing on these results, we made a comparison between urea, tetramethylurea, guanidinium chloride and tetramethylguanidinium chloride in chapter 11. In line with previous results we found that methylation of urea and guanidinium chloride results in a large fraction of water molecules with slower dynamics. These four compounds were compared in their ability to denature a model peptide. We found that the methyl substituted compounds likely have a different mechanism of denaturation compared to the unmethylated compounds.

Samenvatting

WATER IS MEER DAN EEN OPLOSMIDDEL Het leven op aarde is gebaseerd op water: vrijwel alle organismen, of ze nu zo klein zijn als een bacterie of zo groot als een olifant, bestaan voor meer dan 50 procent uit water. Het mag echter duidelijk zijn dat niet het water organismen hun stevigheid of bijzondere mogelijkheden geeft. Puur, vloeibaar water heeft weinig consistentie en valt gemakkelijk uit elkaar in druppels als je er een emmer van leeg gooit. Waarom komt het dan zoveel voor in organismen? Wat voor rol speelt het precies? Deze vragen hebben onderzoekers al decennia lang geïnspireerd.

Het meeste water in organismen zit in hun cellen. Je kunt een cel zien als een microscopisch klein zakje water dat allerlei zouten, eiwitten en andere chemicaliën bevat. Deze bestanddelen voeren taken uit die van belang zijn voor het in leven houden van het organisme als geheel: fotosynthese, het doorgeven van elektrische signalen, celdeling, samentrekking van spieren enz. De meeste van deze bestanddelen zijn oplosbaar in water. Het is daarom ook niet opmerkelijk dat er lange tijd gedacht is dat de enige rol van water was om deze stoffen op te lossen. Water werd gezien als een medium zonder specifieke functie, waarin de eiwitten het echte werk doen. Pas toen er spectroscopische technieken werden ontwikkeld waarmee biologische systemen op moleculaire schaal konden worden bestudeerd, werd het duidelijk dat watermoleculen feitelijk een zeer actieve rol hadden en dat de wisselwerking tussen water, zouten, eiwitten en andere biomoleculen essentieel is voor biologische processen. Het onderzoek dat in dit proefschrift wordt beschreven vormt een bijdrage aan onze kennis over deze interactie tussen watermoleculen en andere moleculen of zouten. Dergelijke inzichten zijn niet alleen relevant voor het begrip van biologische processen. Water beïnvloedt ook processen die ten grondslag liggen aan de werking van diverse technologische vindingen zoals brandstof cellen of batterijen.

WAT ONDERZOEKEN WE EN WAAROM? De rol van water in een cel is veel te gecompliceerd om als zodanig te onderzoeken. Om deze reden passen we vaak reductionistische methoden toe om het grote (te ingewikkelde) probleem op te splitsen in kleinere (meer fundamentele) vraagstukken. Een voorbeeld is de interactie van water met alle eiwitten in een (menselijke) cel. Een lichaamscel bevat vele duizenden soorten eiwitten, elk met hun eigen functie. Op dit moment

is het onmogelijk om al de verschillende interacties van die eiwitten met water te onderscheiden. Sterker, zelfs het doorgronden van alle interacties van een enkel type eiwit met zijn omgeving is al zeer uitdagend. Eiwitten zijn namelijk zeer grote moleculen met heel veel onderdelen die zich verschillend gedragen in water. Een goede vergelijking is een kralenketting, waarbij de eigenschappen en relatieve positie van de individuele kralen bepalen wat de functie van het eiwit als geheel is. Een klein eiwit zoals insuline heeft 51 van dit soort kralen, terwijl sommige er zelfs meer dan 30.000 hebben (titin, aanwezig in spierweefsel). Het grote aantal kralen maakt het erg moeilijk om een gedetailleerde beschrijving te maken van de interactie van watermoleculen met het eiwit. Daarbij zou het erg veel werk zijn om alle duizenden eiwitten apart te onderzoeken.

Het is echter gebleken dat de natuur slechts 21 verschillende types kralen kent waaruit al die eiwitten zijn opgebouwd. Deze kralen, of aminozuren zoals ze eigenlijk heten, zijn vrij klein (iets groter dan een watermolecuul) en verschillen alleen in hun moleculaire structuur. Aminozuren zijn dus zeer fundamenteel in hun eigenschappen, overzichtelijk in aantal en ideaal om met onze experimentele technieken te onderzoeken. We kunnen echter nog een extra reductie stap maken. Alle 21 aminozuren kunnen worden onderscheiden in twee eigenschappen die zeer belangrijk zijn in hun relatie tot water: (1) ze zijn al dan niet elektrisch geladen en (2) ze zijn al dan niet oplosbaar in water. De niet oplosbare aminozuren noemen we hydrofoob, omdat ze (net als bijvoorbeeld vetten en olie) waterafstotend zijn. Deze twee eigenschappen liggen ten grondslag aan bijna alle biologische processen, ze vormen het basis gereedschap van moeder natuur. Om de rol van water in deze processen op het meest fundamentele niveau te begrijpen is het dus cruciaal dat we de eigenschappen en interactie van watermoleculen in de buurt van elektrische ladingen en rond hydrofobe stoffen doorgronden.

HOE KAN JE WATERMOLECULEN ONDERZOEKEN? Er zijn een aantal grote uitdagingen in het onderzoek naar het gedrag van watermoleculen: ze zijn ongelofelijk klein en bewegen zich tegelijkertijd verschrikkelijk snel. Het karakteriseren van een alledaags object, zoals het meten van de snelheid van een auto, zouden we kunnen doen met behulp van een camera. Als we zien dat de auto zich tussen het eerste en tweede frame een meter heeft verplaatst, en de film 24 beelden per seconden heeft, dan kunnen we eenvoudig uitrekenen dat de snelheid van de auto 86 km per uur was. De bewegingen van watermoleculen zijn echter zo snel, dat een betrouwbaar 'filmpje' meer dan een biljoen (1.000.000.000.000) beelden per seconden nodig heeft. Daarbij kan geen enkele microscoop een watermolecuul direct in beeld brengen, aangezien deze meer dan 100.000 keer kleiner zijn dan de diameter van een haar en meer dan 1000 keer kleiner dan de golflengte van zichtbaar licht. Toch kunnen we een soort filmpje maken, en wel met behulp van ultrakorte infrarood laser pulsen (flitsen van laserlicht).

In een meting worden twee laser pulsen gefocusseerd op een dun laagje water, met een variabel tijdsverschil tussen de pulsen. De eerste laser puls zorgt ervoor dat bepaalde watermoleculen gaan trillen, zodat ze in feite een soort label hebben. Deze trillende watermoleculen zorgen voor een kleine veran-

dering in de eigenschappen van de tweede puls, die in een detector kunnen worden gedetecteerd. Het tijdsverschil tussen de pulsen kan eenvoudig worden gevarieerd door de tweede puls een andere weg af te laten leggen dan de eerste puls. Aangezien de snelheid van licht ongeveer 300.000 km per seconde is, zal bij een weglengteverschil van 0.3 mm tussen de pulsen het tijdsverschil een biljoenste van een seconde bedragen. Het signaal wat door de tweede puls gemeten wordt hangt af van de exacte lengte van het tijdsinterval, bijvoorbeeld omdat de gelabelde watermoleculen in de tussentijd een beetje bewogen hebben. Door het tijdsinterval te variëren kunnen we dus een soort filmpje maken. We kunnen allerlei eigenschappen afleiden uit de gedetecteerde pulsen, zoals de snelheid waarmee de watermoleculen bewegen, *hoe* ze bewegen en hoe lang ze blijven trillen na de eerste puls.

WATERMOLECULEN BEWEGEN IN SPRONGEN Op basis van computer simulaties zijn er voorspellingen gedaan over hoe watermoleculen zich precies bewegen. Het blijkt dat dit niet op een willekeurige manier gebeurt, maar dat de moleculen eerder kleine draaiende sprongetjes maken. Waarom watermoleculen zo bewegen hangt samen met de structuur van water. Elk watermolecuul is verbonden met ongeveer vier andere watermoleculen door middel van verbindingen die waterstofbruggen worden genoemd. Als een watermolecuul zich wil bewegen, dan zal minstens één waterstofbrug verbroken moeten worden, waarna een nieuwe waterstofbrug wordt gevormd met een ander watermolecuul. Het verbreken en nieuw vormen van waterstofbruggen gaat met een plotselinge draaibeweging die snel is zelfs in vergelijking met de tijdschaal van de laser pulsen die we gebruiken. De *gemiddelde* draai snelheid van watermoleculen is in feite een stuk langzamer, doordat de watermoleculen tussen de sprongen een tijdje nauwelijks bewegen. Dit is analoog aan de seconde wijzer van een klok die elke seconde een heel snel sprongetje maakt, maar gemiddeld nog steeds een minuut nodig heeft om een rondje te maken. In hoofdstuk 6 beschrijven we resultaten waarmee we een experimenteel bewijs leveren voor deze sprongetjes. We laten ook zien dat voor hogere temperaturen de sprongetjes vaker voorkomen (in de metafoor van de seconde wijzer betekent dit dat de wijzer in minder dan een minuut rond draait).

WATERMOLECULEN ROND VETTE STOFFEN Vet stoot water af en wordt daarom hydrofoob genoemd (angst voor water). Toch is het mogelijk om bepaalde stoffen die deels hydrofoob zijn op te lossen in water, een alledaags voorbeeld is zeep. De stof tetramethylurea (TMU) is ook een voorbeeld van een stof die wel oplosbaar is in water maar verder karakteristiek heeft die bij hydrofobe moleculen horen. In het verleden is er aangetoond dat watermoleculen rond dit soort hydrofobe moleculen gemiddeld langzamer bewegen dan in puur water. Het is echter nog steeds niet helemaal duidelijk hoeveel langzamer en waar dit precies door komt.

Met het experiment dat wij uitgevoerd hebben, konden we een specifieke groep van watermoleculen volgen die een grote kans heeft om een draai sprong te maken. Daarbij vonden we dat rond de hydrofobe groepen van TMU de

watermoleculen heel erg gehinderd worden om draai sprongen te maken. Voor een dergelijke sprong is het nodig dat de afstand tussen twee watermoleculen iets groter wordt, zodat de waterstofbrug verbroken kan worden en een ander watermolecuul in de buurt kan komen om een nieuwe brug te vormen. Juist de beweging die nodig is om de afstand tussen de moleculen groter te maken is moeilijk: het netwerk van waterstof bruggen is rond de hydrofobe stof wat stijver. Dit effect verdwijnt bij hogere temperaturen, en dat klopt precies met eerdere resultaten: hydrofoben hebben aanzienlijk minder watervrees voor warm water.

WATERMOLECULEN ROND ELEKTRISCHE LADINGEN Als je zout oplost in water, dan splitst het zich in elektrisch positief geladen deeltjes en elektrisch negatief geladen deeltjes. Deze deeltjes worden ionen genoemd. Watermoleculen worden door deze ionen aangetrokken en vormen er een waterschilletje omheen. Dat is de reden waarom zouten oplosbaar zijn in water. Wij hebben ontdekt dat de watermoleculen die een schilletje vormen rond negatieve ionen toch nog de vrijheid hebben om binnen dat schilletje te wiebelen. Kleinere ionen zullen de watermoleculen meer vasthouden dan grote ionen, waardoor het water minder kan wiebelen.

Positieve ionen trekken aan een andere kant aan de watermoleculen dan de negatieve ionen. Daardoor kan het gebeuren dat watermoleculen tussen een positief en negatief ion terecht komen en geen kant meer op kunnen. Deze watermoleculen kunnen minder eenvoudig de sprongetjes maken die hierboven staan beschreven en bewegen dus veel langzamer dan in puur water. Ook dit getouwtrek hangt weer af van de grootte van de ionen. Kleine ionen trekken harder aan de watermoleculen dan grote, en zorgen er dus voor dat de watermoleculen zich extra langzaam bewegen.

WAT IS STERKER: DE AFSOTING OF DE AANTREKKING? Er bestaan heel veel verschillende soorten zouten, en sommigen hebben bijzondere eigenschappen. De positieve ionen van tetra-alkylammonium (TAA) zouten hebben een moleculaire structuur die veel aan vetten doet denken. Maar ze zijn ook elektrisch positief geladen. De vraag is dus wat sterker is, de afstotende werking van de vetten of de aantrekkende kracht van de elektrische lading? Uit onze resultaten blijkt dat de watermoleculen rond de vette ionen zich net zo gedragen als ze rond een hydrofobe stof zouden doen. We hebben ook verschillende soorten TAA zouten vergeleken die een hogere of lagere mate van vettigheid hebben. Het bleek dat hoe vetter de ionen worden, des te liever ze samen op een kluitje gaan zitten om maar zo min mogelijk water om zich heen te hebben. Doordat de vette ionen positief geladen zijn, trekken ze echter toch wat van de negatieve ionen en watermoleculen aan. Er ontstaan daardoor eilandjes in het water met een hoge concentratie ionen en een paar water moleculen ertussen. Deze watermoleculen zitten zo klem dat ze zich nog maar nauwelijks kunnen bewegen.

Dankwoord

Er zijn velen wie ik dank verschuldigd ben voor het tot stand komen van dit proefschrift. Allereerst uiteraard mijn promotor Huib Bakker, voor de vele inspirerende discussies en invalshoeken die hij mij heeft gegeven. Ik heb grote bewondering voor zijn uitgebreide kennis en wetenschappelijke intuïtie waarmee hij mij op vele momenten te hulp is gekomen. Ook op persoonlijk vlak heb ik hem altijd als zeer ondersteunend en meelevend ervaren. Niet in de laatste plaats dank ik hem ook om het vertrouwen dat hij mij gaf bij aanvang van mij promotie door mij een positie aan te bieden, ondanks dat mijn kennis van experimentele technieken op dat moment tamelijk gelimiteerd was.

Verder wil ik een aantal mensen bedanken die mij in het bijzonder in het lab hebben bijgestaan. Ellen Backus wil ik bedanken voor alle tijd die zij opgeofferd heeft om mij te leren met femtoseconde laseropstellingen te werken. Hinc Schoenmaker voor zijn technische ondersteuning, in het bijzonder bij het maken en verfijnen van de water-flow-cell. Altijd als ik iets verzon, dan had hij in twee seconde een snellere en meer luxe oplossing. Sjoerd Wouda voor de software ondersteuning. Als er een probleem met Irismet was dan werd het binnen de kortste keren opgelost in het lab. En Henk Dekker, Ronald Buijs en Idsart Attema wil ik bedanken voor de ondersteuning op het gebied van electronica.

There are a number of people I have very much enjoyed working with in close collaboration in different projects and would like to thank for that. Klaas-Jan Tielrooij, for the collaboration on ion hydration; Ronald Ulbricht, for the project on electron dynamics in diamonds; Stefan Scheidelaar, who successfully finished an internship on tetraalkylammonium salts for his masters under my supervision; Marcin Pastorczak, with whom I collaborated on formate salts and GABA; Wagner Homsí Brandeburgo, who's computer simulations provided valuable insights on the hydration of TMU; Sander Woutersen, for the initiation and input on the overtone project; and Johannes Hunger, for our joined work on the hydration of phospholipid headgroups. Our email correspondence on the data would provide for a whole book on the scientific discussions that lead to the paper, in case it gets famous.

I always experienced the atmosphere at AMOLF and within the group as

very pleasant. There was always room for respectful discussions and *gezellige* moments at breaks or after work. For that I am very grateful to you all: Artem, Carien, Christiaan, Christian, Christina, Henco, Jan, Janneke, Jiri, Klaas-Jan, Lianne, Liyuan, Lukasz, Marcin, Niklas, Nuria, Oleg, Roel, Rutger, Simona, Stefan, Stefanie, Stephan, Yves, Wilbert en Wouter. Also the groups of Mischa Bonn and Sander Woutersen contributed a lot to this atmosphere, during work discussions and after work time. I would like to thank especially my room mates Lukasz, Liyuan and Simona, who endured all my grumpy moods in our office, but with whom I also had a lot of laughs. I have good memories of all the whistling/humming/singing concerts with Lukasz.

Before I finish I would also like to thank Ethan Oelman very much for allowing me to use his work 'A Night to Dance with Water' for the front cover of my thesis, and Jorrit van der Post for making the layout.

Ik sluit af met de mensen die het dichtst bij me staan: mijn vriendin Bonnie, mijn ouders en mijn broer Jorrit, die mij in vele opzichten altijd tot steun zijn geweest. Lieve Bonnie, vier en een half jaar lang ben je samen met mij door alle fases van mijn promotie heen gegaan. Het heen en weer fietsen naar het lab in de avond, de klaagzangen over mislukte experimenten en de zorg voor Tobin terwijl ik mijn proefschrift aan het schrijven was: je hebt alles doorstaan en me door vele dalen geholpen. En Tobin, als je dit leest als je later groot bent: zelfs jij hebt me enorm geholpen. Je vroeg veel aandacht in de eerste maanden van je leven, maar door jou vergat je vader om te stressen.